National Library of Canada

Acquisitions and Bibliographic Services Branch

395 Wellington Street
Ottawa, Ontario
K1A 0N4

Bibliothèque nationale du Canada

Direction des acquisitions et des services bibliographiques

395, rue Wellington
Ottawa (Ontario)
K1A 0N4

Your file *Votre référence*

Our file *Notre référence*

NOTICE

The quality of this microform is heavily dependent upon the quality of the original thesis submitted for microfilming. Every effort has been made to ensure the highest quality of reproduction possible.

If pages are missing, contact the university which granted the degree.

Some pages may have indistinct print especially if the original pages were typed with a poor typewriter ribbon or if the university sent us an inferior photocopy.

AVIS

La qualité de cette microforme dépend grandement de la qualité de la thèse soumise au microfilmage. Nous avons tout fait pour assurer une qualité supérieure de reproduction.

S'il manque des pages, veuillez communiquer avec l'université qui a conféré le grade.

La qualité d'impression de certaines pages peut laisser à désirer, surtout si les pages originales ont été dactylographiées à l'aide d'un ruban usé ou si l'université nous a fait parvenir une photocopie de qualité inférieure.

Canada

COORDINATION PROPERTIES OF AMINOPHOSPHINE WITH FIRST ROW TRANSITION METAL NITROSYL COMPLEXES

by

NASRIN ANSARI

A dissertation submitted to the Graduate School in partial fulfillment of the requirements for the degree of Doctor of Philosophy, Ottawa University, Ottawa, Ontario, CANADA

February 1994

ISBN 0-612-00444-9

UNIVERSITÉ D'OTTAWA
UNIVERSITY OF OTTAWA

ABSTRACT

The synthesis of the new thermolabile ironnitrosylhydride complex FeH(NO)(CO)(dppf) is reported. (dppf = 1,1'-bisdiphenyl phosphino-ferrocene). The facile decomposition of FeH(NO)(CO)(dppf) is interpreted in terms of a homolysis of the Fe-H bond and of a nitrosyl transfer reaction.

The synthesis of the structurally characterized iron complex $Fe(O=PPh_2(2\text{-}Py))_3^{2+}\cdot 2BF_4^-$, by the reaction of $Fe(NO)_2(THF)_2^+$ with $PPh_2(2\text{-}Py)$ is described. The proposed mechanism for the formation of $Fe(O=PPh_2(2\text{-}Py))_3^{2+}\cdot 2BF_4^-$ involves a combination of disproportionation and oxygen transfer reactions. This dipositive iron complex is the first example of a first row transition metal chelated by the oxide of diphenyl(2-pyridyl)phosphines.

The synthesis and the reactivity of the cobaltdinitrosyl monometallic $Co(NO)_2(PPh_2(2\text{-}Py))_2^+\cdot BF_4^-$, $Co(NO)_2(Py)_2^+\cdot BF_4^-$, $Co(NO)_2(Py)_2^+\cdot BPh_4^-$ and bimetallic $Co_2(NO)_3(PPh_2(2\text{-}Py))_2^+ -BPh_4^-$ complexes are reported. The single crystal X-ray diffraction study of $Co(NO)_2(PPh_2(2\text{-}Py))_2^+BF_4^-$ shows that the aminophosphine ligands are co-ordinated through their P-donor sites. In solution, $Co(NO)_2(Py)_2^+BF_4^-$ was stable whereas, $Co(NO)_2(Py)_2^+BPh_4^-$ decomposed rapidly. The structural study of $Co(NO)_2(Py)_2^+BF_4^-$ has led to the proposal of a new theoretical

model in which the non-bonded repulsions between the NO and L ligands of the M(NO)(L) moieties provide the most influential factor for fixing the value of the (O)N-M-N(O) angle.

The structurally characterized $Co_2(NO)_3(PPh_2(2\text{-}Py))_2^+$ $-BPh_4^-$ complex is the first example of a bimetallic containing two metal-metal bonded first row transition metals with diphenyl(2-pyridyl)phosphine as a bridging ligand. It is also the first example of a $Co_2(NO)_3^+$ bimetallic core stabilized by two diphenyl(2-pyridyl)phosphine ligands coordinated by the P and N donor sites of the ligands arranged in a head-to-head fashion.

Acknowledgements

I wish to express my deep appreciation to Late Dr. Jean-Louis Roustan, my thesis supervisor, for his continued guidence and expert advice during the course of this work. I also thank him for providing all the facilities for the preparation of this thesis.

I would like to thank Dr. F. R. Ahmed, Dr. E. Gabe, Dr. Y. Lepage, Dr. J. P. Charland and Dr. F. Lee from the National Research Council in Ottawa for the single crystal structure determinations reported in this thesis.

Financial support in the form of teaching assistantship from the Department of Chemistry, Ottawa University, Ottawa, Ont. Canada, is highly appreciated.

Special thanks go to my husband Prof. Shaukat Ali, at the University Of Bridgeport, Connecticut, for his continuous support and encouragement.

I also wish to thank all my family members for their encouragement and help.

Dedicated to:

My sister

Mrs. Seemin A. Ansari

and

brother-in-law

Late Mr. Amjad H. Ansari

Publications from this work

(1) Roustan, J. L.; Ansari, N.; Le Page, Y.; Charland, J. P. *Can. J. Chem.* **1992**, 70, 1650-1657 "Single crystal X-ray structure of $Co(NO)_2(C_5H_5N)_2^+BF_4^-$. Lability of the pyridine ligands of $Co(NO)(C_5H_5N)_2^+$ and its relevance to the formation of the $Co_2(NO)_3^+$bimetallic core".

(2) Roustan, J. L.; Ansari, N.; Lee, F.; Charland, J. P. *Inorg. Chim. Acta* **1989**, 155, 11-12 " Redox reactions involving D_{NO}^{7+2} dinitrosyl iron complexes. Oxidation of 2-pyridyl diphenyl phosphine into the corresponding phosphine oxide chelating a D_{NO}^{6+0} iron".

(3) Roustan, J. L.; Ansari, N.; Charland, J. P. *Acta Cryst.*, **1989**, C45, 680. " Structure of diphenyl(2-pyridyl) Phosphine".

(4) Roustan, J. L.; Ansari, N.; Charland, J. P.; Le Page, Y. *Can. J. Chem.* **1989**, 67, 2016-2022. "Molecular geometry of M(NO)(CO)complexes. Crystal structure of acetonitrile carbony lnitrosyl bis(triphenylphosphine)irontetra fluoro borate dichloromethane".

(5) Roustan, J. L.; Ansari, N.; Ahmed, F. R. *Inorg. Chim. Acta* **1987**, 129, L11-L12 "Synthesis of the $Co_2(NO)_3^+$ metallic core stablized by two bridging aminophosphines, with BPh_4^- as a denitrosylating reagent".

List of Contents Page#

List of Figures Page#

List of Tables Page#

List of Schemes Page#

PURPOSE OF THE PRESENT STUDY

The initial aim of this work was to study the catalytic activity of the already known ironnitrosyl hydride $FeH(CO)(NO)(PPh_3)_2$ in reactions involving syngas (H_2+CO mixtures). The preliminary study readily showed that the predominant reaction was a rapid thermolysis of the hydride into a catalytically inactive mixture of dinitrosyls ($Fe(NO)_2(PPh_3)_2$ and $Fe(NO)_2(CO)(PPh_3)$) and NO-free ($Fe(CO)_3(PPh_3)_2$ and $Fe(CO)_4(PPh_3)$) monometallic degradation products. With the objective of obtaining a more stable hydride, the PPh_3 ligand was replaced by 1,1'-bis(diphenylphosphino)ferrocene more unstable than the PPh_3 analog. Decomposition of FeH(CO)(NO)(dppf) proceeds with the formation of a bimetallic. This shifted our attention towards the synthesis of bimetallic complexes, which might serve as precursors of polymetallic hydrides. Towards this end, the reaction of $Fe(CO)_4^{2-}$ with $Fe(CO)_2(NO)_2$ was studied and $Fe(CO)_3(NO)^-$ was obtained in an almost quantitative yield. The anion $Fe(CO)_3(NO)^-$ being the initial iron reagent was used in the preparation of those nitrosyl hydrides which are catalytically inactive in reactions with syngas. These studies are presented in part II of the thesis ("NO ligand transfers in ironnitrosyl chemistry"), they played a central role in shifting the aim of this research <u>from</u> reactivity studies directed towards the synthesis of organic molecules <u>to</u> inorganic synthesis targeted at the

synthesis of bimetallics containing aminophosphine bridging nitrosylated first row transition metals. Under these new conditions, *the primary aim became the study of the coordination properties of aminophosphines towards nitrosylated first row transition elements* , with part of the emphasis being placed on the identification of conditions favoring the formation of metal-metal bonded bimetallics. On the basis of geometrical considerations, the *rigid* diphenyl(2-pyridyl)phosphine PPh_2(2-Py) molecule was selected as the aminophosphine of choice. The results obtained with this ligand are presented in part III of the thesis ("Diphenyl(2-pyridyl)phosphine as an ancillary ligand of first row transition metal nitrosyl complexes"). The complexes obtained were characterized by single crystal X-ray diffraction studies and some of them displayed unusual features. Part IV ("Analysis and discussion of angular variations in M(NO)(XO) (X = C, N atoms) tetra and pentacoordinated complexes : Proposal of a new stereoelectronic model"), describes how the results obtained in this area have led to questions on the current theoretical interpretation of some of the angular deformations observed in pseudotetrahedral dinitrosyl complexes, and the proposal of an alternate model.

Part I of the thesis, provides a review of the "Structural and chemical aspects of the nitrosyl complexes", which is relevant to the present work.

PART I

STRUCTURAL AND CHEMICAL ASPECTS OF NITROSYL COMPLEXES

I-1 STRUCTURAL FEATURES OF NITROSYL COMPLEXES

The NO molecule contains an odd number of electrons. Its facile oxidation yields the nitrosonium ion (NO^+) which is isoelectronic with CO as shown below :

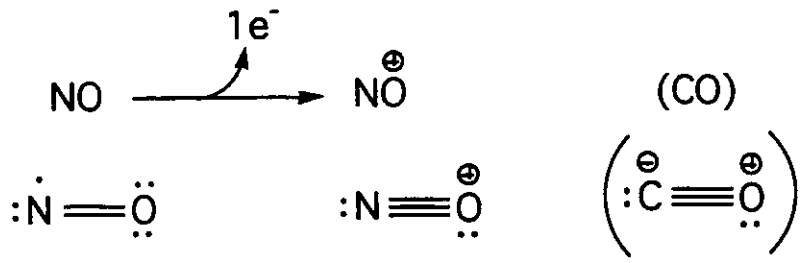

Fig.I-1-1 Lewis formulas of NO and NO^+ (isoelectronic with CO)

Three broad classes of MNO complexes can be distinguished based on the value of the M-N-O angle of the **covalent** MNO linkage, resulting from the complexation of a NO molecule on the metallic center M.

(1) when the M-N-O angle is smaller than 140°, the NO coordination mode is considered as **bent** and the NO ligand is said to display "NO^--character".

(2) when the M-N-O angle falls in the range of 155°-180°, the NO coordination mode is qualified as **linear** and the NO ligand is said to display "NO^+-character".

(3) when the M-N-O angle falls in range 140°-155° the

coordination mode is considered as **intermediate**. This coordination mode is rarely found.

To understand the origin of this NO^+/NO^- dichotomy, frequently referred to in the literature, it suffices to describe the MNO linkage in terms of a localized bonding model.

(a) NO^- character - When the NO molecule is acting as a one-electron ligand, the complexation with a metallic center M results in the formation of a σ bond (Fig. I-1-2).

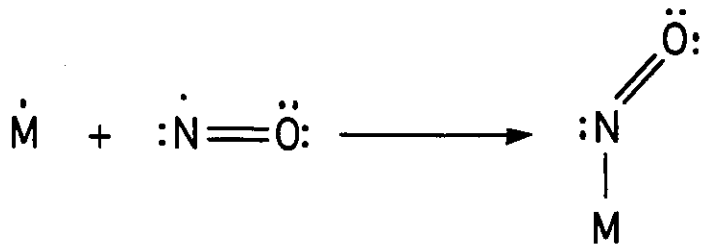

Fig.I-1-2 Bent coordination mode of NO in a neutral MNO fragment

According to the valence shell electron pair repulsion (VSEPR) theory [1], where the lone pair-lone pair > lone pair-bond pair > bond pair- bond pair interactions, the M-N-O bond angle is predicted to be about 120° with a bent coordination mode of the NO ligand. For computing the electronic configuration of the metal M in a MNO complex, the NO in a bent coordination mode must be treated as "NO^-".

(b) NO^+ character - When the M-N-O angle is around 180°, the coordination mode of the NO resembles that of a CO ligand. The formation of the M-N-O linkage can then be interpreted **formally** in the stepwise manner shown in Fig.I-1-3.

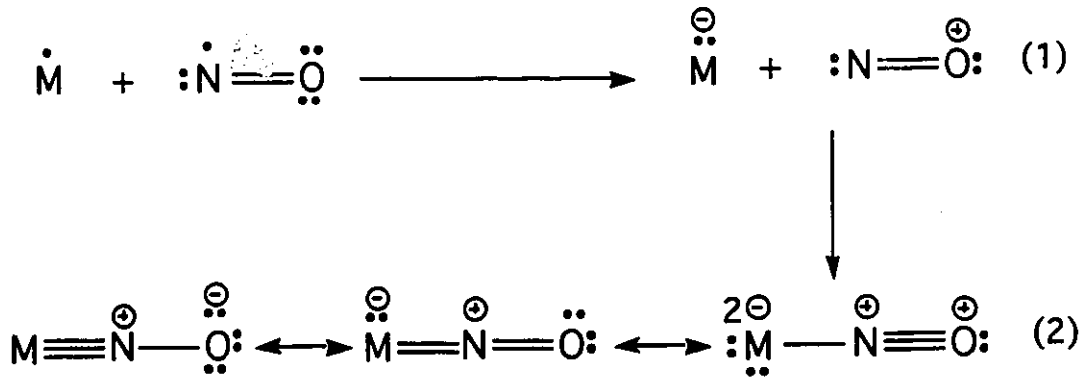

Fig.I-1-3 Linear coordination mode of NO in a neutral MNO fragment

In step (1) transfer of the unpaired electron of NO onto the metal "M" generates NO^+ (which is isoelectronic with CO) which then coordinates in a similar manner on the M^- metallic center (step (2)). Under these conditions, the NO molecule is acting as a three electron donor. To assign the oxidation state and the electronic configuration of the metal, the NO ligand has to be removed in the same electronic configuration as the CO ligand, that is as NO^+.

I-2 Problems in assigning an electronic configuration to the metal attached to a NO ligand

One encounters a difficulty in assigning an electronic configuration to a metal coordinated to a NO ligand, unless the complex is structurally characterized. In order to overcome this problem, it was necessary to consider a NO-free complex such as $Fe(CO)_5$. To find the electronic configuration of Fe, the ligands from the metal are removed in such a way that in each ligand the atom which was directly bonded to the metal achieves a closed shell configuration. With $Fe(CO)_5$ this requirement is fulfilled when the CO ligands are removed as CO molecules according to the formal reaction of ligand detachment.

$$Fe(CO)_5 \rightarrow Fe + 5CO \qquad \text{(Rc I-2-1)}$$

An iron atom is formally produced, and therefore, the electronic configuration of Fe in $Fe(CO)_5$ is d^8. Selecting, $Fe(CO)_2(NO)_2$ as the next example, to assign tentatively an electronic configuration to Fe, as before, each NO ligand can be considered as either a one or a three electron donor. There are, therefore, three possibilities as indicated below:

$$Fe(CO)_2(NO)_2 \rightarrow Fe^{2-}(d^{10}) + 2CO + 2NO^+ \qquad \text{(Rc I-2-2)}$$

$$Fe(CO)_2(NO)_2 \rightarrow Fe^{2+}(d^6) + 2CO + 2NO^- \qquad \text{(Rc I-2-3)}$$

$$Fe(CO)_2(NO)_2 \rightarrow F\ (d^8) + 2CO + NO^+ + NO^- \qquad \text{(Rc I-2-4)}$$

Depending upon which one of these formal processes is selected, the electronic configuration assigned to iron can be either d^{10}, d^6 or d^8. The 'd^a' notation becomes ambiguous with NO complexes.

It is only when the coordination mode of the MNO linkage "linear or bent" is known, that one can know how to treat formally the NO ligand (NO^+ or NO^-) for assigning an electronic configuration to the metal. Consequently, it is only when structural data are available that the electronic configuration of the metal in terms of the usual 'd^a' notation can be used (a = number of d electrons assigned to the metallic center M of the complex under consideration, irrespective of what this complex might be).

To overcome this limitation, two symbolic representations of nitrosyl complexes have been introduced. They are applicable whether the MNO complexes have been structurally characterized or not.

(i) Enemark-Feltham Notation

The number of "d" electrons assigned to the metal is obtained in every case by removing formally the NO ligand as NO^+. The notation $\{M(NO)_n\}^b$ is then used to denote a complex containing **n**NO ligands, such that when they are **removed as NO^+**, **b** "d" electrons are left on the metal M. With this notation $Fe(CO)_2(NO)_2$ is a $\{M(NO)_2\}^{10}$ complex. $(Fe(NO)_2Cl)_2$ contains two

$\{M(NO)_2\}^9$ iron centers and $Co(CO)_3NO$ is a $\{M(NO)\}^{10}$ complex. This notation has been used extensively since it was proposed in 1974 [2].

(2) Roustan-Morrow Notation

This notation was initially proposed to remove any ambiguity regarding the meaning of the terms "Oxidation" and "Reduction", when they are used to describe reactions involving NO complexes deposited on a solid support. However, the notation can be used under any circumstances, irrespective of whether the NO complexes are considered under heterogeneous or homogeneous conditions. According to this notation, any $[M](NO)_n$ complex can be obtained in a formal way by the complexation of nNO molecules on the metallic fragment [M], where "[ ]" represents an unspecified set of non-nitrosylic ligands attached to M. If in the NO-free species [M] the electronic configuration of the metal is d^a, then the same metallic center M in the $[M](NO)_n$ complex is of the type D_{NO}^{a+n}. The number "a" is the number of d electrons left on the metal M in the complex (The oxidation state of metal could be +, 0, or -) obtained by *the formal dissociation (D) of the nNO ligands removed as NO molecules* [3].

A $[M](NO)_n$ complex of the type $\{M(NO)_n\}^b$ according to the Enemark-Feltham notation is a D_{NO}^{a+n} complex with b = a + n, in the Roustan-Morrow notation. The D_{NO}^{a+n} notation applies to any

complex. When there is no NO ligand, the D_{NO}^{a+0} notation becomes equivalent to the usual "d^a" notation. For example, $Co(NO)_3$ is a $\{M(NO)_3\}^{12}$ complex that contains a D_{NO}^{9+3} cobalt. As shown by the notation, this complex could in principle results from the addition of three NO molecules to one $D_{NO}^{9+0}(d^9)$ Co(0) center.

I-3 Redox processes classified in term of the D_{NO} notation

Any conversion (such as the one considered in Scheme I-3-1) of a D_{NO}^{a+n} $[M](NO)_n$ complex **1** into a $D_{NO}^{a'+n'}$ $[M'](NO)_{n'}$ complex **2** can be achieved according to two pathways. The first one involves the *actual* set of reactions required to obtain **2** from **1**. The second and *formal* pathway involves the NO-free progenitors **3** and **4** of species **1** and **2**, respectively, in which the metallic center is of the type D_{NO}^{a+0} for **3** and of the type $D_{NO}^{a'+0}$ for **4**.

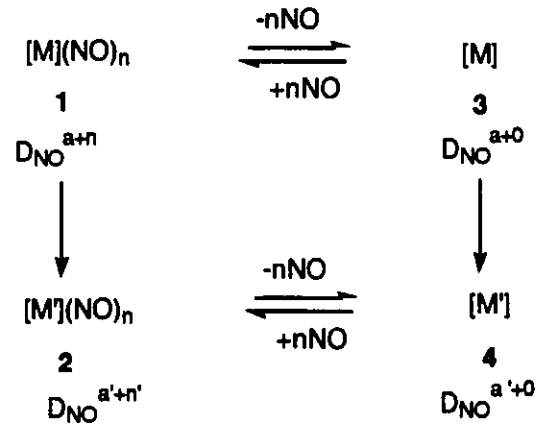

Scheme I-3-1 Conversion of a D_{NO}^{a+n} complex into a $D_{NO}^{a'+n'}$ complex

Along this formal route, the redox changes that accompany the conversion of 1 into 2 can be broken down into two components. The first type pertains to the complexation-decomplexation steps involving the pair 1 and 3 and pair 2 and 4, whereas the second type involves the NO-free species 3 and 4.

Redox changes of the first type pertain exclusively to the transfer of electrons between the metal and NO leading to the formation or rupture of a covalent MNO linkage. Depending upon the coordination modes of the NO ligands in 1 and 2, the complexation-decomplexation steps might result in a formal oxidation or reduction or no redox change at M. These redox processes will be qualified as *temporary*, with the NO ligands acting merely as electron pumps. For example, complexation of nNO ligands on 3 to yield 1 followed by decomplexation of the nNO molecules restore the initial electronic configuration of [M]. According to the present notation, it is readily seen that such temporary redox changes leave invariant the **electronic parameter** "a" of the D_{NO}^{a+n} notation, only the structural parameter "n" is altered. It is solely during the conversion of 3 into 4 that the parameter "a" might be modified and such redox changes will be qualified as *non-temporary* .

In the actual reaction that converts the D_{NO}^{a+n} complex 1 into the $D_{NO}^{a'+n'}$ complex 2, when there is a change in the value of the electronic parameter (a different from a') a non-temporary

redox process is necessarily involved. When a' > a, the reaction is a non-temporary reduction and when a' < a, the reaction is a non-temporary oxidation. In addition, if the value of the structural parameter is also altered the reaction necessarily involves the loss (n' < n) or gain (n' > n) of NO ligands.

In the few selected examples given in Table I-3-1, (p-13), RcI-3-5 to RcI-3-9 are examples of redox inactive (a = constant) nitrosylation reactions with only **n** increasing. RcI-3-10 is an example of a non-temporary redox nitrosylation, the electronic parameter increasing from 8 in the D_{NO}^{8+0} nickelocene Cp_2Ni reactant to 9 in the mononitrosylated D_{NO}^{9+1} CpNi(NO) product. RcI-3-11 provides an example of a non-temporary dismutation reaction, part of the D_{NO}^{7+1} reactants providing the species which will get oxidized into the D_{NO}^{6+0} product, the other part providing the species which will get oxidized into the D_{NO}^{8+2} derivatives.

In the work presented in this thesis, the non-temporary redox changes affecting NO complexes will be referred frequently . To analyze these changes, the D_{NO} notation will be used.

Table I-3-1 Examples of reactions involving NO complexes in relation to the D_{NO}^{a+n} notation

Rc I-3-5 $Co(CO)_3(NO) \xrightarrow{NO} Co(NO)_3$ [4]
D_{NO}^{9+1} D_{NO}^{9+3}

Rc I-3-6 $Cr(CO)_6 \xrightarrow[h\nu]{NO} Cr(NO)_4$ [5]
D_{NO}^{6+0} D_{NO}^{6+4}

Rc I-3-7 $[CpCr(CO)_3]_2 \xrightarrow{NO} CpCr(CO)_2NO$ [6]
$[D_{NO}^{5+0}]_2$ D_{NO}^{5+1} Cp = Cyclopentadienyl

Rc I-3-8 $CpV(CO)_3CN^- \xrightarrow{NO} CpV(NO)_2CO$ [7]
D_{NO}^{4+0} D_{NO}^{4+2}

Rc I-3-9 $[W(O\text{-}tBu)_3]_2 \xrightarrow{NO, Py} W(O\text{-}tBu)_3(NO)(Py)$ [8]
$[D_{NO}^{3+0}]_2$ D_{NO}^{3+1} Py = pyridine

Rc I-3-10 $(Cp)_2Ni \xrightarrow{NO} CpNi(NO)$ [9]
D_{NO}^{8+0} D_{NO}^{9+1}
Non-Temporary Reduction

Rc I-3-11 $2Co(NCS)L_3'(NO)^+ \longrightarrow Co(NO)_2(L_2')^+ + Co(NCS)_2L_4'^+$ [10]
$2D_{NO}^{7+1}$ Dismutation Reaction D_{NO}^{8+2} D_{NO}^{6+0}

I-4 Examples of structurally characterized nitrosyl complexes with linear and bent coordination modes of the NO ligand

$Ru(NO)(diphos)_2^+$ (Fig.I-4-4) [11] and $RuH(NO)(PPh_3)_3$ (Fig.I-4-5) [12] are examples of structurally characterized complexes having a trigonal bipyramidal (TBP) geometry with a linear NO ligand. In $Ru(NO)(diphos)_2^+$, (Fig.I-4-4) NO occupies an equatorial position and the bidentate diphos ligands span equatorial and axial positions, the ν_{NO} was found at 1673 cm^{-1}.

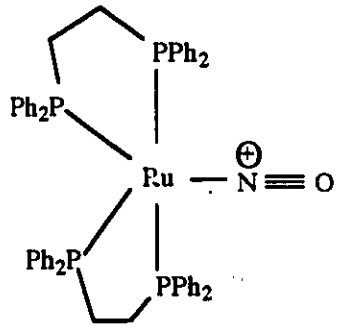

Fig.I-4-4

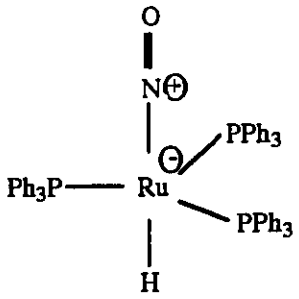

Fig.I-4-5

Figs.I-4-4 and I-4-5 Examples of structurally characterized complexes with linear NO ligands

In $RuH(NO)(PPh_3)_3$, (Fig.I-4-5), the NO ligand is found at an axial coordination site and the ν_{NO} is at1645 cm^{-1}.

The bent coordination mode of NO was first observed by

Hodgson and Ibers [13] in $IrCl(CO)(NO)L_2^+$ (L = PPh_3; ν_{NO} = 1620 cm^{-1} see Fig.I-4-6) .

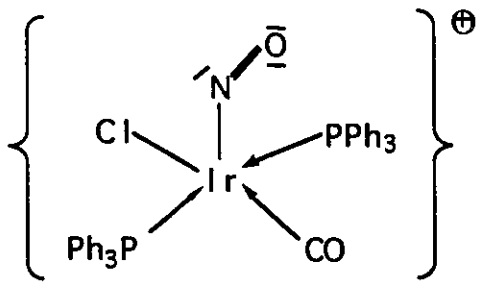

Fig.I-4-6 Example of a structurally characterized complex with a bent NO

An example of a linear to bent conversion of a NO ligand was provided by the reaction of $Co(NO)(diars)_2^{2+}$ (diars = o-phenylenebis(dimethylarsine)) with a two-electron donor ligand X^- [14]. The $Co(NO)(diars)_2^{2+}$ possesses a trigonal bipyramidal geometry with a linearly coordinated NO in an equatorial position (ν_{NO} = 1852 cm^{-1}, Fig.I-4-7, p-16). In the presence of coordinating ion (X^- = Cl^-, Br^-, NCS^-), $Co(NO)(diars)_2^{2+}$ is converted to a six coordinate derivative containing a bent nitrosyl $Co(NO)(diars)_2X^+$ in an axial position (ν_{NO} = 1587 cm^{-1}) (Fig. I-4-8, p-16).

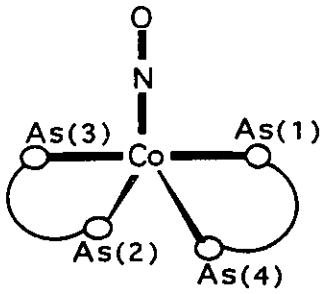

Fig.I-4-7 Representation of $Co(NO)(diars)_2^{2+}$ with a linear NO

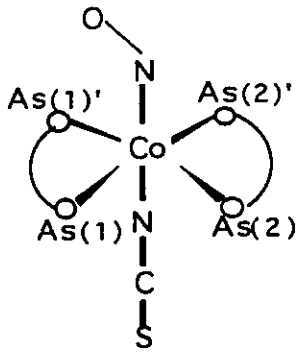

Fig.I-4-8 Representation of $Co(NO)(diars)_2(NCS)^+$ with a bent NO

In terms of the old "NO^+/NO^-" formalism, in this reaction, the cobalt center suffers a 2e- oxidation and the NO ligand a 2e- reduction (from formally NO^+ to formally NO^-). In terms of the D_{NO} notation, these redox changes are of the temporary type and the cobalt reactant and products are both D_{NO}^{7+1} complexes.

I-5 Chemical Reactivity

The reactions of metal nitrosyl complexes are classified into two main groups: (a) reactions which involve modification of the set of atoms bonded to the nitrosylic N atom. This is the case for O-transfer rections which involve a NO ligand, (b) reactions in which the set of atoms bonded to N are not modified from the reactants to the products.

(a) O-transfer reactions involving a NO ligand

(i) Several $M(NO)_2(PPh_3)_2^x$ (M = Rh, Ir; x = 0, +1) derivatives show catalytic activity in the environmentally important degradation reactions of NO-CO mixtures into less noxious atmospheric pollutants (Rc I-5-12 as an example).

$$2NO + CO \rightarrow N_2O + CO_2 \qquad \text{(Rc.I-5-12)}$$

Johnson and coworkers [15,16] have reported that $M(NO)_2(PPh_3)_2^+$ (M = Rh, Ir) catalyzes the reaction.

$$M(NO)_2(PPh_3)_2^+ + 4CO \rightarrow M(CO)_3(PPh_3)_2^+ + N_2O + CO_2 \qquad \text{(RcI-5-13)}$$

$+2NO, -3CO$

(ii) The μ-Cl bridged dimers $[M(NO)_2Cl]_2$ (M = Co, Rh) react with PPh_3 to yield the phosphine oxide and either N_2 (M = Co) or N_2O (M = Rh) [17, 18] as shown below.

$$[Co(NO)_2X]_2 + 6PPh_3 \rightarrow Co(NO)(PPh_3)_3 + CoX_2(OPPh_3)_2 + OPPh_3 + 3/2N_2 \qquad \text{(Rc I-5-14)}$$

$$[Rh(NO)_2Cl]_2 + 6PPh_3 \rightarrow Rh(NO)(PPh_3)_3 + Rh(NO)Cl_2(PPh_3)_2 + OPPh_3 + N_2O \qquad \text{(Rc I-5-15)}$$

(iii) Oxidation of a NO ligand into a NO_2 ligand can be achieved by

molecular oxygen. The NO_2 ligand can subsequently transfer an O-atom onto a suitable oxygen acceptor. For example, the cobaltnitrosyl complex Co(NO)(Saloph) (Saloph = N,N'-bis (salicylidene)-o-phenylenediamine) reacts with molecular oxygen in the presence of pyridine to give the complex Co(Saloph)Py(NO_2), which further catalyzes the oxidation of PPh_3 to $OPPh_3$ by molecular oxygen (Rcl-5-16) [19].

$$Co(NO)(Saloph) + Py + 1/2\ O_2 \rightarrow Co(Saloph)Py(NO_2)$$

$$Co(Saloph)Py(NO_2) + PPh_3 \rightarrow Co(saloph).NO(Py) + OPPh_3 \quad \text{(Rcl-5-16)}$$

In acetonitrile, the dicationic rhodium nitrosyl complexes $(bpy)(CH_3CN)_3Rh(NO)^{2+}.2PF_6^-$ and $(CH_3CN)_4Rh(NO)^{2+}.2BF_4^-$ are similarly oxidized by molecular oxygen to their corresponding nitro complexes $(bpy)(CH_3CN)_2RhNO_2^{2+}.2PF_6^-$ and $(CH_3CN)_4RhNO_2^{2+}.2BF_4^-$. In addition, $(bpy)(CH_3CN)_2RhNO_2^{2+}.2PF_6^-$ oxidizes ethylene or terminal olefins to acetaldehyde or alkanones in the presence of $(PhCN)_2PdCl_2$ (involvement of Pd(II)(Olefin) complexes). In addition, $(CH_3CN)_4RhNO_2^{2+}.2BF_4^-$, catalyzes the transfer of an oxygen atom from the nitro ligand to a coordinated olefin in the presence of nitromethane. As a result, formation of acetaldehyde from ethylene, and 2-alkanones from terminal olefins, takes place [20].

(b) Reaction in which the set of atoms bonded to N is not modified from reactants to products.

(i) Polymerization

A number of reactions have been found in which transition metal nitrosyls are used as catalyst precursors for the polymerization of olefins. For example, the cationic complexes $Fe(NO)_2(L_n)^+Y^-$, where L = acetonitrile, acrylonitrile and Y = PF_6^-, BF_4^-, ClO_4^-, BPh_4^-, $Co(NO)_2L_2^+Y^-$, where L = tertiary phosphine and Y = BF_4^-, BPh_4^-, ClO_4^-, are catalyst precursors for the polymerization of acrylonitrile and of styrene, and for the dimerization of butadiene, isoprene and norbornadiene [21,22].

The rhodiumnitrosyl complex $[Rh(NO)(CH_3CN)_4](BF_4)_2$ is also known to catalyze the oligomerization of branched alkenes and polymerization of 1,3-butadiene to *trans*-1,4-polybutadiene [23].

(ii) Isomerization

Hydrides of ruthenium and osmium of the type $RuH(NO)L_3$ (L = PPh_3, $PPrPh_2$) and $OsH(NO)(PPh_3)_3$,isomerize 1-hexene to internal olefins [24]. $Rh(NO)(PPh_3)_3$ in the presence of traces of air, in CH_2Cl_2 isomerize 1-hexene into internal isomers [25]. $Ir(NO)(PPh_3)_3$ catalyzes the isomerization of 1-hexene to cis- and trans-2-hexenes in benzene at 85°C [26].

(iii) Olefin Metathesis

The metathesis of acyclic and cyclic olefins has been studied extensively [27,28]. With transition metal nitrosyls, the major homogeneous catalyst system for the metathesis of olefins are prepared from either molybdenum or tungsten nitrosyl complexes and alkyl aluminium as cocatalyst. For example, $Mo(NO)_2(PPh_3)_2Cl_2$ and $(CH_3)_3Al_2Cl_2$ result in the formation of 2-pentene to 2-butene and 3-hexene [29].

(iv) Hydrogenation

The rhodium(-1)nitrosyls, $Rh(NO)L_3$, (L = PPh_3, P-(p-tolyl)$_3$, $P(p\text{-}FC_6H_4)_3$, $PMePh_2$ and $AsPh_3$) have been used as catalysts in the homogeneous hydrogenation of terminal and cyclic olefins and alkynes [30,26]. Also, $Ir(NO)(PPh_3)_3$ catalyzes the hydrogenation of heptene, styrene derivatives and 1-hexene [31] . A series of nitrosyl complexes of the type $RuH(NO)L_3$ (L = PPh_3, PPr^iPh_2 or $P(C_6H_{11}Ph_2)$, $P(MePh_2)_3$) have been prepared by Osborn and coworkers [24]. These complexes were found to catalyze the hydrogenation of styrene, propionaldehyde, and crotonaldehyde.

(v) Fe-mediated alkylation reactions

Roustan and coworkers [32] have found that $Na^+Fe(CO)_3(NO)^-$ and $Fe(CO)_2(NO)_2$ are active catalysts for the alkylation of allylic acetate and allylic carbonates.

PART II

NO-TRANSFER REACTIONS IN IRONNITROSYL CHEMISTRY

II-1 Synthesis and thermal lability of a ironnitrosylhydride - NO transfer reaction

In a preliminary study of the catalytic activity of $FeH(NO)(CO)(PPh_3)_2$ in the presence of syngas, it was found that the predominant reaction was the thermolysis of the hydride into a mixture of catalytically inactive $Fe(CO)_x(NO)_2(PPh_3)_y$ (x + y = 2, x = 1, 0) and $Fe(CO)_u(PPh_3)_v$ (u + v = 5, u = 4, 3) decomposition products. This observation provided the incentive to search for other ironnitrosyl hydrides which might display a different reactivity under thermolytic conditions. In place of PPh_3 as a supporting ligand, 1,1'-bis(diphenylphosphino)ferrocene (dppf) containing an iron center was used. Ligand 1,1'-bis(diphenylphosphino)ferrocene (dppf) might participate in a one electron oxidation reaction (as ferrocene itself), a possibility not available with PPh_3, or for that matter with any other classical mono or bidentate phosphines.

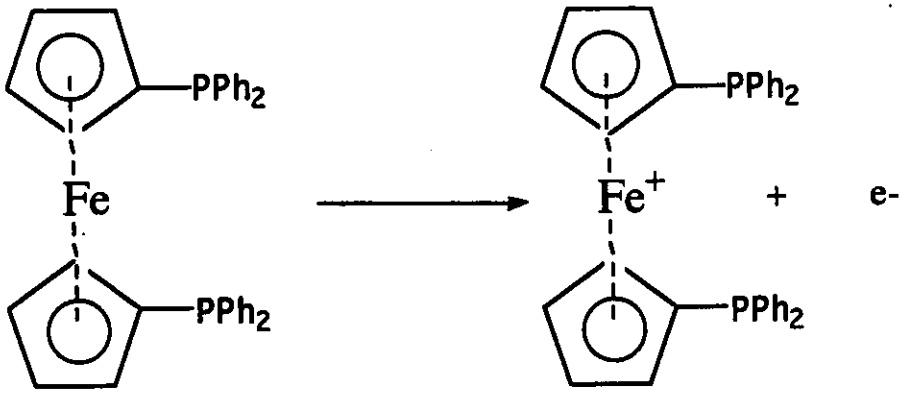

Scheme II-1-1 Representation of one electron oxidation reaction of (dppf)

The first attempt to synthesize the desired FeH(NO)(CO)(dppf) complex, containing the 1,1'-bis(diphenylphosphino)ferrocene (dppf) ligand was to use the same method which was successful in preparing $FeH(CO)(NO)(PPh_3)_2$ 2 as shown in scheme II-1-2 [1].

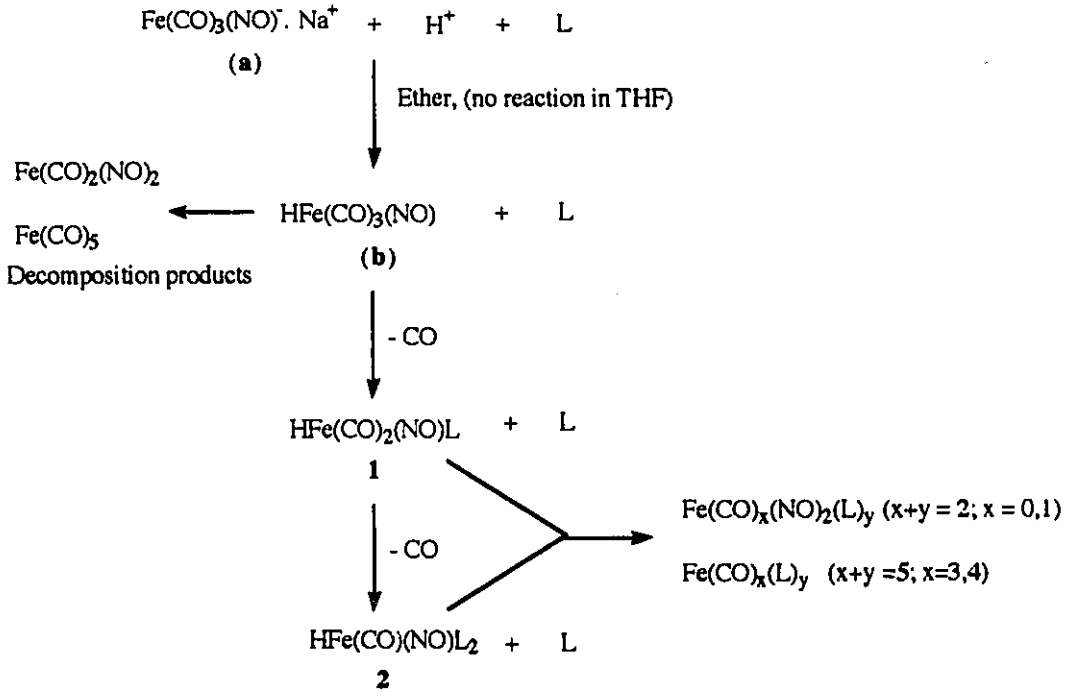

When L = PPh_3 , Ether soluble $Fe(CO)_3(NO)^-Na^+.CH_3OH$ used

When L = dppf , Sparingly Ether soluble $Fe(CO)_3(NO)^-.Na^+$(1,4-dioxane used)

Scheme II-1-2 Synthesis and decomposition pathways of ironnitrosylhydrides

When only one equivalent of PPh_3 was used in the presence of the ether soluble $Fe(CO)_3(NO)^-Na^+.CH_3OH$ complex **(a)**, the mono substituted hydride $HFe(CO)_2(NO)(PPh_3)$ **1** was generated in situ (Scheme II-1-2, p-23). The hydride $HFe(CO)(NO)(PPh_3)_2$ **2** was obtained from the protonation of $Fe(CO)_3(NO)^-Na^+.CH_3OH$ **(a)** in the presence of an excess of triphenylphosphine. Alternatively, when the anion was protonated in the absence of triphenylphosphine only a mixture of $Fe(CO)_2(NO)_2$ and $Fe(CO)_5$ was obtained. This was taken as good evidence for the transient formation of $HFe(CO)_3(NO)$ **(b)**, which rapidly decomposed. (Reported to decompose in the pure state at -45°C, sometimes explosively).

The above reaction was unsuccessful when the protonation of $Fe(CO)_3(NO)^-Na^+.CH_3OH$ was carried out in the presence of an equimolar amount of 1,1'-bis(diphenylphosphino)ferrocene. Only a mixture of $Fe(CO)_5$ and $Fe(CO)_2(NO)_2$ was obtained as confirmed by IR studies. It was postulated that dppf ligand being sparingly soluble in ether, there was not enough ligand present in the solution to allow for a CO to phosphine substitution reaction to compete efficiently with the decomposition of $HFe(CO)_3(NO)$.

Two modifications of this reaction procedure could be considered. First a change of solvent could enhance the solubilization of phosphine. THF proved to be a suitable solvent for this purpose. However, protonation of $Fe(CO)_3(NO)^-Na^+$ **(a)** did

not occur under these conditions. Alternatively, with ether as the solvent, a sparingly soluble form of $Fe(CO)_3(NO)^-Na^+$ could be used in order to maintain the concentration of the $Fe(CO)_3(NO)^-$ anion in solution at a level comparable to that of the 1,1'-bis(diphenylphosphino)ferrocene ligand. The use of $Fe(CO)_3(NO)^-Na^+$-1,4-dioxane proved to be adequate for this purpose.

The desired hydride FeH(CO)(NO)(dppf) **(28)** was obtained following the protonation of a suspension of $Fe(CO)_3(NO)^-Na^+$. 1,4-dioxane and the 1,1'-bis(diphenylphosphino)ferrocene ligand in ether, yielded hydride FeH(NO)(CO)(dppf) **(28)** as an orange powder. However, attempts to obtain single crystals suitable for an X-ray study were unsuccessful.

Compound **(28)** was characterized by its spectral properties and elemental analysis. The presence of one CO and NO ligand per iron was shown in the IR spectra (Nujol or CH_2Cl_2), by the presence of two strong absorption bands centered at 1920 cm^{-1} (ν_{CO}) and at 1700 cm^{-1} (ν_{NO}). (For comparison, $FeH(CO)(NO)(PPh_3)_2$ **2** had ν_{CO} at 1915 cm^{-1} and ν_{NO} at 1690 cm^{-1} [2]). In FeH(CO)(NO)(dppf) **(28)**, the presence of a ν_{NO} band at 1700 cm^{-1} is strongly suggestive of a linearly coordinated NO, as found in the structurally characterized bis-PPh_3 analogue $FeH(CO)(NO)(PPh_3)_2$ [1].

The presence of a hydride ligand was demonstrated by ^1H

and ^{31}P NMR. The ^{1}H NMR ($CDCl_3$, TMS) displayed a 1:2:1 binomial triplet at δ = -4.00 ppm (J = 30 Hz). On the other hand, the undecoupled ^{31}P NMR ($CDCl_3$, 85% H_3PO_4) displayed a doublet at δ = 58.2 ppm (J = 30 Hz), it collapsed to a singlet upon ^{1}H decoupling. These results establish the presence of one hydride ligand coupled with two magnetically equivalent P atoms.

The remaining of the ^{1}H NMR spectrum consisted of:

-Several lines between δ = 7.00-8.00 ppm assigned to the 20 aromatic protons of the phenyl groups.

- Three pseudo singlets at δ = 3.37 ppm (2H), δ = 3.92 ppm(2H) and δ = 4.13 ppm(4H). (The number of protons relative to the hydrido proton are indicated in brackets following each indicated chemical shift). They are assigned to the protons of the cyclopentadienyl ring.

The same resonance pattern was observed in the ^{1}H NMR spectrum of the structurally characterized $Re(dppf)(CO)_3Cl$ complex A [3]. In this compound, the Cp-protons appeared as three pseudosinglets at δ = 4.33 ppm (4H), 4.37 ppm (2H) and 4.39 ppm (2H). A perspective view of this molecule is presented in Fig. II-1-1 (p-29). The labeling letter assigned to each hydrogen (omitted in the figure for clarity) is the same as that of the carbon atom to which it is bound.

The pairs of protons [H(A), H(A')], [H(B), H(B')], [H(C), H(C')] and [H(D), H(D')] are now considered. Each proton of a pair is at a

position close to that of the image of the other proton of the same pair through a mirror plane perpendicular to the equatorial plane P(1)P(2)C(1)C(2) and bissecting the P(1)ReP(2) angle. Consequently, the two protons of each pair are expected to be magnetically equivalent. However, magnetic inequivalence between a proton of any pair and a proton of another pair is also expected. For example, H(A) and H(A') protons are located on the same side of the equatorial plane as the Cl(1) atom whereas, H(B) and H(B') protons together with the C(3)O(3) ligand are located on the other side of the plane. The magnitude of the magnetic inequivalence arising from the rhenium atom and from the other atoms directly bound to it cannot be anticipated, nevertheless, one can expect that it would be less pronounced for [H(C), H(C')] relative to [H(D), H(D')] than for [H(A), H(A')] relative to [H(B), H(B')] which are closer to the Re center. The ^{1}H NMR of complex $Re(dppf)(CO)_3Cl$ can, therefore, be easily interpreted by assigning the singlet at 4.33 ppm integrating as four protons to the pairs [H(C), H(C')] and [H(D), H(D')] and each one of the other two singlets pairs at δ 4.37 and 4.93 ppm, integrating for (two protons each), to each one of the remaing pairs [H(A), H(A')] and [H(B), H(B')].

Following a similar line of reasoning , one then concludes that the ^{1}H NMR of ironnitrosylhydride FeH(NO)(CO)(dppf) **(28)**, is supportive of a square pyramidal coordination around iron with H

in the apical position with NO ligand trans to one phosphorus (P2) atom and CO ligand in trans to the other phosphorus atom (P1). This arrangement would imply two magnetically inequivalent phosphorus. However, the decoupled ^{31}P NMR indicates two equivalent phosphorus as singlet at δ = 58.2 ppm; suggesting the two ligands (NO and CO) are exchangeable at NMR time scale. Fig.II-1-2 (p-30).

The other possible structure could be a trigonal bipyramid with H atom either in the equatorial or axial position. The structure with H in the equatorial position is unlikely because the two P atoms would become magnetically inequivalent and would give rise to two different J_{P-H} coupling constants. However, with H in the axial position in trans to CO or NO ligands would be another possible trigonal bipyramidal arrangement. If it is so, ^{1}H and ^{31}P NMR data would comply the above chemical shifts as observed in square pyramidal structure.

(Note : The number in brackets such as FeH(NO)(CO)(dppf) (28) corresponds to the numbers of complexes in the experimental section hence forth).

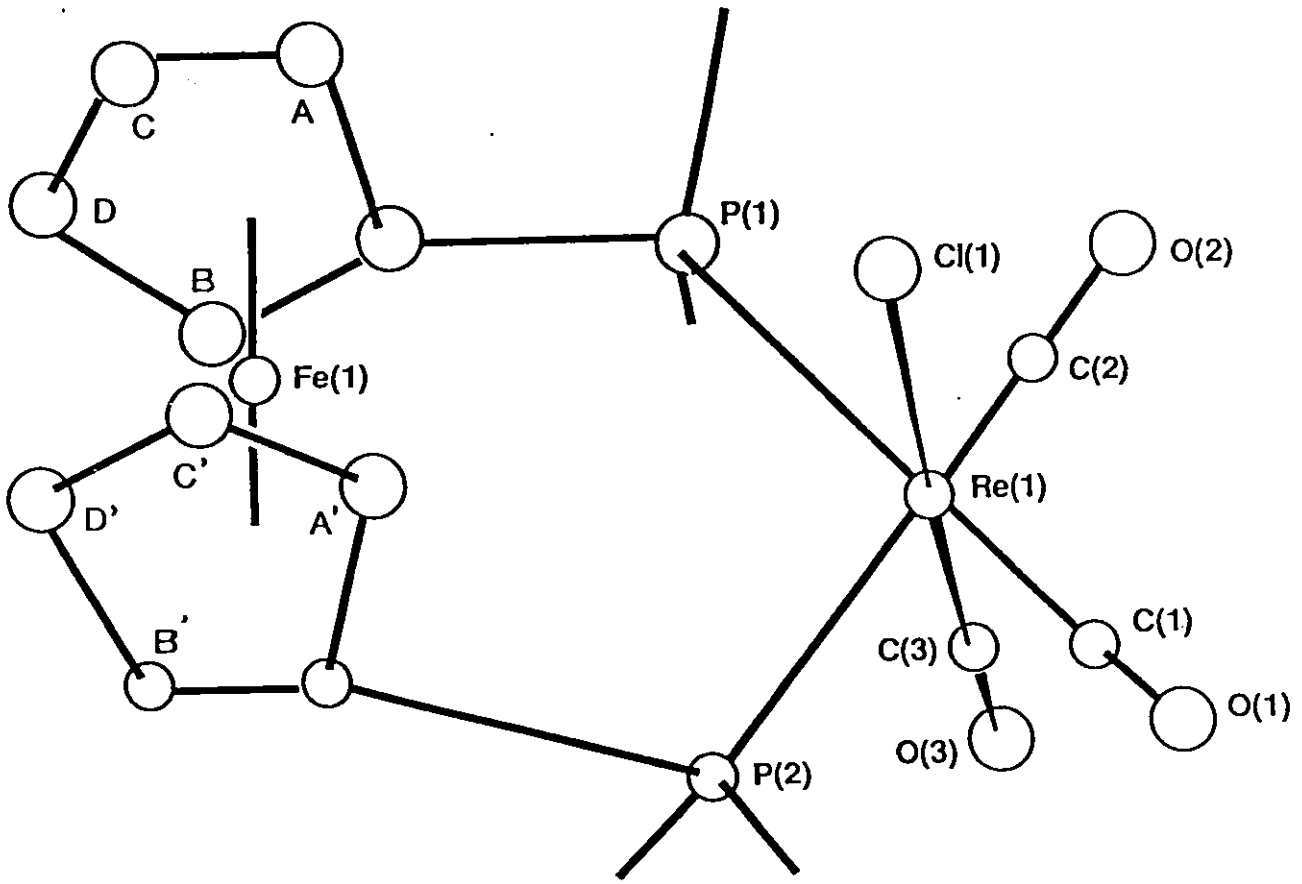

Fig. II-1-1 A perspective view of the structurally characterized

$Re(dppf)(CO)_3Cl$ - **A**

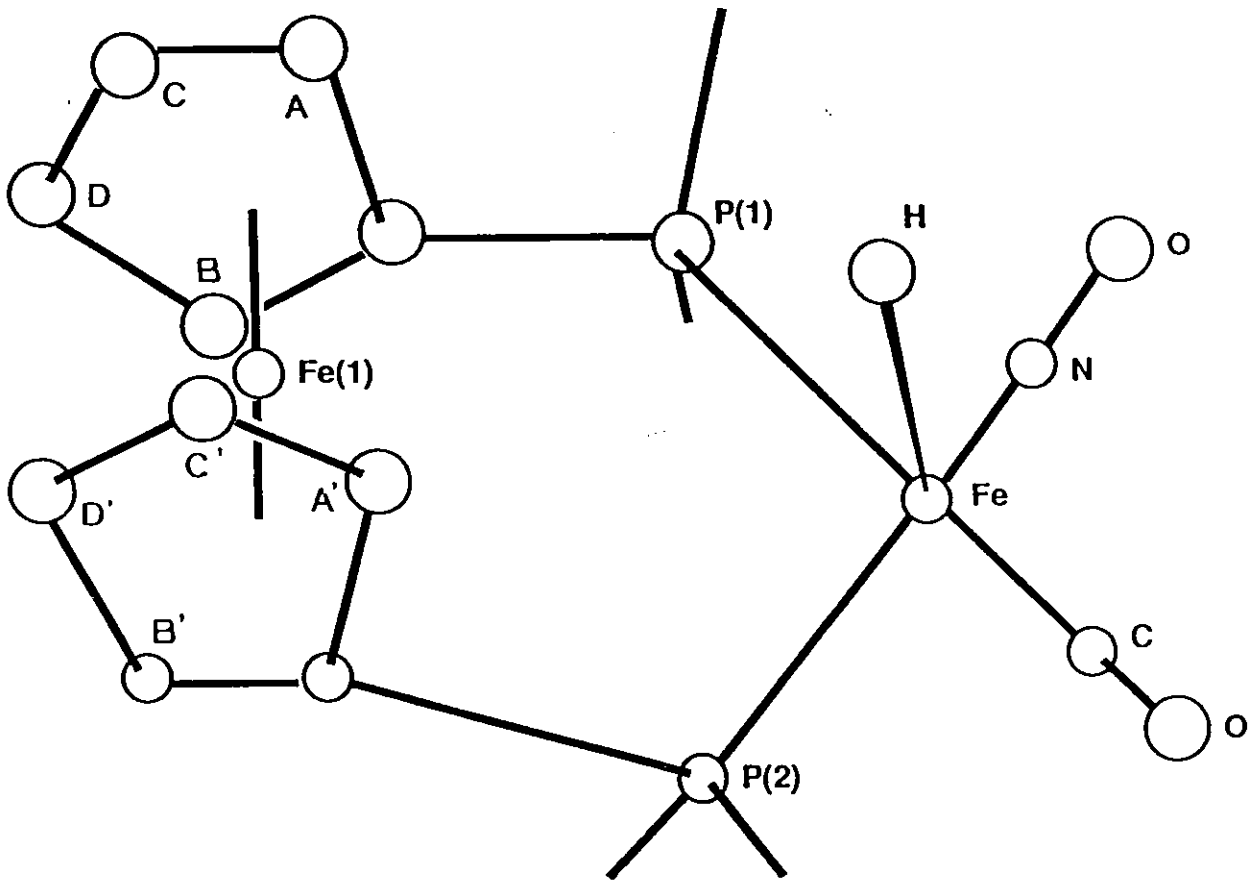

Fig. II-1-2 A representation of the assigned coordination polyhedra in Fe(dppf)(NO)(CO)H **(28)**

One probable cause of failure to obtain single crystal of FeH(NO)(CO)(dppf) **(28)** is its thermal unstability. In solution (CH_2Cl_2, C_6H_6, CS_2) at 20°C, it slowly decomposes with time, as observed by the progressive decrease in the intensity of its NO and CO bands concomittant with the development of several other bands in the 2200-1650 cm^{-1} region. The hydride FeH(NO)(CO)(dppf) **(28)** is also unstable in the solid state when kept at this temperature.

A comparison of the IR spectra of the decomposed solutions of $HFe(NO)(CO)_2(PPh_3)$ **1** and of $HFe(NO)(CO)(PPh_3)_2$ **2** (scheme II-1-2, p-23) with those obtained starting with FeH(NO)(CO)(dppf) **(28)** showed that the latter displayed the characteristic absorption bands of a mixture of degradation products of types $Fe(CO)_x(L)_y$ (x + y = 5; x = 3, 4) and $Fe(NO)_2(CO)_x(L)_y$ (x + y = 2; x = 0, 1). (Scheme II-1-2; p-23, L = PPh_3 starting with $HFe(NO)(CO)(PPh_3)_2$ **2**, L = P donor site of the dppf ligand starting with **(28)**). Consequently, FeH(NO)(CO)(dppf), like $FeH(CO)_x(NO)(PPh_3)_y$ (x + y = 3; x = 2,1) decomposes by routes involving the relocation of NO ligands. Such reactions are also occuring following the protonation of $Fe(CO)_3NO^-Na^+$ in ether in the absence of phosphine but in that case a mixture of $Fe(CO)_2(NO)_2$ and $Fe(CO)_5$ is obtained [2].

II-2 $Fe(CO)_2(NO)_2$ as a NO ligand donor

The observation that dinitrosyl derivatives are invariably formed in the decomposition of the known mononitrosyliron hydrides, suggested that, provided low activation energy pathways are available, a "$Fe(NO)_2$" functional group might be significantly more thermodynamically stable than a "Fe(NO)" group. For that reason, monometallic "$Fe(NO)_2$" complexes were used as building blocks in the synthesis of polymetallics, which might subsequently serve as precursors of hydrides. It was anticipated that the "$Fe(NO)_2$" unit will retain its integrity throughout. The first reaction attempted sufficed to show that this was not the case.

In $Fe(CO)_2(NO)_2$, the CO ligands are easily substituted by two electron ligands such as phosphines. (e.g. $Fe(CO)_2(NO)_2 + PPh_3 \rightarrow Fe(CO)(NO)_2(PPh_3) + CO$). It was expected that using a metalate M^- as the two electron ligand, would provide an entry to anionic bimetallics and subsequently to metallic hydrides.

$$M^- + Fe(CO)_2(NO)_2 \xrightarrow{-CO} [M\text{-}Fe(CO)(NO)_2]^- \xrightarrow{H^+} MFe(H)(CO)(NO)_2 \qquad \text{(Rc II-2-1)}$$

It was found that $Fe(CO)_4^{2-}$ reacts rapidly with $Fe(NO)_2(CO)_2$ in THF, but the reaction proceeds all the way to the formation of $Fe(CO)_3(NO)^-$ (Rc II-2-2).

$$Fe(CO)_4^{2-} + Fe(CO)_2(NO)_2 \xrightarrow[-78°C \text{ to } 20°C]{THF} 2Fe(CO)_3(NO)^-$$

(Rc II-2-2)

The reactions were conducted by adding a solution of $Fe(CO)_2(NO)_2$ dropwise, in THF to an equimolar suspension of $Fe(CO)_4^{2-}\cdot 2Na^+.1.5$(1,4-dioxane) in the same solvent, which resulted in air sensitive microcrystals of $Fe(CO)_3(NO)^-\cdot Na^+$ 1,4-dioxane **(23)**. The IR spectrum in THF displays (tight ion pairs) νCO bands at 1990, 1890 cm^{-1}; νNO at 1615 cm^{-1} and (loose ion pairs) νCO bands at 1995, 1905 cm^{-1}; νNO at 1585 cm^{-1}, which are comparable to that of the ether soluble $Fe(CO)_3(NO)^-Na^+$ [a] prepared from $Fe(CO)_5$ and $NaNO_2$ in methanol [4] which retains CH_3OH in the solid state.

Discussion

The results reported in this part of the thesis bring into light the facile occurence of NO ligand relocation reactions in the chemistry of mixed carbonyl-nitrosyl iron complexes, with the possibility of having a dinitrosyl "$Fe(NO)_2$" complex as either a reactant or a product. These NO ligand relocation reactions will be analyzed in terms of the D_{NO} notation which provides a convenient method of classification. A possible reaction mechanism will be proposed for the reactions just described.

II-3 (i) Symbolic representation of a NO-ligand transfer

In scheme II-3-3, reaction R is taken as a representative example of a NO ligand transfer reaction. The complex [M](NO) is the **NO-donor** which is converted to a complex denoted [M]* . The complex [M'] is the **NO-acceptor** which yields a complex denoted [M']*(NO).

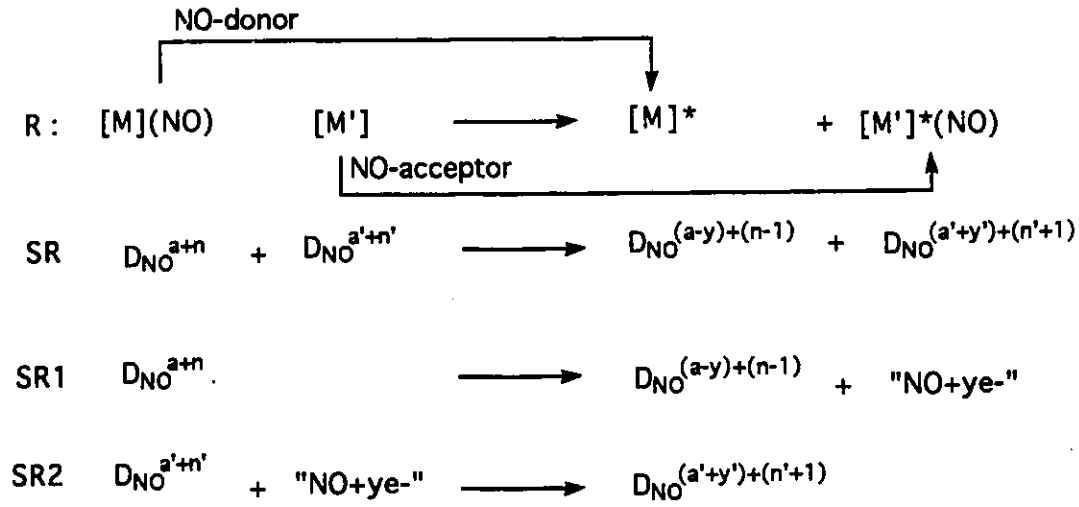

Scheme II-3-3 Symbolic representation of a NO-ligand transfers in terms of D_{NO}^{a+n} notation

The symbolic reaction SR identifies the D_{NO} type of the metallic reactants and products directly involved in the transfer considered. It shows that the D_{NO}^{a+n} [M](NO) complex (NO-donor) suffers the net loss of a "NO+ye$^-$" unit ($y > 0, < 0, = 0$) to yield

the $D_{NO}^{(a-y)+(n-1)}$ [M*] product, as indicated by a decrease in the structural and electronic parameters of 1 and y units, respectively. The unit "NO+ye-" is gained by the $D_{NO}^{a'+n'}$, [M'] complex (NO-acceptor), which yields the $D_{NO}^{(a'+y')+(n'+1)}$ [M*](NO) product. The net chemical change can be easily formalized by writing SR as the sum of equations SR1 and SR2, as shown in scheme II-3-3 (p-34).

The three simplest types of NO-ligand transfer concievable are obtained for y = -1, +1 or 0. This leads to the following classification

"NO+"- transfer (y = -1): "NO-1e-" = "NO+" - Reactions of this type can be readily identified by observing that the electronic parameter of the NO donor *increases* by one unit, as shown by equation Rc II-3-3 of Table II-3-1 (p-36).

"NO-"- transfer (y = +1): "NO+1e-" = "NO-" - Reactions of this type can be easily recognized by observing a *decrease* in the electronic parameter by one unit, as shown in Rc II-3-4 and in Rc II-3-5 of Table II-3-1 (p-36).

"NO"- transfer (y = 0): "NO +0e-" = "NO" - In this type of reactions, there is *no change* in the electronic parameter as seen in equation Rc II-3-6 of Table II-3-1 (p-36).

Table II-3-1 Types of NO-ligand transfer Reactions

y = -1, "NO^+"transfer

Rc II-3-3 $Hg[Fe(CO)_3(NO)]_2 \longrightarrow HgFe(CO)_4 + Fe(CO)_2(NO)_2$ [5]

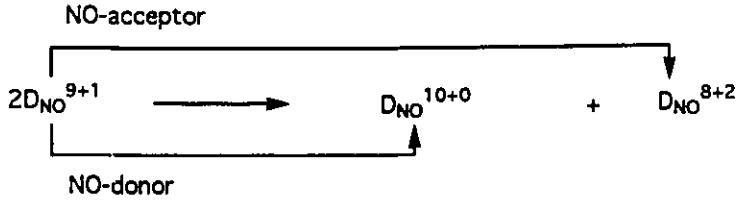

y = +1, "NO^-"transfer

Rc II-3-4 $Co(DMG)_2(NO) + Co(NO)(L)_2Cl_2 \longrightarrow Co(DMG)_2Cl + Co(NO)_2(L)Cl$ [6]

$Co(NO)_2(L)_2^+$

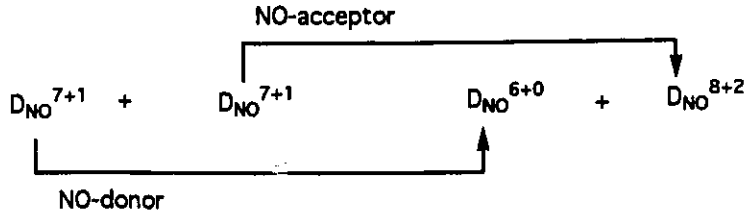

DMG = Dimethyl glyoxime L = PPh_3

Rc II-3-5 $2Fe(CO)(NO)(L)_2^+ \longrightarrow Fe(NO)_2(L)_2 + Fe^{2+} + 2CO + 2L$ [7]

$2D_{NO}^{7+1}$ D_{NO}^{8+2} D_{NO}^{6+0}

[8]

y = 0, "NO"transfer On an alumina surface

Co_s = superficial cobalt

Rc II-3-6 $O{=}Co_s(NO) + O{=}Co_s(NO) \longrightarrow O{=}Co_s + O{=}Co_s(NO)_2$

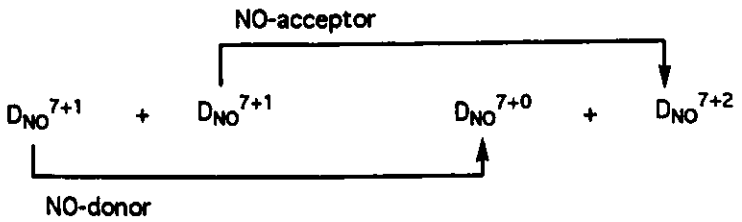

II-3 (ii) Application to the Fe/CO/NO complexes studied in this chapter

The formation of $Fe(CO)_3(NO)^-$ from $Fe(CO)_4^{2-}$ and $Fe(CO)_2(NO)_2$ is a simple "NO^+-transfer. The associated D_{NO} equation $D_{NO}^{8+2} + D_{NO}^{10+0} \rightarrow 2D_{NO}^{9+1}$ is nothing other than the reverse of the equivalent equation associated with Rc II-3-3 in Table II-3-1 (P-36). A possible associative mechanism is presented below.

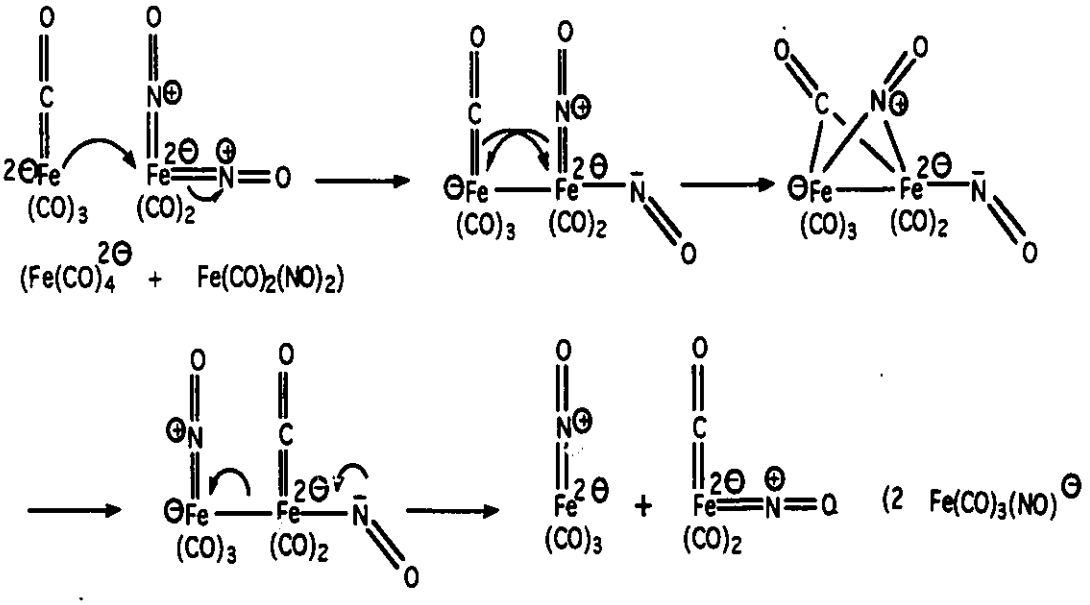

Scheme II-3-4 Proposed associative mechanism for the formation of the monometallic $Fe(CO)_3(NO)^-$ complex

The analysis of the thermolysis of the D_{NO}^{7+1} Fe/CO/NO hydrides considered in Rc II-3-7 to Rc II-3-10 (Scheme II-3-5) is necessarily more involved. In every case, a relocation reaction of the NO ligand takes place but it is not of the simple NO-ligand transfer type. This is shown by an increase in the electronic parameters (7→8) from all of the Fe-reactants to all of the Fe-products.

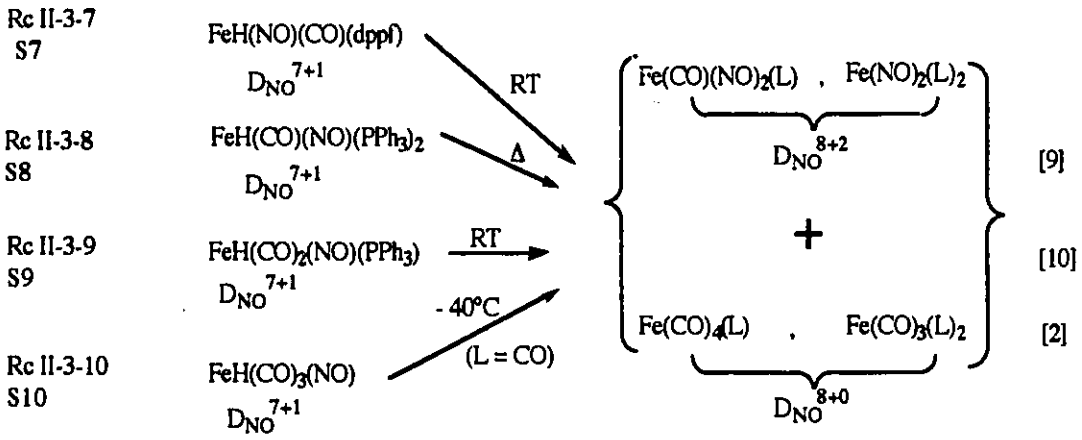

Scheme II-3-5 (Unbalanced equations identifying solely the D_{NO} types of the iron reactants and the observed products)

In all of these reactions, if only a NO-ligand transfer reaction had taken place, the electronic parameter of one part of the reactants would have increased and that of the other part would have decreased ("NO^+", "NO^-" -transfers) or there would have been no change at all in the electronic parameters ("NO"-transfer).

The simplest pathways which can be considered to account for the observed changes in the D_{NO} types from reactants (D_{NO}^{7+1})to products (D_{NO}^{8+2} and D_{NO}^{8+0}) are shown in scheme II-3-6 below.

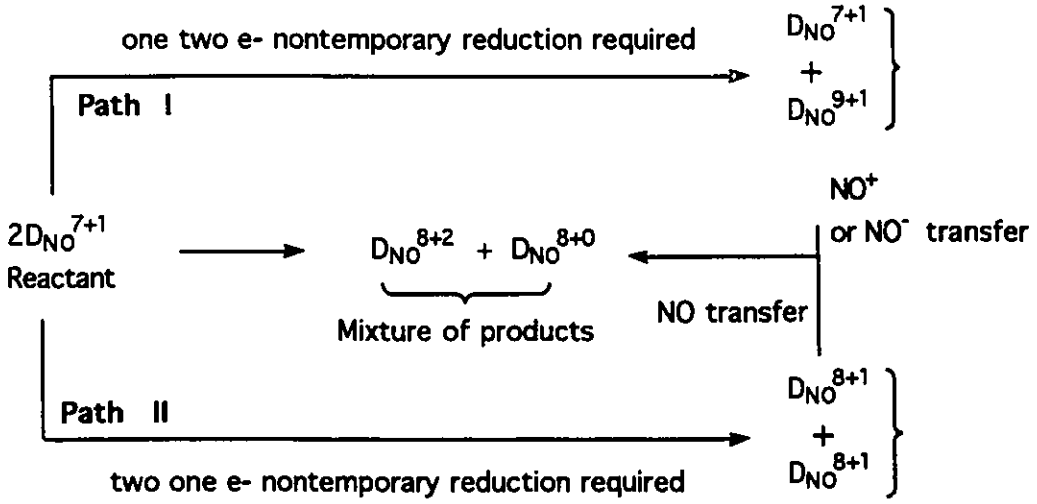

Scheme II-3-6 Thermolysis of the D_{NO}^{7+1} ironnitrosyl hydride : Changes involved in the D_{NO} types from reactants to products

Path I : The mixture of D_{NO}^{8+2} and D_{NO}^{8+0} products might result from a "NO^+" or "NO^-" transfer involving one D_{NO}^{9+1} and one D_{NO}^{7+1} species. This would require a two-electron -non-temporary reduction of part of the initial D_{NO}^{7+1} molecules of the Fe/CO/NO hydrides to yield D_{NO}^{9+1} anionic species. This appears unlikely under the reaction conditions.

Path II : The mixture of the D_{NO}^{8+2} and D_{NO}^{8+0} products are considered to result from a "NO"-transfer, involving two D_{NO}^{8+1}

precursors. The latter have to be generated in situ by two one-electron-non-temporary reductions of two molecules of the initial monometallic D_{NO}^{7+1} hydrides.

The homolysis of a M-H bond, (most likely upon a reaction with a radical initiator such as traces of O_2 or any other suitable organic or metallic impurity), being a well documented process [11], path II is favored. The homolysis of the Fe-H bond of a D_{NO}^{7+1} hydride necessarily generates a D_{NO}^{8+1} radical. (scheme II-3-7(p-41). Once formed, such a radical is expected to dimerize into a dimer of type (D). An alternate route to the same dimer might be provided by the oxidative addition of the Fe-H bond of one molecule of hydride onto the Fe center of another followed by elimination of H_2. A fast NO/CO ligand exchange ((D) → (E) → (F)) (scheme II-3-7(p-41), followed by the rupture of the Fe-Fe bond provides all that is needed to account for the formation of the observed mixture of the D_{NO}^{8+2} and D_{NO}^{8+0} degradation products.

In preparing the hydride **(28)**, it was anticipated that the dppf ligand might prevent the dimerization of a D_{NO}^{8+1} radical by allowing the formation of a zwitterionic derivative (as shown in scheme II-3-8 (p-42), however this did not happen.

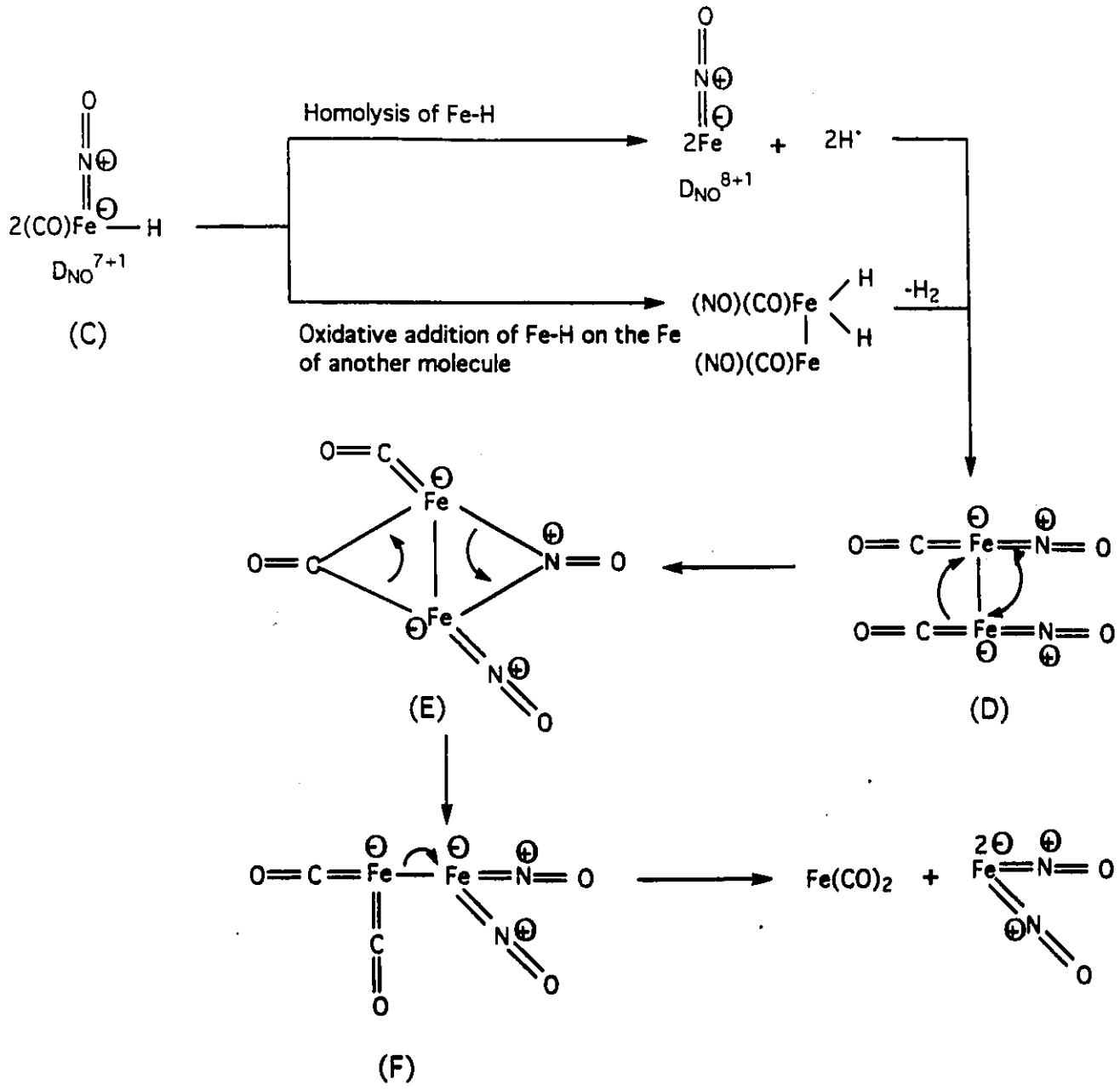

Scheme II-3-7 Suggested decomposition pathway for iron introsyl hydride

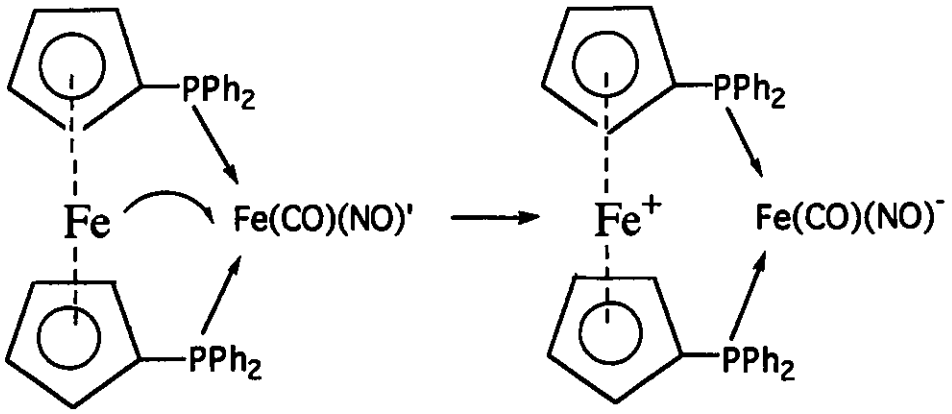

Scheme II-3-8 Suggested pathway for the formation of zwitterion derivative

According to scheme II-3-7 (p-41), it can be predicted that a decrease in the steric protection around the H ligand of the starting hydride would ease the access to the Fe-H bond and would therefore enhance the rate of formation of a dimer of type (D). The X-ray structure of $FeH(CO)(NO)(PPh_3)_2$ has shown [1] that each PPh_3 bends towards the coordination site of the H ligand, the latter being shielded from the outside by the manner the phenyl subsituents are disposed. This shielding is expected to increase with the number of PPh_3 ligands. The decrease in the thermal stability along the sequence $FeH(CO)(NO)(PPh_3)_2$ > $FeH(CO)_2(NO)(PPh_3)$ > $FeH(CO)_3(NO)$ becomes readily rationalized on this basis. In FeH(CO)(NO)(dppf) **(28)**, assuming the coordination polyhedron shown in Fig. II-1-2 (p-29) and supported by the NMR data, the steric protection of the H ligand should be less than in $FeH(CO)(NO)(PPh_3)_2$ and the thermal instability

should be more pronounced, as observed.

Conclusion

In catalytic systems involving a metallic hydride M-H as the active catalyst, formation of a metallic dimer M-M frequently occurs according to the following reactions [12].

$$2M{-}H \rightleftharpoons M{-}M + H_2 \quad (\text{e.g. } 2HCo(CO)_4 \rightleftharpoons Co_2(CO)_8 + H_2)$$

(Rc II-3-11)

However, these reactions are *reversible* . In the presence of H_2, there is always a sufficient amount of M-H present to maintain an efficient catalytic cycle. Such an equilibrium is not established when ironnitrosyl hydrides are used. According to the mechanistic interpretation shown in scheme II-3-7 (p-41), dimers are indeed formed, but only as mere reaction intermediates, which irreversibly disintegrate into monometallic products *following* NO/CO exchanges. Depending upon the nature of the dimeric species involved, these exchange reactions can occur in the direction converting "Fe(NO)" species into "$Fe(NO)_2$" (scheme II-3-7, p-41) or in the *reverse* direction in which "$Fe(NO)_2$" species act as the NO-donor (scheme II-3-4, p-37). The implication of the mechanistic interpretations are clear. The design of catalysts for syngas chemistry based on inexpensive

iron complexes might be accomplished only when ways have been found to stabilize NO/CO iron bimetallics such as those shown in schemes II-3-4 (p-37) and II-3-7 (p-41). One possible approach to this problem was to establish a mechanical link by using an appropriate bidentate ligand between the two metal-metal bonded metallic centers so that the latter are forced to remain in a closed vicinity. Research are conducted in this direction and the results obtained are presented in part III of the thesis.

PART III

DIPHENYL(2-PYRIDYL)PHOSPHINE AS AN ANCILLIARY LIGAND OF FIRST ROW TRANSITION METALS

GENERAL INTRODUCTION

To allow as much flexibility as possible, bidentate ligands L – L' were selected, which might allow for a facile access to heterobimetallics, with one metallic center M attached to L and another metallic center M' attached to L' as shown below :

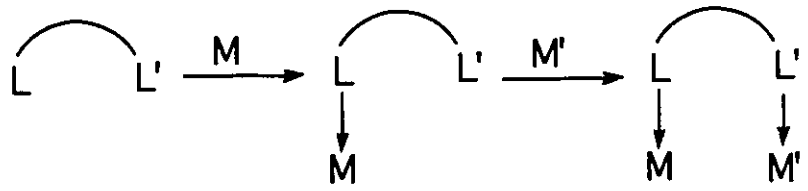

Scheme III-1 Suggested mechanism for the formation of bimetallic using bidentate ligand

In 1982, Roustan and coworkers [1-3] had shown that the aminophosphine **(I)** , Fig.III-1 could be used to functionalize sequentially the P-donor site with one nitrosylated Fe center, then the N-donor site with a different metallic fragment (e.g. **(II)** → **(III)** → **(IV)**) as depicted in scheme III-2, p-47)

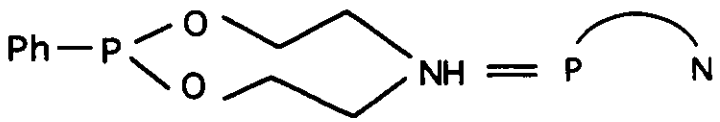

(I)

Fig. III-1 Structural representation of cyclic aminophosphine ligand

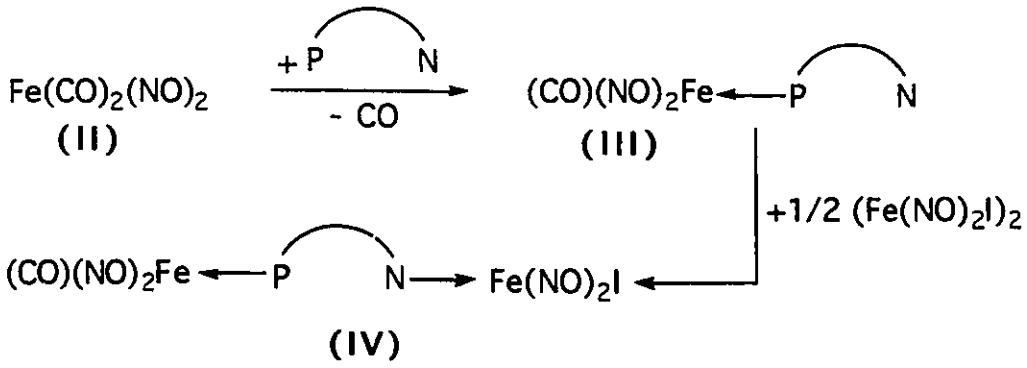

Scheme III-2 Formation of bimetallic with the P and N donor site of the ligand

Also of interest was the reaction of (I) in methanol, with the iron dimer $(Fe(NO)_2I)_2$ containing D_{NO}^{7+2} Fe centers in the presence of $NaBPh_4$. Complex (V) containing a D_{NO}^{8+2} center was isolated and structurally characterized. The increase of the electronic parameter of the D_{NO} type by one unit (from 7 in the iron reactant to 8 in the product) implied the occurence of a non-temporary reduction at the metal.

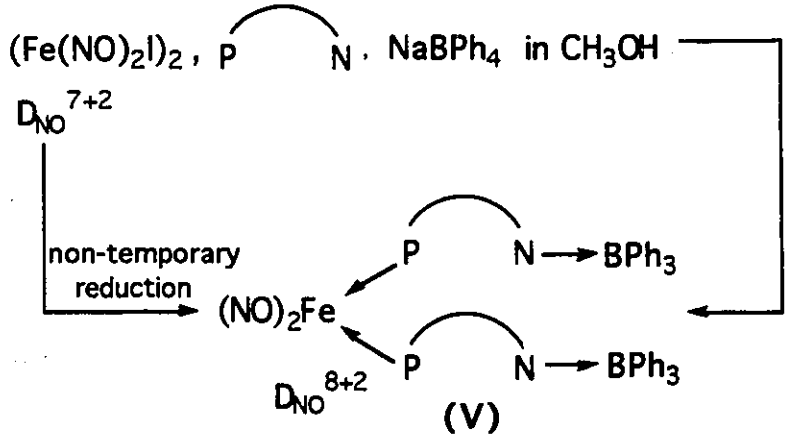

Scheme III-3 Representation of a Non-temporary reduction at the metallic center

The cyclic aminophosphine used in these studies is very flexible, due to the presence of an eight membered ring. Therefore, in order to favor conditions more prone to the formation of stable metal-metal bonded complexes in this present work, diphenyl(2-pyridyl)phosphine, $PPh_2(2\text{-}Py)$, has been selected as an ancillary ligand.

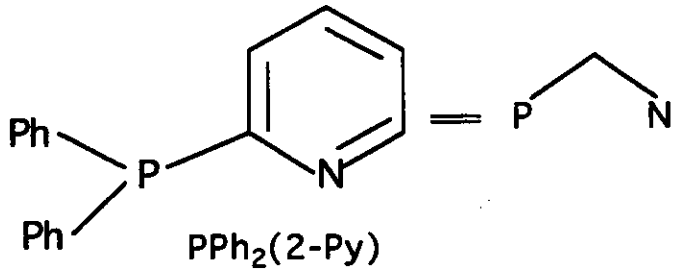

$PPh_2(2\text{-}Py)$

(VI)

Fig. III-2 Structural representation of Diphenyl(2-pyridyl)phosphine

Diphenyl(2-pyridyl)phosphine can bind to two metallic centers either in a Head-to-Head fashion (H-H) or Head-to-Tail (H-T) arrangement as shown in Fig.III-3 and Fig.III-4 respectively (p-49).

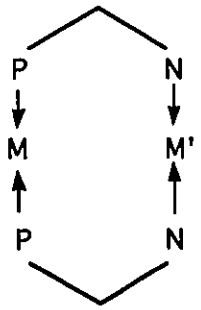

Fig.III-3 Head -to- Head (H-H) arrangement of the P^N ligand

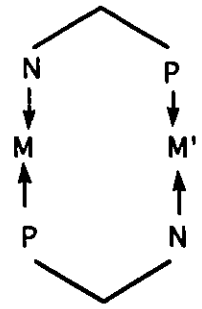

Fig.III-4 Head -to-Tail (H-T) arrangement of the P^N ligand

Diphenyl(2-pyridyl)phosphine has been used extensively by Alan Balch and coworkers [4-10] to construct metal-metal bonded bimetallics with second and/or third row metals. However, at the beginning of the present work, no complex containing this ligand and first row transition metals was known. In an M-M bonded $M_2(PPh_2(2\text{-}Py))$ unit, replacement of the second or third row metals by first row metal was expected to decrease the M-P, M-N, and M-M bond lengths. Consequently, at the outset, there was a legitimate concern that these structural changes might cause a severe destablizing strain in the bridge and it could not be taken for granted that $PPh_2(2\text{-}Py)$ could be successfully used with the first row transition elements.

The general synthetic scheme selected was the simplest one conceivable. It is depicted in scheme III-4 (p-51). Following route (a), functionalization of the P-donor site of the P^N ligand is achieved with a metallic fragment containing a M-X bond (X = halogen). A subsequent heterolysis of M-X with a suitable halogen

abstractor creates an empty coordination site at the metal for complexation of the N-site of the ligand. Due to the geometry of the latter, the formation of a monometallic chelate (intramolecular complexation) would not be favored relative to the formation of a bimetallic (intermolecular complexation). In principle, the latter could also be accessed according to route (b) in which the M-X bond is cleaved first, followed by the addition of the PPh_2(2-Py) ligand. Halogenated iron, then cobalt complexes were selected to provide the M-X complexes.

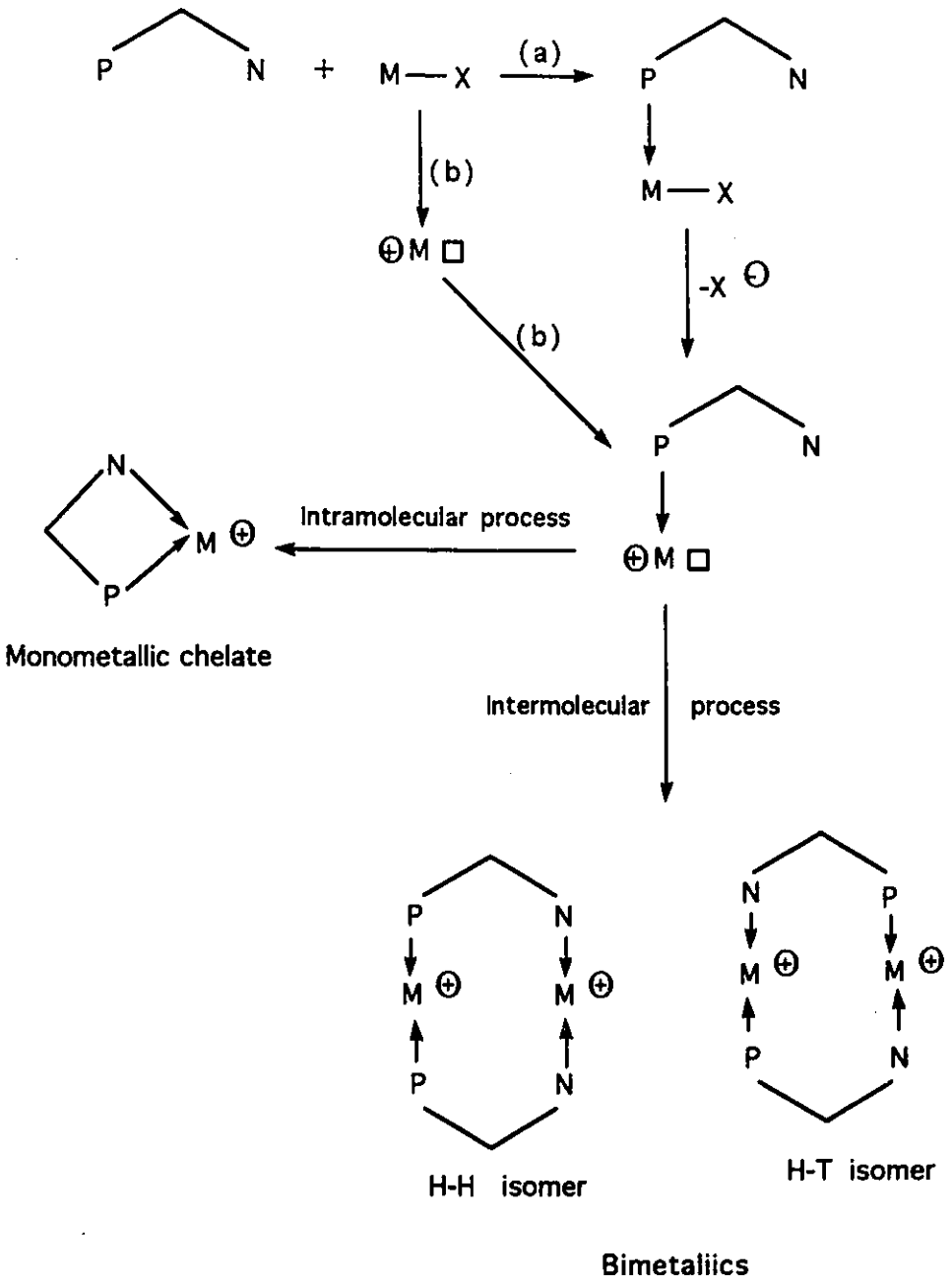

Scheme III-4 General synthetic scheme selected

CHAPTER 1 THE IRON SYSTEM

III-1-1 Electron transfer and ligand centered O-transfer

The preliminary work by Roustan and coworkers quoted in the general introduction led to selecting $(Fe(NO)_2I)_2$, as the precursor of the metallic fragment required in the general synthetic scheme III-4 (p-51).

Results

Reaction of $(Fe(NO)_2I)_2$ and $PPh_2(2\text{-}Py)$ (P/Fe =1) in EtOH at room temperature resulted in the formation of a precipitate. The latter was separated, washed with ether and recrystalllized from CH_2Cl_2-hexane. The IR spectrum in CH_2Cl_2 displayed ν_{NO} bands at 1785, 1735 cm^{-1} comparable to the ν_{NO}'s at 1789 and 1731 cm^{-1} of $Fe(NO)_2(PPh_3)I$ [11]. This supports the formation of the D_{NO}^{7+2}, $Fe(NO)_2(PPh_2(2\text{-}Py))I$ complex **(20)**.

$$(Fe(NO)_2I)_2 + 2PPh_2(2\text{-}Py) \rightarrow 2Fe(NO)_2(PPh_2(2\text{-}Py))I \qquad \text{(Rc III-1-1-1)}$$

(20)

However, the latter is unstable. Upon standing at room temperature, crystals of **(20)** slowly evolve iodine which appeared as tiny red crystals. To an ethanolic solution of **(20)**, either a stoichiometric amount or an excess of $AgBF_4$ or $NaBPh_4$ were added. In both cases, an untractable solid material was

obtained, which was found to be insoluble in CH_2Cl_2, CH_3CN or DMSO solvents. The same results were obtained when $(Fe(NO)_2Cl)_2$ was used.

The alternate approach identified as route (b) in the general synthetic scheme III-4 (p-51), was therefore attempted. The cation $Fe(NO)_2(THF)_2^+$ was formed first, followed by the addition of the diphenyl(2-pyridyl)phosphine ligand.

$(Fe(NO)_2Cl)_2$ was dissolved in THF. Addition of $AgBF_4$ to a THF solution of $(Fe(NO)_2Cl)_2$ resulted in the formation of AgCl, which was separated by filtration. In the filtrate, the cationic species $Fe(NO)_2(THF)_2^+BF_4^-$ was formed (ν_{NO} = 1776, 1710 cm^{-1}, comparable to the literature value ν_{NO} = 1780,1714 cm^{-1} [12]). To the homogenous solution of $Fe(NO)_2(THF)_2^+BF_4^-$, two equivalents of diphenyl(2-pyridyl)phosphine per iron atom was added. A yellow precipitate was formed, which was separated by filtration, the solution was evaporated to dryness. The solid residue was redissolved in a minimum amount of methylene chloride and subjected to a chromatographic separation (chromatotron with silica/alumina plate, elution with 1:1 methylene chloride/ethylacetate). Two products were separated. One was unreacted diphenyl(2-pyridyl)phosphine, $PPh_2(2\text{-}Py)$ ligand. The other, obtained as dark crystals, was identified as $Fe(NO)_2(PPh_2(2\text{-}Py))_2$ 8 (p-56), by comparing its IR spectrum with that of an authentic sample $Fe(NO)_2(PPh_2(2\text{-}Py))_2$ prepared

independently from $Fe(NO)_2(CO)_2$ and an excess of $PPh_2(2\text{-}Py)$ ligand ($\nu NO(CH_2Cl_2)$ = 1720, 1680 cm^{-1}) [13].

A single crystal X-ray diffraction study identified the yellow product as $Fe(O{=}PPh_2(2\text{-}Py))_3^{2+}.2BF_4^-$ **(21)**, indicating the oxidation of diphenyl(2-pyridyl)phosphine and chelation with iron center. The IR spectrum of **(21)** showed an absorption band at 1115 cm^{-1} suggesting the coordination of the phosphine oxide in the complex. This complex provides the first example of a first row metal coordinated by the phosphine oxide derived from the initial $PPh_2(2\text{-}Py)$ molecule.

According to the plausible mechanism in scheme III-I-3-8 (p-56), N_2O could be one of the end products. To confirm that N_2O was evolved during the process, the reaction with $Fe(NO)_2(THF)_2^+BF_4^-$ and $PPh_2(2\text{-}Py)$ in THF was conducted on a small scale in a flask directly attached to the inlet of a mass spectrometer. Mass spectrometric analysis of the gas phase showed that the reactions proceeded with the evolution of N_2, indicating that N_2O was formed.

The reaction of diphenyl(2-pyridyl)phosphine ($PPh_2(2\text{-}Py)$) was compared with triphenyl phosphine (PPh_3) to confirm the oxidation and coordination of the phosphine with iron center. For this, PPh_3 was reacted with $Fe(NO)_2(THF)_2^+BF_4^-$ in THF. An IR spectrum of the solution showed two new bands at 1720 and 1680 cm^{-1}, suggesting that the initial compound $Fe(NO)_2(THF)_2^+BF_4^-$ 5

(p-56) has been consumed. The solution was evaporated to dryness and the solid residue was recrystallized in methylene chloride/diethylether allowing the separation of two complexes, one was $OPPh_3$ (triphenyl phosphine oxide) as white crystal ($\nu_{O=P}$ (nujol) = 1200 cm^{-1}. The other complex was identified as the reduction product $Fe(NO)_2(PPh_3)_2$ ν_{NO} (CH_2Cl_2) = 1720, 1680 cm^{-1}. (Compared with the lit. value of $Fe(NO)_2(PPh_3)_2$ (νNO = 1724, 1678 cm-1) [14].

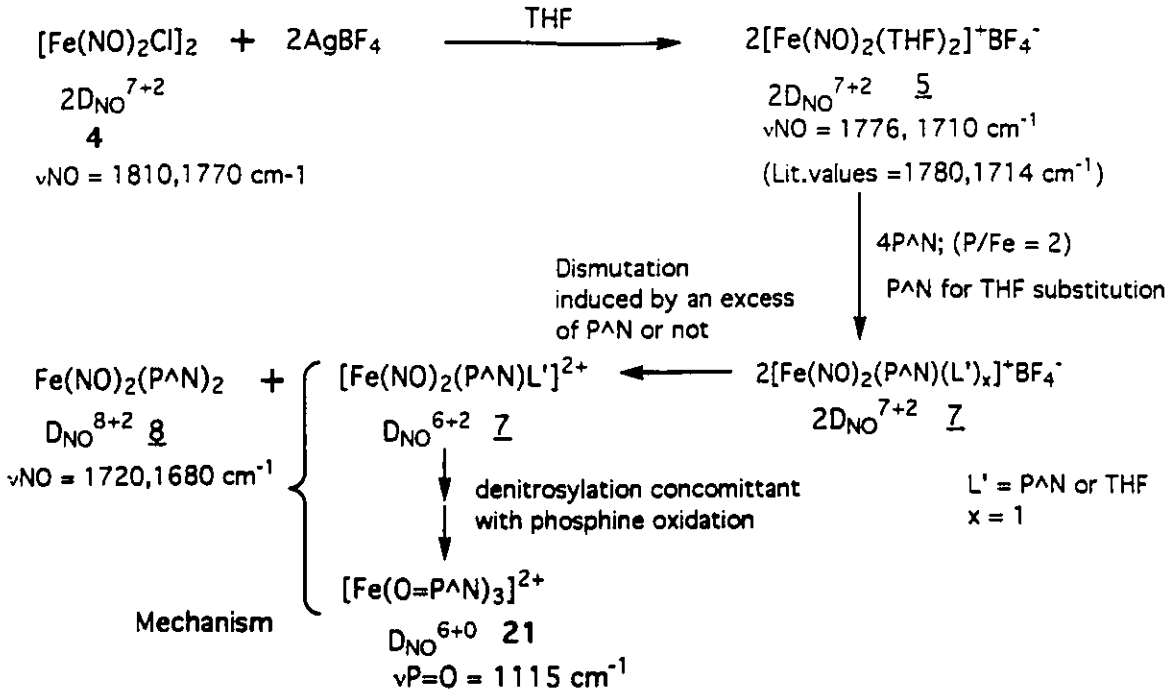

Mechanism

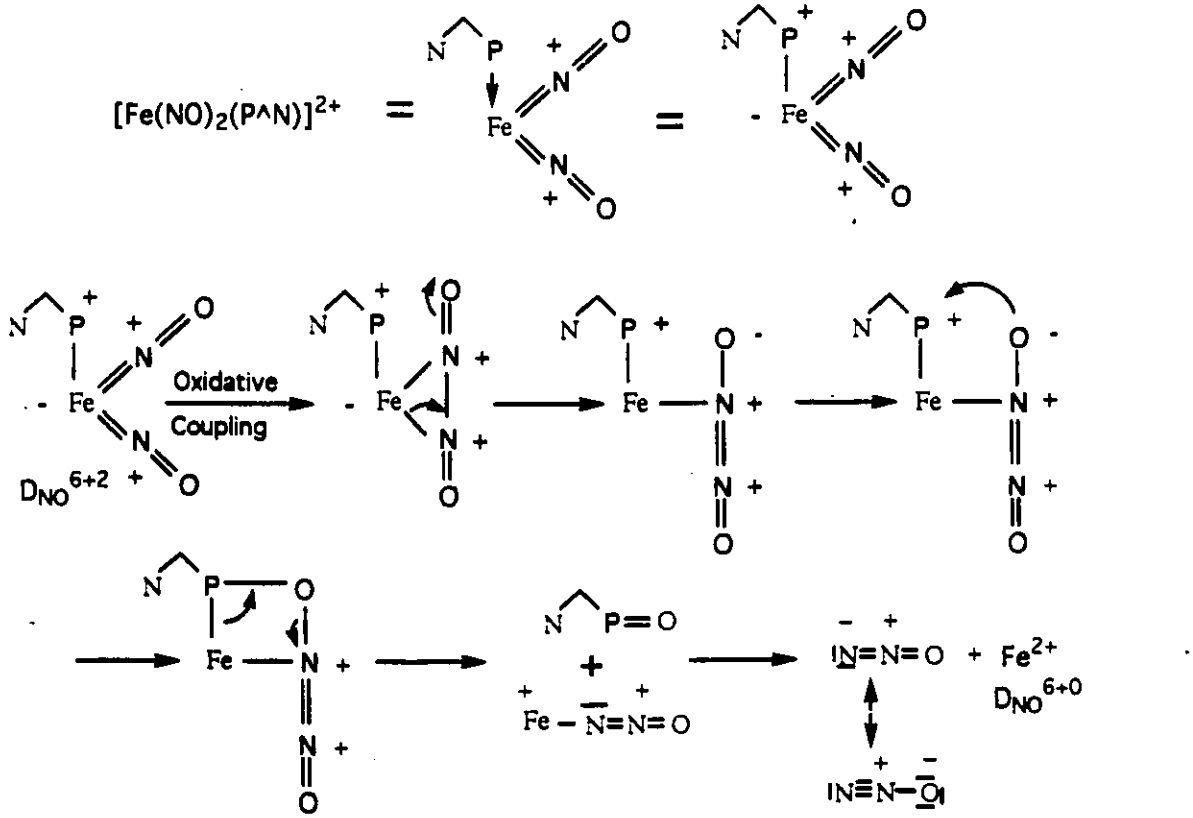

Scheme III-1-3-8 Suggested decomposition pathway of a $[Fe(NO)_2(P\wedge N)]^{2+}$ moiety using a representation with localized bonds

Discussion

The formation of a mixture of $Fe(NO)_2(PPh_2(2\text{-}Py))_2$ (D_{NO}^{8+2}) and $Fe(O{=}PPh_2(2\text{-}Py))_3^{2+}.2BF_4^-$ (D_{NO}^{6+0}) from $Fe(NO)_2(THF)_2^+BF_4^-$ (D_{NO}^{7+2}) implies the occurence of non-temporary redox reactions and complete denitrosylation of part of the initial iron centers. These reactions necessarily occur after the complexation of at least one $PPh_2(2\text{-}Py)$ molecule (in solution, and in the absence of the added ligand, $Fe(NO)_2(THF)_2^+BF_4^-$ is stable). In addition, the evolution of N_2 implies the cleavage of the N-O bonds of some of the NO ligands and at least part of the initial nitrosylic O-"atoms" serve to oxidize $PPh_2(2\text{-}Py)$ into the corresponding phosphine oxide. In search of a possible mechanistic model which might account for the observations, the simplest D_{NO} equation relating the iron reactant and products was used as a guideline :

$$2D_{NO}^{7+2} \rightarrow D_{NO}^{8+2} + D_{NO}^{6+0} + 2\text{"NO"}$$

This equation can be rewritten as the sum of (i) a dismutation reaction forming a mixture of D_{NO}^{8+2} + D_{NO}^{6+2} products and in which the total content of NO ligands remains constant (ii) a complete denitrosylation of the D_{NO}^{6+0} derivative :

$2D_{NO}^{7+2} \rightarrow D_{NO}^{8+2} + D_{NO}^{6+2}$ dismutation

$D_{NO}^{6+2} \rightarrow D_{NO}^{6+0} + 2\text{"NO"}$ denitrosylation

---

$2D_{NO}^{7+2} \rightarrow D_{NO}^{8+2} + D_{NO}^{6+0} + 2\text{"NO"}$

This analysis leads to the proposal of the reaction pathways presented in scheme III-1-3-8 (p-56). In this scheme addition of an excess of $PPh_2(2\text{-Py})$ to the solution containing the $Fe(NO)_2(THF)_2^+$ cation should yield a D_{NO}^{7+2} intermediate $Fe(NO)_2(PPh_2(2\text{-Py}))L'^+$ **6** (L' = $PPh_2(2\text{-Py})$ or THF). The latter might undergo a dismutation reaction into $Fe(NO)_2(PPh_2(2\text{-Py}))_2$ **8**, one of the observed products, and the D_{NO}^{6+2} new intermediate $Fe(NO)_2(PPh_2(2\text{-Py}))^{2+}$ **7**. A subsequent complete denitrosylation of **7** might then occur to yield the D_{NO}^{6+0} Fe^{2+} cation and the phosphine oxide required to construct the observed trichelated cation $Fe(O{=}PPh_2(2\text{-Py}))_3^{2+}$ found in **(21)**. A plausible mechanism shown in scheme III-1-3-8(p-56), is a mere adaptation of scheme II in ref [15]. A simple oxidative coupling of the two NO ligands of intermediate **7** is selected as the first step, followed by a ring opening which places a nucleophillic oxygen in the vicinity of the coordinated P-donor site of the $PPh_2(2\text{-Py})$ ligand. This situation is favorable for the formation of a P-O bond which becomes part of a four membered ring. This cyclic intermediate subsequently fragments, with the formation

of N_2O, phosphine oxide and Fe^{2+}, required to ultimately yield (21). What remains unknown is the nature of the subsequent O-transfer involving N_2O, in order to account for the evolution of N_2. However, it is well known that N_2O can oxidize metallic centers in a low oxidation state, with the formation of N_2 [16].

A similar reaction pathway can be suggested for the reactions involving PPh_3. The main difference between the two systems resides in the ability of the diphenyl(2-pyridyl) -phosphine oxide $O{=}PPh_2(2\text{-}Py)$ to chelate the Fe^{2+} cation, forming dipositive iron complex.

Conclusion

Undoubtedly, study of the $Fe(NO)_2^{+}/PPh_2(2\text{-}Py)$ system has contributed to a better knowledge of the course of reactions in which $D_{NO}{}^{7+2}$ irondinitrosyl species are involved in non-temporary redox processes. But it failed to provide any evidence for the formation of a bimetallic with $PPh_2(2\text{-}Py)$ as a bridging ligand. This evidence was finally obtained when $(Co(NO)_2I)_2$ was selected as the precursor of the metallic fragments.

Chapter 2 THE COBALT SYSTEM

III-2-1 Synthesis of $Co(NO)_2(PPh_2(2\text{-}Py))I$

$(Co(NO)_2I)_2$ was reacted with an ethanolic solution of $PPh_2(2\text{-}Py)$ (2equiv) at room temperature. After stirring for 15 min, shiny microcrystals were separated from the solution and washed with ether. Single crystals were obtained from CH_2Cl_2-hexane. The IR spectrum recorded in CH_2Cl_2 displayed ν_{NO} bands at 1827, 1770 cm^{-1}. The formation of the D_{NO}^{8+2} complex $Co(NO)_2(PPh_2(2\text{-}Py))I$ **(8)** was supported by a single crystal X-ray diffraction study, which revealed that the $PPh_2(2\text{-}Py)$ ligand is coordinated to cobalt through its P atom. This complex was subsequently placed under conditions favoring the heterolysis of the Co-I bond.

$$(Co(NO)_2I)_2 + 2\ PPh_2(2\text{-}Py) \rightarrow 2Co(NO)_2(PPh_2(2\text{-}Py))I \quad \text{(Rc. III-2-1-1)}$$

(8)

$\nu_{NO}(CH_2Cl_2) =$ 1827, 1770 cm^{-1}

III-2-2. Synthesis of a cationic monometallic derivative with diphenyl(2-pyridyl)phosphine

$Co(NO)_2(PPh_2(2\text{-}Py))I$ **(8)** was dissolved in ethanol and reacted with a stoichiometric amount of $AgBF_4$. A new monometallic D_{NO}^{8+2} $Co(NO)_2(PPh_2(2\text{-}Py))_2^+BF_4^-$ derivative **(9)**

was obtained. Single crystals were grown from toluene-CH_2Cl_2 solvents. An X-ray study showed that both $PPh_2(2\text{-}Py)$ ligands were coordinated to Co through the P donor sites.

$$2Co(NO)_2(PPh_2(2\text{-}Py))I \xrightarrow[\text{Ethanol}]{AgBF_4} Co(NO)_2(PPh_2(2\text{-}Py))_2{}^+BF_4{}^- \quad \text{(Rc. III-2-2-2)}$$

(8) **(9)**

ν_{NO}(nujol) = 1855, 1795 cm^{-1}

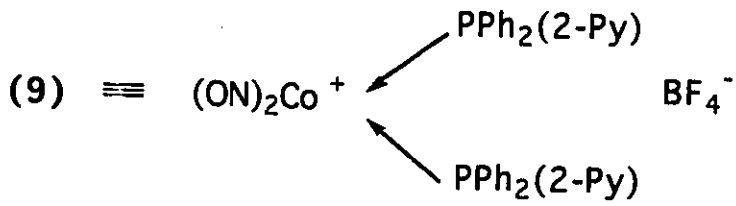

(In reaction Rc.III-2-2-2, there are necessarily at least two $Co(NO)_2(PPh_2(2\text{-}Py))I$ molecules involved in the formation of one $Co(NO)_2(PPh_2(2\text{-}Py))_2{}^+BF_4{}^-$).

III-2-3 First synthesis of a bimetallic containing a $Co_2(NO)_3{}^+$ core

The course of the reaction was drastically altered when $NaBPh_4$ was used as the halide abstractor. Addition of $NaBPh_4$ to an ethanolic solution of $Co(NO)_2(PPh_2(2\text{-}Py))I$ **(8)** at 37°C resulted in the rapid formation of a precipitate. The precipitate

was separated by filtration and dissolved in THF followed by a moderate heating at 40°C. A new crystalline product was obtained after removal of THF and recrystallization from CH_2Cl_2-hexane. The chemical identity of the compound $Co_2(NO)_3(PPh_2(2\text{-}Py)_3)^+.BPh_4^-$ **(12)** Fig.III-2-3-1, (p-63), had to be established by a single crystal X-ray diffraction study. Complex **(12)** contains an unprecedented $Co_2(NO)_3^+$ metallic core stablized by two bridging $PPh_2(2\text{-}Py)$ ligands coordinated in a Head-to-Head fashion. The $Co_2(NO)_3^+$ core can be viewed as two $Co(NO)_2$ units sharing a μ_2-NO ligand, each cobalt center having an additional terminal NO. The separation of 2.527(1)Å between the two metals is in agreement with the presence of a metal-metal bond. In the IR spectrum of complex **(12)**, the two terminal NO ligands are characterized by a strong absorption band at 1775 cm^{-1} flanked by a shoulder at 1750 cm^{-1}, an additional band at 1570 cm^{-1} can be confidently identified as the NO-absorption band of the μ_2-NO ligand.

This complex dissolved in CH_2Cl_2 proved to be unreactive towards syngas (H_2 : CO =1, P = 1 atm.) at room temperature.

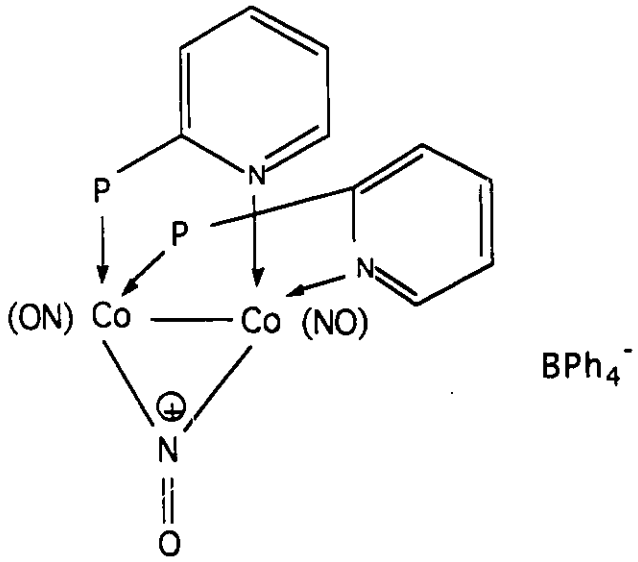

The pheny substituents of each P atom have been omitted for clarity

Fig. III-2-3-1. Arrangement of ligands around each cobalt atom in complex (12)

The bimetallic cation $Co_2(NO)_3(PPh_2(2\text{-}Py))_2^+$ is of the $D_{NO(2Co)}{}^{17\ +3}$ type (the formal removal of the NO's as NO molecules and of the $PPh_2(2\text{-}Py)$ ligand leaves a Co_2^+ bimetallic core containing 17 metallic d electrons), its formation, starting from two $D_{NO}{}^{8+2}$ $Co(NO)_2(PPh_2(2\text{-}Py))$I molecules, implies a reductive partial denitrosylation. A simple condensation of two mono--metallic $D_{NO}{}^{8+2}$ species would yield a $D_{NO(2Co)}{}^{16+4}$ dimer with an electronic parameter and a structural parameter one unit below (16 vs. 17) and one unit above (4 vs. 3) respectively. A less involved, and already known case of a reductive partial

denitrosylation is provided by the room temperature reaction of $NaBPh_4$ in THF, with a mixture of the D_{NO}^{8+2} complexes $Co(NO)_2(PPh_3)Cl$ and $Co(NO)_2(PPh_3)_2^+Cl^-$, in the presence of an excess of PPh_3, and an almost quantitative yield of $Co(NO)(PPh_3)(D_{NO}^{9+1})$ was reported [17].

Under the present reaction conditions yielding ultimately $Co_2(NO)_3(PPh_2(2\text{-}Py))_2^+$, with no hydride donor being present, the reductive nitrosylation had to involve the BPh_4^- anion. Unfortunately, a survey of the literature did not provide any case of an unusual reaction between BPh_4^- and nitrosyl complexes which could be used to suggest a feasible reaction pathway leading to $Co_2(NO)_3(PPh_2(2\text{-}Py))_2^+$. In the latter, one cobalt center is connected to two NO and two P-donor sites, and there is nothing unusual about this ligand arrangement when BPh_4^- is present. For example $Co(NO)_2(PPh_3)_2^+BPh_4^-$ was described years ago and was found to be stable in solution [17]. The other cobalt center of the complex **(12)** is of more interest, besides the two NO, it is connected to the two pyridinyl portions of the bridging $PPh_2(2\text{-}Py)$ ligands. At the time speculations were made about the reactions involved in the formation of $Co_2(NO)_3(PPh_2(2\text{-}Py))_2^+$, this ligand arrangement was unprecedented, the monometallic counterpart $Co(NO)_2(pyridine)_2^+$ $-BPh_4^-$ being then unknown . This bispyridine cobalt complex became a necessary target. The synthesis of this new

monometallic complex is described in the following paragraph. Its behavior in solution provided the information required to propose a pathway leading to bimetallic (12), a matter which will be described later on. The solution behavior of $Co(NO)_2(Py)_2^+BPh_4^-$ was so unexpected that the molecular structure of $Co(NO)_2(Py)_2^+BF_4^-$, which provided single crystals, was established by X-ray diffraction. This later study provided structural data which will be used in part IV of the thesis.

III-2-4 Synthesis of the $Co(NO)_2(Py)_2^+$ cation

The cobaltdinitrosylbispyridine cation $Co(NO)_2(Py)_2^+$ (Py = pyridine) was synthesized by the reaction of an ethanolic solution of $(Co(NO)_2I)_2$ (2) and an excess of pyridine with either BF_4^- or BPh_4^-. In the reactions using $AgBF_4$ as the halide abstractor, after separation by filtration of solid AgI, the solution was evaporated to dryness and the residue was crystallized in methylene chloride-hexane mixtures to yield $Co(NO)_2(Py)_2^+BF_4^-$ (10). The chemical formulation was confirmed by a single crystal X-ray diffraction study. The IR spectrum of the complex (10) in CH_2Cl_2 displayed two strong NO-absorption bands at 1876 and 1798 cm-1. They are at positions comparable to those reported for other D_{NO}^{8+2} cationic dinitrosyl cobalt complexes (see for example the data in Table IV-1-2-1 (p-156) and Table IV-1-2-2 (p- 157).

When $NaBPh_4$ was used in place of $AgBF_4$, olive green microcrystals gradually precipitated from the ethanolic solution consisting initially of $(Co(NO)_2I)_2$, pyridine and $NaBPh_4$. The IR spectrum of the crystals in a nujol mull displayed two strong NO-bands at 1870 and 1790 cm^{-1}, as expected for the formation of $Co(NO)_2(Py)_2^+BPh_4^-$ **(11)**. However, when dissolved in CH_2Cl_2, this complex decomposed rapidly, in sharp contrast to the behavior of $Co(NO)_2(Py)_2^+BF_4^-$ **(10)** which was stable under the same experimental conditions. The progress of the decomposition was monitored by IR spectroscopy. This showed the transient appearance of a new band at 1720 cm^{-1}, clearly distinguishable from the ν_{NO}'s of the cationic complex, which provides a good indication for the formation of an uncharged reaction intermediate. However, the latter was also unstable and after a few minutes no absorption remained in the frequency range 1900-1700 cm^{-1}, indicating a complete loss of terminal NO ligands. No cobalt derivative could be isolated from the decomposed solutions. The decomposition reaction was also monitored using ^{11}B NMR spectroscopy. The initial sharp resonance at δ = -5.9 ppm of the BPh_4^- anion present in the initial ionic complex was rapidly replaced by a broad resonance centered at δ = + 6.0 ppm which is strongly suggestive of the formation of BPh_3 [18].

Alternatively, $Co(NO)_2(Py)_2^+BPh_4^-$ could be recrystallized

without decomposition from a CH_2Cl_2 solution containing an excess of pyridine.

Discussion

From this inhibitory effect of an excess of pyridine upon the decomposition of $Co(NO)_2(Py)_2^+$, it can be concluded that the dissociation of the pyridine ligand from $Co(NO)_2(Py)_2^+$ is a *prerequisite* for the decomposition to take place. In addition, the BF_4^- derivative of $Co(NO)_2(Py)_2^+$ being stable, BPh_4^- has to be actively involved in the decomposition of the cation, after one of its coordination sites has been made available by the departure of a pyridine ligand. Consequently, in line with the documented ability of BPh_4^- to phenylate metallic centers [19], one might suspect the involvement of an uncharged η^1-phenyl intermediate such as $Co(NO)_2(Py)$-Ph. This suggests the following decomposition pathway as a likely one :

$Co(NO)_2(Py)_2^+ \rightleftharpoons Co(NO)_2(Py)^+ + Py$ (shifted to the left with an excess of Py)

$Co(NO)_2(Py)^+ + BPh_4^- \rightarrow BPh_3 + Co(NO)_2(Py)\text{-}Ph \rightarrow$ decomposition (intermediate to which the transient ν_{NO} at 1720 cm^{-1} is tentatively assigned).

Scheme III-2-3-1 Suggested decomposition pathway of $Co(NO)_2(Py)^+ BPh_4^-$

This unexpected lability of the pyridine ligands when they are bound to a $Co(NO)_2^+$ functional group immediately provides a rationale for the formation of $Co_2(NO)_3(PPh_2(2\text{-}Py))_2^+BPh_4^-$.

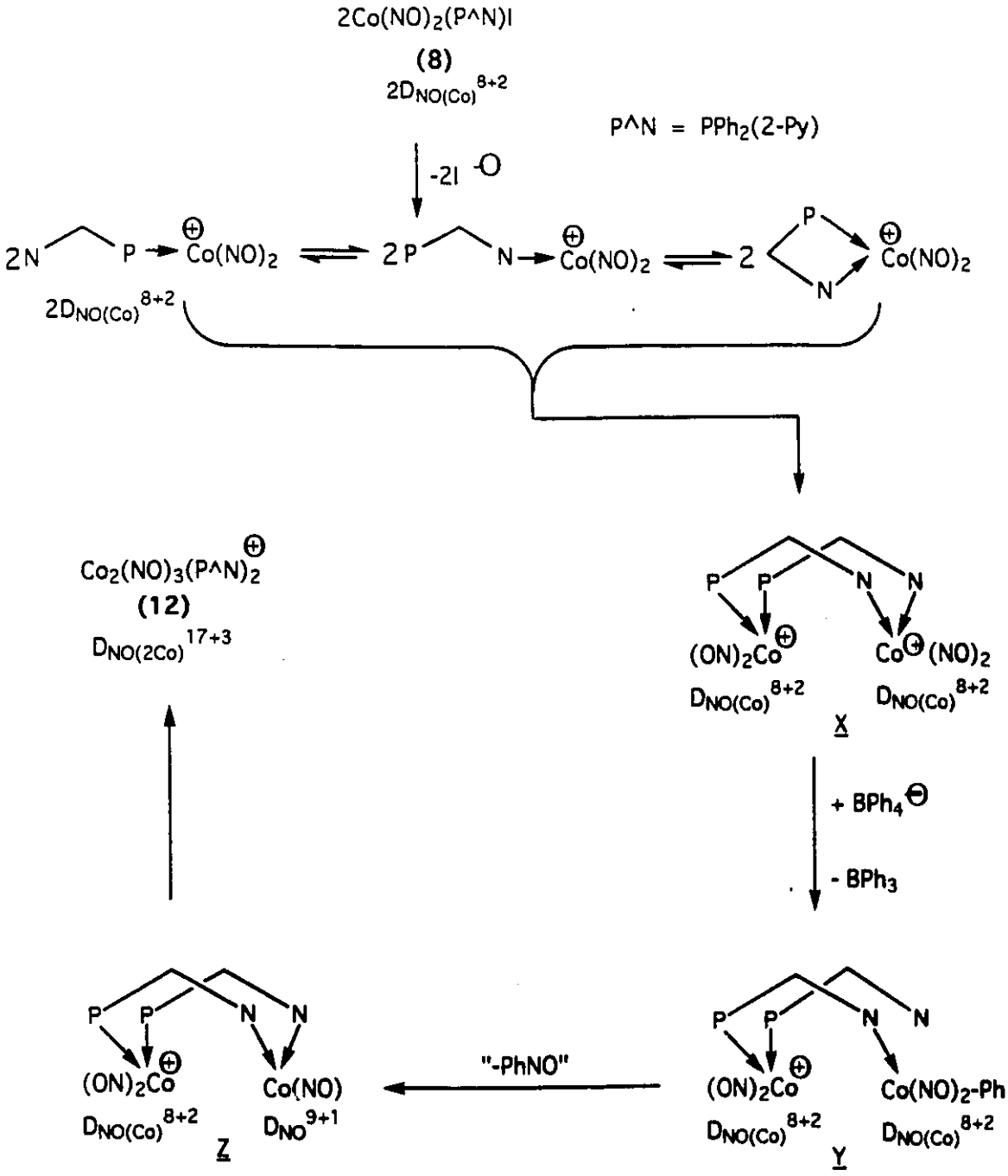

Scheme III-2-3-2 A proposed mechanism for the formation of bimetallic

According to scheme III-2-3-2 (p-69), in an intermediate such as X , one of the two possible bimetallics which could result from the ionization of the Co-I bond of $Co(NO)_2(PPh_2(2\text{-}Py))I$ **(8)**, only the cobalt center attached to the N-sites of the $PPh_2(2\text{-}Py)$ ligands would be prone to a phenyl transfer involving BPh_4^-. However, contrary to $Co(NO)_2(Py)^+$, due to the geometry of the $PPh_2(2\text{-}Py)$ ligand, the pyridinyl moiety which has to dissociate prior to the phenylation step is forced to stay in the vicinity of the metallic center. Consequently, it remains available for recomplexation when the suggested intermediate Z has formed after the elimination of PhNO as unidentified reaction product. The formation of the $Co_2(NO)_3^+$ core from intermediate Z can be rationalized by applying general principles to this particular case. The important features of the postulated intermediate Z are the presence of a coordinatively unsaturated $Co(NO)(N\text{-})_2$ metallic center maintained within a bonding distance of the coordinatively saturated $Co(NO)_2(P\text{-})_2^+$ center. The latter can act as a two electron donor according to scheme III-2-3-3 (p-71).

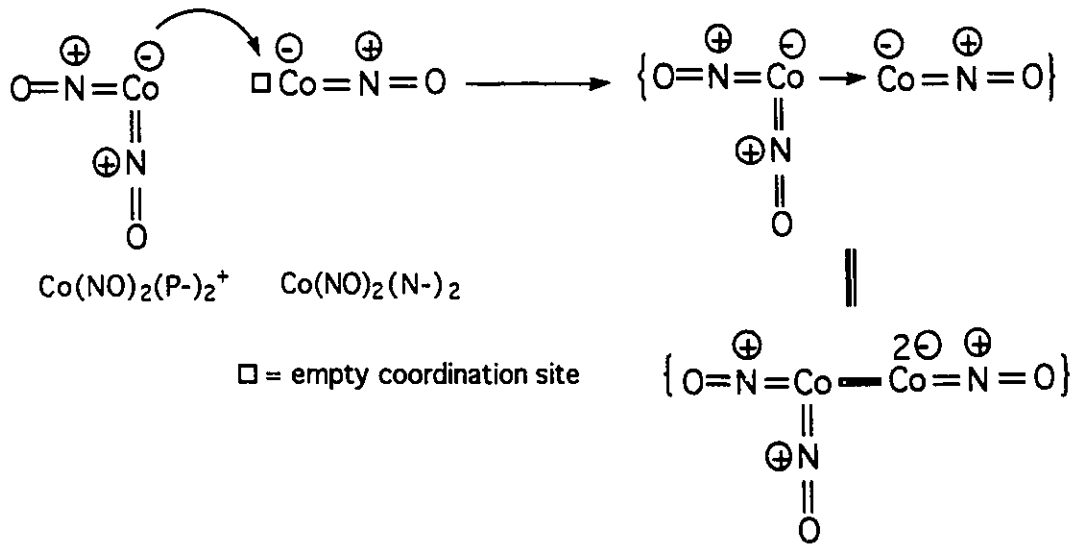

Scheme III-2-3-3 Suggested mechanism for the formation of a metal-metal bond between $Co(NO)_2$ and Co(NO)moiety

The formation of the μ_2-NO bridge might then proceed as follows

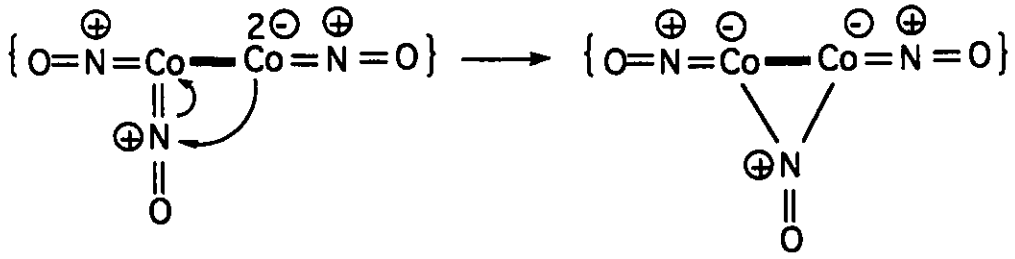

Scheme III-2-3-4 Formation of a μ_2-NO bridge between two metallic center

When BPh_4^- is not available, the bimetallic intermediate might also decompose by forming the $Co(NO)_2(PPh_2(2\text{-}Py))_2^+$ cation, and the formation of $Co(NO)_2(PPh_2(2\text{-}Py))_2^+BF_4^-$ can be accounted for on this basis.

Conclusion

In the design of catalytic systems capable of operating under mild conditions (e.g. at room temperature), one of the requirements is the facile formation of coordinatively unsaturated species. The results reported here demonstrate that this requirement is fulfilled in $Co(NO)_2(Py)_2^+$ which contains a labile pyridine ligand. Consequently, this complex should be considered in future studies aimed at screening its catalytic activity under a variety of conditions.

It is also the lability of the pyridine ligands, coupled with a subsequent reaction with BPh_4^-, which has been tentatively identified as the key factor for allowing the formation of the bimetallic $Co_2(NO)_3(PPh_2(2\text{-}Py))^+$ cation. The synthesis of the latter demonstrates that the aminophosphine $PPh_2(2\text{-}Py)$ can be used as a bridging ligand to construct bimetallics containing nitrosylated first row metallic elements.

Unfortunately, when the results presented in part IV are taken into account , it is likely that the access to a bimetallic of this type will be limited to derivatives in which the interligand

repulsions in the metallic center attached to the N-site of the aminophosphine have been minimized by a judicious choice of the ligand set.

In this context, the notion that interligand repulsions are significant factors to consider, derives from the conclusion regarding the nature of the factors responsible for the contrasting behavior of the $Co(NO)_2(Py)_2^+$ and $Co(NO)_2(phosphine)_2^+$ cations. In solution and in the presence of BPh_4^-, whereas $Co(NO)_2(Py)_2^+$ decomposes rapidly, $Co(NO)_2(PPh_3)_2^+$ and $Co(NO)_2(P(OCH_3)_2)_2^+$ are inert. From this observation it can be concluded that contrary to a pyridine ligand, a phosphine ligand does not dissociate to any appreciable extent from $Co(NO)_2^+$. This suggests the hypothesis that a comparison of the solid structures of $Co(NO)_2(py)_2^+$, $Co(NO)_2(PPh_3)_2^+$ and $Co(NO)_2(P(OCH_3)_2)_2^+$ might provide useful information to rationalize the observed difference in reactivity upon going from the cobalt-pyridine to cobalt-phosphines complexes. Indeed, it seems that this comparision is a fruitful one, and will be in a position to show why it is so only at the end of Chapter I of Part IV.

CHAPTER 3 CRYSTAL AND MOLECULAR STRUCTURES

III-3 Theory of Crystallography

This part of the thesis describes briefly some theoretical aspects of X-ray diffraction studies. This chapter gives a general idea of some of the terms commonly used in solving a crystal structure.

III-3-1 UNIT CELL

A crystal consists of atoms arranged in a pattern that repeats periodically in three dimensions. One can divide two dimensional space into parallelograms. In three dimensions, the space is divided into parallelpipeds. Repetition of these parallelpipeds by translation from one lattice point to another generates the lattice. The generating parallelpiped is called a unit cell. A unit cell is the smallest volume of the crystal which contains all the structural and symmetry information for the crystal. The size and shape of the unit cell may be specified by means of length a, b, and c for the three independent edges and three angles α, β, and γ between these edges as shown in Fig.III-3-1-1 (p-75).

III-3-2 BRAGG'S LAW [20, 21]

The X-ray was discovered by Rontgen (1895), but at that time its nature was not known. It was Max von Laue (1912), who discovered the diffraction of X-rays by crystals. In the same year

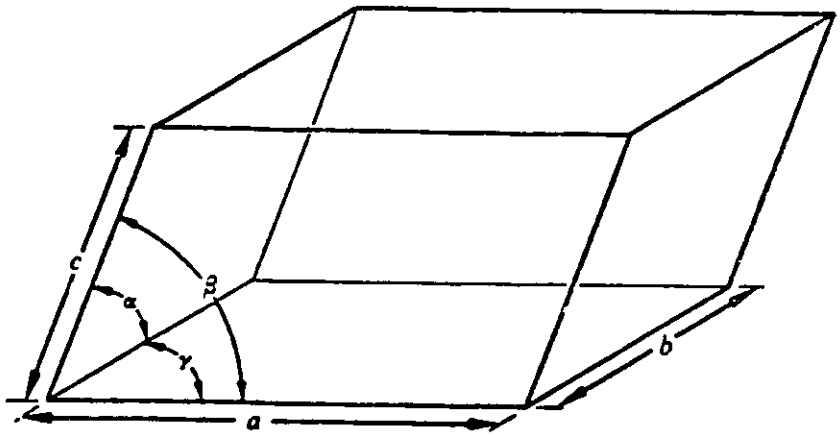

Fig. III-3-1-1 Representation of a Unit Cell

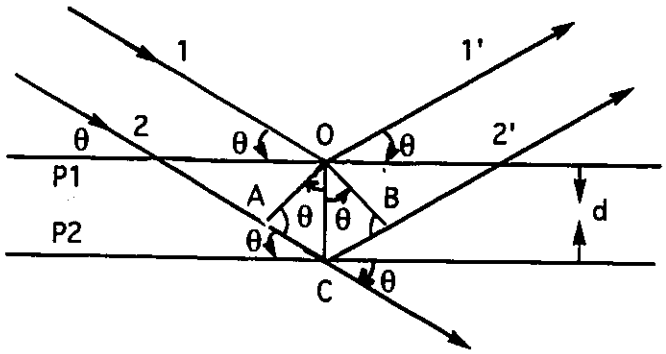

Fig. III-3-2-2 Representation of Bragg's Law

W. L. Bragg noted the similarity of diffraction to ordinary reflection and deduced a simple equation treating diffraction as reflection.

When an electromagnetic wave (having wavelength λ) strikes two parallel planes, separated by 'd' making an angle θ, the constructive interference of the waves generated at points O and C will occur only when θ is adjusted such that following equation is satisfied. Fig. III-3-2-2 (p-75).

$$n\lambda = 2d\sin\theta \qquad \text{----------} \quad \text{(III-3-2-1)}$$

This equation is known as Bragg's law. This concept can be applied to crystal lattices as they contain various sets of parallel planes of a stack (hkl) with spacing d_{hkl}.

$$n\lambda = 2d_{hkl}\sin\theta_{hkl} \qquad \text{----------} \quad \text{(III-3-2-2)}$$

III-3-3 CONCEPT OF RECIPROCAL LATTICE [22]

Reciprocal space is best described as a mathematical concept to represent diffraction geometry. Thus, a diffraction plane (hkl) in the (crystal) direct space is represented in reciprocal space by a vector from the origin normal to the diffraction plane. These vectors, are then diffraction vectors that register on the X-ray film or on the scintillation counter of the

diffractometer. The planes in direct space are represented by vectors in the reciprocal space. This concept is helpful for data collection, but the structure determination is still carried out in the direct space of the unit cell.

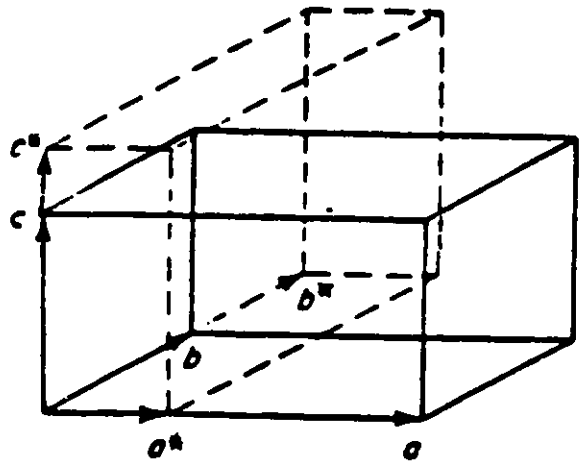

Fig. III-3-3-3 Relationship between the orthorhombic direct and reciprocal cell

The reciprocal lattice is a representation of the unit cell in reciprocal space. The spacings between the lattice points are

inversely proportional to the spacings between the parallel diffraction planes of the crystal. For orthorhombic space groups, with cell dimensions (a, b, c), the reciprocal unit cell has dimensions (1/a, 1/b, 1/c). Fig. III-3-3-3 (p-77) shows the relationship between the orthorhombic direct and reciprocal cell.

III-3-4 CHOICE OF RADIATION

A diffraction pattern with Cu radiation (λ = 1.5418 Å) is stronger (more intense) than with Mo radiation (λ = 0.7107 Å). However, X-ray absorption is more severe for Cu than Mo. Thus, when the compound contains heavy atoms, which produce a strong diffraction pattern anyway, it is best to use Mo radiation in order to reduce the absorption effect. For very accurate work, the measured intensities of organometallic compounds should be corrected for absorption.

III-3-5 ELIMINATION OF BACKGROUND RADIATION

Each peak count is converted into a net intensity by substracting the background radiation:

$$I = C - (B1 + B2)\, t_s/t_b \quad \text{----------} \quad \text{(III-3-5-3)}$$

Here, 'I' represents the observed intensity, 'C' is the peak count, 'B1' and 'B2' are the high and low background counts respectively,

't_s' is the reflection scan time and 't_b' is the total background time. The standard deviation $\sigma(I)$ of the intensity I is computed adopting the equation :

$$\sigma (I) = [C + (B1 + B2)/2 (t_s/t_b)^2 + (NC)^2]^{1/2} \quad \text{------} \quad \text{(III-3-5-4)}$$

Here, 'N' is the instrumental constant known as 'ignorance factor' and was usually taken as 0.003 during the least-square refinement of atomic parameters. Intensities less than a predetermined threshold $3\sigma(I)$ are rejected along with the reflections which are systematically absent.

III-3-6 Lorentz and Polarization Correction [23]

The intensity is converted into the structure factor amplitude by the equation:

$$|F_{hkl}| = \sqrt{K I_{hkl} / LP} \quad \text{----------} \quad \text{(III-3-6-5)}$$

where 'K' is the scaling factor which depends on the crystal size, beam intensity and a number of other fundamental constants. 'LP' is the Lorentz-Polarization correction. The unpolarized x-ray beam is partially polarized after the reflection from the monochromator and sample crystal and this reduces the measured intensity. The polarization factor corrects the reflection for this

effect.

$$P = (\cos^2 2\theta_m + \cos^2 2\theta_c) / (\cos^2 2\theta_m + 1) \text{ -------} \quad \text{(III-3-6-6)}$$

'θ_m' and 'θ_c' represent the diffraction angles at the monochromator and crystal respectively. The time required for a reciprocal lattice point to pass through the sphere of reflection is not constant but varies with its position in the reciprocal space and the direction in which it appproaches the sphere. The Lorentz factor corrects for the time it takes for each reciprocal lattice point to pass through the sphere of reflection. For a four circle diffractometer this factor is:

$$L = 1/\sin 2\theta \text{ ----------} \quad \text{(III-3-6-7)}$$

These corrections are usually combined as:

$$LP = (\cos^2 \theta_m + \cos^2 \theta_c) / \sin 2\theta_c (\cos^2 \theta_m + 1) \text{ ---- (III-3-6-8)}$$

III-3-7 STUCTURE FACTOR DEFINITION [24]

The structure factor F_{hkl} of a particular reflection expresses the resultant scattering of all the atoms in the unit cell. If N atoms are present in the unit cell, the stucture factor for a reflection hkl can be written as:

$$F_{hkl} = \sum_{j=1}^{N} f_j e^{2\pi i(hx_j+ky_j+lz_j)} \quad \text{----------} \quad \text{(III-3-7-9)}$$

where (x_j, y_j, z_j) are the fractional coordinates of the j^{th} atom and

$$f_j = f_{oj} e^{-B_j(\sin^2\theta/\lambda^2)} \quad \text{----------} \quad \text{(III-3-7-10)}$$

The 'f_j' and 'f_{oj}' are the scattering factors of the j^{th} atom in the vibrating and stationary conditiion respectively.

The structure factor is identified as a complex number, therefore can be analyzed to its real and imaginary parts as :

$$F_{hkl} = A_{hkl} + iB_{hkl} \quad \text{----------} \quad \text{(III-3-7-11)}$$

where,

$$A_{hkl} = \sum_{j=1}^{N} f_j \cos 2\pi(hx_j+ky_j+lz_j) \quad \text{--------} \quad \text{(III-3-7-12)}$$

$$B_{hkl} = \sum_{j=1}^{N} f_j \sin 2\pi(hx_j+ky_j+lz_j) \quad \text{--------} \quad \text{(III-3-7-13)}$$

Further the phase δ and amplitude of the structure factor can be expressed as :

$$\delta = 2\pi(hx_j+ky_j+lz_j) \quad \text{----------} \quad \text{(III-3-7-14)}$$

and

$$F_{hkl} = \sqrt{A^2_{hkl} + B^2_{hkl}} \quad \text{----------} \quad \text{(III-3-7-15)}$$

The phase angle 'α_{hkl}' can be calculated using

$$\alpha_{hkl} = \tan^{-1}(B_{hkl} / A_{hkl}) \quad \text{---------} \quad \text{(III-3-7-16)}$$

III-3-8 THE RELATIONSHIP OF STRUCTURE FACTORS AND INTENSITIES [25]

In the X-ray diffraction experiment the most important quantity that is measured is the relative intensity of a reflection hkl. The observed intensity I_o is related to the structure factor by

$$I_o(hkl) = K^2 C(hkl) \; |Fo(hkl)|^2 \quad \text{----------} \quad \text{(III-3-8-17)}$$

Here,'K' is the scale factor associated with $F_o(hkl)$ and 'C(hkl)' depends upon a number of experimental conditions, especially Lorentz and Polarization and sometimes absorption corrections as explained above.

The complex quantity, F_{hkl} can be represented on an Argand diagram (Fig.III-3-8-4, p-83).

The complex conjugate of F_{hkl} is $\tilde{F}_{hkl}$.

$$F_{hkl} = A_{hkl} + iB_{hkl} \quad \text{----------} \quad \text{(III-3-8-18)}$$

$$\tilde{F}_{hkl} = F_{\bar{h}\bar{k}\bar{l}} = A_{hkl} - iB_{hkl} \quad \text{----------} \quad \text{(III-3-8-19)}$$

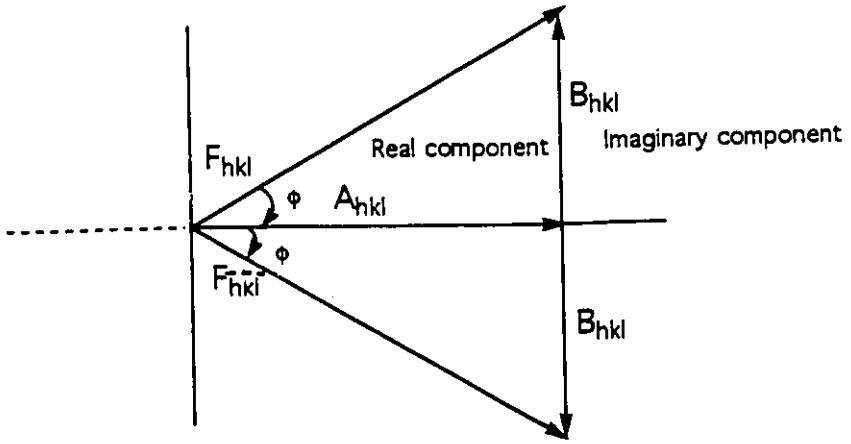

Fig. III-3-8-4 Representation of an Argand diagram

when F_{hkl} and $F_{\bar{h}\bar{k}\bar{l}}$ are multiplied together:

$$F_{hkl}.\tilde{F}_{hkl} = (A_{hkl} + iB_{hkl}).(A_{hkl} - iB_{hkl}) \quad \text{----} \quad \text{(III-3-8-20)}$$

$$I_{hkl} = |F_{hkl}|^2 = A^2_{hkl} + B^2_{hkl} \quad \text{---------} \quad \text{(III-3-8-21)}$$

It can also be shown that for reflections hkl and their centrosymmetric related partners $\bar{h}\bar{k}\bar{l}$,

$$F(hkl) = F(\bar{h}\bar{k}\bar{l}) \quad \text{----------} \quad \text{(III-3-8-22)}$$

which means,

$$I_o(hkl) = I_o\ (\bar{h}\bar{k}\bar{l}) \quad \text{----------} \quad \text{(III-3-8-23)}$$

This is Friedel's law. The recorded diffraction pattern will appear

centrosymmetric, even though the structure itself does not possess a centre of symmetry. Deviation from Friedel's law occurs when an anomalous scatterer is present in the structure.

III-3-9 FOURIER SYNTHESIS [25]

Since crystals are periodic in stucture, the electron density can be described as a periodic function by means of a Fourier series which is the sum of sine and cosine terms with appropriate co-efficients. The electron density thus calculated is the Fourier transform of the structure factors and related to F_{hkl} by equation :

$$\rho(x,y,z) = 1/V \sum_{h}\sum_{k}\sum_{l} |Fhkl| \cos 2\pi(hx+ky+lz - \alpha_{hkl}) \quad \text{----} \quad \text{(III-3-9-24)}$$

An electron density distribution calculated by a Fourier synthesis using the observed structure factors is called an "Observed Fourier" map. A "Difference Fourier" is frequently used when a structure is partially solved, to search for for comparitively light atoms e.g. hydrogen. The co-efficient ΔF can be used in the difference Fourier summation.

$$\Delta\rho(x,y,z) = 1/V \sum_{h}\sum_{k}\sum_{l} \Delta F \cos 2\pi(hx+ly+kz - \alpha'_{hkl}) \quad \text{----} \quad \text{(III-3-9-25)}$$

where,

$$\Delta F = |F_O| - |F_C| \text{ ---------- ---} \quad \text{(III-3-9-26)}$$

and $$\cos \alpha = A/|F_C| \text{ ----------} \quad \text{(III-3-9-27)}$$

$$\sin \alpha = B/|Fc| \text{ ----------} \quad \text{(III-3-9-28)}$$

Here, 'F_O' is the observed structure factor, 'F_C' is the structure calculated using equation (III-3-7-9), 'A' and 'B' are the cosine and sine terms in the structure factor calculation. For a centrosymetric case the sine term is zero. The usefulness of a D-Fourier arises because it removes the contribution to $\rho(x,y,z)$ of all atoms included in structure factor calculation at that stage.

III-3-10 THE PHASE PROBLEM [24]

The structure factor $F_{(hkl)}$ is related to the intensity as has already been described. Unfortunately, the structure factor is not just a real number but a complex number having both magnitude and phase. The magnitude can be calculated by measuring the intensities of reflections, but there is no way to measure the phase of the structure factor; hence the "Phase Problem". There are two basic ways to overcome this problem.

(i) the heavy atom method

(ii) direct methods

(i) THE HEAVY ATOM METHOD [26]

It is possible to locate the heavy atom in the crystal cell by this method. Once the heavy atom in the cell is located it can serve as a phasing model from which the other atomic positions can be developed. A Patterson synthesis provides a vector map of the contents of the unit cell and is expressed as :

$$P(u,v,w) = 1/V \sum_{h}\sum_{k}\sum_{l} |Fhkl|^2 \cos 2\pi(hu+kv+lw) \quad \text{------} \quad \text{(III-3-10-29)}$$

Thus a peak at the point u,v,w in a Patterson map indicates that atoms are present at x_1,y_1,z_1 and x_2,y_2,z_2 in the crystal such that :

$u = x_1 - x_2$

$v = y_1 - y_2$

$w = z_1 - z_2$

A unit cell containing N atoms will have $(N^2-N)/2$ independent Patterson peaks, excluding the intense peak at the origin. Since the cell of the Patterson synthesis is of the same size as that of the crystal, the peaks are obviously much more densely packed and they overlap each other.

This can be minimized by using "Sharpened Structure Factors" (where atoms are considered as point scatterers.

$$(Fsharp)^2_{hkl} = \frac{[0.1667+(\sin^2\theta/\lambda^2)]\,[F_{obs}]^2_{hkl}}{[\Sigma f_{oj} e^{-B(\sin^2\theta/\lambda^2)}]} \qquad \text{---(III-3-10-30)}$$

The term 'B' is the average thermal parameter, and 'f_{oj}' is the mean atomic scattering factor of the j^{th} atom. The weight of the Patterson peak depends upon the product of the atomic numbers of atoms defining the vectors. The major significance of this peak height relationship is that the vectors between like heavy atoms appear with weights corresponding to the square of their atomic numbers, and they may be very prominent against the background of heavy-light and light-light atom vectors. If the asymmetric unit contains few heavy atoms, their location is straightforward. However, if the structure is more complex then with or without heavy atoms it will be more difficult to assign peaks to specific vectors.

(ii) DIRECT METHODS [27]

In the early days of its development, direct methods were limited almost entirely to centrosymmetric space groups. Phasing consisted of assigning a plus or minus sign to each observed structure amplitude. However, the phase solution of non-centrosymmetric crystals by direct methods is now becoming quite common. Sayre (1952) [28] described a method which

provides the basis for the routine application of direct methods for the case of centrosymmetric crystals.

$S(F_{hkl}) \sim S(F_{h'k'l'}).S(F_{h-h',k-k',\ l-l'})$ -------- (III-3-10-31)

or

$S(F_{hkl}).\ S(F_{h'k'l'}).S(F_{h-h',k-k',\ l-l'}) \sim +1$ ------ (III-3-10-32)

where,'S' means sign and '~' means probably equal to:

The same result is also obtained from the equation of Karle [29]

$$S(E_A) = S\left(\sum_{A=B+C} E_B.\ E_C\right) \qquad \text{---------- (III-3-10-33)}$$

Here, 'S' means 'sign of'; A,B,C, are the vectors (hkl) for reflections A,B,C; E_A, E_B, E_C are the normalized structure factor for reflections A, B, C. The normalized structure factor is defined as:

$$E_h = F_h / \in [\sum f^2{}_j h]^{1/2} \qquad \text{---------- (III-3-10-34)}$$

'F_h' is the structure factor for reflection h; N is the total number of atoms in the unit cell. '$f_j h$' represents the atomic scattering factor for the j^{th} atom for the value of associated with h and $\in$ is a "statistical fudge factor" adjusting for the degeneracy in F for reflections at symmetry locations in reciprocal space. A typical

procedure, the one used in MULTAN, is as follows :

A list of both observed and calculated values of E vs 2θ is obtained. The E's are scaled in such a way that the mean $E^2 = 1$. All the strong reflections are chosen which have the value of E greater than a specified value. In addition some of the weakest reflections are also chosen All strong triples h, k, l; h', k', l'; h-h', k-k', l-l' (called $\sum^2$ relationships) are found within this set, plus those for the weak hkl's where the other two reflections are strong. This weak group is known as the ϕ_o reflections.

Phases are assigned to origin defining reflections (usually three) and "arbitrary" phases to a small number of other reflections with high E values. This set of "starting phases" can then be extended using $\sum^2$ relationships with high probability, until all reflections have been phased. This extension may not be correct however, as indicated by measures of statistical consistency. In this case other "arbitrary" phases can be assigned and the procedure repeated. Even when many attempts are made some structures fail to yield sensible solutions.

III-3-11 LSTSQ REFINEMENT THEORY [30]

The structure factor for a particular reflection hkl is calculated using

$$F_c = \sum f^c_{oj} e^{-2B_j(\sin^2\theta/\lambda^2)} e^{2\pi i(hx_j+ky_j+lz_j)} \quad \text{-------} \quad \text{(III-3-11-35)}$$

where

F_C = calculated structure factor

f^C_{oj} = free atom scattering factor of the j^{th} atom

x,y,z = positional co-ordinates

B_j = isotropic thermal parameters

For anisotropic vibration,'B' is replaced by six parameters and 'f' is given by the equation:

$$f= f_{oj}e^{-(\beta_{11}h + \beta_{22}k + \beta_{33}l +2\beta_{12}hk + 2\beta_{13}hl + 2\beta_{23}kl)} \text{ --}$$

----- (III-3-11-36)

The equation represents the amplitude and direction of vibration as an ellipsoid. An equivalent and preferable expression for the temperature factor argument is :

$$[-2\pi^2U_{11}h^2a^*+U_{22}k^2b^*+U_{33}l^2c^*+U_{12}hka^*b^*+U_{13}hla^*c^*+U_{23}klb^*c^*]$$

----- (III-3-11-37)

Here, 'U' represents the thermal parameter expressed in terms of mean square amplitude of vibration in Å.

Free electron scattering factors are corrected for relativistic effects before use in the structure factor calculations. Due to the very fast movement of the core electrons, the scattered x-ray photons are out of phase with the incident

photons. Thus scattering is considered as inelastic to a significant degree. These corrections are significant in the case of 'heavy atoms' and take the form of a real 'Δf' and imaginary "Δf" known as dispersion correction.

$$f^{c}_{oj} = f_{oj} + \Delta f_{oj}' + i\Delta f_{oj}'' \quad \text{--------} \quad \text{(III-3-11-38)}$$

Each atom requires positional and thermal parameters as expressed by the eq. III-3-11-35. The parameters are optimized by minimizing the differences 'D' between the observed $|F_{obs}|$ and calculated $|F_c|$ structure factors.

$$D = w_{hkl} (|F_{obs}| - |KF_c|) \quad \text{------} \quad \text{(III-3-11-39)}$$

where

k = scale factor for F_c and $w_{hkl} = 1/\sigma^2(F_{hkl})$

and $\sum D$ is to be minimized.

The differential of the equation III-3-11-39, with respect to each of the parameters is set to zero. The equations obtained are non-linear and use of a truncated Taylor series is required. Thus 'n' linear equations in parameter shifts, ΔPn are obtained and can be expressed in the form of matrix. In case where a large number of parameters are refined, the use of block diagonal matrix may

be necessary. In the anisotropic case nine parameters are involved per atom : six thermal and three positional parameters. More cycles are required for the block diagonal Least-Square method than with full matrix to reach convergence.

The correctness and degree of refinement of the strcture are related to the residual factor 'R_f' also known as the "discrepancy factor".

$$R_f = \Sigma \left| |F_{obs}| - |F_{cal}| \right| / \Sigma |F_{obs}| \quad \text{------- (III-3-11-40)}$$

$$R_w = \Sigma w |F_{obs}| - |F_{cal}| / \Sigma |F_{obs}| \quad \text{------ (III-3-11-41)}$$

where R_w = weighted R factor

The lowest value of 'R_f' and 'R_w' corresponds to the best fit. Usually, refinement is stopped when the parameter shifts are less than some fraction (e.g.1/10) of the standard deviation of the parameters.

III-3-12 Structural Study of $Fe(O=PPh_2(2\text{-}Py))_3^{2+}\cdot 2BF_4^-$

Single crystals of complex (21) were obtained after a number of unsuccessful trials. Crystals were very small therefore CuKα radiation was used to obtain as much diffraction data as possible. The purpose of this structure determination was to find only the coordination around the iron atom.

(i) Crystal Data and Refinement

Single crystals of $Fe(O=PPh_2(2\text{-}Py))_3^{2+}.2BF_4^-$ (21) were obtained by crystallization in CH_2Cl_2-toluene. The crystal selected was 0.05x0.10x0.2 mm in dimension. CuKα radiation was used. Crystal data and refinement indicators are presented in appendix (p-236).

A total of 10975 reflections were measured out of which 10965 reflections were unique and 2968 reflections were considered to be significant with $I_{net} > 2.5\ \sigma(I_{net})$. No correction was made for the absorption effect (μ = 3.85 mm^{-1}). The cell parameters were derived from the angular settings of 30 strong reflections in the 2θ range 60.0-80.0°. The residual factors converged to R_f = 0.097, R_w = 0.047, this was sufficient to establish the chemical identity of the compound.

(ii) Description of the Structure

The bond distances and angles of complex (21) are presented in Table III-3-12-1(p-97). A perspective drawing of the molecule with the numbering scheme is presented in Fig

III-3-12-1(p-96). Fractional coordinates are presented in appendix (p-237). The coordination around the dipositive iron cation is octahedral with the following average bond lengths and angles : <Fe-O> = 2.099(5)Å , <P-O> = 1.508(17)Å, <Fe-N> = 2.247(4)°, <Fe-O-P> = 118.4(36)°. The angular disposition of ligands about the iron deviates little from the ideal with the *cis* -angles ranging from 77-98° and the*trans*-angles from 162-172°. The <P-O> bond distance (1.508(17)Å) is also within the range of distances found for the closely related triphenylphosphine oxide ligand bound to transition metals (see for example the data in Table V of reference [10]). As expected, coordination to a metal causes this distance to be longer than that found in free triphenylphosphine oxide, whose P-O is 1.46(1)Å [31]. The tetrahedral coordination around the phosphorus atom is fairly close to a regular geometry with the angles ranging from 105.0(5)° to 115.3(6)°. The phenyl rings are nearly perfectly planar and there are no significant departures from the expected structural parameters.

The most interesting feature of this structure is the chelation of three phosphine oxides to the metal and degree of bending of Fe-O-P unit, which is necessary to form a chelate ring. The degree of variability in the M-O-P angle (180-118°) is presented in Table V of ref [10]. It was observed that there is no correlation between the M-O-P angles and P-O bond distance,

angle. The other angles and distances within the chelate rings are normal. The <Fe-O> bond length of 2.099(5)Å is in the range of other iron complexes [32, 33].

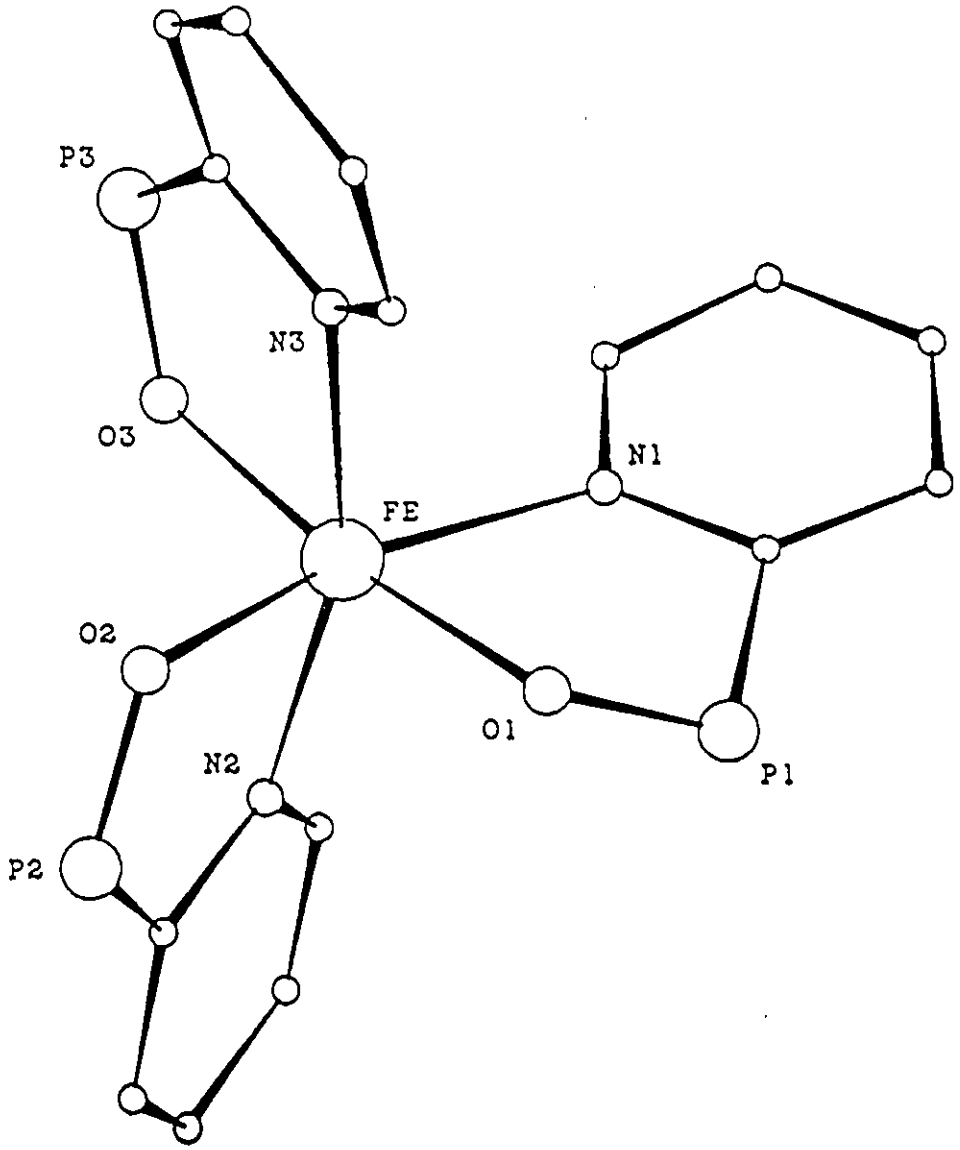

Fig. III-3-12-1

A perspective drawing of the $Fe(O=PPh_2(2\text{-}Py))_3^{2+}.2BF_4^-$ **(21)** with the numbering scheme (The phenyl substituents and the BF_4^- anions have been omitted for clarity)

Table III-3-12-1

Selected bond distances (Å) and angles (°) of

$Fe(O{=}PPh_2(2\text{-}Py))_3^{2+}{\cdot}2BF_4^-$

Bond Distances			
Fe-N1	2.294(2)	Fe-N2	2.205(2)
Fe-N3	2.244(5)	Fe-O1	2.063(8)
Fe-O2	2.157(8)	Fe-O3	2.079(8)
P1-O1	1.488(4)	P2-O2	1.521(5)
P3-O3	1.514(4)	N1-C11	1.337(2)
N1-C15	1.338(2)	N2-C41	1.371(2)
N2-C45	1.289(2)	N3-C71	1.354(2)
N3-C75	1.281(2)		

Bond angles			
N1-Fe-O1	77.31(3)	N1-Fe-N3	97.52(3)
N2-Fe-O1	95.82(4)	N2-Fe-O2	83.02(3)
O2-Fe-O3	98.05(3)	O3-Fe-N3	80.34(3)
N1-Fe-N2	96.61(3)	N1-Fe-O3	96.15(4)
N2-Fe-O3	88.75(3)	N3-Fe-O1	97.56(4)
N3-Fe-O2	85.74(4)	O1-Fe-O2	87.94(4)
N2-Fe-N3	162.80(3)	N1-Fe-O2	165.13(3)
O3-Fe-O1	172.05(3)	Fe-O1-P1	120.96(5)
Fe-O2-P2	114.33(5)	Fe-O3-P3	120.15(5)

III-3-13 Structural study of $Co(NO)_2(PPh_2(2\text{-}Py))I$

The crystal structure of this complex was solved only to see whether diphenyl(2-pyridyl)phosphine ligand is coordinated to the metal with its P or N donor sites.

(i) Crystal data

Single crystals of $Co(NO)_2(PPh_2(2\text{-}Py))I$ **(8)** were grown under argon by slow diffusion of an upper layer of hexane into a concentrated solution of the complex in CH_2Cl_2. The crystal studied was brown in colour with cell dimension 0.10x0.10x0.30 mm. The crystal data and refinement indicators are presented in appendix (p-238).

A total of 4248 reflections were measured out of which 2497 were unique and 1980 were considered to be significant with $I_{net} > 3.0\ \sigma\ (I_{net})$. The cell parameters were obtained using least-squares refinement of the setting angles of 30 reflections ($40 < 2\theta < 45°$). The final residual factor converged to $R_f = 0.052$ and $R_w = 0.045$ with GOF of 1.87.

(ii) Description of the structure

In $Co(NO)_2(PPh_2(2\text{-}Py))I$, the ligand $PPh_2(2\text{-}Py)$ is coordinated to the cobalt atom through its P atom. A perspective view of the molecule with the numbering scheme is presented in Fig. III-3-13-2 (p-100). Bond distances and angles of interest are presented in Table III-3-13-2 (p-101). Fractional coordinates and thermal parameters are presented in appendix (p-239) and

(p-240). The geometry around the cobalt atom was found to be pseudotetrahedral. The smallest interligand angle about cobalt is the P-Co-I angle at 100.48(5)°, and the largest is the N1-Co-N2 angle at 126.90(3)°. The atoms N1 and N2 are displaced more towards the P atom away from the I atom. This is presumably caused by the larger effective size of the large iodine atom. The two nitrosyl ligands are linearly bonded to metal with <M-N-O> angle of 169.65(9)°. The Co-P and Co-N bond lengths of 2.252(2)Å and 1.632(7)Å respectively, compares well with other cobalt phosphine complexes as shown in Table III-3-16-9 (p-140).

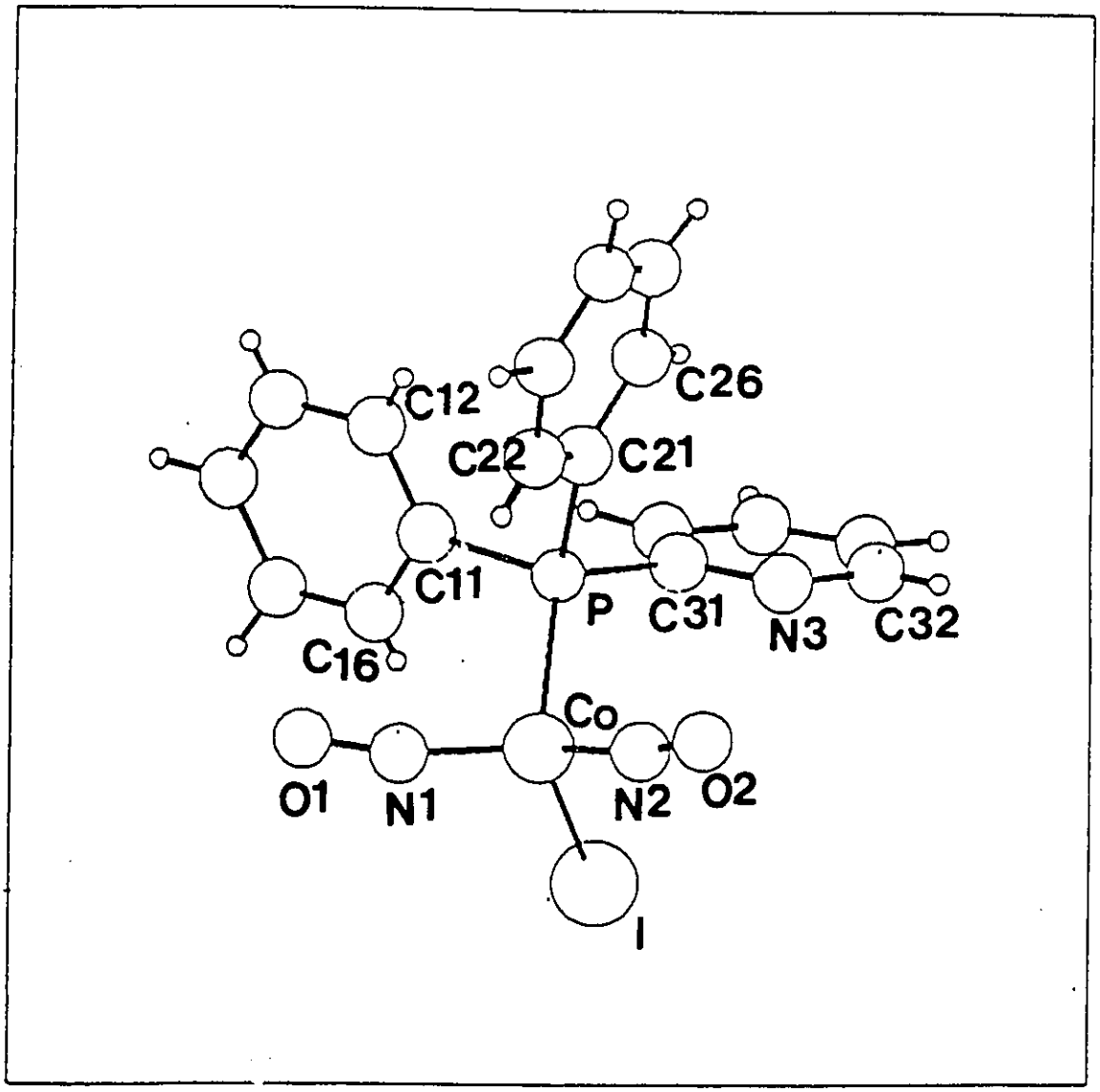

Fig. III-3-13-2

A perspective drawing of the $Co(NO)_2(PPh_2(2\text{-}Py))I$ **(8)**

Table III-3-13-2

Bond distances (Å) and angles (°) with esd's for $Co(NO)_2(PPh_2(2\text{-}Py))I$

Bond distances

Cc-N(1)	1.640(6)	Co-N(2)	1.625(7)
Co-I	2.578(6)	Co-P	2.252(2)
N(1)-O(1)	1.156(8)	N(2)-O(2)	1.130(6)
N(3)-C(31)	1.337(8)	N(3)-C(32)	1.352(6)
P-C(11)	1.820(6)	P-C(21)	1.806(5)
P-C(31)	1.820(6)	C(11)-C(12)	1.365(6)
C(11)-C(16)	1.377(2)	C(12)-C(13)	1.367(2)
C(12)-H(12)	0.760(6)	C(13)-C(14)	1.355(2)
C(13)-H(13)	0.780(6)	C(14)-C(15)	1.382(2)
C(14)-H(14)	0.950(7)	C(15)-C(16)	1.354(2)
C(15)-H(15)	0.93(7)	C(16)-H(16)	0.620(6)
C(21)-C(22)	1.375(8)	C(21)-C(26)	1.380(8)
C(22)-C(23)	1.369(2)	C(22)-H(22)	0.790(5)
C(23)-C(24)	1.365(2)	C(23)-H(23)	1.170(7)
C(24)-C(25)	1.379(2)	C(24)-H(24)	1.010(6)
C(25)-C(26)	1.367(2)	C(25)-H(25)	0.950(7)
C(26)-H(26)	0.780(7)	C(31)-C(35)	1.367(6)
C(32)-C(33)	1.378(2)	C(32)-H(32)	0.840(7)
C(33)-C(34)	1.323(2)	C(33)-H(33)	0.980(6)
C(34)-C(35)	1.401(6)	C(34)-H(34)	0.990(6)
C935)-H(35)	0.950(6)		

Bond angles

N(1)-Co-N(2)	126.90(3)	P-C(21)-C(22)	120.30(4)
N(1)-Co-I	109.40(2)	P-C(21)-C(26)	121.90(5)
N(1)-Co-P	101.37(2)	C(22)-C(21)-C(26)	117.70(6)
N(2)-Co-I	109.42(3)	C(21)-C(22)-C(23)	121.70(6)
N(2)-Co-P	105.62(2)	C(21)-C(22)-H(22)	116.00(3)
I-Co-P	100.48(5)	C(23)-C(22)-H(22)	121.00(3)
Co-(N1)-O(1)	169.00(5)	C(22)-C(23)-H(24)	119.90(7)
Co-(N2)-O(2)	170.30(7)	C(22)-C(23)-H(23)	116.00(3)
C(31)-N(3)-C(32)	116.60(6)	C(24)-C(23)-H(23)	123.00(3)
Co-P-C(11)	112.05(2)	C(23)-C(24)-H(25)	119.60(7)
Co-P-C(21)	113.76(2)	C(23)-C(24)-H(24)	120.00(3)
Co-P-C(31)	115.93(2)	C(25)-C(24)-H(24)	119.00(3)
C(11)-P-C(21)	103.90(3)	C(24)-C(25)-H(26)	120.00(7)
C(11)-P-C(31)	106.30(3)	C(24)-C(25)-H(25)	127.00(4)
C(21)-P-C(31)	103.79(2)	C(26)-C(25)-H(25)	112.00(4)
P-C(11)-C(12)	122.60(5)	C(21)-C(26)-C(25)	121.20(7)
P-C(11)-C(16)	119.70(5)	C(21)-C(26)-H(26)	122.00(5)
C(12)-C(11)-C(16)	117.70(6)	C(25)-C(26)-H(26)	115.00(5)
C(11)-C(12)-C(13)	120.50(7)	N(3)-C(31)-P	113.60(4)
C(11)-C(12)-H(12)	122.00(5)	N(3)-C(31)-C(35)	123.00(5)
C(13)-C(12)-H(12)	117.00(5)	P-C(31)-C(35)	123.40(5)
C(12)-C(13)-C(14)	121.10(8)	N(3)-C(32)-C(33)	122.90(7)
C(12)-C(13)-H(13)	118.00(5)	N(3)-C(32)-H(32)	112.00(4)

C(14)-C(13)-H(13)	120.00(5)	C(33)-C(32)-H(32)	124.00(4)
C(13)-C(14)-C(15)	119.50(7)	C(32)-C(33)-C(34)	119.70(7)
C(13)-C(14)-H(14)	119.00(4)	C(32)-C(33)-H(33)	115.00(4)
C(15)-C(14)-H(14)	121.00(4)	C(34)-C(33)-H(33)	124.00(4)
C(14)-C(15)-C(16)	118.70(8)	C(33)-C(34)-C(35)	119.20(7)
C(14)-C(15)-H(15)	119.00(4)	C(33)-C(34)-H(34)	123.00(3)
C(16)-C(15)-H(15)	120.00(5)	C(35)-C(34)-H(34)	117.00(3)
C(11)-C(16)-C(15)	122.50(8)	C(31)-C(35)-C(34)	118.50(7)
C(11)-C(16)-H(16)	117.00(6)	C(31)-C(35)-H(35)	120.00(3)
C(15)-C(16)-H(16)	119.00(6)	C(34)-C(35)-H(35)	120.00(3)

III-3-14 Structural study of $Co(NO)_2(PPh_2(2\text{-}Py))_2^+BF_4^-$

(i) Crystal Data and Refinement

Single crystals of complex $Co(NO)_2(PPh_2(2\text{-}Py))_2^+BF_4^-$, **(9)** were grown under argon at 20°C by slow diffusion of an upper layer of toluene into a concentrated solution of the complex in CH_2Cl_2. The crystal studied was brown in color with dimensions 0.10x0.10x0.30 mm. Crystal data and refinement indicators are presented in appendix (p-241).

A total of 5909 reflections were measured out of which 4325 were unique reflections and 2754 were considered to be significant with $I_{net} > 2.5\ \sigma(I_{net})$. No correction was made for the absorption effect (μ = 2.76 mm^{-1}). The cell parameters were obtained using least-squares refinement of the setting angles of 25 reflections ($20° < 2\theta < 25°$). The residual factors converged to R_f = 0.038, R_w = 0.039 with GOF = 1.37.

(ii) Description of the structure

Complex $Co(NO)_2(PPh_2(2\text{-}Py))_2^+BF_4^-$ **(9)** consists of discrete cobalt cations $Co(NO)_2(PPh_2(2\text{-}Py))_2^+$ and ordered BF_4^- anions. Two independent molecules of $Co(NO)_2(PPh_2(2\text{-}Py))_2^+BF_4^-$ represented by A and B crystallize in the unit cell. The asymmetric unit contains only one half of each cation and anion due to the presence of a two-fold axis.

An ORTEP drawing of cations A and B with the numbering scheme is shown in Fig. III-3-14-3 (p-107). Stereoviews of

cation B and of the unit cell contents are presented in Fig. III-3-14-4 (p-108) and Fig. III-3-14-5 (p-108), respectively. Selected bond lengths and angles for molecules A and B are presented in Table III-3-14-3 (p-109). Fractional coordinates and thermal parameters are presented in appendix (p-242). Table III-3-14-4 (p-111) presents a comparison of the bond distances and angles of $Co(NO)_2(PPh_2(2\text{-}Py))_2^+BF_4^-$ with the triphenylphosphine analogues. The geometry around each cobalt atom in both molecules A and B is pseudotetrahedral. The cobalt atom is coordinated with two P atoms of the aminophosphines and two N atoms of the nitrosyl ligands. The most interesting feature of this structure is the difference between the two independent molecules A and B. These differences are in the disposition of the pyridyl rings and the angular deformation of the $M(NO)_2$ moities. In molecule A, the dihedral angle between P-Co-P and N-Co-N planes is 87.8(2)° which is close to the ideal value of 90°, whereas, in molecule B it is 79.5(2)° which is one of the lowest values found for pseudotetrahedral $M(NO)_2(L)_2^x$ (x = +1, 0) complexes shown in Table III-3-14-4 (p-111). The Co-N, N-O, and Co-P bond lengths compare well with the equivalent distances in the PF_6^- and ClO_4^- derivatives of $Co(NO)_2(PPh_3)_2^+$.

The differences between molecules A and B are the disposition of the pyridyl ring. In molecule B the pyridyl rings are arranged in such a way that they are parallel to each other and

are in an eclipsed conformation, whereas, this type of arrangement is not observed in molecule **A**. The pyridyl rings of the two independent molecules differ from each other in their bond lengths and angles. The C-N bond lengths of 1.339(6)Å and 1.340(7)Å in molecule **B** are significantly shorter than the C-C bonds (average = 1.370(6)Å [34]. The same is found in the solid state structure of the PPh_2(2-Py) in an uncoordinated form (C-N = 1.342(5), 1.343(3)Å, <C-C> = 1.374(11)Å [35], which also has a P-C-N(Py) angle of 111.7(2)° identical to that found for **B**.

On the other hand, the C-N bond lengths of 1.370(6)Å and 1.366(8)Å for molecule **A**, are significantly longer and the P-C-N(Py) angle opens up by 5° to 116.9(3)° which can be accounted for by the disposition of the pyridyl rings.

The most significant structural change from molecule **A** to molecule **B** involves the M-N-O linkages. In molecule **A** the Co-N-O angle is 178.4(4)° whereas, in molecule **B** it is 172.9(4)°. The measurement of the M-N-O (γ) angle in a $M(NO)_2$ moiety will be described in Part IV of the thesis taking into account the in-plane and out-of-plane bending of a nitrosyl ligand respectively in and out of the NMN plane.

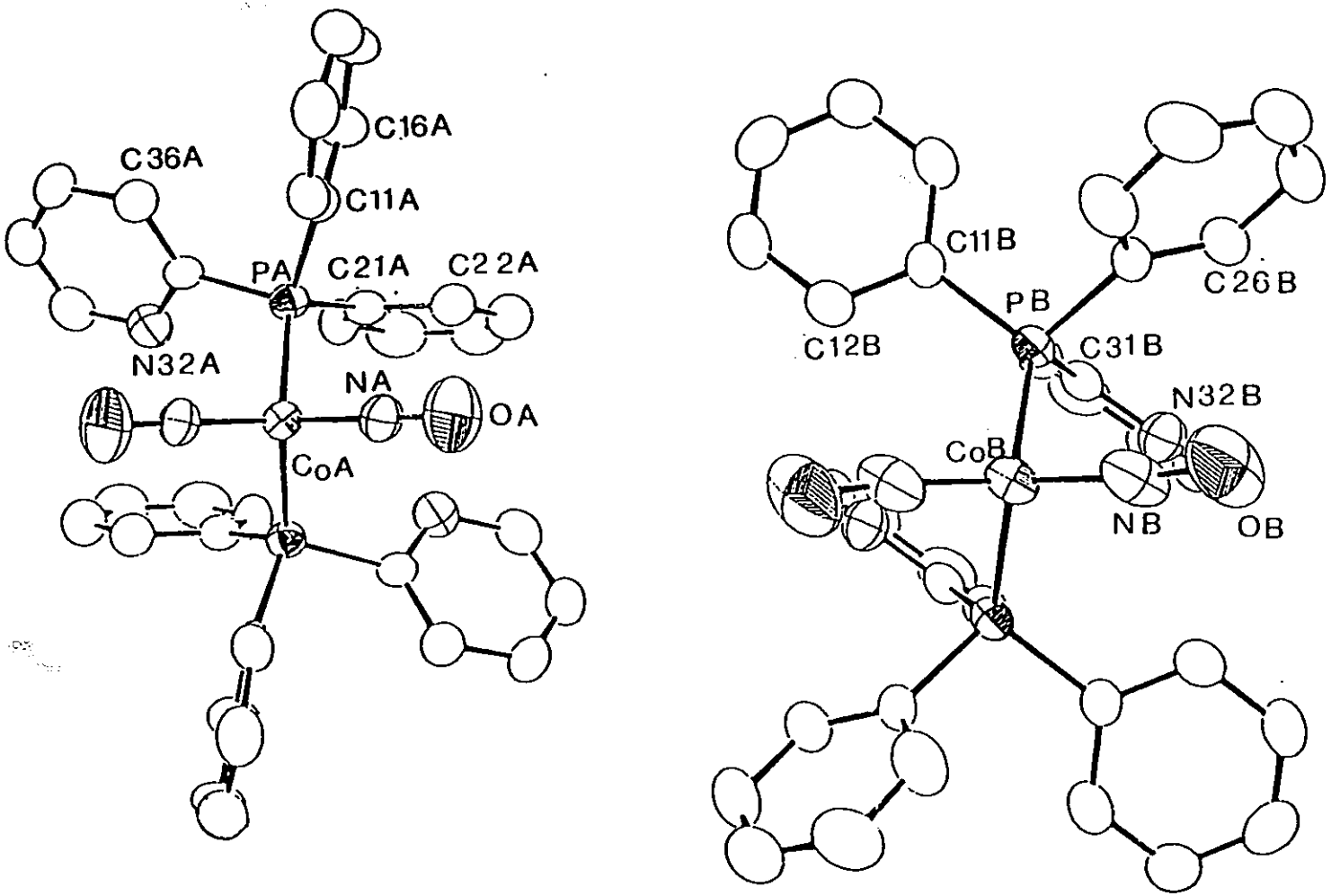

Fig. III-3-14-3

An ORTEP drawing of the two independent cations A and B of $Co(NO)_2(PPh_2(2\text{-}Py))_2^+$ with numbering scheme . The molecules are on a crystallographic two fold axis.

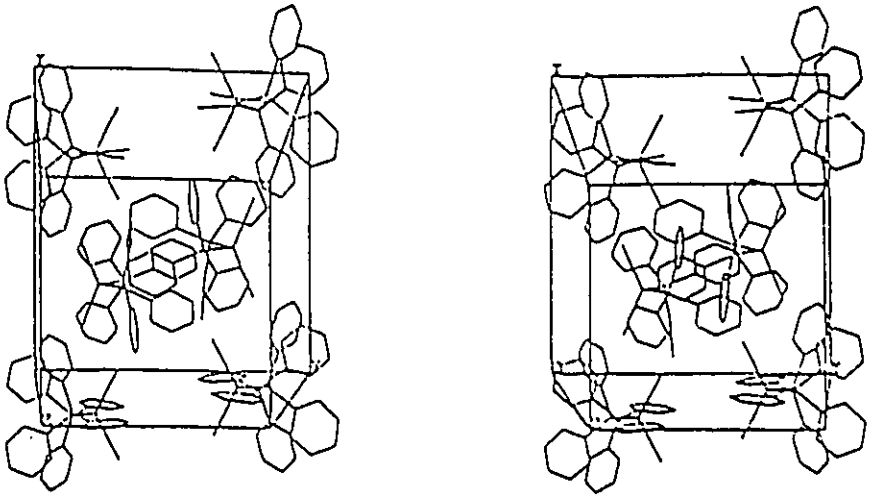

Fig. III-3-14-4 Stereoview of the unit cell of cation $Co(NO)_2(PPh_2(2\text{-}Py))_2^+$

(For clarity BF_4^- is omitted)

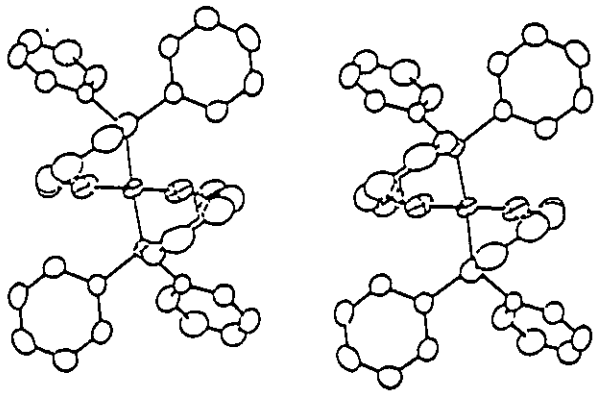

Fig. III-3-14-5 Stereoview of cation $Co(NO)_2(PPh_2(2\text{-}Py))_2^+$ of molecule B

Table III-3-14-3

Selected distances (Å) and angles(°) with esd's in the two independent molecules A and B of $Co(NO)_2(PPh_2(2\text{-}Py))_2^+.BF_4^-$

Molecule A		Molecule B	
Bond Distances			
Co(A)-P(A)	2.275(2)	Co(B)-P(B)	2.264(2)
Co(A)-N(A)	1.637(5)	Co(B)-N(B)	1.652(5)
N(A)-O(A)	1.146(6)	N(B)-O(B)	1.144(7)
P(A)-C(11A)	1.818(4)	P(B)-C(11B)	1.812(5)
P(A)-C(21A)	1.818(5)	P(B)-C(21B)	1.818(5)
P(A)-C(31A)	1.821(5)	P(B)-C(31B)	1.827(4)
C(31A)-N(32A)	1.370(6)	C(31B)-N(32B)	1.339(6)
N(32A)-C(33A)	1.366(8)	N(32B)-C(33B)	1.340(7)
B(A)-F(1A)	1.327(7)	B(B)-F(1B)	1.335(6)
B(A)-F(2A)	1.324(7)	B(B)-F(2B)	1.376(7)
Bond Angles			
P(A)-Co(A)-P(A)'	108.97(6)	P(B)-Co(B)-P(B)'	107.09(6)
N(A)-Co(A)-N(A)'	126.1(2)	N(B)-Co(B)-N(B)'	131.8(2)
Co(A)-N(A)-O(A)	178.4(4)	Co(B)-N(B)-O(B)	172.9(4)
P(A)-Co(A)-N(A)	103.6(2)	P(B)-Co(B)-N(B)	96.3(2)
P(A)-Co(A)-N(A)'	107.0(2)	P(B)-Co(B)-N(B)'	112.1(2)
Co(A)-P(A)-C(11A)	109.9(2)	Co(B)-P(B)-C(11B)	117.9(2)
Co(A)-P(A)-C(21A)	116.6(2)	Co(B)-P(B)-C(21B)	108.3(2)
Co(A)-P(A)-C(31A)	112.6(1)	Co(B)-P(B)-C(31B)	114.2(1)
C(11A)-P(A)-C(21A)	105.5(2)	C(11B)-P(B)-C(21B)	103.6(2)
C(11A)-P(A)-C(31A)	102.3(2)	C(11B)-P(B)-C(31B)	106.6(2)
C(21A)-P(A)-(C31A)	108.7(2)	C(21B)-P(B)-C(31B)	104.9(2)
P(A)-C(31A)-N(32A)	116.9(3)	P(B)-C(31B)-N(32B)	111.7(3)

P(A)-C(31A)-C(36A)	121.6(4)	P(B)-C(31B)-C(36B)	124.9(4)
C(31A)-N(32A)-C(33A)	117.6(4)	C(31B)-N(32B)-C(33B)	117.1(4)
N(32A)-C(31A)-C(36A)	121.2(5)	N(32B-C(31B)-C(36B)	123.3(4)
N(32A)-C(33A)-C(34A)	121.8(5)	N(32B)-C(33B)-C(34B)	122.9(6)

	Range (<average> b)		
C-C	1.348(7)-1.391(6) (1.369[14])	C-C	1.343(5)-1.390(7) (1.372[14])
P-C-C	117.6(4)-121.6(4) (120.5[18])	P-C-C	117.1(4)-124.9(4) (121.7[32])
C-C-C	118.3(4)-121.2(6) (119.9[8])	C-C-C	118.2(5)-120.9(6) (119.8[10])
F-B-F	103.1(7)-114.1(7) (109[5])	F-B-F	103.9(7)-113.9(7) (109[4])

Selected intra and intermolecular van der waals contacts in Å

P(A)·····N(32A)	2.73(5)
P(B)·····N(32B)	2.63(4)
N(A)·····N(A)'	3.92(9)
N(B)·····N(B)'	3.02(11)
N(A)·····P(A)	3.10(4)
N(B)·····P(B)	2.95(4)
N(A)·····P(A)'	3.17(4)
N(B)·····P(B)'	3.27(5)
O(B)·····C(33A)'	2.99(7)
O(A)·····O(B)	3.06(8)
O(B)·····C(34A)'	3.16(7)

Table III-3-14-4

Angular deformations(°) in selected M(NO)(XO) (X=N,CO) molecular fragments

$M(NO)_2(L)_2{}^nA^-$				Dihedral	M-N-O	γ^i/γ^o	N-M-N	O ···M ···O	[Ref]
M	L	n	A^-	Angle(b)	(γ)				
Co	PN	+1	BF_4^-	87.8	178.4(4)	179.2/1.3	126.1(2)	125.5	[TW]
Co	PN	+1	BF_4^-	79.5	172.9(4)	183.4/6.3	131.8(2)	134.6	[TW]
Co	PPh_3	+1	ClO_4^-	NA	171.2(3)	NA/NA	132.4(1)	134.6	[36]
					171.1(3)				
Co	PPh_3	+1	PF_6^-	87.9	171.0(5)	188.8/1.8	136.7(4)	144.0	[37]
Co	DPP	+1	PF_6^-	88.0	176.6(14)	182.7/2.1	131.7(5)	135.9	[38]
					172.3(11)	187.7/0			
Co	$P(OMe)_3$	+1	BPh_4^-	87.3	177.0(13)	182.8/1.2	128.0(8)	129.2	[39]
					179.7(12)	179.9/0.3			
Co	Py	+1	BF_4^-	89.3	170.2(6)	170.3/1.5	115.6(3)	107.6	[40]
					170.7(6)	171.0/1.7			
Co	Py	+1	BF4-	89.2	170.7(6)	170.8/1.4	115.9(3)	107.7	
					169.1(7)	169.2/1.4			
Co	SacSac	0	---	90.0	168.9(5)	169.0/1.1	115.5(3)	106.6	[35]

Co	PPh_3	0	I^-	88.8	165.2(22)	174.9/13.9	121.73(11)	115.09	[36]
					163.3(22)	170.9/1.4			
Rh	PPh_3	+1	ClO_4^-	86.0	158.9(14)	200.9/2.6	157.5(3)	173.7	[41]
Ir	PPh_3	+1	ClO_4^-	85.7	163.5(10)	196.4/1.4	154.2(2)	167.5	[42]
Ir	NO,CO,PPh_3		----	84.3	174.1(17)	182.1/5.5	128.7(2)	128.8	[43]
					177.8(9)	178.0/1.1			

(a) Values indicated are taken from the references quoted. All the others, except otherwise stated have been caculated from the data available in the literature.

TW = this work; NA = not available ; PN = diphenyl(2-pyridyl)phosphine; Py = pyridine; DPP = diphenyl phosphine; $P(OMe)_3$ = trimethyl phosphite; SacSac = dithioacetylacetanato; γ^i = in-plane bending of the M-N-O (γ) angle γ^o = out-of-plane bending of the M-N-O (γ) angle (See Part IV of the thesis for full description) . (b) Dihedral angle is that between the P-M-P and N-M-N planes.

III-3-15 Structural Study of $Co(NO)_2(Py)_2^+BF_4^-$

(i) Crystal Data and Refinement

Single crystals of $Co(NO)_2(Py)_2^+BF_4^-$ (10) were grown by slow diffusion of an upper layer of toluene into a concentrated solution of $Co(NO)_2(Py)_2^+BF_4^-$ in CH_2Cl_2. The crystal studied was dark brown with dimensions 0.15x0.15x0.30 mm. It was mounted on a glass rod and subsequently coated with a protective layer of epoxy resin. Crystal data and refinement indicators are presented in appendix (p-243).

The intensities were measured at 296K with $2\theta_{max} = 45°$ and graphite monochromatized MoKα radiation on an Enraf-Nonius CAD-4 diffractometer. A total of 6038 reflections were measured which reduced to 3820 unique reflections. Among these 2225 reflections have $I_{net} > 2.5\ \sigma(I_{net})$. Lorentz and polarization corrections were applied, but no absorption correction was made ($\mu = 1.21 mm^{-1}$). The cell parameters were derived from the angular settings of 45 strong reflections with $40° < 2\theta < 45°$ using MoKα1 ($\lambda = 0.70926$Å). The positions of the heavy atoms were located using MULTAN . Difference Fourier maps revealed the positions of all the other atoms including hydrogen. Refinement by full-matrix least-squares on all atoms, with fixed isotropic thermal motion for hydrogen and anisotropic motion for the others and including extinction correction, converged to $R_f = 0.054$ and $R_w = 0.023$ with GOF = 2.462. The largest shift was 0.1σ in the final cycle and the highest residual electron density

was 0.47e/Å^3.

(ii) Description of the Structure

The crystal consists of discrete $Co(NO)_2(Py)_2^+$ cations and BF_4^- anions. No unusual intramolecular Van der Waals contacts were observed. A perspective view of the molecule is presented in Fig. III-3-15-6 (p-116), together with the numbering scheme. A stereo representation of the unit cell contents is shown in Fig.III-3-15-7 (p-117) and a summary of selected bond lengths and angles is given in Table III-3-15-5 (p-120). The fractional coordinates and thermal parameters are given in appendix (p-244). The compound crystallizes with two independent molecules A and B in the asymmetric unit. The geometry around each cobalt atom was found to be distorted tetrahedral and it is coordinated to the two pyridine and two nitrosylic N atoms. The (Py)N-Co-N(Py) and (O)N-Co-N(O) planes are perpendicular to each other as shown by the dihedral angles of 89.3(3)° for molecule A and 89.2(3)° for molecule B. A composite structure of the pyridine ligand with distances and angles are given in Fig. III-3-15-8 (p-117). The results are comparable to several other pyridine complexes [18]. The cobalt atoms are slightly distorted out of the pyridine mean plane (range 0.04(2)-0.15(2)Å). The Co-N(Py) bond lengths are 2.012(6)Å (CoA-N1A; CoA-N2A) for molecule A and 2.013(6)Å (CoB-N1B) and 2.016(6)Å (CoB-N2B) for molecule B. They fall near the lower range of values reported for Co-N(Py) bond lengths which can vary by as much as 0.2Å as

shown by the values of 1.917(2)Å and 2.203(10)Å for complexes (η5-C_5H_5)CoCl(Py) [19] and $Co_2(DBA)_2(Py)_4$ [44] respectively (DBA = 1,5-diphenyl 3,5 -pentane-trionato).

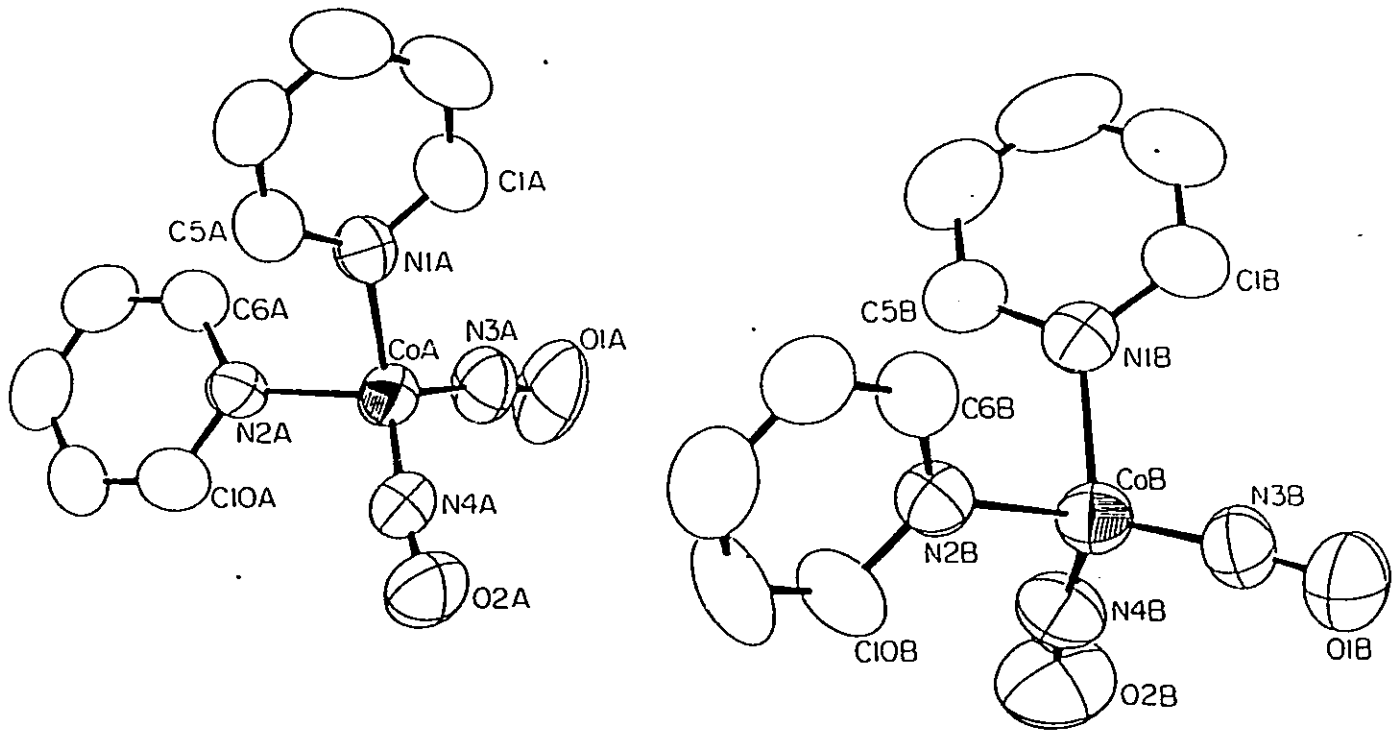

Fig. III-3-15-6

A perspective view of $Co(NO)_2(Py)_2^+BF_4^-$ with numbering scheme.

(For clarity BF_4^- is omitted)

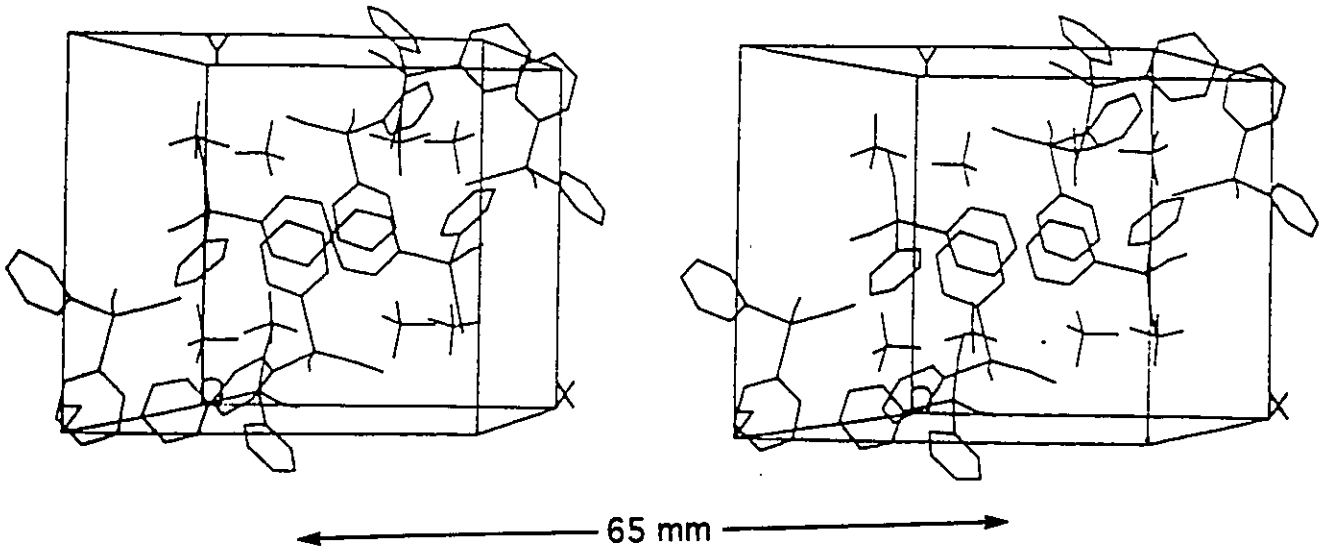

Fig. III-3-15-7 A representation of a stereopairs of the $Co(NO)_2(Py)_2^+BF_4^-$ molecule

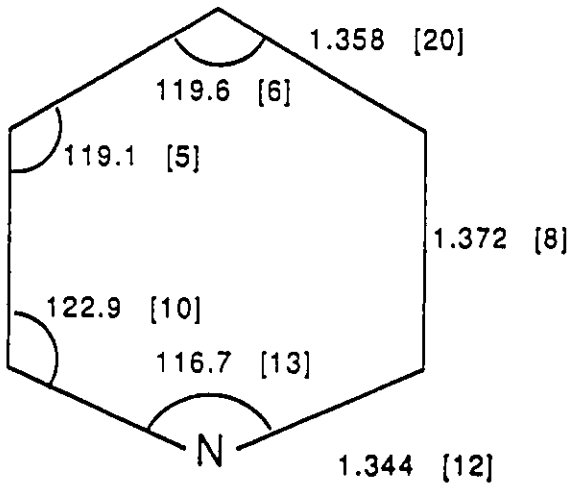

Fig. III-3-15-8 A Composite structure of pyridine

An interesting feature of the $Co(Py)_2^+$ moieties is the disposition of the pyridine rings of molecule A relative to those of molecule B as shown by the dihedral angle of 1.2(4)° (Plane1 and Plane 4; Table III-3-15-6; p-123). The mean plane of the pyridine ring containing N1A of molecule A (plane 1) is parallel to that of molecule B containing N2B (plane 4). Furthermore, these rings are stacked as seen in Fig. III-3-15-7 (p-117), whereas, such an arrangement is not found for the rings containing N2A and N1B atoms. In each molecule the position of the NO ligands relative to the pyridine mean plane is non-symmetrical as seen by the distances of the nitrosylic N and O atoms from the pyridine mean plane (Table III-3-15-6; p-123), and in the intramolecular non-bonded distances between the nitrosylic N atoms and the pyridine ortho hydrogens. The Co-N and N-O bond lengths are normal. The Co-N-O angles are close to 170° indicating a linear NO coordination mode. The cobalt center is therefore, formally d^{10} in $Co(NO)_2(Py)_2^+BF_4^-$ when the old formalism based on the "NO^+/NO^-" dichotomy is used.

The shortest intramolecular non-bonded distances in molecule A are 2.81(16)Å and 2.86(7)Å between N3A···H1A and N4A···H10A respectively. In molecule B the equivalent distances are 2.77(5)Å and 2.65(6)Å for N3B···H1B and N4B···H10B respectively. For comparison the shortest N-H intramolecular separations observed for complexes $Rh(NO)_2(PPh_3)_2^+$ [41] $Ir(NO)_2(PPh_3)_2^+$ [41] and $Ru(NO)_2(PPh_3)_2$ [38] are 2.74Å, 2.61Å,

2.7Å respectively. These values fall in the range 2.66-2.89 Å reported for the H(phenyl)···C/N(O) intramolecular separations in $Co(CO)_x(NO)(PPh_3)_y$ (x + y = 3; x = 1, 2) [45] and the latter have been qualified as short contacts.

The most interesting feature of the geometry of molecules **A** and **B** is the value of the N-Co-N angles (115.6(3)°(**A**), 115.9(3)°(**B**)). They will be considered in part IV of the thesis.

Tables III-3-15-5

Selected bond distances (Å) and angles (°) with esd's for the two independent molecules A and B of $Co(NO)_2(Py)_2^+BF_4^-$

	Molecule A	Molecule B
Pyridine Ligand		
	Range [average]	Range [average]
C-N	1.324(14)-1.360(13) [1.344(15)]	1.333(12)-1.356(12) [1.344(10)]
C-C	1.338(17)-1.390(16) [1.368(19)]	1.347(16)-1.377(17) [1.362(13)]
C-H	0.69(5)-1.25(6) [1.04(11)]	0.85(6)-1.24(5) [1.05(11)]
N-C-C	122.8(8)-124.3(7) [123.3(7)]	120.8(8)-123.3(7) [122.4(1.2)]
C-C-C	118.6(8)-119.5(8) [119.1(4)]	118.7(1.0)-120.1(1.1) [119.4(6)]
C1-N1-C5	115.4(7)	116.1(7)
C6-N2-C10	117.0(7)	118.4(7)
Nitrosyl Ligand		
N3A-O1A	1.130(8)	N3B-O1B 1.149(8)
N4A-O2A	1.156(8)	N4B-O2B 1.142(7)
CoA-N3A-O1A	170.2(6)	CoB-N3B-O1B 170.7(6)

CoA-N4A-O2A	170.1(6)	CoB-N4B-O2B	169.1(7)

Cobalt coordination sphere

CoA-N1A	2.012(6)	CoB-N1B	2.013(6)
CoA-N2A	2.012(6)	CoB-N2B	2.016(6)
CoA-N3A	1.654(6)	CoB-N3B	1.650(6)
CoA-N4B	1.644(6)	CoB-N4B	1.648(6)
N1A-CoA-N2A	93.5(3)	N1B-CoB-N2B	93.0(3)
N3A-CoA-N4A	115.6(3)	N3B-CoB-N4B	115.9(3)
N1A-CoA-N3A	112.0(3)	N1B-CoB-N3B	112.1(3)
N1A-CoA-N4A	111.6(3)	N1B-CoB-N4B	110.2(3)
N2A-CoA-N3A	110.2(3)	N2B-CoB-N3B	111.6(3)
N2A-CoA-N4A	111.7(3)	N2B-CoB-N4B	111.9(3)
O1A-CoA-O2A	107.6(2)	O1B-CoB-O2B	107.7(2)

BF_4^- anions

	Range [average]	Range [average]
B-F	1.259(15)-1.322(14) [1.288(29)]	1.260(14)-1.357(13) [1.327(45)]
F-B-F	105.2(10)-116.0(11) [109(4)]	102.5(9)-115.0(10) [109(4)]

Selected nonbonded intramolecular contacts between nitrosylic N atoms and pyridino N and H(ortho) atoms in (Å)

N1A·····N3A	3.045(3)	N1B·····N3B	3.044(9)
N1A·····N4A	3.032(8)	N1B·····N4B	3.010(8)
N2A·····N3A	3.014(9)	N2B·····N3B	3.038(9)

N2A·····N4A	3.033(9)	N2B·····N4B	3.041(11)
N3A·····H1A	2.81(16)	N3B·····H1B	2.77(5)
N3A·····H5A	4.53(5)	N3B·····H5B	4.48(6)
N3A·····H6A	3.42(6)	N3B·····H6B	3.44(5)
N3A·····H10A	3.95(6)	N3B·····H10B	3.86(7)
N4A·····H1A	3.85(5)	N4B·····H1B	4.21(7)
N4A·····H5A	3.44(7)	N4B·····H5B	3.22(6)
N4A·····H6A	4.42(6)	N4B·····H6B	4.50(5)
N4A·····H10A	2.86(7)	N4B·····H10B	2.65(6)

Standard deviation of mean values are calculated as $\sigma(x) = [\sum (xi-x)^2/(n-1)]^{1/2}$

Table III-3-15-6

Selected least-squares planes. The equations are of the form $kx + ly + mz = n$, where, x, y, z are the fractional coordinates. Distances of atoms from planes (Å) are given in square brackets

	k	l	m	n
Plane#1				
N1A-C1A-C5A	-2.69(7)	1.28(7)	14.925(14)	12.997(10)
[N1A 0.002(11), C1A -0.007(14), C2A -0.014(15), C3A 0.017(18), C4A 0.002(16), C5A -0.007(13), CoA -0.151(16), N4A -1.625(19), O2A -2.650(21), N3A 0.349(22), O1A 0.54(3)]				
Plane#2				
N2A-C6A-C10A	9.32(5)	8.52(5)	3.69(6)	6.16(6)
[N2A -0.002(9), C6A 0.004(12), C7A 0.005(14), C8A -0.015(14), C9A 0.013(14), C10A -0.003(13), CoA 0.044(13), N3A 1.530(17), O1A 2.554(18), N4A -0.0509(18), O2A -0.712(22)]				
Plane#3				
N1B-C1B-C5B	8.65(6)	9.86(5)	2.76(7)	4.20(3)
[N1B 0.002(9), C1B -0.002(13), C2B -0.009(18), C3B 0.019(18), C4B -0.010(15) C5B 0.000(14), CoB 0.077(14), N3B -0.291(19), O1B 0.376(23), N4B 1.491(19), O2B 2.474(21)]				
Plane#4				
N2B-C6B-C10B	-2.52(6)	1.52(7)	14.872(19)	5.486(4)
[N2B -0.003(1), C6B 0.002(12), C7B 0.003(14), C8B -0.007(15), C9B 0.003(14), C10B 0.003(14), C10B 0.004(14), CoB 0.080(14), N3B				

-1.546(17), O1B -2.553(18), N4B 0.469(19), O2B 0.652(23)]

Plane#5				
CoA-N1A-N2A	8.37(5)	-0.56(6)	8.93(5)	7.92(4)
Plane#6				
CoA-N3A-N4A	-5.61(7)	12.28(4)	6.05(6)	8.37(4)
[O1A 0.029(13), O2A 0.034(13)]				
Plane#7				
CoB-N1B-N2B	-3.56(5)	10.69(3)	9.75(4)	3.66(2)
Plane#8				
CoB-N3B-N4B	10.84(5)	-3.81(6)	5.21(6)	4.96(2)
[O1B 0.027(13), O2B -0.028(14)]				

Dihedral angles between planes

1-2	65.8(4)	1-3	69.6(4)
1-4	1.2(4)	2-3	7.6(4)
2-4	64.6(4)	3-4	68.5(4)
5-6	89.3(3)	7-8	89.2(3)

III-3-16 Structural study of $Co_2(NO)_3(PPh_2(2\text{-}Py))_2{}^+BPh_4{}^-$

(i) Crystal data and refinement

Single crystals of $Co_2(NO)_3(PPh_2(2\text{-}Py))_2{}^+BPh_4{}^-$ (12) were obtained by slow diffusion of toluene into a concentrated solution of the complex in CH_2Cl_2 at room temperature. The crystal selected was brown in colour. A table of crystal data and refinement indicators for the complex is presented in appendix (p-245).

The intensities were measured with $2\theta_{max} = 130°$ and CuKα radiation (1.5418Å) on an Enraf-Nonius CAD-4 diffractometer. A total of 9275 reflections were measured with 9275 unique reflections. Among these 6579 reflections have $I_{net} > 3.0\sigma(I_{net})$. Absorption correction was applied to the measured intensity (μ = 6.877 mm^{-1}). The structure was determined by the heavy-atom method using Patterson and electron-density maps. The hydrogen atoms were located from a difference electron-density map.

The structure refinement was by the least-squares method minimizing $\Sigma w (|F_o| - |F_c|)^2$, the weights were evaluated from the expression $w = 1/ [1+ (|Fo| \div P_2/P_1)^2]$, with P_1=25 and P_2 = 12. In the final cycle of refinement, the mean shift in the atomic parameters was 0.06 σ, and the maximum shift was 0.27 σ for the ordered atoms and 0.57 σ for the solvent.

(ii) Description of the Structure

The structure consists of discrete unipositive bimetallic cations, BPh_4^- anions and CH_2Cl_2 molecules. The latter were found to be disordered over three positions. An ORTEP drawing of the cationic portion of bimetallic $Co_2(NO)_3(PPh_2(2\text{-}Py))_2^+BPh_4^-$ and the atomic numbering scheme used are presented in Fig. III-3-16-9 (p-128) and Fig. III-3-16-10 (p-129) respectively. An orthogonal projection of various atoms on the Co1Co2N3 plane of the $Co_2(NO)_3^+$ core is presented in Fig. III-3-16-11 (p-130). Selected bond lengths and angles are listed in Table III-3-16-7 (p-137) and dihedral angles between the planes are given in Table III-3-16-8 (p-139). Atomic parameters and thermal parameters are presented in Appendix on (p-246) and (p-247) respectively. In the complex $Co_2(NO)_3(PPh_2(2\text{-}Py))_2^+BPh_4^-$ the two cobalt atoms are connected by a triple bridge consisting of one μ_2-NO and two aminophosphines coordinated in a head-to-head fashion. Each cobalt atom is also coordinated to one terminal NO. The intramolecular cobalt-cobalt separation of 2.527(1)Å indicates the formation of a metal-metal bond, therefore each cobalt atom is pentacoordinated. The Co-N and N-O bond lengths are normal within the experimental range [46-48].

The $Co_2(NO)_3^+$ metallic core can be viewed as derived from two monometallic cobaltdinitrosyl moieties, Co1(N1O1)(N3O3) represented as"*cobaltdinitrosyl*-1" and Co2(N2O2)(N3O3) as "*cobaltdinitrosyl*-2" sharing the same μ_2-N3O3 ligand but

differing in the geometrical conformation adopted by the linearly bonded NO ligand. For each of the "*cobaltdinitrosyl*-1" and "*cobaltdinitrosyl*-2" moieties, the projected geometry on the corresponding (O)NCoN(O) plane (not shown) is qualitatively similar to that of Fig.III-3-16-11(p-130) with the projected NO vector of the terminal NO ligand pointing towards (Co2N4) and away from Co1(N5) and the μ_2-N3O3 ligand. This conformational orientation is associated with an opening of the N2-Co2-N3 angle from 100.5(2)° in "*cobaltdinitrosyl*-2" to 117.1(2)° for (N1-Co1-N3) in "*cobaltdinitrosyl*-1"

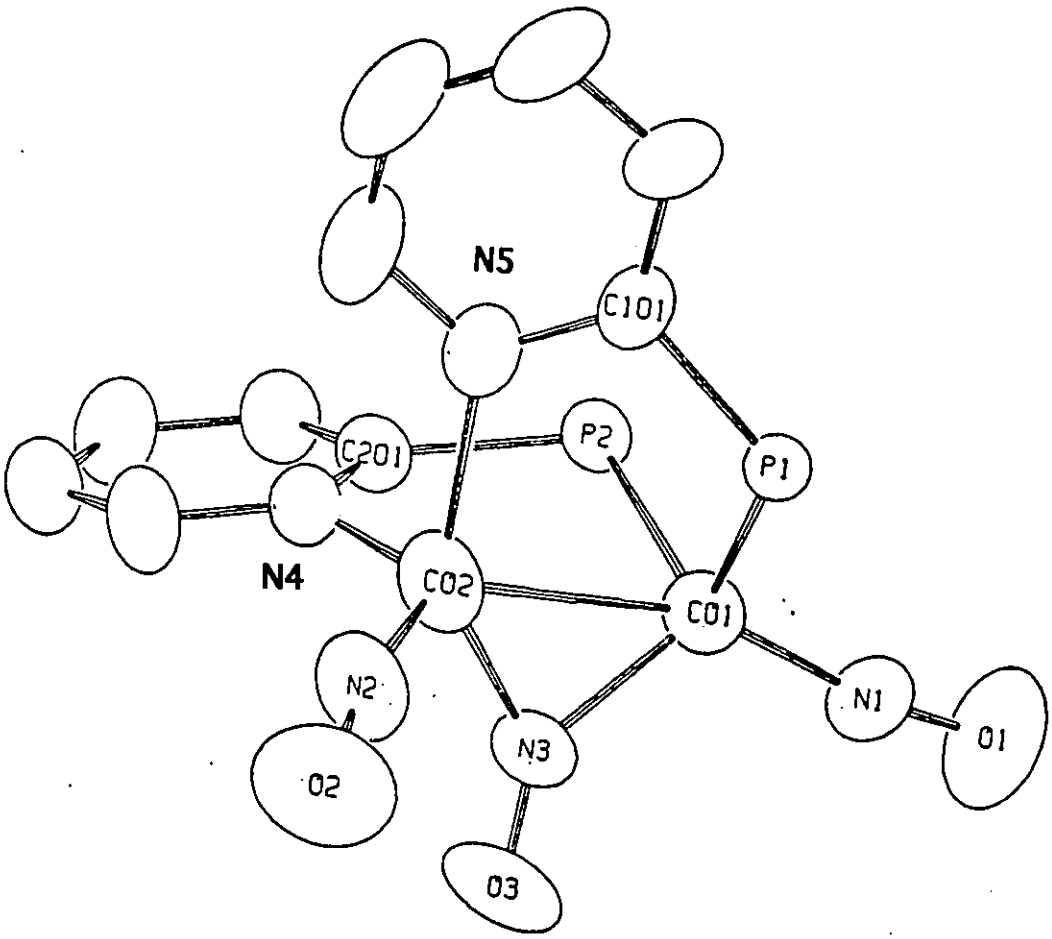

Fig. III-3-16-9 An ORTEP drawing of the cationic portion of $Co_2(NO)_3(PPh_2(2\text{-}Py))_2^+$

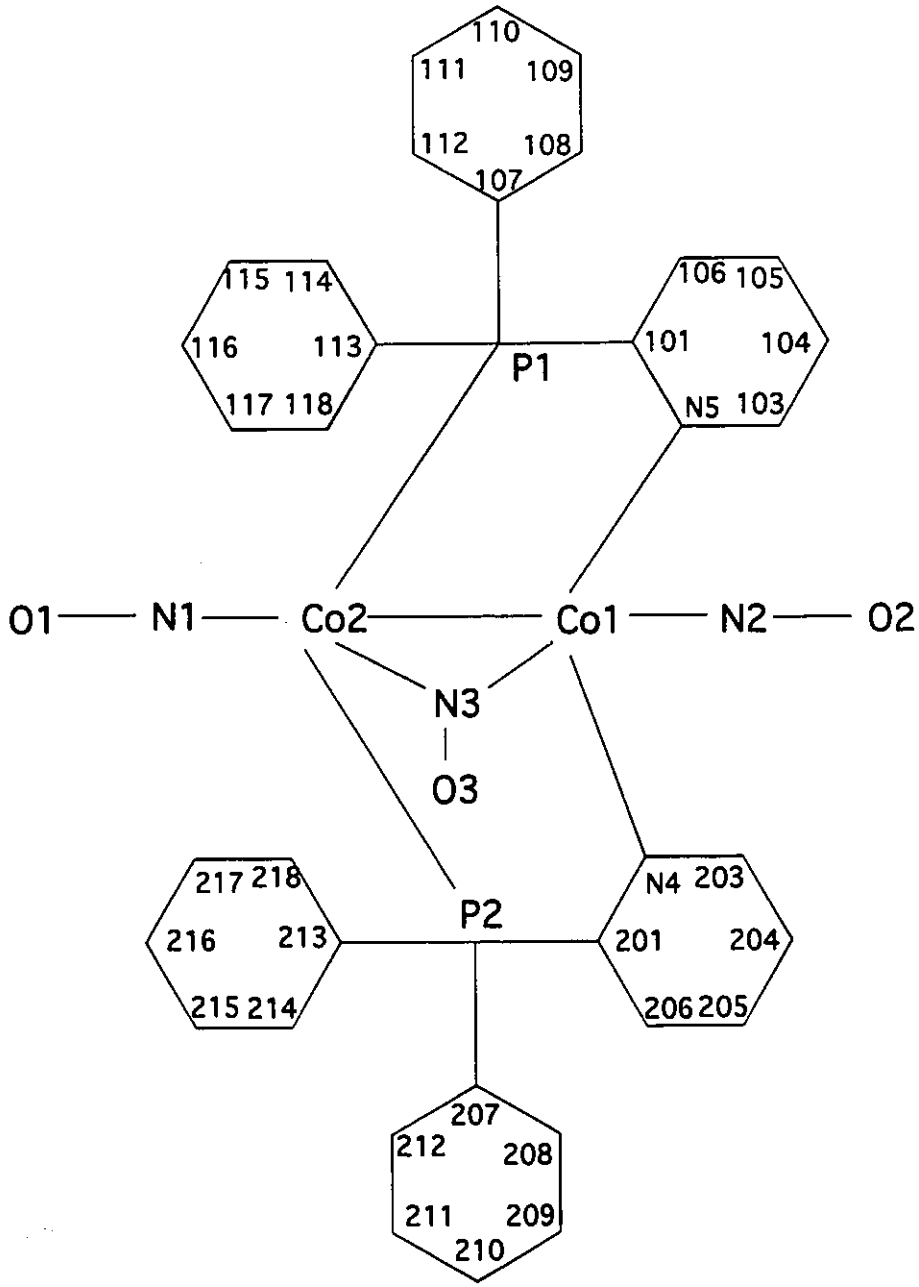

Fig. III-3-16-10 A representation of the atomic numbering scheme used in $Co_2(NO)_3(PPh_2(2\text{-}Py))_2^+$ cation

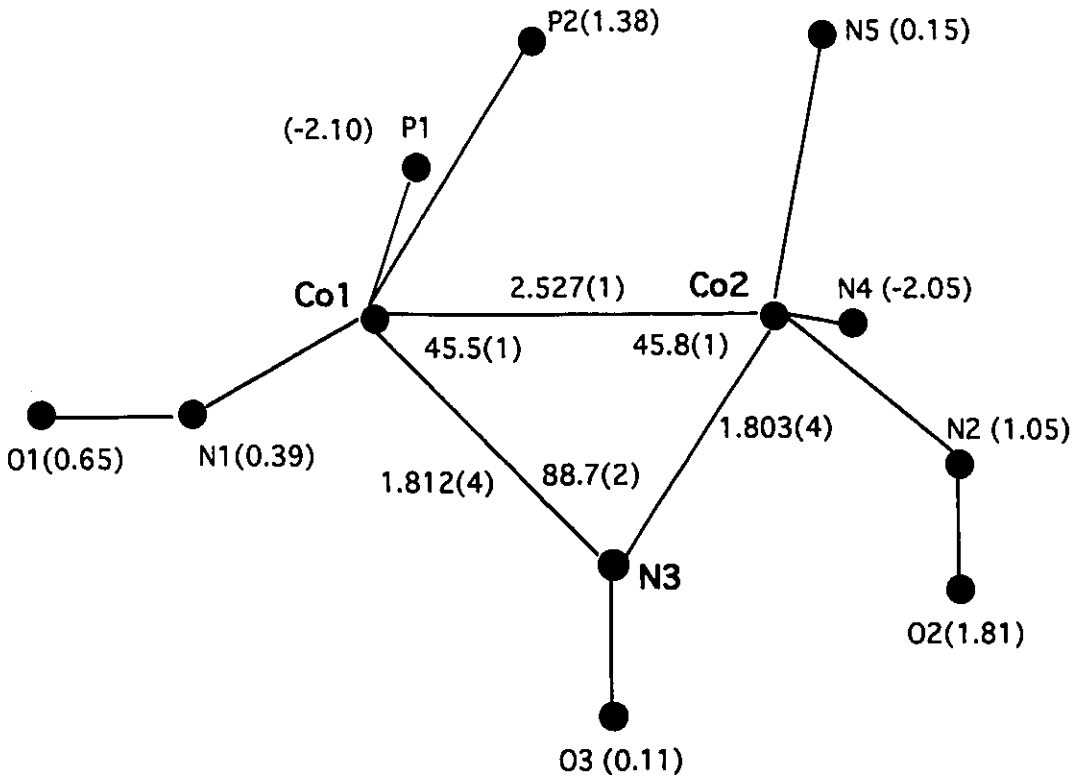

Fig.III-3-16-11 Projections of selected atoms on the Co1Co2N3 plane. Two atoms with elevations of the same sign (shown in brackets)are on the same side of the plane

The coordination polyhedron around each cobalt atom of the bimetallic **(12)**, which is coordinated to the P and N-donor sites of the $PPh_2(2\text{-}Py)$ ligand is compared with the two closest monometallic model compounds. The crystal structure of $Co(NO)_2(PPh_2(2\text{-}Py))_2^+BF_4^-$ **(9)** provides an example for the comparison of the P-donor site of the ligand $PPh_2(2\text{-}Py)$ coordinated to cobalt in the bimetallic **(12)**, whereas the crystal structure of $Co(NO)_2(Py)_2^+BF_4^-$ **(10)** is used to compare the N-donor site of the ligand $PPh_2(2\text{-}Py)$ in bimetallic **(12)**.

The coordination polyhedron of the pentacoordinated "*cobaltdinitrosyl* -1" center of the bimetallic **(12)** is almost the same as that found for Co in complex **(9)**, which is tetracoordinated having a pseudotetrahedral geometry. Based on the comparison of the intervalence angles involving Co1, the P atoms, and the nitrosylic nitrogen atoms (Table III-3-16-9, p-140) of complex **(12)** with the equivalent angles of complex **(9)**, the coordination polyhedron around Co1 is best described as a face-capped tetrahedron formed by P1, P2, N1 and N3 with the Co1Co2 vector passing through the P1P2N3 face as shown in Fig. III-3-16-12 (p-133). Comparing the structures of these three cobalt complexes, presented in Table III-3-16-9 (p-140), the P-Co-P angle of 107.3(1)° around "*cobaltdinitrosyl* -1" in **(12)** is very similar to those found for the two independent molecules **(9A)** 108.97(6)° and **(9B)** 107.09(6)° of $Co(NO)_2(PPh_2(2\text{-}Py))_2^+$ BF_4^- **(9)**. However, the Co1-P bond length of 2.219(1)Å and

2.251(1)Å in **(12)** are shorter than those of 2.275(2)Å and 2.264(2)Å for **(9A)** and **(9B)** respectively, which contains a less electron rich metallic centre, as shown by the ν_{NO} frequencies (1775, 1590 cm-1 for **(12)** and 1855, 1795 cm^{-1} for **(9)**). The Co-P bond length shortens, with an increase in the metal basicity as found for a variety of iron complexes containing the $Fe(CO)(PPh_3)$ subunit [49]. The ligand arrangement around "*cobaltdinitrosyl* -2" in **(12)** bears no resemblance to that found in $Co(NO)_2(Py)_2{}^+BF_4{}^-$ **(10)**. The least unsatisfactory description is that of a square pyramid with N4 in the axial position and N5, N3 and Co1 defining the basal plane. (Fig. III-3-16-13 (p-133). In agreement with this description, the valence angles involving Co2N4 with Co2N3, Co2Co1 and Co2N5 of 45.8(1)°, 95.6(1)° and 97.0(1)° respectively are in the range expected for a coordination of that type. The N5-Co2-Co1 angle of 97.0(1)° is also adequate for two basal ligands in a *syn*-relationship. The N3 atom however is displaced from the position corresponding to a regular geometry due to the geometrical constraint imposed by the formation of the μ_2-N3O3 bridge which forces the Co1Co2N3 angle to close down to 45.8(1)°. More interestingly , there is a second more severe distortion which involves the terminal N2O2 ligand. The N2 atom is more or less symmetrically disposed relative to the basal N5 and N3 atoms as far as the N5-Co2-N2 and N3-Co2-N2 angles of 105.4(2)° and 100.5(2)° respectively are concerned, but N2 is displaced by a very large 0.96 Å out of the

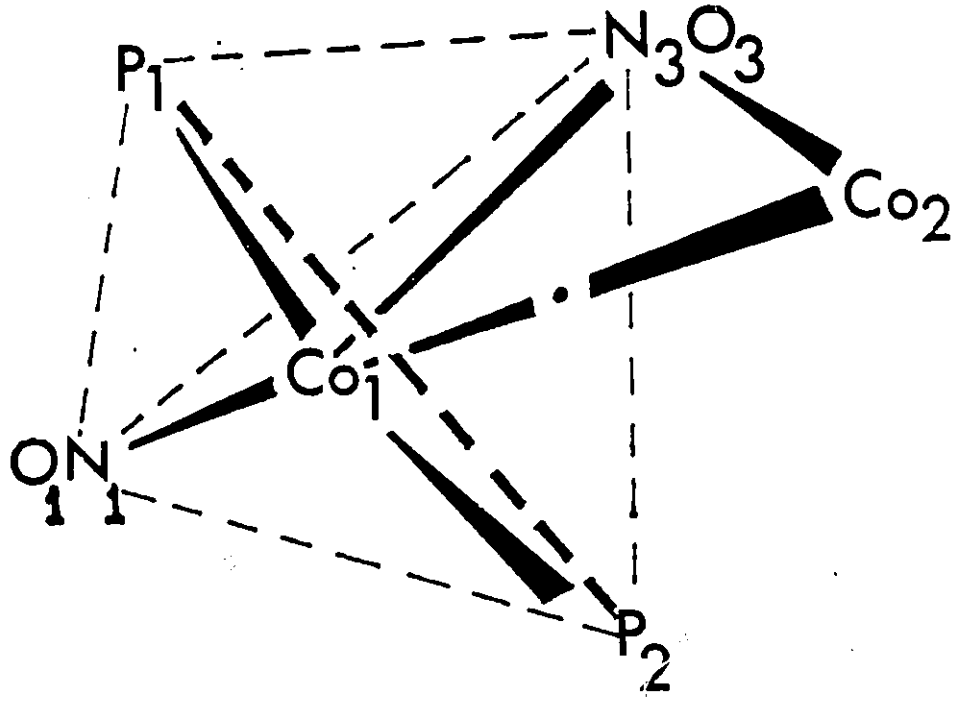

Fig. III-3-16-12

Representation of a face capped tetrahedron geometry around Co1 in $Co_2(NO)_3(PPh_2(2\text{-}Py))_2^+$ cation

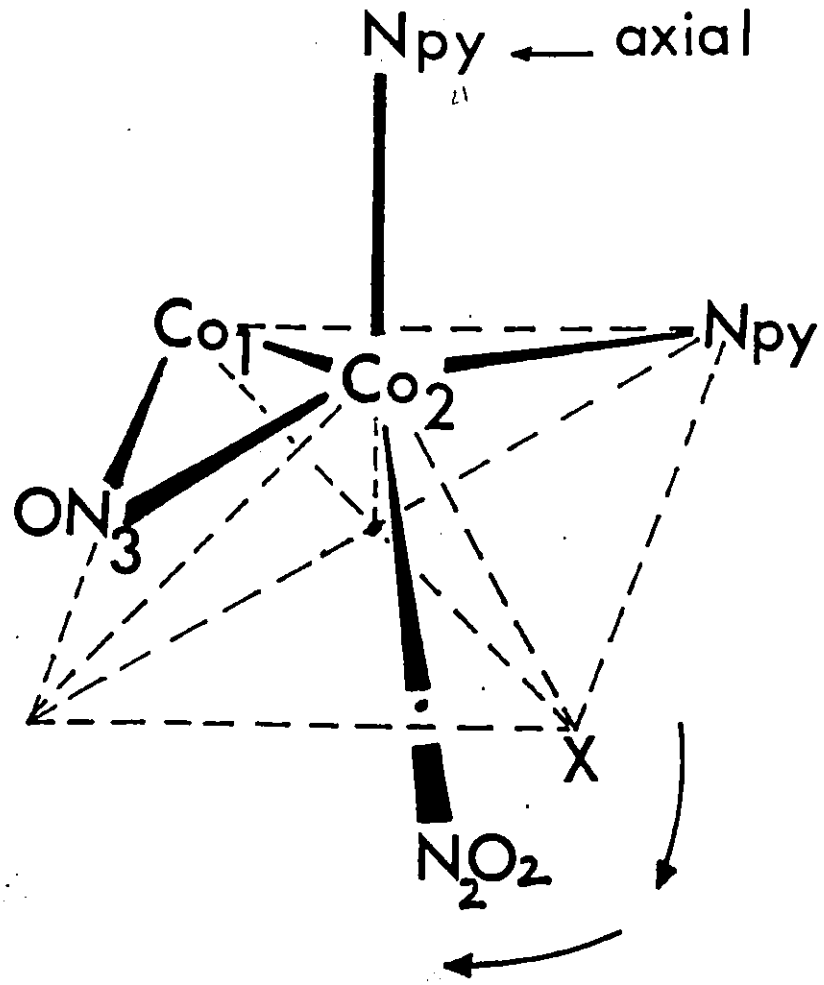

Fig. III-3-16-13

Representation of a square pyramidal geometry around Co2 in $Co_2(NO)_3(PPh_2(2\text{-}Py))_2^+$ cation

basal plane away from the axial N4 atom towards the least sterically hindered portion of the cation.

In the "*cobaltdinitrosyl* -2" moiety of $Co_2(NO)_3(PPh_2(2\text{-}Py))_2{}^+BPh_4{}^-$, the pyridinyl angle (N5-Co2-N4 95.2(2)°) can be compared with 93.5(3)° and 93.0(3)° found in the two independent molecules **(10A)** and **(10B)** of $Co(NO)_2(Py)_2{}^+BF_4{}^-$ **(10)** respectively, whereas the Co2-N4 and Co2-N5 bond lengths of 2.066(4) and 2.062(4)Å in "*cobaltdinitrosyl*-2" are longer than the equivalent distances found in $Co(NO)_2(Py)_2{}^+BF_4{}^-$ by ca. 0.05-0.06Å. Overall, the presence of a mechanical link between the phosphorus and the pyridinyl nitrogen atom of the $PPh_2(2\text{-py})$ ligand does not affect the angular parameters of the $Co(NO)_2(L)_2$ moieties of complex **(12)** when they are compared to those of the two closest monometallic model compounds **(9)** and **(10)**. Finally, it was observed that the ligand arrangement around each cobalt atom of complex **(12)** is unusual for the family of bimetallic coordinated with the P and N donor sites of $PPh_2(2\text{-Py})$. For example, in $Rh_2(Cl)_2(\mu_2\text{-}CO)(PPh_2(2\text{-Py}))_2$ [50] in which the bimetallic core can be regarded as formed from two Rh(CO)(Cl) units sharing the same μ_2-CO bridge, each rhodium was found to form a triangular bipyramid, with the most significant deviation from regular geometry being caused by the formation of the bridge. From this bimetallic rhodium derivative $Rh_2(Cl)_2(\mu_2\text{-}CO)(PPh_2(2\text{-}Py))_2$ to the complex $Co_2(NO)_3(PPh_2(2\text{-Py}))_2{}^+ BPh_4{}^-$, the M-P and M-N(Py) bond lengths

decrease by ca. 0.05 and 0.1Å respectively, which in turn increases the repulsions between the ligands bound to the same metal. The change in the type of coordination polyhedron might therefore be required to achieve an acceptable rebalancing of bonding and non-bonding repulsive forces.

Table III-3-16-7

Selected Bond lengths (Å) and angles (°) with esd's in

$Co_2(NO)_3(PPh_2(2\text{-}Py))_2^+BPh_4^-$

Bond lengths

Co1-N1	1.649(4)	N1-O1	1.146(7)
Co1-N3	1.812(4)	Co1-P1	2.219(1)
Co1-P2	2.251(1)	Co1-Co2	2.527(1)
Co2-N2	1.655(4)	N2-O2	1.149(7)
Co2-N3	1.803(4)	Co2-N4	2.066(4)
Co2-N5	2.062(4)	N3-O3	1.184(7)
P1-C107	1.813(5)	C107-C108	1.385(7)
C107-C112	1.383(7)	P1-C113	1.823(5)
C113-C114	1.389(7)	P1-C101	1.832(5)
C101-N5	1.345(7)	C101-C106	1.384(7)
P2-C201	1.845(5)	C201-N4	1.348(6)
C201-C206	1.375(6)	P2-C207	1.812(5)
C207-C208	1.383(7)	C207-C212	1.390(6)
P2-C213	1.831(5)	C213-C214	1.388(6)
C213-C218	1.403(7)	N5-C103	1.355(6)
N4-C203	1.343(6)		

Bond angles

N1-Co1-Co2	158.8(2)	N1-Co1-N3	117.1(2)
N1-Co1-P1	105.4(2)	N1-Co1-P2	112.4(2)
Co2-Co1-N3	45.5 (1)	Co2-Co1-P1	77.5 (1)
Co2-Co1-P2	85.9 (1)	N3-Co1-P1	112.8(1)
N3-Co1-P2	101.6(1)	P1-Co1-P2	107.3(1)
N2-Co2-Co1	131.7(2)	N2-Co2-N3	100.5(2)
N2-Co2-N5	105.4(2)	N2-Co2-N4	123.5(2)

Co1-Co2-N3	45.8 (1)	Co1-Co2-N5	97.0 (1)
Co1-Co2-N4	95.6 (1)	N3-Co2-N5	142.6(2)
N3-Co2-N4	92.4 (2)	N5-Co2-N4	95.2 (2)
Co1-N1-O1	170.5(5)	Co2-N2-O2	167.0(5)
Co1-N3-Co2	88.7 (2)	Co1-N3-O3	136.9(4)
Co2-N3-O3	133.7(4)	Co1-P1-C101	114.4(2)
Co1-P1-C107	112.9(2)	Co1-P1-C113	117.4(2)
C101-P1-C107	106.8(2)	C101-P1-C113	101.3(2)
C107-P1-C113	102.7(2)	Co1-P2-C201	110.5(2)
Co1-P2-C207	120.6(2)	Co1-P2-C213	114.5(2)
C201-P2-C207	102.0(2)	C201-P2-C213	103.9(2)
C207-P2-C213	103.5(2)		

Table III-3-16-8

Dihedral angles (°) (σ = 0.3) between selected planes in bimetallic

$Co_2(NO)_3(PPh_2(2\text{-}Py))_2{}^+BPh_4{}^-$ (12)

Planes	Dihedral Angles
Plane#1 / Plane#2	82.7
Plane#3 / Plane#4	86.3
Plane#3 / Plane#5	85.5
Plane#5 / Plane#6	64.2
Plane#7 / Plane#8	84.7
Plane#3/ Plane#9	88.7

Plane#1 = P1Co1P2; Plane#2 = N1Co1N3; Plane#3 = Co1N3N5; Plane#4 = Co1Co2N4

Plane#5 = N5Co2N4; Plane#6 = N2Co2N3; Plane#7 = Co1N3N4; Plane#8 = N3Co2N4 Plane#9 = N2Co2N4

Table III-3-16-9

Comparision of selected bond lengths (Å) and angles (°) between Complexes **(12)**, **(9)** and **(10)**

$Co_2(NO)_3(PPh_2(2\text{-}Py))_2^+BPh_4^-$ **(12)** (ca. ν_{NO} = 1775, 1750, 1590(s) cm^{-1})

Cobaltdinitrosyl-1

M-L	N-O	M-N-O	N-M-N	O ···M ···O	L-M-L	N-M-L
2.219(1)	1.146(7)	170.5(5)	117.1(2)	104.39(2)	107.3(1)	105.4(2), 112.4(2)
2.251(1)	1.184(7)	136.9(4)				112.8(1), 101.6(1)

Cobaltdinitrosyl-2

2.062(4)	1.149(7)	167.0(5)	100.5(2)	79.5(2)	95.2(2)	92.4(2),123.5(2)
2.066(4)	1.184(7)	133.7(5)				105.4(2),142.6(2)

$Co(NO)_2(PPh_2(2\text{-}Py))_2^+BF_4^-$ **(9)** (ca. ν_{NO} = 1855, 1795 cm^{-1})

Molecule **A**

2.275(2)	1.146(6)	178.4(4)	126.1(2)	125.5(2)	108.97(6)	103.6(2),107.0(2)

Molecule **B**

2.264(2)	1.144(7)	172.9(4)	131.8(2)	134.6(1)	107.09(6)	96.3(2),112.1(2)

$Co(NO)_2(Py)_2^+BF_4^-$ **(10)** (ca. ν_{NO} = 1876, 1798 cm^{-1})

Molecule **A**

2.012(6)	1.130(8)	170.2(6)	115.6(3)	107.6(2)	93.5(3)	111.4(3),112.0(3)
2.012(6)	1.156(8)	170.1(6)				110.2(3),111.7(3)

Molecule **B**

2.013(6)	1.149(8)	170.7(6)	115.9(3)	107.7(2)	93.0(3)	110.2(3),112.1(3), 111.6(3),111.9(3)
2.016(6)	1.142(7)	169.1(7)				

III-3-17 Structural study of diphenyl(2-pyridyl)phosphine

During the structural studies of the complexes of first row transition metals containing diphenyl(2-pyridyl)phosphine, PPh_2(2-Py) as ligand, it was neccessary to determine its crystal structure in an uncoordinated state. The structural parameters are compared with triphenylphosphine (PPh_3) [51]

(i) Crystal Data and Refinement

Crystals of diphenyl(2-pyridyl)phosphine were grown from a diethylether and hexane solvent system. The crystal studied was white with dimensions 0.15x0.35x0.35 mm. The crystal data and refinement indicators are presented in appendix (p-250).

A total of 3376 reflections were measured out of which 3346 were unique and 1680 reflections were considered to be significant with $I_{net} > 3.0\ \sigma\ (I_{net})$. These data were corrected for Lorentz and polarization effects, but no absorption correction was applied. The cell parameters were obtained using least-squares refinement of the setting angles of 100 reflections ($35° < 2\theta < 45°$). The positions of the non-hydrogen atoms were determined by direct methods using MULTAN. At the beginning all the ring atoms were considered as C atoms. Then the atoms ortho to the carbon atoms linked to phosphorus were examined. The structure was refined isotropically and the thermal motion of one of the atoms under examination indicated the possibility of it being a nitrogen atom. Later the atoms were refined by fixing the

isotropic U value at 0.04 and refining occupancies. The position assumed to be the nitrogen atom refined as 1.2 carbon while the others had occupancies close to 1.00. A difference map revealed the positions of all the hydrogen atoms, and as expected no peak was found in the vicinity of the N position. The coordinates of the hydrogen atoms were refined with isotropic parameters, while the other atoms were refined anisotropically by full-matrix least-squares. Weights based on counting statistics were used throughout. The final residual converged to R_f = 0.043 and R_w = 0.023 with a GOF of 2.15. The maximum shift to error ratio in the last cycle was 0.004.

Bond distances and angles of interest are presented in Table III-3-17-10 (p-147). The dihedral angles between the basal plane, and the planes defined in each ring by the C atom bonded to P and the two ortho atoms, are listed in Table III-3-17-11 (p-148). The least squares planes through the aromatic rings of diphenyl(2-pyridyl)phosphine are presented in Table III-3-17-12 (p-149). Atomic coordinates with thermal parameters are presented in Appendix (p-251). A stereo pair of the molecule is presented in Fig. III-3-17-14 (p-146). An orthogonal projection of PPh_2(2-Py) (solid lines) and of PPh_3 (dotted lines) on the basal plane formed by the C1, C7, C13 atoms bonded to P is shown in Fig. III-3-17-15 (p-145). The elevations of the ortho atoms relative to that plane are also indicated. The data in parenthesis are for PPh_3.

(ii) **Description of the structure**

In PPh_2(2-Py) the three aromatic rings A, B (phenyl rings) and C (pyridyl ring), are planar within experimental errors. The endocyclic C-N-C angle of 116.6(3)° is considerably smaller than the corresponding C-C-C angles of 120.4(3)- 122.3(3)° in the phenyl rings. Conversely, the N-C-C angles subtended at C13 and C17 ortho to N, which are 122.1(3) and 124.6(3)°, are more than 4.0° larger than the corresponding angles in the phenyl rings. The C-N bond lengths of 1.343(3)Å and 1.342(5)Å in the pyridyl ring are smaller than the C-C bond lengths (average = 1.378(11)Å). These differences confirm the presence and location of the N atom. As in PPh_3 the aromatic substituents of PPh_2(2-Py) adopt a propeller conformation as seen in Fig.III-3-17-15 (p-145), by the sequence of alternating +ve and -ve elevations of the ortho atoms. Replacing the H-C18 grouping of PPh_3 by N18 of PPh_2(2-Py) results in a closing of C1-P-C13 angle from 103.2(2)° to 99.7(1)°. At the same time ring C rotates around the P-C13 bond so that it becomes significantly less inclined relative to the basal plane, as shown by the large variation of the dihedral angle from 64.8° to 45°. Concomitantly ring B becomes more inclined by 10°, whereas, ring A is affected to a much lesser extent. The combined effect of these displacements allows the N atom to move closer to ring A. The major change in the intramolecular non-bonded contacts between the ortho atoms pertains to the shortening, by 0.5Å, of the separation involving the C6 and C2 atoms with C18 in

PPh_3 (4.72, 4.03 Å respectively) and with N18 in PPh_2(2-Py) (4.22, 3.53Å respectively).

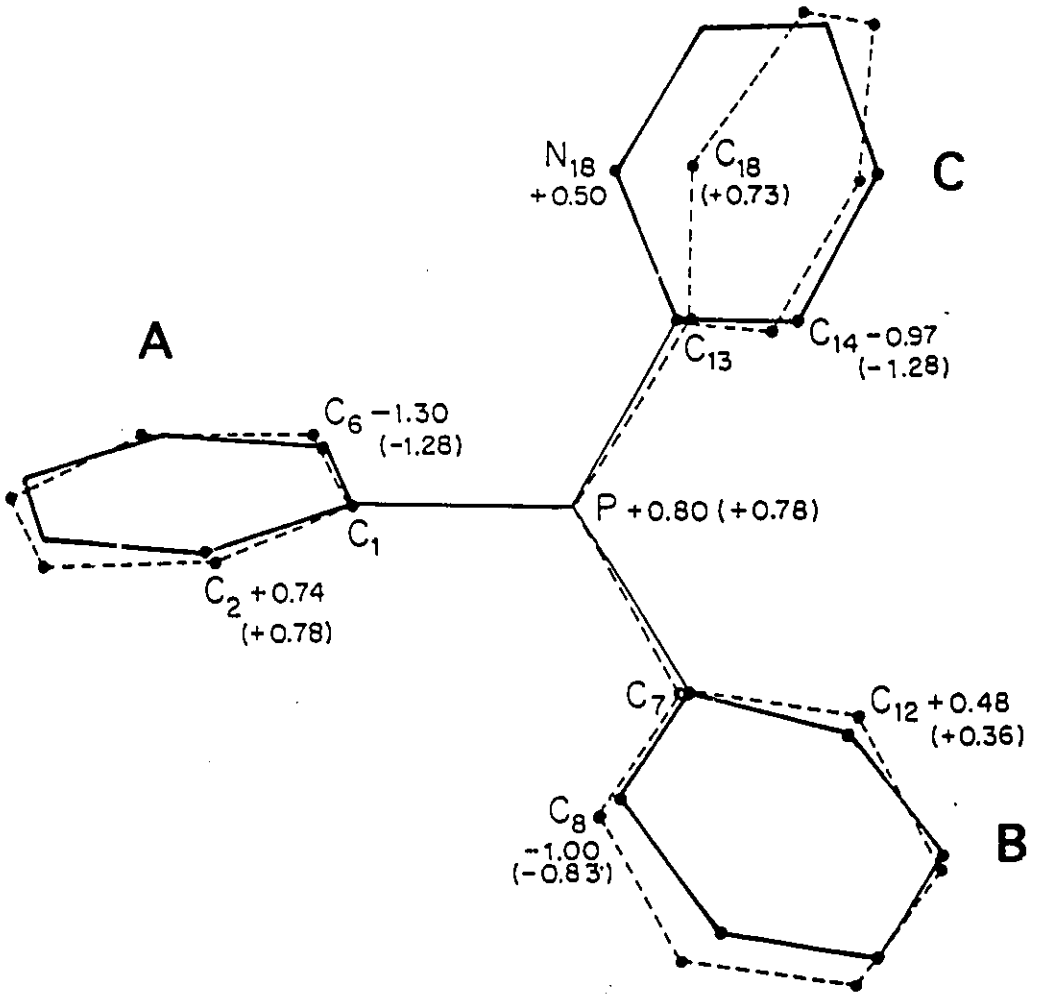

Fig. III-3-17-14

An Orthogonal projection of the $PPh_2(2\text{-}Py)$ molecule (solid lines) and of the PPh_3 molecule (dotted lines) on the basal plane formed in each molecule by the C1, C7, C13 atoms bonded to P.

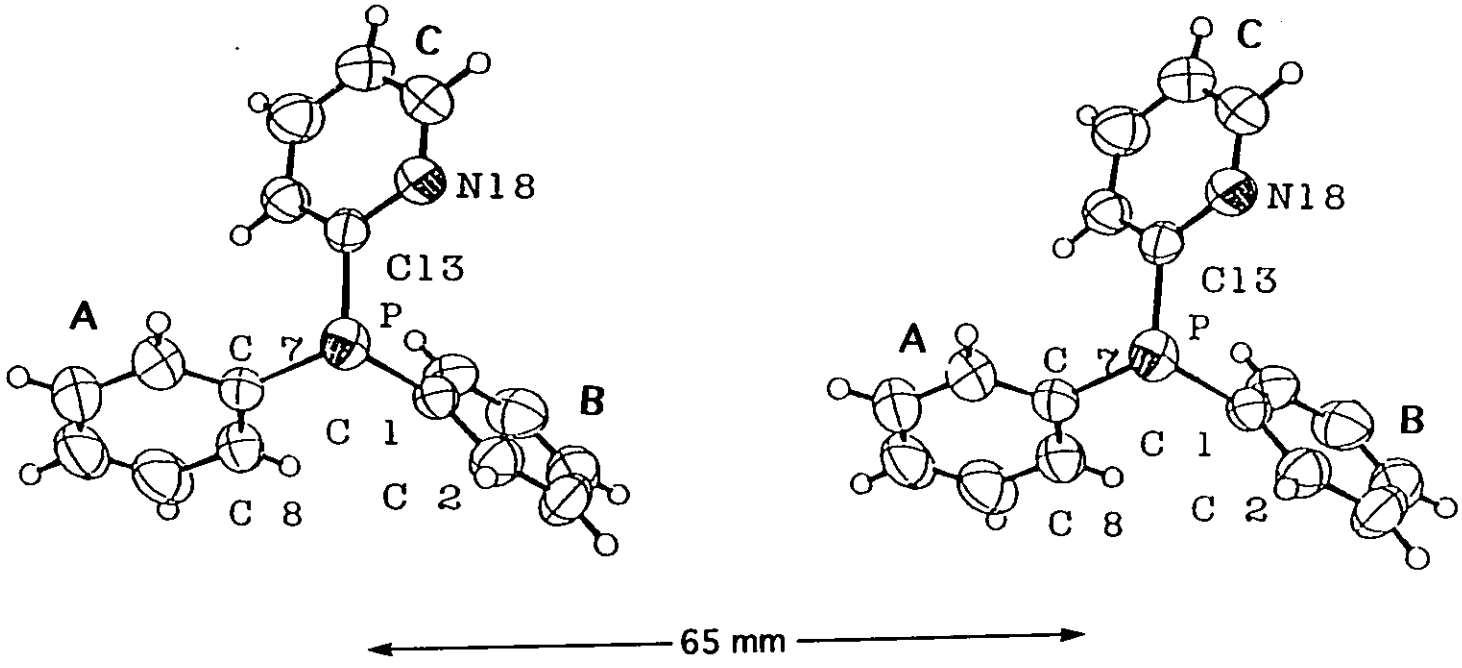

Fig. III-3-17-15 An ORTEP drawing of the $PPh_2(2\text{-}Py)$ molecule

Table III-3-17-10

Bond distances (Å) and angles (°) with esd's for $PPh_2(2\text{-}Py)$

Ring A		Ring B		Ring C	
Bond distances					
P-C1	1.823(2)	P-C7	1.820(2)	P-C13	1.835(3)
C1-C2	1.373(4)	C7-C8	1.380(4)	C13-C14	1.370(4)
C2-C3	1.383(5)	C8-C9	1.400(4)	C14-C15	1.380(5)
C3-C4	1.364(7)	C9-C10	1.364(6)	C15-C16	1.363(5)
C4-C5	1.366(6)	C10-C11	1.359(6)	C16-C17	1.363(6)
C5-C6	1.384(5)	C11-C12	1.369(5)	C17-N18	1.342(5)
C6-C1	1.383(4)	C12-C7	1.379(4)	N18-C13	1.343(3)
Bond angles					
C1-C2-C3	121.1(3)	C7-C8-C9	120.4(3)	C13-C14-C15	119.7(3)
C2-C3-C4	119.6(3)	C8-C9-C10	120.2(4)	C14-C15-C16	118.9(3)
C3-C4-C5	120.6(3)	C9-C10-C11	120.0(3)	C15-C16-C17	118.1(3)
C4-C5-C6	119.5(4)	C10-C11-C12	119.8(3)	C16-C17-N18	124.6(3)
C5-C6-C1	120.9(3)	C11-C12-C7	122.3(3)	C17-N18-C13	116.6(3)
C6-C1-C2	118.3(3)	C12-C7-C8	117.4(2)	N18-C13-C14	122.1(3)
C2-C1-P	118.1(2)	C8-C7-P	125.8(2)	C14-C13-P	126.2(2)
C6-C1-P	123.6(2)	C12-C7-P	116.8(2)	N18-C13-P	111.7(2)
C1-P-C7	104.5(1)	C7-P-C13	101.9(1)	C13-P-C1	99.7(1)
P·····N 1 8	2.645(3)	< C-H >	0.95(4)	< C-C-H>	120.0(3]

TABLE III-3-17-11

Dihedral angles (°) between the basal plane and the three aromatic rings in the $PPh_2(2\text{-}Py)$ and PPh_3 molecules

Plane	$PPh_2(2\text{-}Py)$	PPh_3
A	71.7	67.8
B	46.6	36.6
C	45.1	64.8

Plane A = C1C2C6; Plane B = C7C8C12; Plane C = C13C14N18(C18)

TABLE III-3-17-12

Least-Squares planes through the aromatic rings of $PPh_2(2\text{-}Py)$

The equations are in the form kx + ly + mz = n, where x, y, z are the fractional coordinates. Distances of atoms from planes (Å) are given in square brackets.

	k	l	m	n
Plane A				
(C1-C6)	8.799(7)	3.233(14)	-5.459(22)	7.321(7)
[C1 0.001(4),C2 0.000(4), C3 -0.003(5),C4 0.002(6), C5 0.002(5), C6 -0.002(4)]				
Plane B				
(C7-C12)	0.260(20)	9.8469(12)	1.093(22)	2.157(15)
[C7 0.005(3), C8 0.001(4), C9 -0.008(5),C10 0.008(5),C11 0.003(5), C12 -0.009(4)]				
Plane C				
(C13-N18)	5.499(12)	-2.785(13)	11.211(14)	8.224(13)
[C13 -0.002(3), C14 -0.003(4), C15 0.008(4), C16 -0.005(5), C17 -0.005(5), N18 0.004(3)]				

PART IV

ANALYSIS AND DISCUSSION OF ANGULAR VARIATIONS IN M(NO)(XO) (X = C, N) TETRA AND PENTA COORDINATED COMPLEXES. PROPOSAL OF A NEW STEREOELECTRONIC MODEL

General Introduction

Pseudotetrahedral dinitrosyl complexes of the type $M(NO)_2(L)_2^x$ (x = o, +1; $(L)_2$ = bidentate ligand or set of two monodentate ligands) have provided interesting objects to study from a structural viewpoint (Fig. IV-1), in light of the angular deformations which can affect the $M(NO)_2$ moiety and, to a lesser extent, the $M(L)_2$ moiety.

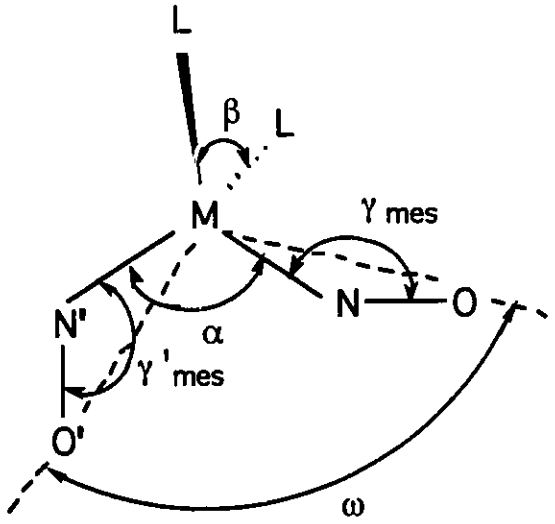

Fig IV-1 Angular representation in $M(NO)_2$ moiety

In general, in such complexes, the M-N and N-O vectors of a MNO linkage are not colinear. In the literature, it has been a standard practice to express the extent of bending of a MNO linkage in terms of the angle γ_{mes} sustained at N by the M and O atoms (γ'_{mes} is the equivalent angle when the M-N'-O' linkage of Fig.IV-1 is

considered). *In the particular case of symmetry related nitrosyl ligands* ($\gamma_{mes} = \gamma'_{mes}$), when the rotation about M-N bond is such that the O atoms move towards each other, the $M(NO)_2$ subunit is said to be in an "**endo**" conformation, when the bending moves the O atoms away from each other, the conformation is said to be '**exo**" as presented in Fig. IV-2. Later in the text, a new terminology will be proposed for identifying all of the possible conformations which might be encountered when the two nitrosyl ligands are crystallographically independent.

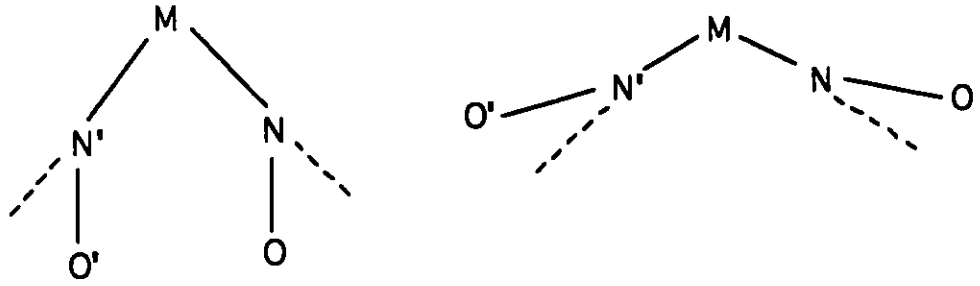

Endo conformation (a)

Exo conformation (b)

Fig. IV-2 (a) (b) Representation of endo and exo conformations in M(NO)(N'O') moiety respectively.

Upon going from one complex to another, changing either the nature of the ancillary ligands L and/or the nature of the metal M, usually causes a change in either all or part of the angles denoted α, β, γ_{mes}, γ'_{mes} and ω in Fig.IV-1 (p-151).

The first chapter of this section describes, the variations of the N'-M-N = α angle and proposes a new model to rationalize the observed changes and the observed differences in solution behaviour upon going from the cobalt-pyridine to cobalt-phosphines complexes. The second chapter describes the changes affecting the O···M···O' = ω angle and the extent of bending of the nitrosyl ligands.

Chapter I

IV-1-1 Variation of the α angle : the current electronic model

From one $M(NO)_2(L)_2^x$ (x = 0, +1) complex to another one, the N'-M-N = α angle can vary by a substantial amount, for example, in $Fe(NO)_2(PPh_3)_2$ (α = 123.8(4)°) whereas in $Rh(NO)_2(PPh_3)_2^+$ (α = 157.5(3)°). These variations of the α angle have been rationalized in terms of electronic influences using either M.O. or valence bond theories. The M.O. theory describes the bonding in $M(NO)_2$ moiety in terms of delocalized bonds, whereas the valence bond approach considers localized bonds between the metal and each one of the NO ligands. When the valence bond theory is used the variations in the α angle have been tentatively rationalized by what is essentially an application of the Gillespie's theory of electron pair-electron pair repulsions.

According to this electron pair repulsion model, referred to as the "electronic model" henceforth, as the π-back bonding from M to NO increases, the electron population of the M-N bond increases, and this causes an enhancement of the mutual electrostatic repulsion of these bonds. In other words, as the back bonding from M to NO increases the non-bonded covalent radius of the nitrosylic N atom increases at a fixed α angle, this raises the steric compression within the $M(NO)_2$ moiety. In order to reduce the compression, the α angle has to increase.

Prior to the present work, the lessening of the electrostatic repulsions within the $M(NO)_2$ moiety has been considered as the predominant factor involved in the variation of α from one complex to another. The steric influence of the supporting ligand L was assumed to have a minor importance.

IV-1-2 Observations in agreement with the electronic model

The following observations are in agreement with this model. A series of dinitrosyl complexes have been selected from Table IV-I-2-1 (p-156) and Table IV-I-2-2 (p-157).

(i) Upon going from $Co(NO)_2(PPh_3)_2^+PF_6^-$ (ν_{NO}(Nujol) = 1836, 1784 cm^{-1}; α = 136.7(4)°) to $Co(NO)_2(P(OMe)_3)_2^+BPh_4^-$ ($\nu_{NO}(CH_2Cl_2)$ = 1876, 1817 cm^{-1}; α = 128.0(8)°) (Table IV-1-2-1, p-156), the observed closing of α by ca. 9° is in agreement with a decrease in the Co to N back bonding, as inferred by the changes in the ν_{NO} frequencies from 1836, 1784 cm^{-1} to 1876, 1817 cm^{-1}.

(ii) From $Co(NO)_2(PPh_3)_2^+PF_6^-$ ($\nu_{NO}(CH_2Cl_2)$ = 1836, 1784 cm^{-1}; α = 136.7(4)°) to $Rh(NO)_2(PPh_3)_2^+ClO_4^-$ ($\nu_{NO}(CH_2Cl_2)$ = 1759, 1714 cm^{-1}; α = 157.5(3)°) (Table IV-1-2-2, p-157), the metal to NO back bonding increases, as shown by the change in the ν_{NO} values, and this is in line with the expected increase in the metal basicity from a first row to a second row transitional element. The electronic model predicts an increase in the α angle and this is indeed observed.

Table IV-1-2-1

Selected distances (Å), angles (°) and ν_{NO}'s (cm^{-1}) in $Co(NO)_2(L_2)^+X^-$ and $Fe(NO)_2(L)_2$ complexes

Compound		M-L	M-N	α	β	L···N	L···L	N···N	ν_{NO}	Ref.
$Co(NO)_2L_2^+X^-$										
# L	X^-									
10 Py	BF_4^-	2.012(6)	1.654(6)	115.6(3)	93.5(3)	3.03	2.93	2.79	1876,1798	[1]
	Mol. A	2.012(6)	1.644(6)							
		2.013(6)	1.650(6)	115.9(3)	93.0(3)					
	Mol. B	2.016(6)	1.648(6)							
A $P(OMe)_3$	BPh_4^-	2.209(4)	1.594(13)	128.0(8)	99.5(3)	3.07	3.38	2.88	1876,1817	[2]
		2.214(5)	1.613(12)							
B PPh_3	PF_6^-	2.266(3)	1.645(6)	136.7(4)	113.5(2)	3.06	3.79	3.05	1836, 1784	[3]
$Fe(NO)_2(L)_2$										
C PPh_3		2.267(2)	1.650(7)	123.8(4)	111.9(1)	3.14	3.75	2.91	1724, 1678	[4]

Table IV-1-2-2

Selected distances (Å), angles (°) and ν_{NO}'s (cm^{-1}) in $M(NO)_2(PPh_3)_2^n$ (n = o,+1) complexes.

Compound			M-L	M-N	α	β	L···N	L···L	N···N	ν_{NO}	Ref.
$M(NO)_2(PPh_3)_2$											
#	**L**	**M**									
C	PPh_3	Fe	2.267(2)	1.650(7)	123.8(4)	111.9(1)	3.14	3.75	2.91	1724,1678	[5]
D	PPh_3	Ru	2.337(2)	1.762(6)	139.2(3)	103.85(6)	3.22	3.69	3.32	1665, 1615	[6]
			2.353(2)	1.776(6)						<1640>	
E	PPh_3	Os	2.324(2)	1.776(7)	139.1(3)	103.51(6)	3.22	3.66	3.32	1645, 1597	[7]
			2.340(2)	1.771(12)							
F	PPh_3	Ir	2.324(2)	1.787(8)	128.7(4)	103.9(1)	3.44	3.65	3.22	1660, 1645*	[8]
	CO		2.323(2)				3.17			1640 ($CHCl_3$)	
	NO										
$M(NO)_2(PPh_3)_2^+X^-$											
	X^-	**M**									
B	PF_6^-	Co	2.266(3)	1.645(6)	136.7(4)	113.5(2)	3.06	3.79	3.05	1836, 1784	[5]
G	ClO_4^-	Rh	2.355(1)	1.818(4)	157.5(3)	115.8(5)	3.12	3.98	3.56	1759, 1714	[9]
H	ClO_4^-	Ir	2.339(3)	1.771(12)	154.2(7)	116.3(2)	3.09	3.97	3.45	1760, 1715	[10]

Py = pyridine; $P(OMe)_3$ = trimethyl phosphite; Tw = This work, * = Nujol

(iii) Similar support is provided by the opening of α from $Fe(NO)_2(PPh_3)_2$ (ν_{NO} (CH_2Cl_2) = 1724, 1678 cm^{-1}; α = 123.8(4)°) to $Ru(NO)_2(PPh_3)_2$ (ν_{NO}(CH_2Cl_2) = 1665, 1615 cm^{-1}; α =139.2(3)°) (Table IV-1-2-2, p-157). However, with this pair of electro neutral complexes another angular deformation becomes significant. The P-M-P = β angle decreases from Fe (β = 111.9(1)°) to Ru (β = 103.85(6)°) derivative. The electronic model remains silent about what might be responsible for this closing of β.

IV-1-3 Observations not in agreement with the electronic model

(i) From $Fe(NO)_2(PPh_3)_2$ ($\nu_{NO}(CCl_4)$) = 1724, 1678 cm^{-1}; α = 123.8(4)°) to $Co(NO)_2(PPh_3)_2{}^+PF_6{}^-$ (ν_{NO} = 1836, 1784 cm^{-1}; α = 136.7(4)°) (Table IV-1-2-1, p-156), the M to NO back bonding decreases, as inferred by the ν_{NO} values, but the α angle opens up, whereas the electronic model predicts a closing of α.

(ii) In every case moving across the same series of the periodic table from a neutral $M(NO)_2(PPh_3)_2$, (M = Ru, Os) to a cationic $M'(NO)_2(PPh_3)_2{}^+$ (M' = Rh^+, Ir^+), as the M to NO back bonding decreases (ν_{NO} increases), the α angle increases instead of decreasing.

(iii) As a last example of a direct relevance to the present work, the pair of cationic cobalt derivative $Co(NO)_2(P(OMe)_3)_2{}^+$ $-BPh_4{}^-$ (ν_{NO}= (CH_2Cl_2) = 1876, 1817 cm^{-1}; α = 128.0(8)°) and

$Co(NO)_2(Py)_2^+BF_4^-$ (ν_{NO} = 1876, 1798 cm^{-1}; α = 115.6(3)°/115.9(3)°) (Table IV-1-2-1, p-156) were selected. From the $P(CMe)_3$ to the pyridine derivative, the Co to NO back bonding *does not decrease* (ν_{NO} does not increase). Consequently, the electronic model predicts that there should not be a decrease in α angle and this is in obvious conflict with the observed closing of α by ca.13°.

IV-1-4 A new proposal : the stereoelectronic model

In the new model proposed, the basic postulate that the non-bonded covalent radius of a nitrosylic N-atom is an increasing function of the extent of M to NO back bonding was kept. *However, the possibility that the non-bonded interactions in the M(NO)L moieties of a $M(NO)(L)_2^X$ complex might be more influential that the non-bonded interactions within the $M(NO)_2$ subunit is not ruled out at the outset.* For deciding which of these two types of repulsive interactions might be identified as the predominant one, the following approach was taken.

Fig.IV-1-4-3 (p-160) represents an idealized case of a pseudotetrahedral dinitrosyl complex with mm2 point symmetry at M. Consider a chemical change in the $M(L)_2$ portion which *lessens* the NO repulsive influence (i.e. decrease the M to NO backbonding), but leaves *invariant* geometrical parameters r_N, r_L, and β . This change would result in either a decrease in the

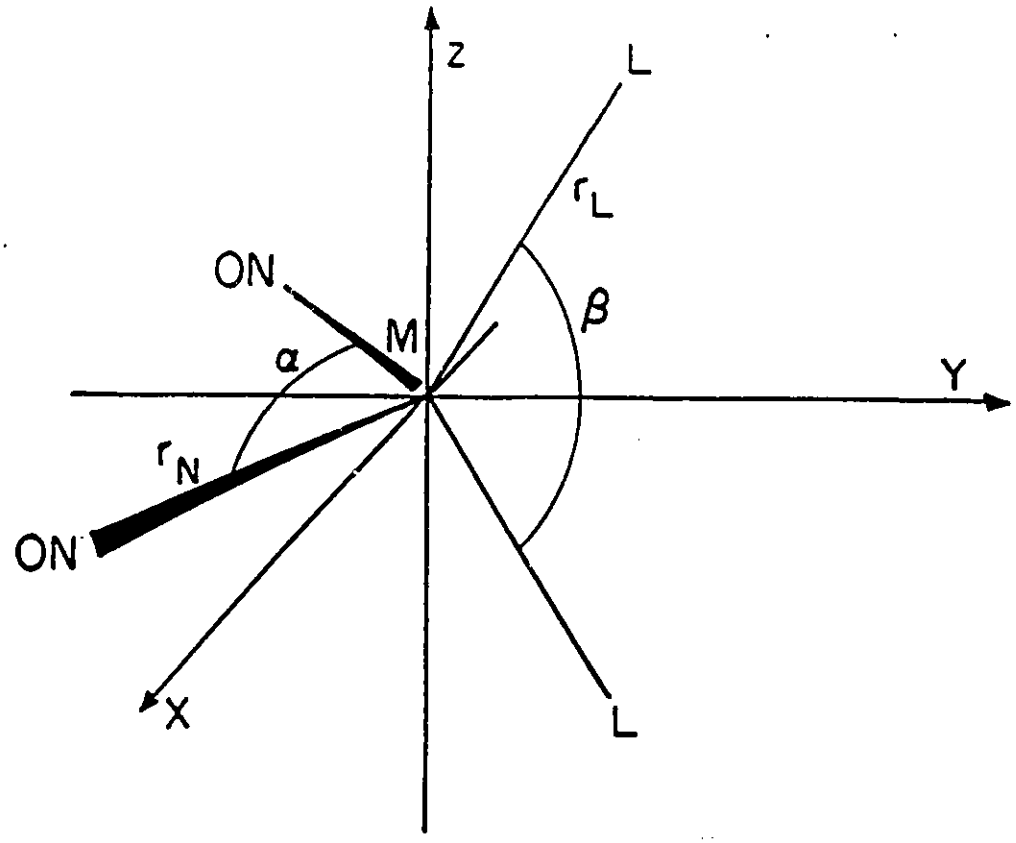

$$\text{Eq 1} \qquad d^2_{LN} = r^2_L + r^2_N + 2 \cdot r_L \cdot r_N \cdot \cos(\alpha/2) \cdot \cos(\beta/2)$$

$$\text{Eq 2} \qquad d_{LL} = 2 \cdot r_L \cdot \sin(\beta/2)$$

$$\text{Eq 3} \qquad d_{NN} = 2 \cdot r_N \cdot \sin(\alpha/2)$$

Fig. IV-1-4-3

Representation of a pseudotetrahedral $M(NO)_2$, D_{NO}^{8+2} complex in mm2 symmetry

$d_{N\cdots N}$ separation or a decrease in the $d_{L\cdots N}$ distance. A decrease in $d_{N\cdots N}$ separation would occur, if the repulsive interactions in M(NO)(L) moieties are the predominant one, and this will imply a closing of the α angle (eq.3 Fig.IV-1-4-4, p-160). A decrease in $d_{L\cdots N}$ separation would take place, if the repulsive interactions in the $M(NO)_2$ moieties are the most influential, and this will imply an opening of the α angle (eq.1 Fig.IV-1-4-4, p-160).

To decide which one of these two possibilities are supported by experimental data, it suffices to consider the structures of $Fe(NO)_2(PPh_3)_2$ ($\nu_{NO}(CCl_4)$ = 1724, 1678 cm^{-1}, α = 123.8(4)°) and $Co(NO)_2(PPh_3)_2{}^+PF_6{}^-$ ($\nu_{NO(nujol)}$ = 1836, 1784 cm^{-1}, α = 136.7(4)° from Table IV-1-2-1(p-156). Upon going from the Fe complex to the Co^+ complex, the increase in the ν_{NO} values implies a decrease in the extent of M to NO backbonding in cobalt complexes. In addition the geometrical parameters r_N, r_L and β vary little. *The observed increase in α by ca. 13° from the neutral Fe complex to the cationic Co complex supports the view that it is the repulsive interactions in M(NO)L which have the predominant role in controlling the value of α.*

The same conclusion is also valid for pentacoordinated dinitrosyl complexes. This is shown by comparing the data belonging to the pair of manganese complexes from $Mn(NO)_2(P(OMe)_2Ph)_3{}^+BF_4{}^-$ (ν_{NO} = 1760, 1712 cm^{-1}; α =

116.5(5)°) to $Mn(NO)_2(P(OMe)_2Ph)_2Cl$ (ν_{NO} = 1713, 1674 cm^{-1}; $\alpha 1$ = 111.5(5)°, $\alpha 2$ = 112.1(5)°, $\alpha 3$ = 113.5(5)°) (two crystalline forms and three independent molecules) [11]. The M to NO back bonding is less in the BF_4^- derivative compared to the chloro derivative as inferred from the ν_{NO} values. The standard electronic model predicts an opening of the α angle from BF_4^- to chloro complex. Instead, the α angle closes. The closing of the α angle can be interpreted in terms of the changes in electrostatic repulsions within the M(NO)(L') moieties. As the M to NO back bonding increases in the Mn-chloro complex, the electrostatic repulsion in the M(NO)(L') moieties also increases and is the predominant factor for the closing of α from BF_4^- complex to chloro complex.

To distiguish the new model from the electronic model, which exclusively placed the attention on $M(NO)_2$ moieties, one can refer to the former as the "stereoelectronic model". It has an "electronic" component because of its extent of M to NO backbonding, which imposes the NO steric demand, and it has a "steric" component because the non-bonded (i.e. steric) component of its steric interactions between L and NO play the predominant role in controlling the value of the N-M-N = α angle.

Another question which also deserves consideration is the behavior of the P-M-P = β angle in the triphenylphosphine complexes. For example in two pairs of $M(NO)_2(PPh_3)_2^x$ (x = 0, +1)

complexes, in the first pair M = Fe, Ru and x = 0, in the second one M = Co, Rh and x = +1, in Table IV-1-2-2 (p-157) one observes that from M = Fe to M = Ru or M = Co to M = Rh, the α angle increases systematically upon replacing a first row transition element by the second row element in the same group of the periodic table. One also observes that the P-M-P = β angle is little affected in the cationic series (113.5(2)° (Co), 115.8(5)° (Rh)), but decreases significantly in the electroneutral one (111.9(1)° (Fe), 103.85(6)° (Ru)). The old electronic model, with the emphasis placed solely on the interactions within $M(NO)_2$, was incapable of offering a simple rationalization. Alternatively, the stereoelectronic model allows such a simple explanation. With the attention placed on the involvement of steric interactions between L and NO, one can view the M(NO)(L) portions as providing a *mechanical link* between the $M(NO)_2$ and $M(L)_2$ subunits. *One can then assume the existence of a threshold such that* :

- as long as the extent of M to NO backdonation places the non-bonded influence of a NO below the threshold, the compression strain remains confined within the $M(NO)_2$ and M(NO)(L) portions. This assumption implies that in Fe, Co and Rh complexes, the non-bonded influence of a NO is below threshold. This is the only conclusion in agreement with the similarities in the β angle (range ca. 112°-116°).

- when the extent of backbonding is sufficiently large to place the non-bonded influence of a NO at, or above, the threshold, the β angle closes in order to achieve a more favorable rebalancing of the non-bonded forces within the $M(NO)_2$, M(NO)L and $M(L)_2$ portions. This assumption implies that the non-bonded influence of the NO is above the threshold in the Ru complexes with a β angle of 103.85(6)°. The average ν_{NO} value of $<\nu_{NO}>$ (nujol) = (1665 + 1615)/2 cm^{-1} = 1640 cm^{-1} of this Ru complex can serve as an indicator of the magnitude of the M to NO backbonding required to be at or above the threshold.

Now comparing the data pertaining to the pair of Ir complexes $Ir(NO)_2(PPh_3)_2^+ClO_4^-$ (ν_{NO}(nujol) = 1760, 1715 cm^{-1}) and $Ir(CO)(NO)(PPh_3)_2$ ($\nu_{NO}(CHCl_3)$ = 1640 cm^{-1}). Upon replacing a NO^+ by a CO and going from the cationic complex to the electroneutral one, the M to NO backbonding is expected to increase. This is indeed well reflected by the decrease in the ν_{NO}'s values. In addition, regarding in $Ir(CO)(NO)(PPh_3)_2$, the ν_{NO} of 1640 cm^{-1} implies that the Ir to NO backbonding should have reached the postulated threshold. Consequently, the β angle should close significantly for $Ir(NO)_2(PPh_3)_2^+ClO_4^-$ to $Ir(CO)(NO)(PPh_3)_2$. This is exactly what is observed. In $Ir(NO)_2(PPh_3)_2^+$, the β angle is equal to 116.3(2)°, which is comparable to that of 115.8(5)° for $Rh(NO)_2(PPh_3)_2^+$, whereas in $Ir(CO)(NO)(PPh_3)_2$, the β angle has closed to a value of 103.9(1)°

which does not differ significantly from that of 103.85(6)° found for $Ru(NO)_2(PPh_3)_2$.

We are now in a position to comment upon the α angle observed in $Co(NO)_2(Py)_2^+$. Considering the pair of complexes $Co(NO)_2(P(OCH_3)_3)_2^+ BPh_4^-$ ($\nu_{NO}(CH_2Cl_2)$ = 1876, 1817 cm^{-1}, α = 128.0(8)°) and $Co(NO)_2(Py)_2^+BF_4^-$ ($\nu_{NO}(CH_2Cl_2)$ = 1876, 1798 cm^{-1}, α = 115.6(3)° cation A and 115.9(3)° cation B)), Table IV-1-2-1 (p-156). It has already been indicated that from the $P(OCH_3)_3$ derivative to the pyridine derivative, the closing of α by ca. 13° is not associated with a lessening of the Co to NO backdonation. This implies that:

-the $Co(NO)_2$ is more compressed in the pyridine complex than in the $P(OCH_3)_3$ analog.

-the repulsions in Co(NO)(Py) predominate over those in $Co(NO)_2$ for fixing the value of the α angle.

This closing of α then becomes readily interpreted as the response to the large decrease in the Co-L bond lengths from 2.209(4)-2.214(5)Å in $Co(NO)_2(P(OCH_3)_3)_2^+$ to 2.012(6) -2.016(6)Å in $Co(NO)_2(Py)_2^+$ in order to prevent an excessive build up of compression in the Co(NO)(Py) fragments. The facile dissociation of a pyridine ligand from $Co(NO)_2(Py)_2^+$ then becomes easily understandable as a means to provide a steric decompression of the $Co(NO)_2$ molecular portion.

The displacement of the N2 atom in bimetallic **(12)** can be

rationalized in terms of the compression strain experienced by the Co(NO)(Py) moiety. In order to relieve part of the steric pressure exerted by the pyridinyl N donor sites on the least rigidly held terminal NO, the N2 atom is severely displaced out of the Co1N3N5 plane.(See Fig. III-3-16-13; p =134).

Conclusion

The main difference between the interpretation of the observed changes in the (O)N-M-N(O) = α angle of $M(NO)_2(L)_2^x$ complexes and the currently accepted model resides in the extent of involvement of the repulsive forces in the $M(NO)_2$ molecular portion. Rather than placing an exclusive emphasis on these interactions, the preceeding discussion has offered a rationalization of the angular variations by considering the interplay of the non-bonded interactions pertaining to the $M(NO)_2$, M(NO)(L) and $M(L)_2$ moieties. In several instances, notably in $Co(NO)_2(Py)_2^+$, the interactions in M(NO)(L) are viewed as the controlling factor, so that an opening of α can no longer be taken as reflecting an increase in the metal to NO back-donation. In addition, we have presented literature data which sustain the notion that the M(NO)(L) moities can act as a mechanical relay between the $M(NO)_2$ and $M(L)_2$ portions, a relay which is activated when the repulsions in M(NO)(L) have reached a threshold causing the β angle to close.

Chapter 2 A theoretical and experimental analysis of the angular parameters in $M(NO)_2$ fragments

IV-2-1 The relationship between O-M-O = ω, N-M-N = α and M-N-O = γ angles in a M(NO)(N'O') moiety

When the structure of a nitrosyl complex is reported in the literature, the angle γ^{mes} sustended at N by the M and O atoms of a MNO linkage is invariably reported. Very frequently this is the sole angular parameter which is given and this fails to describe the finer details of the geometry of the MNO group. This section presents the additional angular parameters needed to describe more fully the geometry of a MNO linkage in a dinitrosyl M(NO)(N'O') molecular fragment. The family of dinitrosyl complexes listed in Table IV-2-1-3 (p-176) and Table IV-2-1-4 (p-180) will be selected as representative examples.

Taking the NMN' plane as the *reference* plane, the bending affecting each M-N-O linkage of the $M(NO)_2$ fragment can be separated into two components, referred to as the *in-plane* and the *out-of-plane* bendings.

In Fig. IV-2-1-4 (p-170) and Fig. IV-2-1-5 (p-171) one nitrosyl ligand has been labelled NO and the other N'O'. What will be said about NO will apply fully to N'O'. The actual location of the oxygen atom of the nitrosyl ligand NO is on a sphere of center N, and radius r_O equal to the observed NO bond length, and can be

described in terms of two angular deformations. Starting from the atom placed on point O_{li} on the MN vector, an in-plane bending moves the oxygen atom from O_{li} to O_{in} in the NMN' plane. Subsequently an out-of-plane bending perpendicular to the NMN' plane moves the atom to its actual location O. The atom projects orthogonally from its actual location O, onto point O_p.

(i) In-plane bending of a nitrosyl ligand in $M(NO)_2$: the γ_{in} angle

For a given nitrosyl ligand the in-plane bending can move the oxygen atom towards the other nitrosyl ligand or away from it. In the first case the nitrosyl ligand will be defined as **syn**-NO and in the second one it will be referred to as **anti**-NO. Accordingly, in Fig. IV-2-1-4 (p-170) and Fig. IV-2-1-5 (p-171) the conformation of NO is syn, while that of the ligand N'O' is anti.

When the in-plane bending is such that the Ol_i-N-O_{in} angle is less than ca. 0.5° the conformation of the nitrosyl ligand will be qualified as **in-plane-linear**. With this terminology, any possible conformation of the pair of nitrosyl ligands of a M(NO)(N'O') moiety can be easily identified by specifying the conformation of each nitrosyl ligand. The **[syn,syn]** and **[anti,anti]** conformations are commonly referred to in the literature as **endo** = **attracto** and **exo** = **repulso** (Fig. IV-2-1-4 (p-170) and Fig. IV-2-1-5 (p-171)). This attracto-repulso terminology conveys descriptive information about the pair of nitrosyl ligands considered as a unit,

but does not cover all the possible cases which include the **[syn-anti]**, **[syn,in-plane-linear]** , **[anti, in-plane linear]** and **[in-plane-linear, in-planelinear]** conformations. It is well suited to describe the geometry of a M(NO)(N'O') moiety when the bisector of the NMN' angle is a C_2 axis. In that case, what is known about one MNO linkage applies to the symmetry related one. However, in many structures the two MNO ligands are crystallographically independent.

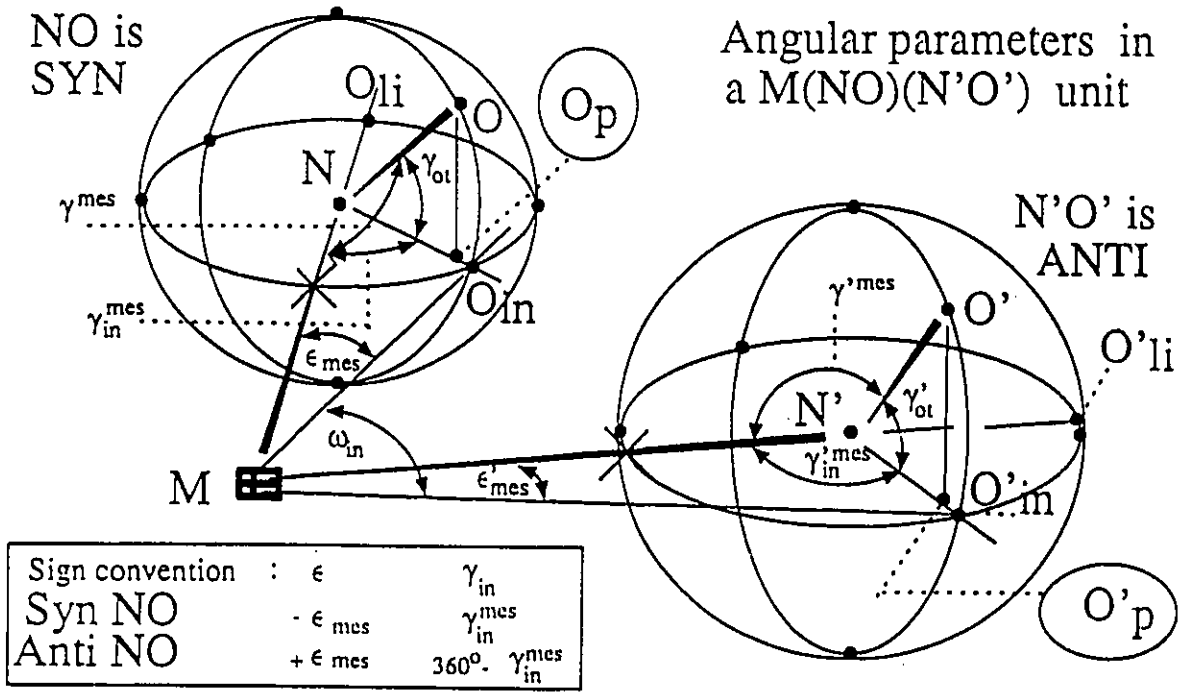
NO is SYN
Angular parameters in a M(NO)(N'O') unit
Oli
O
Op
N
γ_{ot}
γ^{mes}
γ_{in}^{mes}
Oin
ϵ_{mes}
ω_{in}
M
N'O' is ANTI
γ'^{mes}
O'
O'li
N'
γ'_{ot}
γ'^{mes}_{in}
ϵ'_{mes}
O'in
O'p
Sign convention : ϵ γ_{in}
Syn NO $-\epsilon_{mes}$ γ_{in}^{mes}
Anti NO $+\epsilon_{mes}$ $360^{o}-\gamma_{in}^{mes}$

Fig. IV-2-1-4

Angular relationships in an
in-plane M(NO$_{in}$)(N'O'$_{in}$) unit

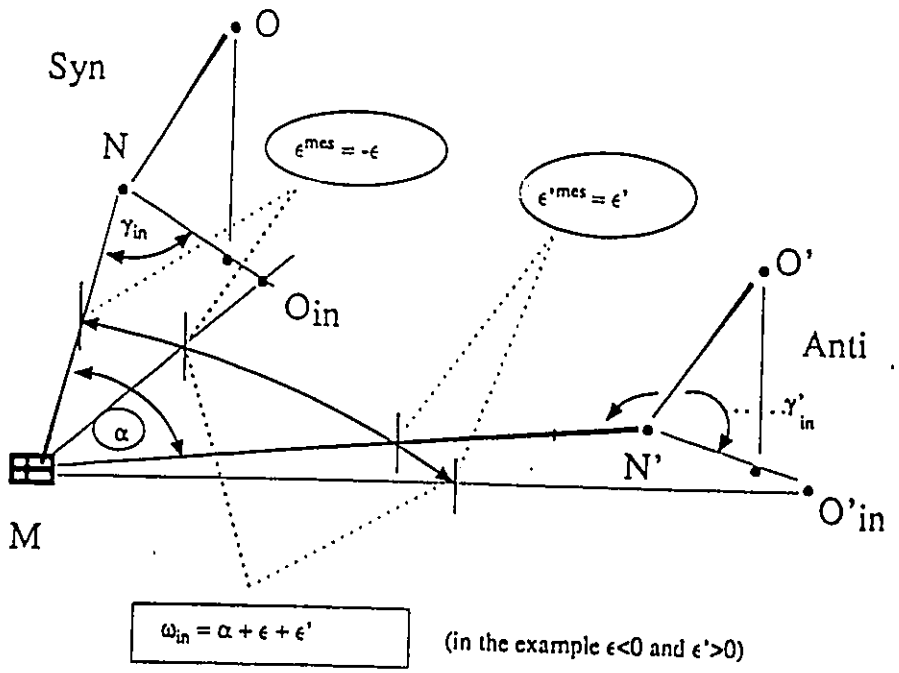

Fig. IV-2-1-5

(ii) The γ_{in} angle : In-plane bending of a nitrosyl ligand in $M(NO)_2$ moiety

To specify the direction of the in-plane bending of a nitrosyl ligand it suffices to adopt the following convention.

The γ_{in}^{mes} angle is the angle M-N-O_{in} and γ_{in} is the angle required to set the MN vector colinear with the NO_{in} by a rotation around N in a way that the NO ligand is **towards** the other nitrosyl ligand (i.e. N'O'). It follows that :

- When the NO conformation is syn (or in the extreme case in-plane-linear) one has :

$$\gamma_{in} = \gamma_{in}^{mes} = < 180°$$

- When the N'O' conformation is anti, one has :

$$\gamma'_{in} = 360° - \gamma'^{mes}_{in} > 180°$$

In every case, the in-plane bending $\delta\gamma_{in}$ measuring the extent of deviation of the ligand NO from an in-plane linear conformation is the angle O_{li}-N-O_{in} given by $\delta\gamma_{in} = |180° - \gamma_{in}|$ The equivalent angle for the ligand N'O' is O'_{li}-N'-O'_{in}.

(iii) The γ_{ot} angle : Out-of-plane bending of a nitrosyl $M(NO)_2$ moiety

Taking the NO ligand of Fig. IV-2-1-4 (p-170) and Fig. IV-2-1-5 (171) as an example this second deformation is conveniently described by the angle γ_{ot} between the NO_{in} and NO vectors (for the ligand N'O' the equivalent angle is γ'_{ot} as shown on the same figure).

For each of the nitrosyl ligands of a M(NO)(N'O') moiety, after having computed the in-plane and out-of plane bendings, one can calculate the parent in-plane geometry of the in-plane MNO_{in} ($N'O'_{in}$) subunit from which the $\omega_{in} = O_{in}\cdots M\cdots O'_{in}$ angle can be calculated.

(iv) Analysis of the structures listed in Table IV-2-1-3

The angles γ^{mes}, γ_{in}^{mes}, γ_{ot} and $\delta\gamma_{in}$ have been computed for each of the NO ligands of the complexes of Table IV-2-1-3 (p-176). When two crystallographically independent NO ligands are present in a given structure, the arithmetic mean $< \gamma_{in} >$ has also been included in Table IV-2-1-3 (p-176). In Table IV-2-1-4 (p-180) ω_{in}, $\omega_{in} - \alpha$, α and ω are presented.

For most of the complexes of the class I and IV $M(NO)_2(L_2)^x$ complexes (x = 0, +1), the out of plane bending is usually small ($\gamma_{ot} < 3°$). In selected cases, however, the bending becomes more significant as for example with $Ru(NO)_2(PPh_3)$ u. (γ_{ot} ca. 5°) and

with the cationic complex $Co(NO)_2(P\wedge N)_2^+$ 9B (γ_{ot} ca. 6°). For the latter, the out-of plane bending is about twice that of the in-plane bending. The in-plane-bending $\delta\gamma_{in}$ falls in the range 0 to 22°. Among the bridged dimer complexes belonging to class III, the sulphido-bridged diirontetra nitrosyl complex q_1 and q_2 stands out for having the largest of both the in-plane and out-of-plane bending (γ_{ot} = 9.5° for one NO, $\delta\gamma_{in}$ = 30.0° respectively for the other NO belonging to the same metallic fragment).

A pronounced out-of-plane bending is also observed with the $M(NO)_2LX$ complexes class II (X = halide, L = Phosphines). With one exception, γ_{ot} falls in the range 8-14°. For the $Co(NO)_2(PPh_3)I$ j and $Co(NO)_2(P\wedge N)I$ 8 complexes, γ_{ot} is comparable to or larger than $\delta\gamma_{in}$. The reverse is observed with the $Fe(NO)_2(PPh_3)Cl$ k iron derivative. In every case, the out-of-plane bendings move the nitrosylic O atoms away from the halide X atom.

Whatever the magnitude of the out of plane bending, the data of Table IV-2-1-4 (p-180), also show that in every case the ω = O···M···O' angle differs by less than 1° from ω_{in} = O_{in}-M-O'_{in} angle of the corresponding in-plane geometry. *Consequently, the observed linear correlation between ω and α implies a linear correlation between ω_{in} and α. The latter is expressed geometrically by the plot of Fig.IV-2-1-6 (p-184) and it is the one which will be considered from now on.*

The equation of the linear regression line is given by

(1) $\omega_{in} = a \times \alpha + b$

$a = 1.606$; $b = -78.343$; $r = 0.9972$; $\sigma = 1.42°$

The linear relationship between ω_{in} and α (and also between ω and α) holds fairly well over the wide range of observations for $\alpha \approx 110°$ to $155°$. The general trend is that for $\alpha = 110°$ to $130°$, ω_{in} is less than α, while the reverse is true for $\alpha > 130°$.

Table IV-2-1-3 The family of dinitrosyl complexes selected as representative examples to account for the angular variations

Complexes

$M(NO)_2(L)_2^x$(x = 0, +1) First row metals

class I

M	L	#	γ^{mes}	$<\gamma^{mes}>$	γ_{in}^{mes}	γ_{in}	$<\gamma_{in}>$	DA[a]	$\gamma_{ot}/\delta\gamma_{in}$	Ref
Co	Py	10A	170.2(6)	170.15	170.3	170.3	170.7	89.3	1.5/9.7	[1]
			170.1(6)		171.1	171.1			1.7/8.9	
Co	Py	10B	170.7(6)	169.9	170.8	170.8	170.0	89.2	1.4/9.2	[1]
			169.1(7)		169.2	169.2			1.4/10.8	
Co	PAN	9A	178.4(4)	178.4	179.2	179.2	179.2	87.8	1.3/0.8	TW
Co	PAN	9B	172.9(4)		176.6	183.4	183.4	79.5	6.3/3.4	
Co	PPh_3	a	171.0(5)	171.0	171.2	188.8	188.8	87.9	1.8/8.8	[3]
Co	$P(OMe)_3$	b	177.0(13)	178.4	177.2	182.8	181.4	87.3	1.2/2.8	[2]
			179.7(13)						0.3/0.1	
Co	DPP	c	176.6(14)	174.5	172.3	182.7	185.2	88.0	2.1/2.7	[12]
			172.3(11)						0/7.7	
Co	SacSac	d	168.9(5)	168.9	169.0	169.0	169.0	90	1.1/11	[13]

$M(NO)_2(L)_2^x$ (x = 0, +1) First row metals

Class I

M	L	#	γ^{mes}	$<\gamma^{mes}>$	γ_{in}^{mes}	γ_{in}	$<\gamma_{in}>$	DA[a]	$\gamma_{ot}/\delta\gamma_{in}$	Ref
Fe	PPh_3	e	178.2(7)	178.2	178.4	178.4	178.4	87.4	1.0/1.6	[4]
Fe	BCP	f	177.6(6)	177.8	179.0	181.0	179.7	86.2	2.2/1.0	[9]
			177.9(5)						1.3/1.6	
Fe	$BCPBPh_3$	g	175.9(9)	175.9	176.5	183.5	183.5	81.2	2.3/3.5	[9]
Fe	f6fos	h	177.8(7)	177.4	177.8	178.1	178.0	83.3	1.1/1.9	[14]
			176.9(7)						2.3/2.2	
Fe	L'	i	169.8(3)	169.8	169.8	169.9	169.9	84.8	1.2/10.1	[15]
			169.8(3)						0.9/0.2	

$M(NO)_2XL$

Class II

Co	PANI	8	169.0(5)	170.4(7)	178.9	181.1	177.9	88.3	10.9/11	TW
(syn-anti)										
Co	PPh_3I	j	165.2(29)	164.2	170.8	174.9	172.9	89.5	13.9/5.1	[16]
			163.2(22)						14.1/5.1	
$FePPh_3Cl$		k	166.4(5)	166.1	166.5	169.0	167.8	89.5	7.9/11	[17]
			165.7(5)							

M	L	#	γ^{mes}	$<\gamma^{mes}>$	γ_{in}^{mes}	γ_{in}	$<\gamma_{in}>$	DA[a]	$\gamma_{ot}/\delta\gamma_{in}$	Ref
Class III, Bridged complexes										
FePYRA		l_1	163.4(2)	165.8	168.3	163.4	165.8	89.5	0.2/16.6	[5]
			168.2(2)						0.9/11.7	
FePYRA		l_2	158.5(3)	162.8	167.0	158.5	162.8	88.6	0.2/21.5	[5]
			167.0(3)						0/13	
CoPYRA		m_1	173.5(3)	169.3	165.2	173.5	169.4	89.9	0.3/6.5	[5]
			165.1(2)						1.4/14.8	
CoPYRA		m_2	173.0(4)	167.3	161.7	173.0	167.4	87.9	0.7/7	[5]
			161.6(3)						1.0/18.3	
Fe L*		n	175.2(3)	174.6	174.0	175.5	174.8	___	1.7/4.5	[18]
			174.0(4)						0.6/6.0	
Fe L**		o	175.2(5)	175.6	175.9	175.9	175.9	___	2.8/4.1	[19]
			175.9(5)						0.7/4.1	
FeL***		p	176.4(8)	175.4	174.3	176.6	175.5	___	1.15/3.4	[2]
			174.3(7)						0/5.7	
Pt-S-Fe-Fe		q_1	149.6	158.4	171.2	149.6	160.4	v.l.	0.8/30.4	[20]
			167.1						9.5/8.8	
		q_2	150.0	168.5	179.9	150.0	165.0	___	2.2/30.0	[20]
			176.0						3.1/0.1.	

M	L	#	γ^{mes}	$<\gamma^{mes}>$	γ_{in}^{mes}	γ_{in}	$<\gamma_{in}>$	DA[a]	$\gamma_{ot}/\delta\gamma_{in}$	Ref

Second and third row metals

$M(NO)_2(L)_2^X$

Class IV

Rh	PPh_3	r	158.9	158.9	159.1	200.9	200.9	86.0	2.6/20.9	[12]
Ir	PPh_3	s	163.5(1)	163.5	163.6	196.4	196.4	85.7	1.4/16.4	[10]
Ru	BPh_3	t	177.8(60	173.2	187.6	181.5	188.4	84.5	1.8/1.5	[6]
			170.6(5)						5.3/7.6	
Ru	PPh_3	u	168.0(15)	171.4	184.7	192	188.4	84.4	0.67/12	[7]
			174.7(16)						5.3/4.7	
Os	PPh_3	v	178.7	174.1	179.1	180.9	182.9	84.3	0.9/0.9	[7]
									3.6/4.8	

DPP = Diphenyl phosphine; P(OMe)3 = trimethyl phosphite; SacSac = dithioacetylacetanato

TW = this work DA[a] = Dihedral angle between the NMX (X = C,N) and LML plane

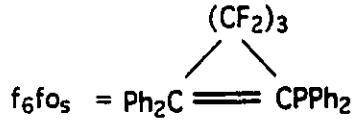

BCP = Ph-P(OCH2CH2)2NH

BCP(BPh3) = Ph-P(OCH2CH2)2NHBPh3

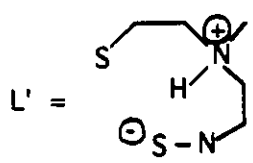

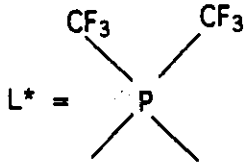

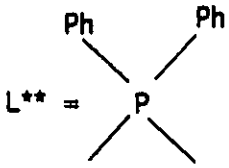

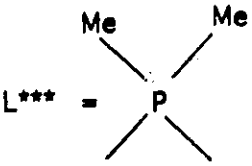

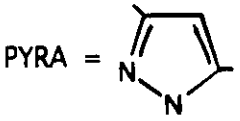

Table IV-2-1-4 The family of dinitrosyl complexes selected as representative examples to account for the angular variations

Complexes

$M(NO)_2(L)_2^x$(x = 0, 1) First row metals

Class I

M	L	#	α	ω	ω_{in}	M-N	N-O	ω_{in}-α	Ref
Co	Py	10A	115.6(3)	107.6(2)	107.6(2)	1.654(6)	1.130(8)	-8.0	[1]
						1.644(6)	1.156(8)		
Co	Py	10B	115.9(3)	107.7(2)	107.7(2)	1.650(6)	1.149(8)	-8.2	[1]
						1.648(6)	1.142(7)		
Co	PAN	9A	126.1(2)	125.5(1)	125.2(1)	1.637(5)	1.146(6)	-0.9	TW
Co	PAN	9B	131.8(2)	134.6(1)	134.3(1)	1.652(5)	1.144(7)	2.5	TW
Co	PPh_3	a	136.7(4)	144.0(1)	144.0(1)	1.645(6)	1.174(6)	7.5	[3]
Co	$P(OMe)_3$	b	128.0(8)	129.2(2)	129.2(2)	1.594(13)	1.16(2)	1.2	[2]
						1.613(12)	1.15(2)		
Co	DPP	c	131.7(5)	135.9(4)	136.0(4)	1.656(10)	1.130(14)	4.3	[12]
						1.671(11)	1.142(13)		
Co	SacSac	d	115.5(3)	106.6(2)	106.6(2)	1.649(2)	1.120(8)	-8.9	[13]
Fe	PPh_3	e	123.8(4)	122.4(4)	122.4(4)	1.650(7)	1.190(10)	-1.4	[4]
Fe	BCP	f	128.3(3)	128.0(3)	128.0(3)	1.646(5)	1.176(6)	-0.3	[9]
						1.638(5)	1.194(6)		

M	L	#	α	ω	ω_{in}	M-N	N-O	ω_{in}-α	Ref
Fe	$BCPBPh_3$	g	132.0(7)	134.9(8)	134.7(8)	1.659(11)	1.195(12)	2.7	[9]
Fe	f6fos	h	125.4(4)	123.8(4)	123.7(4)	1.645(7)	1.181(4)	-1.7	[14]
						1.661(7)			
Fe	L'	i	118.1(1)	109.8(2)	109.8(2)	1.678(3)	1.165(4)	-8.3	[15]
						1.681(3)	1.156(4)		

$M(NO)_2X(L)$, X = halide

Class II

Co	P^NI	8	126.90(3)	124.6(3)	125.1(8)	1.625(7)	1.130(9)	-1.8	Tw
(syn-anti)						1.640(6)	1.156(8)		
Co	PPh_3I	j	121.7(1)	115.1(1)	116.0(1)	1.662(2)	1.154(2)	-5.7	[16]
						1.665(2)	1.153(3)		
Fe	PPh_3Cl	k	115.6(3)	105.492)	105.6(2)	1.679(5)	1.136(7)	-10.0	[17]
						1.681(5)	1.163(7)		

Class III Bridged complexes

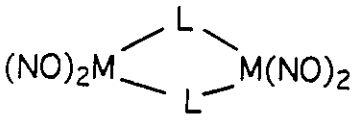

Fe	PYRA	I[1]	112.26(8)	100.8(8)	100.8(8)	1.696(2) 1.692(2)	1.157(2) 1.162(2)	-11.5	[5]
M	L	#	α	ω	ω_{in}	M-N	N-O	ω_{in}-α	Ref
Fe	PYRA	I[2]	109.0(1)	95.0(1)	95.0(1)	1.692(2) 1.694(2)	1.157(2) 1.162(2)	-14.0	[5]
Co	PYRA	m1	113.9(1)	105.3	105.3	1.656(2) 1.669(2)	1.147(3) 1.145(3)	-8.6	[5]
Co	PYRA	m2	110.4(1)	100.2(1)	100.2(1)	1.643(3) 1.677(3)	1.145(3) 1.135(3)	-10.2	[5]
Fe	L*	n	122.4(1)	118.1(1)	118.1(1)	1.661(3) 1.653(3)	1.158(4) 1.156(4)	-4.3	[18]
Fe	L**	o	124.5(3)	121.1(2)	121.1(2)	1.649(5) 1.650(4)	1.165(6) 1.163(6)	-3.4	[19]
Fe	L***	p	125.7(4)	121.9(4)	121.9(4)	1.650(6) 1.646(8)	1.171(1) 1.180(1)	-3.8	[2]
	Pt S								
Fe	Fe	q_1	112.9(8)	97.3(7)	97.3(7)	1.68(2) 1.65(2)	1.164(2) 1.204(3)	-15.6	[20]
		q_2	114.0(9)	102.2(8)	102.2(4)	1.69(2) 1.61(2)	1.185(2) 1.193(2)	-11.8	[20]

M	L	#	α	ω	ω_{in}	M-N	N-O	ω_{in}-α	Ref
Second and third row metals									
$M(NO)_2(L)_2^X$									
Class IV									
Rh	PPh_3	r	157.5(3)	173.7(3)	173.4(3)	1.181(4)	1.158(6)	16.2	[12]
Ir	PPh_3	s	154.2(7)	167.5(7)	167.5(70	1.771(12)	1.213(13)	13.3	[10]
Ru	Ph_3	t	139.2(3)	142.7(2)	142.8(3)	1.762(6)	1.190(11)	3.6	[6]
						1.776(6)	1.194913)		
Ru	PPh_3	u	139.9(7)	146.8(4)	146.8(4)	1.748(20)	1.215(18)	6.9	[7]
						1.688(20)	1.229(18)		
Os	PPh_3	v	139.1(3)	140.6(3)	140.7(3)	1.776(7)	1.211(7)	1.5	[7]
						1.776(6)	1.211(7)		

DPP = Diphenyl phosphine; P(OMe)3 = trimethyl phosphite; SacSac = dithioacetylacetanato

TW = this work DA[a] = Dihedral angle between the NMX (X = C,N) and LML plane

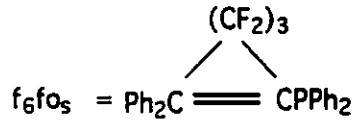

BCP = Ph-P(OCH2CH2)2NH

BCP(BPh3) = Ph-P(OCH2CH2)2NHBPh3

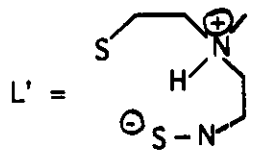

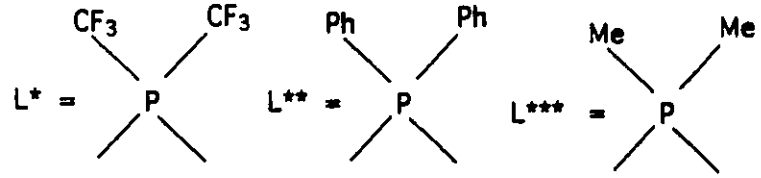

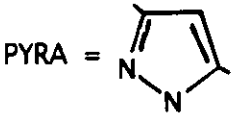

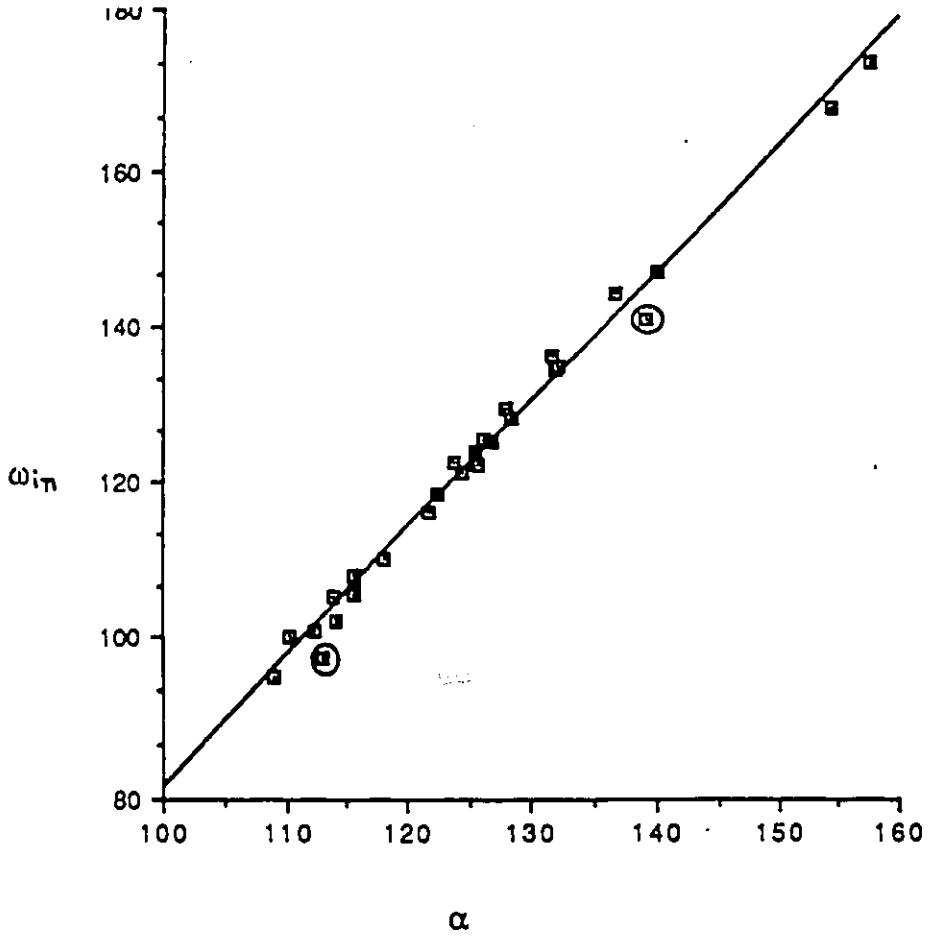

Fig. IV-2-1-6 Plot of ω_{in} VS α

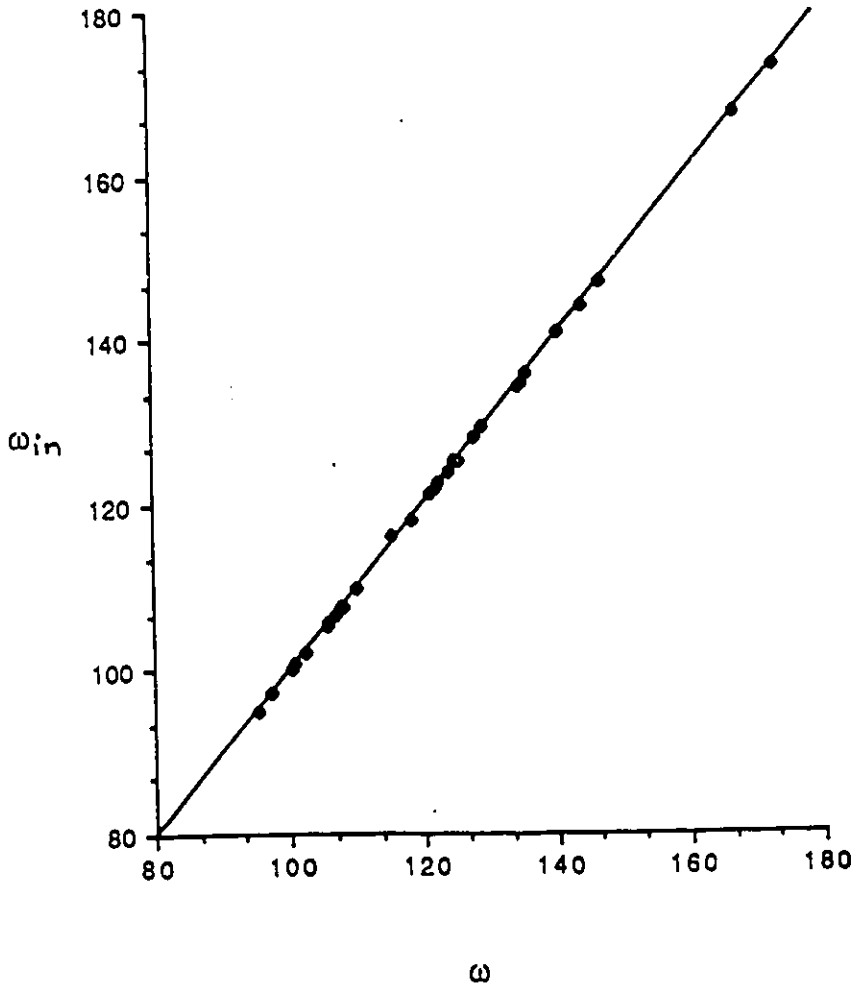

Fig. IV-2-1-7 Plot of ω_{in} VS ω

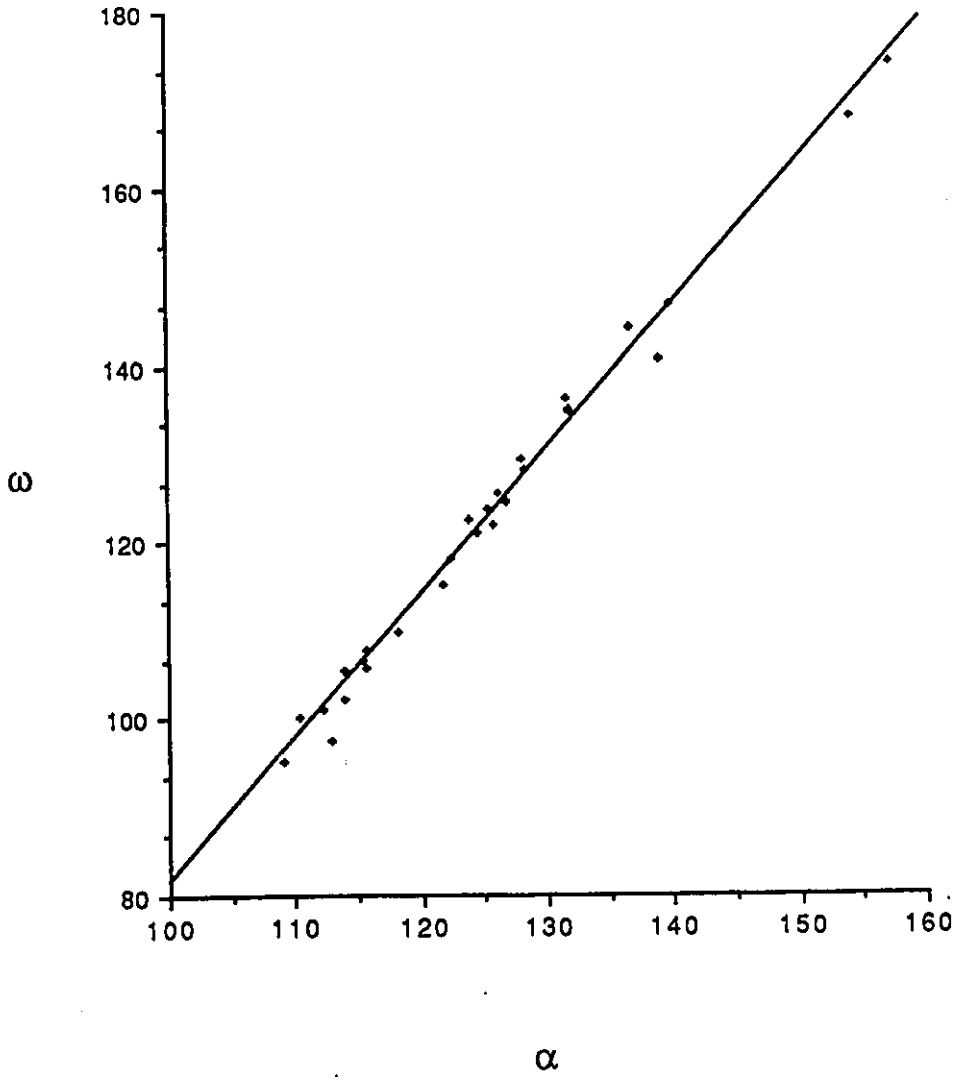

Fig. IV-2-1-8 Plot of ω VS α

IV-2-2 Factors influencing the angle $(O_{in}\cdot\cdot M\cdot\cdot O'_{in})= \omega_{in}$ of the M(NO)(N'O') subunit in an in-plane geometry

(i) Geometrical parameters

When two crystallographically independent nitrosyl ligands are present, the $\omega_{in} = (O\cdot\cdot M\cdot\cdot O')_{in}$ angle is a function of (i) the N-M-N' (α) angle; (ii) the angle $\in_{mes}$ subtended at M by N and O_{in} in the MNO_{in} triangle ;(iii) the angle $\in'_{mes}$, equivalent to $\in_{mes}$, belonging to the $MN'O'_{in}$ triangle. To obtain the ω_{in} angle, when the conformation of nitrosyl ligand is **anti**, the corresponding $\in_{mes}$ must be added to α, when the conformation is **syn**, the corresponding $\in_{mes}$ must be substracted to α.

In order to use a single relationship for calculating ω_{in} , whatever the conformation of the nitrosyl ligands, a signed $\in$ angle will be used with the following sign convention.

-when the NO is anti, $\in$ is counted positively and :

$$\in = \in_{mes}$$

- when the NO is syn, $\in$ is counted negatively and :

$$\in = -\in_{mes}$$

Irrespective of the conformation of each NO ligand, in every case,

one then has :

(2) $\omega_{in} = \alpha + \in + \in'$ (Fig.IV-2-1-5, p-171)

(ii) Factors influencing a $\in_{mes}$ angle

In the NMO_{in} triangle, the $\in_{mes}$ angle is a function of the M-N (r_N) and N-O (r_O) bond lengths and of the M-N-O_{in} = γ_{in}^{mes} angle. Table IV-2-1-5 (p-189). The relative contributions of these three parameters is evaluated in the next paragraphs.

Table IV-2-1-5
Variation of $\in_{mes}$ with r_N and r_O at a given γ_{in}^{mes}

$\langle r_N \rangle$ = 1.657(21)Å

r_N^{max} = (1.657+0.021)Å = 1.678Å

r_N^{mean} = 1.657Å

r_N^{min} = (1.657-0.021)Å = 1.636Å

$\langle r_O \rangle$ = 1.158(20)Å

r_O^{max} = (1.158+0.020)Å = 1.178Å

r_O^{mean} = 1.158Å

r_O^{min} = (1.158-0.020)Å = 1.138Å

$(\gamma_{in}^{mes})^\circ$	$(\in_{mes}^{max})(^\circ)$	$(\in_{mes}^{mean})(^\circ)$*	$(\in_{mes}^{min})(^\circ)$
150	12.5	12.3	12.1
155	10.4	10.2	10.1
160	8.4	8.2	8.1
165	6.3	6.2	6.1
170	4.2	4.1	4.0
175	2.1	2.1	2.0
179	0.4	0.4	0.4

* results rounded to the first decimal place

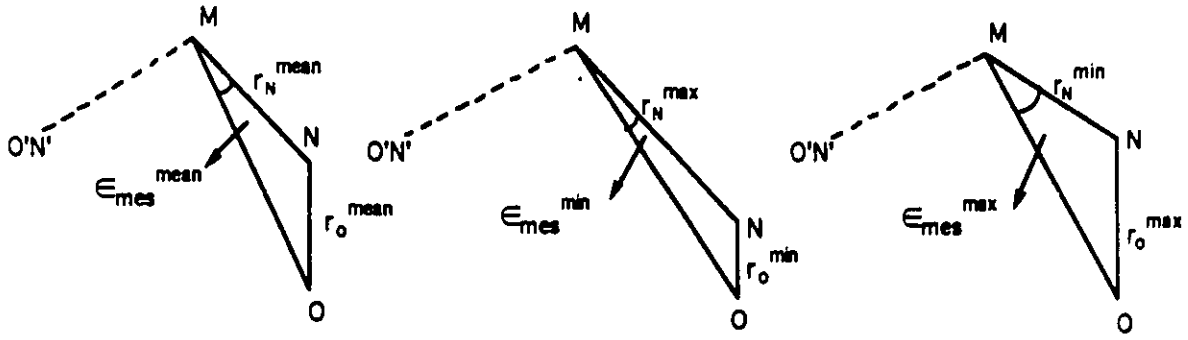

Fig.IV-2-1-9 Variation of $\in_{mes}$ with r_N and r_O

(iii) Variation of the M-N and N-O bond lengths at a fixed γ_{in}^{mes}

The arithmetic means $<r_N>$ and $<r_O>$ of the values of the M-N and N-O bond lengths of the first row metal complexes listed in Table IV-I-2-1 (p-156) and Table IV-I-2-2 (p-157) have been calculated, as well as the standard deviations $\sigma(r_N)$ and $\sigma(r_O)$ from the means. In sample calculations, for each of the M-N and N-O bond lengths, two extreme values have been considered, $<r_N> \pm \sigma(r_N)$ and $<r_O> \pm \sigma(r_O)$ respectively.

As shown in Fig.IV-2-1-9 (p-189), the N-M-O angle = $\in_{mes}$ for a given γ_{in}^{mes}, will have:

- Its lowest value $\in_{mes}^{(min)}$ when the longest M-N and shortest N-O bond lengths are selected

- Its largest value $\in_{mes}^{(max)}$ when the shortest M-N and longest N-O bond lengths are chosen.

The results of the calculations are presented in Table IV-2-1-5 (p-189), for seven different values of γ_{in}^{mes} ($[150 + 5k]°$ with k = 0 to 5, and 179°). It can be seen that at a given γ_{in}^{mes} angle, the maximum relative variation of $\in_{mes}$ due to a change in the M-N and N-O bond lengths is only at most 5% of the angle $\in_{mes}^{(mean)}$.

One can then conclude that *the predominant factor which fixes the value of* $\in_{mes}$ *is the* γ_{in}^{mes} *angle* , while the M-N = r_N and N-O = r_O lengths provide only a secondary contribution.

(iv) Variation of γ_{in} at fixed M-N and N-O bond lengths

In Fig. IV-2-1-10 (p-193) an oxygen atom O is free to move on the circle of center N and of radius r_O . Relative to the M-N vector taken as a reference direction, when O is placed towards the second N'O' ligand, the conformation of the NO ligand is **syn** (consequently, $\in = -\in^{mes}$ and $\gamma_{in} = \gamma_{in}^{mes}$), when it is placed away from N'O' the conformation is **anti** (consequently : $\in = \in_{mes}$ and $\gamma_{in} = 360° - \gamma_{in}^{mes}$). Setting r_N and r_O equal respectively to the mean values $\langle r_N \rangle = 1.657Å$ and $\langle r_O \rangle = 1.158Å$ respectively. The $\in$ angles have been calculated for each $\gamma_{in} = (10 \times k)°$, (k = 1 to 36). The results of the calculation are tabulated in Table IV-2-1-6 (p-193) and presented graphically by the $\in$ vs γ_{in} plot of Fig. IV-2-1-11 (p-194). It can be seen that from $\gamma_{in} = 100°$ to 260° the curvature of the $\in$ vs (γ_{in}) curve is so small that $\in$ appears as being linearly correlated to γ_{in}. Within this range of γ_{in} values, the least squares regression straight line (3) represents, to an excellent approximation, the variations of $\in$ imparted by the variation in γ_{in}.

(3) $\quad \in = A \times \gamma_{in} + B$

with A = 0.4092, B = -73.66 (r = 0.99999)

(Note that in every case one must have B = -180°xA, as 0° and

180° are points of inverse symmetry).

In principle, the values of A and B are a function of r_N and r_O. In practice however, for the range of values spanned by the r_N and r_O bond lengths of all the complexes listed in Table IV-2-1-3 (p-176) the variation in A and B are small. This is shown by the results of calculation presented in Table IV-2-1-7 (p-195).

For all of these complexes A should be around 0.4 and B = -180°xA around -72.

Table IV-2-1-6 Computation of $\in$ for each γ_{in} angle

r_N = M-N = 1.65Å ; r_O = N-O = 1.158Å

γ_{in}	$\in$
10	-21.2687
20	-34.8482
30	-41.5131
40	-44.0327
50	-44.1861
60	-42.9321
70	-40.7937
80	-38.0715
90	-34.9481
100	-31.5399
110	-27.9247
120	-24.1567
130	-20.2749
140	-16.3087
150	-12.2809
160	-8.20996
170	-4.11182
179	-.412352
190	4.11182
200	8.20996
210	12.2808
220	16.3086
230	20.2748
240	24.1566
250	27.9247
260	31.5399
270	34.9481
280	38.0715
290	40.7936
300	42.9321
310	44.1861
320	44.0327
330	41.5132
340	34.8483
350	21.2689
360	00.0000

($\in$ = 0, for γ_{in} = 0°,180°,360°)

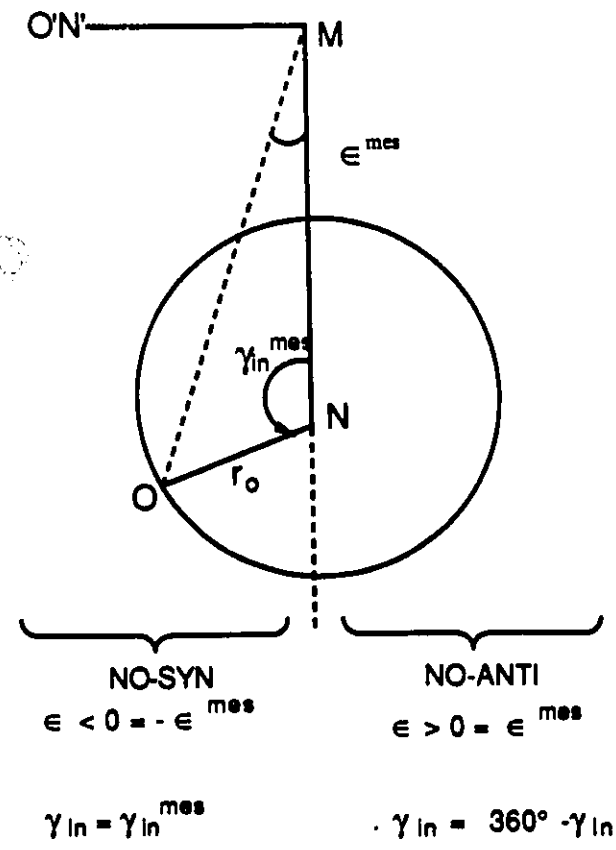

γ_{in}^{mes} = angle sustended at N by the M and O atoms

Fig. IV-2-1-10 Variation of the γ_{In} angle at fixed r_N and r_O

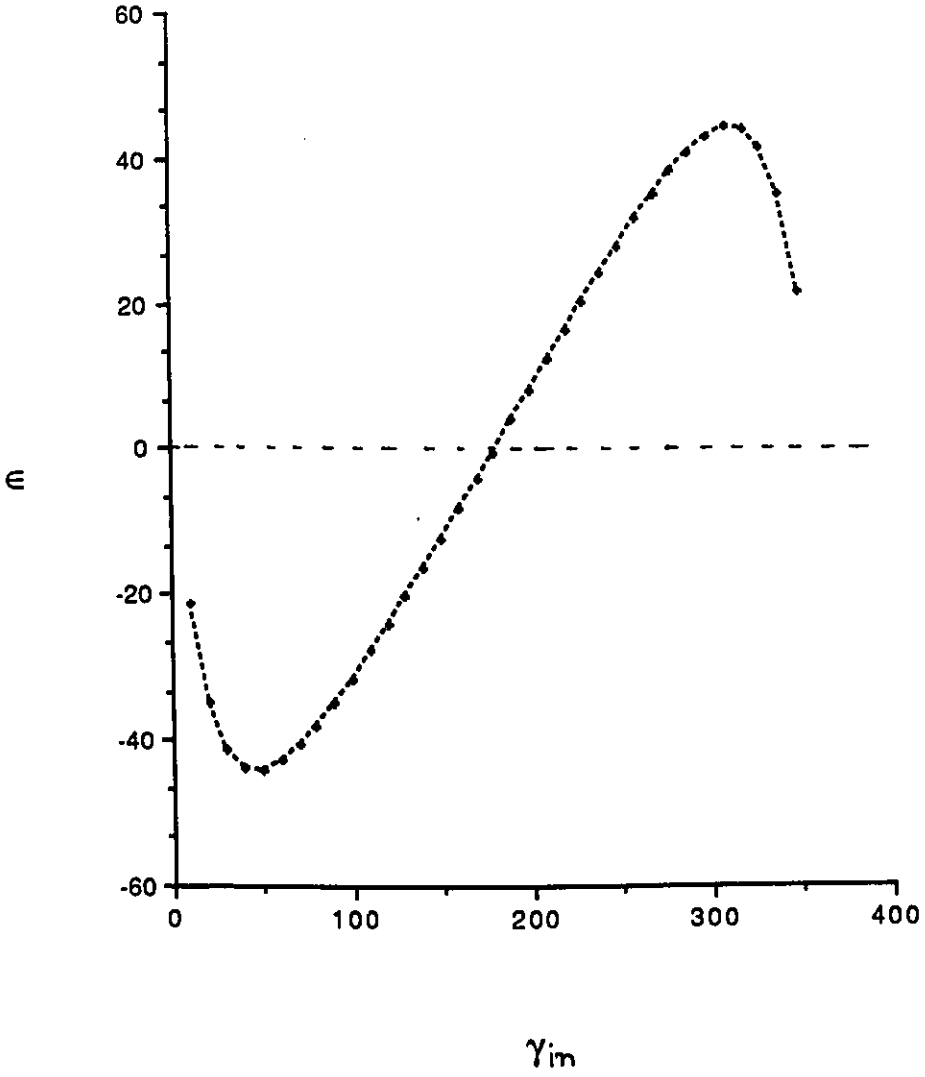

Fig. IV-2-1-11 Plot of $\in$ VS γ_{in}

Table IV-2-1-7 Calculations for A and B for all the complexes listed in table Iv-2-1-3

$$\in = A \times \gamma_{in} + B$$

$$B = -180° \times A$$

$$\text{or } \in = A(\gamma_{in} - 180°)$$

First Row Metals*

$\langle r_N \rangle$ = 1.657(21), $\langle r_O \rangle$ = 1.158(20)

Second Row Metals**

$\langle r_N \rangle$ = 1.764(36), $\langle r_O \rangle$ = 1.200(30)

r_N	1.636	1.657	1.678	1.728	1.764	1.800
r_O	1.178	1.158	1.138	1.230	1.200	1.170
A	0.4175	0.4092	0.4031	0.4144	0.4037	0.3918
B	-75.15	-73.73	-72.58	-74.59	-72.67	-70.52

In every case, correlation coefficient = 0.99999·· for $\in$ vs γ_{in} in the range 100° -260° with σ = 0.03°.

* mean values of r_N and r_O (Å) computed for the first row complexes of class I, II ,III of Table IV-2-1-3.

** mean values of r_N and r_O (Å) computed for the five second and third row complexes of Class IV of Table IV-2-1-3.

IV-2-3 **The geometrically imposed relationship of (ω_{in}-α) vs $<\gamma_{in}>$**

When a planar $M(NO)_2$ moiety is considered with two crystallographically independent MNO and MN'O' linkages, the $\omega_{in} = O_{in}\cdot\cdot M\cdot\cdot O_{in}'$ and α = N-M-N' angles are related according to equation (4), (see also Fig. IV-2-1-5 (p-171))

$$(4) \qquad \omega_{in} = \alpha + \in + \in'$$

The $\in$ and $\in'$ angles are related to the corresponding γ_{in} and γ'_{in} angles by the relationships (Eq.5) and (Eq.6)

$$(5) \qquad \in = A_{in} \times \gamma_{in} + B_{in}$$

$$(6) \qquad \in' = A'_{in} \times \gamma'_{in} + B'_{in}$$

The calculations presented in the preceding paragraph have shown that A_{in} and B_{in} will differ little from A'_{in} and B'_{in} respectively. Consequently, the same relationship between $\in$ and γ_{in} can be selected for all of the complexes listed in Table IV-2-1-3 (p-176). Under these conditions (Eq.4) is written as (Eq.7)

$$(7) \qquad \omega_{in} = \alpha + (A_{in} \times \gamma_{in} + B_{in}) + (A_{in} \times \gamma'_{in} + B_{in})$$

$$= \alpha + A_{in} \times (\gamma_{in} + \gamma'_{in}) + 2B_{in}$$

and finally (Eq.7) can be written as (Eq.8) and then (Eq.9)

(8) $\omega_{in} = \alpha + 2x\, A_{in}\, (\gamma_{in} + \gamma'_{in})/2 + 2B_{in}$

(9) $\omega_{in} - \alpha = A' \times \langle \gamma_{in} \rangle + B'$

with

(10) $\langle \gamma_{in} \rangle = (\gamma_{in} + \gamma'_{in})/2$

(11) $A' = 2A_{in} \cong 0.40x2 = 0.80$

(12) $B' = 2B_{in} = -(180xA_{in}) \times 2 = -360° \times A_{in} \cong (-360°x0.4)° = -144.$

From purely geometrical arguments it can be concluded that the difference $\omega_{in} - \alpha$ should be linearly correlated to the mean value $\langle \gamma_{in} \rangle$ (See Eq.(9)) . Note that this geometrical analysis requires the use of the mean value $\langle \gamma_{in} \rangle$.

This predicted behaviour is indeed observed as shown by the $\omega_{in} - \alpha$ vs $\langle \gamma_{in} \rangle$ plot of Fig. IV-2-3-12 (p-199) . The equation of the least squares linear regression line is given by Eq. (13)

(13) $\omega_{in} - \alpha = A'_{exp} \times \langle \gamma_{in} \rangle + B'_{exp}$

with

$A'_{exp} = 0.80$; $B'_{exp} = -144.3$; $r = 0.99956$; $\sigma = 0.22°$

The agreement between the experimental values A'_{exp} and B'_{exp} and the theoretical $A' \cong 0.80$ and $B' \cong -144.0$ given by Eq.11 and Eq.12 is indeed excellent.

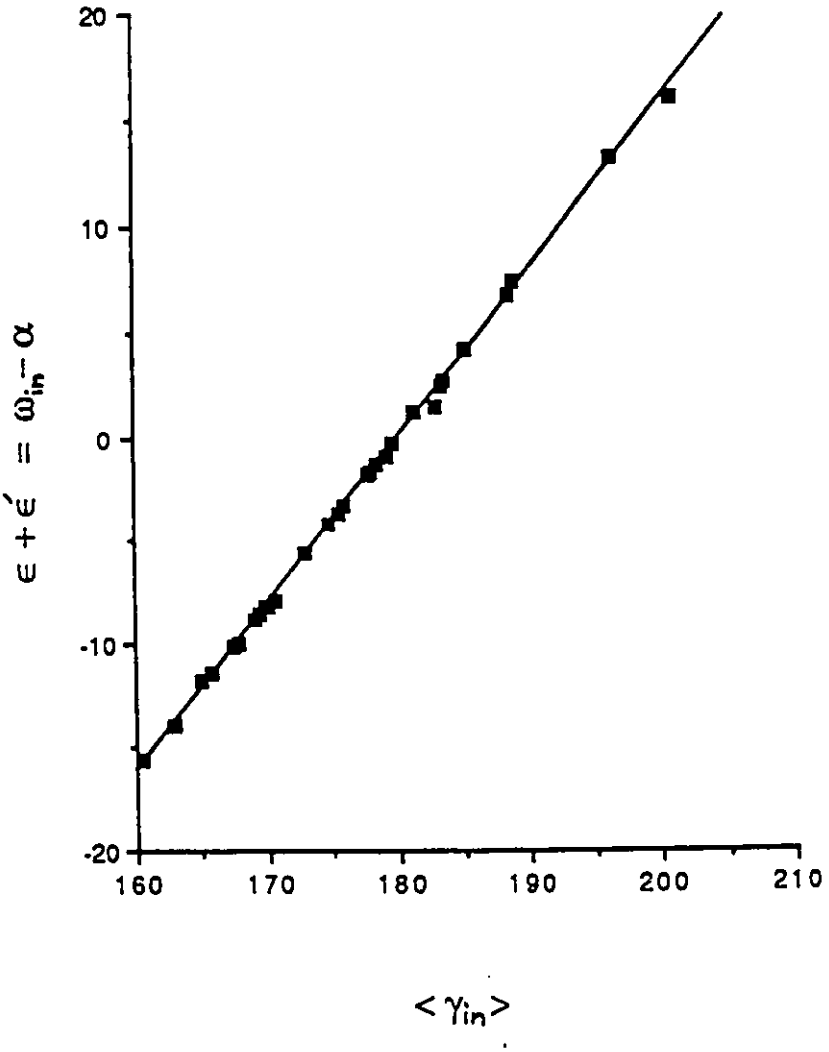

Fig. IV-2-1-12 Plot of $\omega_{in} - \alpha$ VS $<\gamma_{in}>$

PART V

EXPERIMENTAL

V-1 General Procedures

Air sensitive reagents and products were manipulated in a nitrogen or argon atmosphere or under vacuum in Schlenk tubes.

All commercial reagents were of reagent grade. Solvents were purified and dried by standard techniques. THF was refluxed over sodium and benzophenone. Ether was dried over $LiAlH_4$ and freshly distilled under nitrogen. CH_2Cl_2 and CH_3CN were distilled over P_2O_5 under nitrogen before use. Acetone was dried over anhydrous $CaSO_4$ and distilled under nitrogen. DMSO was dried over BaO and distilled under nitrogen. 1,4-dioxane was dried over KOH pellets and distilled over sodium under nitrogen.

n-Butyllithium, 2-chloropyridine, $NaBPh_4$, triphenyl phosphine were purchased from Aldrich Chemical Co.; Diphenyl phosphine, Ferrocene from Strem Co.; $Fe(CO)_4^{-2}.2Na^+$, $AgBF_4$, $AgPF_6$ from Ventrom.

^1H NMR spectra were recorded on Varian XL-300 spectrometer. ^1H chemical shifts are relative to external standard TMS (δ = 0 ppm). ^{31}P shifts are relative to 85% H_3PO_4 and ^{11}B shifts are relative to $BF_3.Et_2O$ used as external standards.

Infrared spectra were recorded on a Perkin-Elmer 783 spetrophotometer.

X-ray diffraction studies on single crystals were conducted using an Enraf-Nonius CAD-4 diffractometer controlled by the NRCCAD software [1]. All computations were performed with the

NRCVAX system of programs [2].

Elemental analyses were performed by Guelph Chemical Laboratoratories Ltd. Guelph, Ontario.

Preparation of NO gas (1)

Nitric oxide was prepared by the action of sodium nitrite with sulphuric acid according to the following reaction.

$$3NaNO_2 + H_2SO_4 \rightarrow Na_2SO_4 + NaNO_3 + H_2O + 2NO$$

$NaNO_2$ (46.6 g, 0.67 mol) was placed in a two necked 500 ml round bottom flask. Sulphuric acid (2 M, 202 ml) was added dropwise under a slow flow of argon with continous stirring. The gas evolved was purified and dried by passing it through a solution of 30% NaOH and subsequently through a column packed with glass wool and Celite.

Cobaltdinitrosyliodide, $(Co(NO)_2I)_2$ (2) (Adapted from [3])

Anhydrous deoxygenated acetone (250 ml) and 35.5 g (0.60 mol) of cobalt powder were placed in a 1000 ml three necked round bottom flask equipped with a mechanical stirrer. A solution of 38.1 g (0.15 mol) of iodine in 300 ml ether was added dropwise over a period of 30 min. at 25°C. The dropping funnel was then replaced by a nitric oxide inlet and the gas was allowed to pass

until the presence of NO was detected in the exit bubbler (brown fumes of NO_2) indicating the completion of the reaction (2-3 hrs). The solvent was removed under vacuum at 25°C. The solid obtained was transferred to a sublimation apparatus. The desired cobalt compound sublimed as a black microcrystalline solid at 120-125°C under vacuum. The compound thus obtained was transferred to a storage bottle in a glove box (30.2 g, 40% yield based on iodine). IR (CH_2Cl_2) : ν_{NO} 1860, 1800 cm^{-1}.

Irondinitrosyliodide, $(Fe(NO)_2I)_2$ (3)

Anhydrous deoxygenated acetone (250 ml) and 33.5 g(0.30 mol) of iron powder were placed in a 1000 ml three necked round bottom flask equipped with a mechanical stirrer. A solution of 38.1g (0.15 mol) of iodine in 300 ml ether was added dropwise over a period of 30 min. at 25°C. The dropping funnel was then replaced by a nitric oxide inlet and the gas was allowed to pass until the presence of NO was detected in the exit bubbler (brown fumes of NO_2) indicating the completion of the reaction (2-3 hrs). The solvent was removed under vacuum at 25°C. The solid obtained was transferred to a sublimation apparatus. The iron compound sublimed as a black microcrystalline solid at 110-115°C . The compound was transferred to a storage bottle in a glove box (33.5 g, 46% yield based on iodine). IR (CH_2Cl_2) : ν_{NO} 1810, 1760 cm-1.

Irondinitrosylchloride, $(Fe(NO)_2Cl)_2$ (4)

Anhydrous $FeCl_3$ (16.2 g) and iron powder (10 g) were placed in a 500 ml three necked round bottom flask. Freshly distilled degassed THF (150 ml) was added and the mixture was stirred with a mechanical stirrer. Nitric oxide was passed into the solution for a period of 5-6 hrs. After filtration the solvent was removed under vacuum. The desired product was obtained by sublimation of the solid residue under vacuum at 100-110°C (14.5 g, 48% yield based on $FeCl_3$). IR (CH_2Cl_2) : ν_{NO} 1810, 1775 cm^{-1}.

Diphenyl(2-pyridyl)phosphine, PPh_2(2-Py) (5) (Adapted from [4])

A solution of *n*-butyllithium (9.58 ml of 2.4 M in hexane, 23 mmol) was slowly added at room temperature over a period of 30 min. to a solution of diphenylphosphine ($HPPh_2$) (4 ml, 23 mmol) in dry THF (100 ml). The resulting red solution was stirred for 1 hr. A solution of 2-chloropyridine (2.2 ml, 23 mmol) was added dropwise to the solution cooled to -78°C with an acetone-dry ice bath surrounding the reaction flask. The colour of the solution slowly changed from red to yellow. After stirring overnight at 25°C the solvent was removed under vacuum. The pale solid was extracted twice with degassed anhydrous Et_2O (2x40 ml). The ether extract was evaporated to dryness on a rotatory evaporator. The resulting crude solid (5.6 g) was recrystallized from

methanol to give (5) as a white solid (4.23 g, 70%). m.p. 83-84°C. ^{31}P NMR (δ = -3.18 ppm)

$Co(NO)_2(PPh_3)I$ (6)

To a solution of $(Co(NO)_2I)_2$ (1.02 g, 2.08 mmol) in degassed absolute EtOH (20 ml) placed in an argon filled Schlenk tube, PPh_3 (1.1 g, 4.15 mmol) dissolved in 15 ml of EtOH was added. After stirring for a few minutes a shiny microcrystalline product started to appear. After an additional 30 min. of stirring the product was separated from the solution, dried under vacuum and recrystallized from CH_2Cl_2-hexane to yield **(6)**,1.64 g, 78%. IR(CH_2Cl_2): ν_{NO} 1830,1775 cm^{-1} .

$Co(NO)_2(PPh_3)_2^+BPh_4^-$ (7)

$NaBPh_4$ (1.2 g, 3.5 mmol) in degassed absolute EtOH (15 ml) was added to a solution of **(6)** (0.68 g,1.33 mmol) and triphenylphosphine (0.55 g, 2.1 mmol) in hot EtOH (30 ml) and stirred for 20 min. A crystalline precipitate was formed during an additional stirring for 30 min. at room temperature. Crystals were separated and dried under vacuum. The crude product was recrystallized in CH_2Cl_2-hexane to yield **(7)** 1.02 g, 80%. IR(CH_2Cl_2) : ν_{NO} 1840,1795 cm^{-1}. IR(Nujol) : 1860, 1800 cm^{-1}.

$Co(NO)_2(PPh_2(2\text{-}Py))I$ (8)

$(Co(NO)_2I)_2$ (0.98 g, 2 mmol) placed in a Schlenk tube was evacuated and filled with argon. Degassed EtOH (25 ml) was added and stirred for 15 min. at room temprature. A solution of diphenyl(2-pyridyl)phosphine (1.05 g, 4 mmol) in 15 ml EtOH was added to the reaction mixture. After 20 minutes of stirring, compound (8) was obtained as a shiny microcrystalline solid. It was then separated by filtration at room temperature, dried under vacuum and recrystallized from CH_2Cl_2-hexane to yield 1.97 g ; 97%. IR(CH_2Cl_2) : ν_{NO} 1827,1770 cm^{-1}. Anal. Calcd. (found) for $C_{17}H_{14}CoPN_3O_2I$: %C 40.10 (40.40), %H 2.77 (3.13), %N 8.25 (9.89). Single crystals for X-ray studies were grown at 20°C by slow diffusion of toluene into CH_2Cl_2 layer.

$Co(NO)_2(PPh_2(2\text{-}Py))_2^+BF_4^-$ (9)

Compound (8) (0.46 g, 0.91 mmol) was suspended in degassed EtOH (80 ml) in a Schlenk tube and stirred for 45 min. at 37°C to achieve dissolution. $AgBF_4$ (0.18 g, 0.91 mmlol) in degassed EtOH (15 ml) was added to the above solution maintained at 37°C and stirred for 10 min. during which the AgI was precipitated. The reaction mixture was brought to room temperature and stirred for an additional 10 min. The filtrate was evaporated to dryness under vacuum and the resulting solid residue was dissolved in CH_2Cl_2 and recrystallized from hexane

to yield **(8)** ; 0.24 g, 36%. IR (CH_2Cl_2) : ν_{NO} 1855,1795 cm^{-1}. ^{31}P NMR($CDCl_3$) : Singlet at δ 45.44 ppm. ^{11}B ($CDCl_3$) : Singlet at δ -0.97 ppm. Anal. Calcd. (Found) for $C_{34}H_{28}CoPN_6O_2BF_4.CH_2Cl_2$: %C 55.76 (55.34), %H 3.85 (3.83), %N 7.65 (7.65). Single crystals for X-ray studies were grown under an argon flow at 20°C by slow diffusion of an upper layer of toluene into a concentrated solution of the product in CH_2Cl_2.

$Co(NO)_2(Py)_2^+BF_4^-$ (10)

A mixture of $(Co(NO)_2I)_2$ (2.38 g, 4.84 mmol) and (1.6 ml,19.34 mmol) pyridine was dissolved in degassed absolute EtOH (20 ml) at room temperature . A solution of $AgBF_4$ (1.88 g, 9.67 mmol) in 10 ml of EtOH was added dropwise to the above stirred solution. After stirring for 1 hr, solid AgI was separated by filtration and the filtrate was evaporated to dryness under vacuum at room temperature. The solid residue obtained was recrystallized from CH_2Cl_2-hexane in the presence of an additional 1.6 ml of pyridine to yield **(10)** 2.68 g, 76% as a dark microcrystalline solid. IR (CH_2Cl_2): ν_{NO} 1876, 1798 cm^{-1}. Anal. Calcd. (Found) for $C_{10}H_{10}BCoF_4N_4O_2$: %C 33.0 (33.2), %H 2.8 (3.1), %N 15.4 (15.0). Crystals suitable for x-ray studies were grown by slow diffusion of an upper layer of toluene into a concentrated CH_2Cl_2 solution of **(10)** at room temperature.

$Co(NO)_2(Py)_2^+BPh_4^-$ (11)

A solution of $NaBPh_4$ (0.77 g, 2.25 mmol) in EtOH was added dropwise to a stirred solution of $(Co(NO)_2I)_2$ (0.55 g,1.13 mmol) and (0.37 g, 4.51 mmol) pyridine in 20 ml of absolute EtOH at 25°C. Olive green microcrystals precipitated . After stirring for 30 min. the crystals were separated and dried under vacuum. The crystals obtained were recrystalized from CH_2Cl_2-hexane in the presence of pyridine to give (11), 1.18 g, 70%. IR (CH_2Cl_2 and excess pyridine): ν_{NO} 1870,1790 cm^{-1}. Anal. Calcd. (Found) for $C_{34}H_{30}BCoN_4O_2$ CH_2Cl_2 : %C 61.7 (62.4), %H 4.7(5.1), %N 8.2 (9.0).

$Co_2(NO)_3(PPh_2(2\text{-}Py))_2^+BPh_4^-$ (12)

Compound (8) (0.58 g, 1.14 mmol) was placed in a previously evacuated Schlenk tube and degassed absolute EtOH (80 ml) was added. The solution was stirred continously for 45 min. at 37°C on a water bath for the complete dissolution of the compound. $NaBPh_4$ (0.78 g, 2.3 mmol) in degassed EtOH (15 ml) was added at 38°C to the above solution and stirred for 30 min. at that temperature and later for another 30 min. at room temperature. A crystalline precipitate was separated , washed with Et_2O and dried under vacuum. The precipitate was dissolved in freshly distilled THF (15 ml) and heated to 45-48°C for 20 min. The THF solution was evaporated to dryness and the solid was

recrystallized in CH_2Cl_2-hexane to give **(12)**, 0.37 g, 62% IR(Nujol) : ν_{NO} 1775(sh), 1750(s), and at 1570 cm^{-1}. ^{11}B NMR exihibits a sharp singlet at δ -6.59 ppm. ^{31}P NMR exihibits a broad signal at δ 61.76 ppm. Anal. Calcd. (found) for $C_{58}H_{48}N_5O_3Co_2P_2B_1$: %C 66.11 (66.46), %N 6.64 (6.14), %H 4.59 (5.0). Crystals suitable for X-ray studies were grown by slow diffusion of toluene into a concentrated solution of the product in CH_2Cl_2 at 25°C.

$Co(NO)_2(PPh_2(2\text{-}Py))_2^+BPh_4^-$ (13)

A solution of compound **(8)** (0.29 g, 0.57 mmol) in degassed EtOH (30 ml) was heated to 45°C on a water bath with continous stirring. $PPh_2(2\text{-}Py)$ (0.30 g, 1.15 mmol) was added and the solution stirred at 45°C for 20 min. $NaBPh_4$ (0.59 g, 1.7 mmol) dissolved in 15 ml EtOH was added to the reaction mixture and stirring for 20 min. yielded brown precipitate. The precipitate was separated, dried under vacuum and the product **(13)** was recrystallized from CH_2Cl_2-hexane (0.49 g, 88% yield). IR(Nujol) (CH_2Cl_2): ν_{NO} 1845, 1795 cm^{-1}. Anal. Calc. (found) for $C_{58}H_{48}BCoN_4O_2P_2.CH_2Cl_2$: %C 67.44 (67.67), %H 4.76 (5.04), %N 5.53 (5.43).

$Co(NO)_2(Py)_2^+PF_6^-$ (14)

To a methanolic solution of $(Co(NO)_2I)_2$ (0.54 g, 1.1 mmol)

at 37°C, pyridine (0.6 ml, 7.23 mmol) was added and stirred for 30 min. at room temperature. To this stirred solution, $AgPF_6$ (0.5 g, 2 mmol) dissolved in MeOH (15 ml) was added. Yellow precipitate of AgI was filtered through sintered glass funnel and the filtrate was concentrated under vacuum, during which needle shaped black crystals appeared. Crystals were separated and dried under vacuum. IR (CH_2Cl_2): ν_{NO} 1870, 1790 cm^{-1}.

$Co(NO)_2(Py\text{-}CH_3)_2^+PF_6^-$ (15)

To a methanolic solution of $(Co(NO)_2I)_2$ (0.54 g, 1.1 mmol), 2-methyl pyridine; ($Py\text{-}CH_3$), (0.8 ml, 8 mmol) was added and stirred for 30 min. at room temperature. $AgPF_6$ (0.51 g, 2 mmol) in MeOH (15 ml) was added to it and stirred at room temperature for 20 min. The precipitate of AgI was removed by filtration and the filtrate was concentrated under vacuum. While concentrating an oil was obtained and no solid product could be isolated. IR (CH_2Cl_2) : ν_{NO} 1870, 1790 cm^{-1}.

$Co(NO)_2(3,5\text{-}DMP)_2^+PF_6^-$ (16)

3,5-DMP (0.91 ml, 8 mmol; DMP= dimethyl pyridine) was added to a methanolic solution of $(Co(NO)_2I)_2$ (0.54 g, 1.09 mmol) and stirred for 10 min. $AgPF_6$ (0.5 g, 2 mmol) dissolved in MeOH (15 ml) was added to it and stirred for 20 min. at room temperature. During that period of time, a brown precipitate

appeared along with the yellow precipitate of AgI. The precipitate was filtered and washed several times with degassed CH_2Cl_2. The brown precipitate was soluble in CH_2Cl_2. The solution was concentrated and no product could be isolated. However, IR (CH_2Cl_2) showed ν_{NO} 1870, 1790 cm^{-1}.

Reaction of $(Co(NO)_2I)_2$ with cytidine ($C_9H_{13}N_3O_5$) under various experimental conditions (17)

$(Co(NO)_2I)_2$ (0.245 g, 0.5 mmol) was placed in a Schlenk tube which was evacuated and filled with argon. Degassed CH_2Cl_2 (10 ml) was added and stirred for 15 min. at room temperature. To it was added cytidine (1 mmol; 0.24 g) and stirred for 2-3 hrs at room temperature. Cytidine remained insoluble in the solution. No change in the IR spectra of the reaction mixture was observed. Two or three drops of DMSO was added to the reaction mixture to dissolve the cytidine. The solution was stirred for another hour. A change in the IR spectrum was observed with a higher shift of the NO frequency displaying two strong ν_{NO} bands at 1845, 1800 cm^{-1}. A similar spectrum was observed when the reaction was performed without the addition of the cytidine which clearly indictes that it is not cytidine but DMSO which is reacting with the dimer. No product could be isolated from this reaction.

To a solution of $(Co(NO)_2I)_2$ (0.25 g, 0.5 mmol) in degassed CH_3CN (15 ml) placed in an argon filled Schlenk tube, $AgPF_6$

(0.25 g, 1 mmol) dissolved in 5 ml of CH_3CN was added. After stirring for 15 min. at room temperature yellow precipitate of AgI was separated by filtration. The IR of the filtrate displayed two strong NO bands at 1840, 1780 cm^{-1} characteristic of $[Co(NO)_2(CH_3CN)_2]^+ \cdot PF_6^-$ [5].

To this solution was added cytidine (0.12 g, 0.5 mmol) dissolved in 5 ml of CH_3CN and stirred for 1hr. During which time a decomposition occurred. No ν_{NO} bands in the IR spectrum of the mixture was obtained and no product could be isolated.

$Fe(NO)_2(PPh_3)I$ (18)

To a stirred solution of $(Fe(NO)_2I)_2$ (1.4 g, 2.9 mmol) in degassed absolute EtOH (30 ml), a solution of triphenylphosphine (1.53 g, 5.83 mmol) in EtOH was added and stirred for 30 min. at room temperature, a shiny microcrystalline product was separated, dried under vacuum and recrystallized from CH_2Cl_2-hexane. The product **(18)** obtained was 2.15 g, 73%. IR(CH_2Cl_2): ν_{NO} 1785, 1735 cm^{-1}.

$Fe(NO)_2(PPh_3)Cl$ (19)

To a stirred solution of $(Fe(NO)_2Cl)_2$ (0.35 g, 1.16 mmol) in EtOH was added an ethanolic solution of triphenylphosphine (0.61 g, 2.3 mmol) and stirred for 30 min. at room temperature, a shiny microcrystalline product was separated, dried under vacuum and

was recrystallized from CH_2Cl_2-hexane to give **(19)**, 0.8 g, 83%. IR(CH_2Cl_2) ν_{NO} 1785, 1735 cm^{-1}.

$Fe(NO)_2(PPh_2(2\text{-}Py))I$ (20)

A solution of diphenyl(2-pyridyl)phosphine (1.4 g, 5.4 mmol) in EtOH (15 ml) was added to a solution of $(Fe(NO)_2I)_2$ (1.3 g, 2.7 mmol) which was dissolved in degassed absolute EtOH in an argon filled Schlenk tube. The reaction mixture was stirred for 30 min. at room temperature. Shiny crystals were separated from the solution which were dried under vacuum and recrystallized from CH_2Cl_2-hexane to give **(20)**,1.9 g, 70%. IR(CH_2Cl_2) : ν_{NO} 1785,1735 cm^{-1}.

$Fe(OPPh_2(2\text{-}Py))_3^{2+}.2BF_4^-$ (21)

$(Fe(NO)_2Cl)_2$ (0.58 g, 1.93 mmol) was dissolved in freshly distilled degassed THF (20 ml). To it was added $AgBF_4$ (0.75 g, 3.87 mmol) in THF (10 ml) at room temperature . The white precipitate of AgCl which formed was removed by filtration. The IR of the filtrate showed the two ν_{NO} bands at 1776, 1710 cm^{-1} characteristic of the $Fe(NO)_2(THF)_2^+BF_4^-$ (ν_{NO}^{lit} : 1780, 1714 cm^{-1} [6]). Diphenyl (2-pyridyl) -phosphine (2.04 g, 7.7 mmol) was added to the above solution. The formation of a yellow precipitate was observed soon after the addition. The amount of solid material suspended in solution increased with time. After 90 min.

when no further changes were noticed, an IR of the solution indicated the complete removal of the initial nitrosyl ligand (ν_{NO} at 1776 cm^{-1}) and the appearance of a new nitrosyl ligand (ν_{NO} at 1680 cm^{-1}).

The yellow precipitate was separated by filtration. The filtrate was evaporated to dryness and the residue was dissolved in minimum amount of CH_2Cl_2 and passed over a silica column, followed by chromatron separation with CH_2Cl_2-EtOAc as the eluent. The complex $Fe(NO)_2(PPh_2(2\text{-}Py))_2$ was eluted first (IR (CH_2Cl_2): ν_{NO} 1720, 1680 cm^{-1}) and recrystallized in hexane-CH_2Cl_2(1:1) (0.31 g, 3% yield from the recovery of Fe "atom"). PPh_2(2-Py) was subsequently eluted and recrystallized from the same solvent to give (0.17 g, 8% recovery yield based on the initial PPh_2(2-Py) ligand. ^{31}P (δ = -3.18 ppm).

The yellow precipitate was recrystallized from CH_2Cl_2-Et_2OH to give **(21)** (0.55 g, 13% yield from the recovery of Fe "atom"). Crystals suitable for X-ray studies were obtained by slow crystallization in CH_2Cl_2-Et_2O for 24 hr at 5°C.

(i) Reaction of $Fe(NO)_2(PPh_2(2\text{-}Py))I$ with $AgBF_4$

Compound **(20)** (0.56 g, 1mmol) was suspended in degassed EtOH (50 ml) in a Schlenk tube and stirred for 45 minutes at 37°C. $AgBF_4$ (0.37 g, 2 mmol) in degassed EtOH (15 ml) was added dropwise to the above solution at room temperature. A yellow

precipitate of AgI was obtained immediately which turned to brown and eventually to black. After 15 minutes everything from the reaction mixture precipitated out leaving a clear EtOH solution. The precipitate was separated by filteration and was insoluble in CH_2Cl_2, CH_3CN, DMSO, acetone and THF etc. No product could be isolated from this reaction.

(ii) Reaction of $Fe(NO)_2(PPh_2(2\text{-}Py))I$ with $NaBPh_4$

Compound (20) (0.28 g, 0.56 mmol) was suspended in degassed EtOH (40 ml) in a Schlenk tube and stirred for 45 minutes at 37°C for complete dissolution. $NaBPh_4$ (0.39 g, 1.13 mmol) in degassed EtOH was added to the above solution maintained at 37°C and stirred for 30 min. The reaction mixture was brought to room temperature and stirred for an additional 30 min. A yellow precipitate was formed in trace amount. The precipitate was separated by filtration. Its IR in CH_2Cl_2 showed no absorption in the NO region. The filtrate was evaporated to dryness under vacuum and the resulting solid residue was dissolved in CH_2Cl_2. IR of the solution showed the presence of several bands along with two strong bands at 1720, 1680 cm^{-1}. No product could be isolated from this reaction.

$Fe(CO)(NO)(PPh_3)_2(CH_3CN)^+BF_4^-$ (22)

(i) Preparation of the Stock Solution of anhydrous HBF4

The stock solution of anhydrous HBF_4 was prepared by dropwise addition of 2 ml of aqueous 37% HBF_4 (~11 mmol of HBF_4) into 10 ml of acetic anhydride which was stirred, and maintained at 0°C in an ice-bath. The solution was prepared just before its use.

(ii) Preparation of Fe(CO)(NO)(PPh3)2+BF4-

HBF_4/acetic anhydride (1.2 ml (from the stock), 1.8 mmol) was added dropwise over a period of 5 minutes to a stirred ice cold THF : Et_2O (1:1) (40 ml total) solution of $FeH(CO)(NO)(PPh_3)_2(C_6H_6)$ (1 g, 1.4 mmol). Precipitation of a black solid started immediately. Once the addition was completed, the ice bath was removed and stirring was continued at room temperature until H_2 gas evolution ceased (approx.10 min). The mixture was then cooled to 0°C to complete the precipitation. The orange-brown powder was collected, washed with ether and dried in vacuum (0.87 g, 86% yield). The orange-brown complex was found to be unstable in solvents such as methylene chloride, chloroform and acetone.

$Fe(CO)(NO)(PPh_3)_2^+BF_4^-$ was dissolved in minimum amount of acetonitrile. The solution was gradually cooled to 0°C and ether was slowly added to complete the crystallization. These orange-brown crystals were filtered out, washed with pentane and dried in vacuum to give compound (22).

$Fe(CO)_3(NO)^-Na^+(C_4H_8O_2)$ (23) Caution : Pyrophoric iron might be formed as a by product in such reactions.

$Fe(CO)_4^{2-}2Na^+1.5\text{-}C_4H_8O_2$ (0.63 g, 1.83 mmol) was placed in a Schlenk tube and 30 ml of freshly distilled THF was added to it. The suspension was stirred and cooled to -78°C. Argon was continuously bubbled into the solution through a needle. $Fe(CO)_2(NO)_2$ (0.99 ml, 1.89 mmol) was slowly added to the above solution. After the addition, the temperature was raised slowly to room temperature and the reaction mixture was stirred for 2 hr. The solution was then evaporated to dryness at 20-40°C under vacuum. The dry solid obtained was extracted with 4x40 ml of dry ether. The solution was filtered through a sintered funnel over Celite under argon. The filtration apparatus should be completely dry as the reaction product $Fe(CO)_3(NO)^-Na^+$ is very sensitive to air, water and is also deliquescent. The homogenous filtrate was concentrated under vacuum at room temperature to about 30 ml. Dry 1,4-dioxane (2 ml) was then added dropwise which precipitated the complex $Fe(CO)_3(NO)^-Na^+$1,4 -dioxane, as microcrystalline yellow crystals. The crystals obtained were separated, washed with dry ether and dried under vacuum to give (23) 0.85 g, 83%. The air sensitive solid can be stored for several weeks in Schlenk tubes in argon at 5°C. IR(THF) : tight ion pairs ν_{CO} = 1990, 1890 cm^{-1}; ν_{NO} 1615 cm^{-1}; loose ion pairs ν_{CO} 1977, 1873 cm^{-1}; ν_{NO} 1648 cm^{-1}. In ether only tight ion pairs

were detected ν_{CO} 1995 , 1905 cm^{-1}, ν_{NO} 1585 cm^{-1}.

1,1'-Dilithioferrocene,TMEDA (24) [6]

Ferrocene (25 g, 13 mmol) was placed in a large Schlenk tube . To it was added freshly distilled Et_2O (150 ml). A solution of *n*-BuLi in hexane (2.5 M,115 ml) was added dropwise to the above solution. The suspension was rapidly stirred and *N,N,N',N'*-tetramethyl- ethylenediamine (TMEDA) (20 ml) dried over CaH_2 was added very slowly. The ferrocene slurry reacted to give a deep cherry red solution. The reaction mixture was allowed to stir overnight during which a fine orange precipitate deposited. This was separated by filtration through a medium porosity Schlenk filter and washed with degassed hexane (60 ml). Drying in vacuum yielded a fine pyrophoric powder of (24) (28g, 75%). The compound could be stored at 5°C under nitrogen for several months.

1,1'-bis(diphenylphosphino)ferrocene (25) [7]

To a suspension of compound (24) (10 g, 31.9 mmol) in dry hexane (50 ml) in a 250 ml Schlenk tube cooled to -78°C, was added PPh_2Cl (14.5 g, 65 mmol) dropwise. The mixture was slowly brought to room temperature and was stirred for 5 hr. Following hydrolysis with water, a brownish orange solid was separated from the solvent. The solid was recrystallized from a

warm solution of benzene to give fine orange crystals of (25),11.5 g, 65%.

1,1'-(diphenylphosphino)ferrocene (26) [8]

Compound **(24)** (3.4 g, 10.85 mmol) was placed in a Schlenk tube with dry Et_2O (50 ml). The suspension was cooled to -78°C and $PPhCl_2$ (2.21 g (1.68 ml), 12.4 mmol) was added dropwise to it. The solution was slowly brought to room temperature and stirred for 2 hr. Following careful hydrolysis with water the Et_2O layer was separated and was concentrated to about 5 ml and was chromatographed on alumina (100-200 mesh). The bright red layer was eluted with hexane and concentrated under reduced pressure to give compound **(26)** (40%).

Pyridylphenylphosphinoferrocene (27) [Attempted synthesis of a new ligand].

Bromopyridine (1.66 ml,17.4 mmol) was placed in a 250 ml Schlenk tube containing freshly distilled, degassed Et_2O (30 ml). *n*-BuLi in hexane (2.5 M, 6.96 ml) was added dropwise to the reaction mixture maintained at -78°C by a dry ice-acetone bath. The solution was stirred for 1 hr. 1,1'-bis(diphenylphosphino) ferrocene **(25)** (2.6 g, 8.7 mmol) dissolved in Et_2O was added dropwise to the above solution. The suspension was stirred for an additional 1 hr at -78°C and was then slowly brought to the room

temperature and stirred for 2 hr. Upon careful hydrolysis with water, the ether layer was separated and concentrated under reduced pressure. The yellow crystals were separated and dried under vacuum to give **(27)** (2 g, 62%).

Bis-(diphenylphosphino)ferrocene iron carbonyl nitrosyl hydride (28)

To a suspension of $Fe(CO)_3(NO)^-Na^+.(C_4H_8O_2)$ (0.3 g, 0.82 mmol) in dry Et_2O (30 ml) was added 1,1'-bis(diphenylphosphino) ferrocene (0.45 g, 0.82 mmol). The suspension was stirred and cooled to 4°C in a water ice bath. Trifluoroacetic acid (0.08 ml) 1.3 equiv. relative to $Fe(CO)_3(NO)^-Na^+$.1,4-dioxane, was added dropwise. A precipitate readily appeared. The reaction mixture was stirred for 10 min at 4°C and then for 1.5 hr at room temperature. The precipitate was separated by filtration, dried under vacuum and extracted with benzene. The resulting benzene solution was evaporated to dryness. The solid obtained was recrystallized from CH_2Cl_2-Et_2O to yield **(28)** 0.20 g, 37%. IR (CH_2Cl_2) (Nujol) : ν_{CO} 1920 cm^{-1}; ν_{NO} 1700 cm^{-1}. The ^1H and ^{31}P NMR are described in Part I.

Summary and Conclusion

The complex ironnitrosylhydride, $FeH(CO)(NO)(PPh_3)_2$, was synthesized, and its preliminary reaction with syngas and olefin showed no catalytic activity. The hydride was found to be unstable and readily decomposed into a mixture of dinitrosyl $Fe(NO)_2(PPh_3)_2$, mononitrosyl $Fe(NO)(CO)(PPh_3)$, and nitrosyl free $Fe(CO)_4(PPh_3)$ and $Fe(CO)_3(PPh_3)_2$ iron complexes.

In order to obtain a more stable hydride the synthesis of iron nitrosylhydride with 1,1'-bis(diphenylphosphino)ferrocene (dppf) ligand, was performed. No single crystal of the complex FeH(CO)(NO)(dppf) **(28)** was obtained for X-ray study under different experimental conditions. The hydride **(28)** was characterized by its spectral properties and elemental analysis. The coordination around Fe was tentatively assigned to be square pyramidal when the NMR pattern was compared with its closely related $Re(dppf)(CO)_3Cl$ complex. The hydride **(28)** was found to be thermolabile and decomposed in the solid state at 20°C. The decomposition of the hydride is described in terms of the homolysis of Fe-H bond. The decomposition also involves the NO transfer reaction. A suggested mechanism for the decomposition of hydride presented in scheme II-3-7 (p-41), shows the formation of a metal-metal bond in the transient species. This shifted the direction of research to the synthesis of bimetallic complexes which might serve as precursors of polymetallic

hydrides. In an attempted synthesis of bimetallics containing iron nitrosyls, $Fe(CO)_4^{2-}$(D_{NO}^{10+0}), and $Fe(CO)_2(NO)_2$ (D_{NO}^{8+2}) were reacted. Instead of the anticipated bimetallic complex, a monometallic derivative, $Fe(CO)_3(NO)^-$ **(23)**, (D_{NO}^{9+1}) was obtained quantitatively. The mechanism for the formation of this monometallic is presented in scheme II-3-4 (p-37). From these observations, it was concluded that a bimetallic species is indeed formed as an intermediate, but a facile rupture of the metal-metal bond occurs with the exchange of the NO and CO ligands between the metallic centers resulting in the formation of the monometallic species.

To prepare a stable bimetallic a chelating ligand, diphenyl(2-pyridyl)phosphine, PPh_2(2-Py) was selected. The P and N-donor sites of the ligand could be functionalized to form polymetallic complexes.

From the results and observations described in Part III (chapter 1), with iron nitrosyl system and diphenyl(2-pyridyl) phosphine, it can be concluded that diphenyl(2-pyridyl)phosphine is not suitable to construct a bimetallic with the ironnitrosyl system. The reaction of $Fe(NO)_2(THF)_2^+$ (D_{NO}^{7+2}), with PPh_2(2-Py) which resulted in the formation of $Fe(NO)_2(PPh_2(2\text{-}Py))_2$ (D_{NO}^{8+2}) and $Fe(NO)_2(PPh_2(2\text{-}Py))(L')^{2+}$ (L' = THF or PPh_2(2-Py)) (D_{NO}^{6+2}) is presented in scheme III-1-3-8 (p-56). Starting from $2D_{NO}^{7+2}$ species a mixture of D_{NO}^{6+2} and

D_{NO}^{8+2} products were obtained. This clearly indicates the occurrence of a dismutation reaction. Subsequent denitrosylation from a D_{NO}^{6+2} species suggests an O-transfer reaction forming N_2O which decomposes to N_2 , along with diphenyl(2-pyridyl) -phosphine oxide and Fe^{2+} as the co-products. Diphenyl (2-pyridyl) phosphine oxide chelates with Fe^{2+} to form $Fe(O{=}PPh_2(2\text{-}Py))_3^{2+}BF_4^-$ **(21)**.

In an attempted synthesis of bimetallic, the cobaltnitrosyl system was chosen. The synthesis of the cobalt nitrosyl derivatives with diphenyl(2-pyridyl)phosphine has been described in Part III (Chapter 2).

Reaction of $(Co(NO)_2I)_2$ with diphenyl(2-pyridyl)phosphine using $AgBF_4$ as halide abstractor resulted in the formation of a monometallic dinitrosyl complex $Co(NO)_2(PPh_2(2\text{-}Py))_2^+BF_4^-$ **(9)**. An x-ray diffraction study revealed a pseudotetrahedral geometry. When $NaBPh_4$ was used as halide abstractor a bimetallic $Co_2(NO)_3(PPh_2(2\text{-}Py))_2^+BPh_4^-$ **(12)** was obtained. This is one of the rare examples of a compound of a first row element with diphenyl(2-pyridyl)phosphine. In **(12)**, the two $PPh_2(2\text{-}Py)$ ligands are arranged in a head-to-head fashion with a bridging NO ligand. During the process of the formation of a bimetallic, one terminal NO ligand was lost as revealed by the X-ray structure. From this observation, it was concluded that a bimetallic can be obtained with cobalt nitrosyl and diphenyl(2-pyridyl)phosphine in

the presence of BPh_4^- anion.

To compare the reactivity and coordination of the P and N-donor sites of the ligand diphenyl(2-pyridyl)phosphine, which might have a bearing upon the formation of bimetallic $Co_2(NO)_3(PPh_2(2\text{-}Py))_2^+BPh_4^-$ **(12)**, certain cobalt dinitrosyl complexes were prepared. The P-donor site of the ligand could be compared well with the already known $Co(NO)_2(PPh_3)_2$ and $Co(NO)_2(PPh_2(2\text{-}Py))_2^+BF_4^-$ **(9)**. On the other hand to compare the N-donor site of the ligand, previously unknown cobaltdinitrosyl complexes were synthesized with pyridine as a ligand of choice.

The cobaltdinitrosylbispyridine cation $Co(NO)_2(Py)^+$ was synthesized by a reaction of $(Co(NO)_2I)_2$ and excess of pyridine with BF_4^- and BPh_4^-. $Co(NO)_2(Py)^+BF_4^-$ **(10)** was stable in solution whereas, $Co(NO)_2(Py)^+BPh_4^-$ **(11)** was unstable in solution and rapidly decomposes at room temperature. A suggested decomposition pathway is presented in scheme III-2-3-1(p-67). The dissociation of pyridine is a prerequisite for the decomposition to proceed. After the dissociation of the pyridine ligand one of the coordination sites of the metal becomes vacant. It is suspected that the phenyl group of the BPh_4^- anion occupies the vacant coordination site forming an uncharged η^1-phenyl derivative $Co(NO)_2(Py)\text{-}Ph$ with BPh_3 as the coproduct. Both of these decomposition products were identified by NMR and IR. In the presence of an excess of pyridine

$Co(NO)_2(Py)^+BPh_4^-$ **(11)** could be isolated.

Lability of the pyridine ligand and involvement of BPh_4^- have bearings upon the formation of bimetallic $Co_2(NO)_3(PPh_2(2\text{-}Py))_2^+ BPh_4^-$ **(12)** and the mechanism is depicted in scheme III-2-3-2 (p-69). Contrary to $Co(NO)_2(Py)_2^+$ case because of the geometry of the $PPh_2(2\text{-}Py)$ ligand, the pyridinyl moiety, which has to dissociate prior to the phenylation step, remains in the vicinity for recomplexation at the later stage forming $Co_2(NO)_3(PPh_2(2\text{-}Py))_2^+BPh_4^-$ **(12)**.

An X-ray diffraction study of $Co(NO)_2(Py)_2^+BF_4^-$ **(10)** shows a distorted tetrahedral geometry around cobalt atom. The structural study of $Co(NO)_2(Py)_2^+BF_4^-$ **(10)** led to the proposal of a stereoelectronic model in which the non-bonded repulsions between the NO and L ligands of the M(NO)(L) moities provide the most influential factor for fixing the value of the angle α. This model applies for the pseudotetrahedral dinitrosyl complexes as well as for the pentacoordinated complexes having a M(CO)(XO) moiety (X = C, N atoms).

The attempted synthesis of cobalt dinitosyl complexes with DNA bases were unsuccessful. Reacting $(Co(NO)_2I)_2$ with cytidine under many different experimental conditions gave only unidentified decomposition products .

The bimetallic **(12)** did not react with CO in dichloromethane at room temperature.

REFERENCES

PART I

(1) Gillespie, R. J. *J. Chem. Educ.* **1970**, *18*, 47.

(2) Enemark, J. E.; Feltham, R. D. *Coord. Chem. Rev.* **1974**, *13*, 339.

(3) Roustan, J. L.; Morrow, B. A. *Inorg. Chem.* **1988**, *22*, 1667.

(4) Sabherwal, I. H.; Burg, A. B. *J. Chem. Soc. Chem. Commun.*. **1970**, 1001.

(5) (a) Swanson, B. I.; Satija, S. K. *J. Chem. Soc. Chem. Commun.* **1973**, 40.

(6) Fischer, E. O.; Plesske, K. *Chem. Ber.* **1961**, *94*, 93.

(7) Fischer, E. O.; Schneider, R. J.; Muller, J. *J. Organomet. Chem.* **1968**, *94*, 4.

(8) Chisholm, M. H.; Cotton, F. A.; Extine, M. W.; Kelly, R. L. *Inorg. Chem.* **1979**, *18*, 116.

(9) Piper, T. S.; Cotton, F. A.; Wilkinson, G. *J. Inorg. Nuclear. Chem.* **1965**, *1*, 165.

(10) Albertin, G.; Pelizzi, G.; Bordginon, E. *Inorg. Chem.* **1983**, *22*, 515.

(11) Pierpont, C. G.; Eisenberg, R. *Inorg. Chem.* **1973**, *12*, 199.

(12) Pierpont, C. G.; Eisenberg, R. *Inorg. Chem.* **1972**, *11*, 1094.

(13) (a) Hodgson, D. J.; Ibers, J. A. *Inorg. Chem.* **1968**, *7*, 2345. (b) Hodgson, D. J.; Payne, N. C.; McGinnety, J. A.; Pearson, R.

G.; Ibers, J. A. *J. Am. Chem. Soc.* **1968**, *90*, 4486.

(14) Enemark, J. E.; Feltham, R. D. *Proc. Nat. Acad. Sci. U.S.* **1972**, *69*, 3534.

(15) Johnson, B. F. G.; Bhaduri, S. *J. Chem. Soc. Chem. Commun.* **1973**, 650.

(16) Bhaduri, S.; Johnson, B. F. G. *Transition Met. Chem.* **1978**, *3*, 156.

(17) Hieber, W.; Pignot, D. V. *Chem. Ber.* **1965**, *89*, 610.

(18) Hieber, W.; Heinicke, K. *Z. Anorg. Allg. Chem.* **1962**, *316*, 321.

(19) Tovrog, B. S.; Diamond, S. E.; Mares, F. *J. Am. Chem. Soc.* **1979**,*101*, 270.

(20) Mucigrosso, D. A.; Mares, F.; Diamond, S. E.; Solar, J. P. *Inorg. Chem.* **1983**, *22*, 960.

(21) Ballivet, D.; Billard, C.; Tkatchenko, I. *J. Organomet. Chem.* **1977**,*124*, C9.

(22) Ballivet, D.; Tkatchenko, I.; Billard, C.; Revillon, A. *J. Polym. Sci.* **1981**, *19*, 1697.

(23) Connelly, N. G.; Draggett, P. T.; Green, M. *J. Organomet. Chem.* **1977**, *140*, C10.

(24) Wilson, S. T.; Osborn, J. A. *J. Am. Chem. Soc.* **1971**, *93*, 3068.

(25) Collman, J. P.; Hoffman, N. W.; Dolcetti, G.; *Inorg. Chim. Acta.* **1972**, *6*, 531.

(26) Dolcetti, G. *Inorg. Nucl. Chem. Lett.* **1973**, *9*, 705.

(27) Hughes, W. B. *Organomet. Chem. Synth.* **1972**, *1*, 341.

(28) Haines, R. J.; Leigh, G. J. *Chem. Soc. Rev.* **1975**, *4*, 155.

(29) Lavel, J. P.; Latters, A. *J. Chem. Soc. Chem. Commun.* **1977**, 502.

(30) Collman, J. P.; Hoffman, N. W.; Morris, D. E. *J. Am. Chem. Soc.* **1969**, *91*, 5659.

(31) Roustan, J. L.; Cygler, M.; Ahmed, F. R.; Forgues, A. *Inorg. Chem.* **1983**, *22*, 1026.

(32) Roustan, J. L.; Abidin, M.; Baer, H. H. *J. Organomet. Chem.* **1989**, 376, C20-C22.

PART II

(1) Same as ref (31) Part I

(2) Roustan, J. L.; Forgues, A.; Merour, J. Y.; Vinayak, N. D.; Morrow, B. A. *Can. J. Chem.* **1983**, *61*, 1339.

(3) Miller, T. M.; Ahmed, K. Z.; Wrighton, M. S. *Inorg. Chem.* **1989**, *28*, 2347.

(4) Pannell, K. H.; Sen Chen Yu.; Belknap, K. L.; J. *Chem. Soc. Chem. Commun.* **1977**, 362.

(5) Hieber, W.; Beutner, H. *Z. Anorg. Allg. Chem.* **1963**, *320*, 101.

(6) Ungermann, C. B.; Caulton, K. G. *J. Am. Chem. Soc.* **1976**, *98*, 3862.

(7) Roustan, J. L.; Merour, J. Y.; Forgues, A. *J. Organomet. Chem.* **1980**, *184*, C13.

(8) Roustan, J. L.; Lijour, Y.; Morrow, B. A. *Inorg.Chem.* **1987**, *26*, 2509.

(9) Roustan, J. L. Ansari, N. Unpublished results.

(10) Sharf, V. Z.; Freidlin, L. Kn.; Krutti, U. N.; Shekotan, I. S. *Izv. Akad. Nauk, SSSr. Ser. Khim.* **1974**, 1330.

(11) Pignataro, S.; Distefano, G.; Foffani, A. *J. Am. Chem. Soc.* **1970**, *92*, 6425.

(12) Orchin, M.; *Acc. Chem. Res.* **1981**, *14*, 260.

PART III

Chapter 1

(1) Roustan, J. L.; Mordenti, L.; Riess, J. G.*Organometallic.* **1983**, *2*, 843

(2) Roustan, J. L.; Mordenti, L.; Riess, J. G. *Inorg.Chem.* **1984**, *23*, 4503

(3) Roustan, J. L; Mordenti, L.; Riess, J. G. *New J. Chem.* **1986**,*10*, 97.

(4) Olmstead, M. M.; Maissonat, A.; Farr, J. P.; Balch, A. L. *Inorg. Chem.* **1981**, *20*, 4060.

(5) Maissonat, A.; Farr, J. P.; Balch, A. L. *Inorg. Chim. Acta* **1981**, *53*, L217.

(6) Wood, F. E.; Olmstead, M. M.; Balch, A. L. *J. Am. Chem. Soc.* **1983**,*105*, 6332.

(7) Farr, J.P.; Olmstead, M.M.; Balch, A.L. *Inorg. Chem.* **1983**, 22,

1229.

(8) Farr, J. P.; Olmstaed, M. M.; Wood, F. E.; Balch, A. L. *J. Am. Chem. Soc.* **1983**, *105*, 792.

(9) Farr, J. P.; Wood, F. E.; Balch, A. L. *Inorg. Chem.* **1983**, *22*, 3387.

(10) Wood, F. E.; Olmstead, M. M.; Farr, J. P.; Balch, A. L. *Inorg. Chim. Acta* **1985**, *97*, 77.

(11) same as ref (11) in Part II.

(12) Ballivet, D.; Tkatchenko, I. *J. Am. Chem. Soc.* **1979**, *10*, 2763.

(13) Roustan, J. L. ; Bisnaire, M. manuscript in preparation.

(14) Albano, V. G.; Araneo, A.; Bellon, P. L.; Ciani, G.; Manassero, M. *J. Organomet. Chem.* **1974**, *67*, 413.

(15) Same as Ref. (10) in Part II.

(16) McCleverty, J. A.; *Chemical Reviews*, **1979**, *79*, 53.

(17) Bianco, T.; Rossi, M.; Uva, L. *Inorg. Chim. Acta* **1969**, *3*, 443.

(18) Long, G. J.; Clarke, P. J.; *Inorg. Chem.* **1978**, *17*, 1394.

(19) Raabe, E.; Koelle, U. *J. Organomet. Chem.* **1985**, *C29*, 279.

(20) Bragg, W. L.; *Proc. Roy. Soc. (London) (A)*, **1914**, *89*, 468.

(21) Bragg, W. L.; *Proc. Cambridge Phil. Soc.* **1913**, *17*, 43.

(22) Azaroff, L. V.; *"Elements of Crystallography"* McGraw Hill **1968.**

(23) Burger, M. J.; Klein, G. E.; *J. Appl. Phys.* **1945**, 408, 16.

(24) Stout, G. H.; Jensen, L. H.; *" X-ray structure determinations. A Practical Guide"*. The Mc.Milan **1968.**

(25) Lipson, H.; Cochran, W.; " *The Determination of Crystal structures*". G. Bell, London. **1957**, 38-46.

(26) Patterson, A. L.; *Phys. Rev.* **1934**, *46*, 372.

(27) Ladd, M. F. C., Palmer, R.A. " *Theory and Practice of Direct Methods in Crystallography*". Plenum Press **1980**.

(28) Sayer, D.; *Acta. Cryst.* **1952**, 60.

(29) Karle, J.; Karle, I. L. *Acta. Cryst.* **1966**, *21*, 849.

(30) Woolfson, M. M. " *X-ray Crystallography*", Univ.Press **1970**.

(31) Bandoli, G.; Bortolozzo, G.; Clemente, D. A.; Croatto, U.; Panattoni, C. *J. Chem. Soc. A.* **1970**, 277

(32) Haynes, J. S.; Retting, S. J.; Sams, J. R.; Thompson, R. C.; Trotter, *J. Can. J. Chem.* **1986**, *64*, 429.

(33) Humphrey, M. B.; Lamanna, W. M.; Brookhart, M.; Husk, G. R. Inorg. Chem. 1983, 22, 3355.

(34) Kaduk, J. A.; Ibers, J.A. *Inorg. Chem.* **1970**, *9* , 1105.

(35) Martin, R. L.; Taylor, D. *Inorg. Chem.* **1976**, *15*, 2970.

(36) Haymore, B. L.; Hoffman, J. C.; Butler, N. E. *Inorg. Chem.* **1983**, *22*, 168.

(37) Reichert, B. *Acta. Cryst. C*, **1979**, 1934

(38) Kaduk, J. A.; Ibers, J. A. *Inorg. Chem.* **1977**, *16*, 3285.

(39) Manotti, Lanfredi, M. A.; Tiripicchio, A.; Tiripicchio, C. M. *Acta Cryst.* **1983**, *C39*, 1633.

(40) Roustan, J. L.; Ansari, N.; Le Page, Y.; Charland, J. P. *Can. J. Chem.* **1992**, *70*, 1650.

(41) Kaduk, J. A.; Ibers, J. A. *Inorg.Chem.* **1975**, *14*, 3070.

(42) Mingos, D. M. P.; Ibers, J. A. *Inorg. Chem.* **1970**, *9*, 1105.

(43) Pratt, B. C.; Ibers, J. A. *Inorg. Chem.* **1972**, *11*, 2812.

(44) Kuszaj, J. M.; Tomlonovic, B. P.; Murtha, D. P.; Lintvedt, R. L.; Glick, M. D. *Inorg. Chem* . **1973**, *12*, 1297.

(45) Albano, V. G.; Bellon, P. L.; Ciani, G. *J. Organomet. Chem.* **1972**,*38*, 155.

(46) Wockner, F.; Keller, E.; Brintzinger, H. H. *J. Organomet. Chem.* **1982**, *236*, 267.

(47) Bernal, I.; Korp, J. P.; Reisner, G. A.; Hermann, M. A. *J. Organomet. Chem.* **1977**, *139*, 321.

(48) Rabinowitz, H. H.; Karlin, K. D.; Lippard, S. J. *J. Am. Chem. Soc.* **1977**, *99*, 1420.

(49) Ahmed, F. R. ; Roustan, J. L.; Al-Janabi, M. Y. *Inorg. Chem.* **1985**, *24*, 2526.

(50) Farr, J. P.; Olmstead, M. M.; Hunt, C. H.; Balch, A. L.; *Inorg. Chem.* **1981**, *20*, 1182.

(51) Daly, J. *J. Chem. Soc.* **1964**, 3799.

PART IV

Chapter 1

(1) Same as Ref. (40) in Part III.

(2) Same as Ref. (39) in Part III.

(3) Same as Ref. (37) in Part III.

(5) Chong, K. S.; Retting, S. J.; Storr, A.; Trotter, J. *Can. J. Chem.* **1979**, *57*, 3119.

(6) Caughan, A. P.; Corden, B. J.; Eisenberg, R.; Ibers, J. A. *Inorg. Chem.* **1974**, *13*, 786.

(7) Haymore, B. L.; Ibers, J. A. *Inorg. Chem.* **1975**, *14*, 2610.

(8) Same as Ref. (43) in Part III.

(9) LeBorgne, G. L.; Mordenti, L.; Reiss, J. G.; Roustan, J. L. *New. J. Chem.* **1986**, *10*, 102.

(10) Mingos, D. M. P.; Ibers, J. A. *Inorg. Chem.* **1970**, *9*, 1105.

(11) Roustan, J. L.; Ansari, N.; Charland, J. P.; Le Page, Y. *Can. J. Chem.* **1989**, *67*, 2016.

Chapter 2

(12) Same as Ref. (4) in Part III.

(13) Same as Ref. (35) in Part III.

(14) Harrison, W.; Trotter, J. *J. Chem. Soc. (A)*, **1971**, 1542.

(15) Baltusis, L. M.; Karlin, K. D.; Rabinowitz, H. N.; Dewan, J. C.; Lippard, S. J. *Inorg. Chem.* **1980**, *19*, 2627.

(16) Same as Ref. (36) in Part III.

(17) Kopf, J.; Schmidt, J. Z.; *Naturforch.* **1975**, *306*, 149.

(18) Clegg, W. *Inorg. Chem.* **1976**, *15*, 2928.

(19) Keller, E.; Vahrenkamp, H. *Chem. Ber.* **1979**, *112*, 1626.

(20) Mazany, A. M.; Fackler, Jr. J. P.; Gallaher, M. K.; Seyferth, D. *Inorg. Chem.* **1983**, *22*, 2593.

PART V

(1) Le Page, Y.; White, P. S.; Gabe, E. J. 1986 (Proc. Am. Crystallogr. Assoc. Meet. Hamilton, Ontario, Canada, Abs. PA23).

(2) Gabe, E. J.; Lee, F. L.; Le, Page Y. (1985) In Crystallographic computing 3, edited by G. M. Sheldrick, C. Kruger and R. Goddard Oxford, Clarendon press.

(3) (a) Haymore, B.; Feltham, R. D. *Inorg. Syn.* **1973**, 14, 81. (b) *Inorg. Syn.* **1966**, 192.

(4) Newkome, G. R.; Hagen, D. C. *J . Org. Chem.* **1978**, *43*, 947.

(5) Ballivet, D.; Tkatchenko, I. *Inorg. Chem.* **1977**, *16*, 945.

(6) Bishop, J. J.; Davison, A.; Katcher, M. L.; Lichtenberg, D. W.; Merill, R. E. ; Smart, J. C. *J. Organomet. Chem.* **1971**, *27*, 241.

(7) Osborn, A. G.; Whitely, R. H.; Meads, R. E. *J. Organomet. Chem.* **1980**, *193*, 345.

(8) (a) Seyferth, D.; Whithers, H. P.; *Organomet.* **1982**, *1*, 1275. (b) Whithers, H. P.; Seyferth, D.; Fellmann, J. D.; Garron, P. E.; Martin, S. *Organomet.* **1982**, *1*, 1283.

APPENDIX

Table I

Crystal data and Refinement for $Fe(O=PPh_2(2\text{-}Py))_3^{2+}.2BF_4^-$

Parameter	Value
Crystal System	Monoclinic
Space Group	$P2_1/a$
a, Å	18.714(1)
b, Å	13.732(2)
c, Å	21.653(2)
β, deg	109.77(1)
V, $Å^3$	5236.42
Z	4
D_{cal}, gm cm^{-3}	1.352
Radiation	CuKα
λ(Kα), Å	1.5418
μ, mm^{-1}	3.85
$2\theta_{max}$, deg	80
Measured Reflection	10975
Unique Reflections	10965
Observed Reflection	2968
R_f	0.097
R_w	0.047

Table II

Atomic parametrs x, y, z of $Fe(O=PPh_2(2\text{-}Py))_3^{2+}.2BF_4^-$ (21)

Name	x	y	z				
Fe	0.60002	0.08613	0.75826	C(86)	0.63932	0.15957	0.50963
P(1)	0.64652	0.08147	0.91061	C(91)	0.75147	0.09566	0.65017
P(2)	0.42510	0.06127	0.71829	C(92)	0.76979	-0.00014	0.64228
P(3)	0.65501	0.12673	0.63906	C(93)	0.84192	-0.03318	0.65846
O(1)	0.59377	0.12462	0.84877	C(94)	0.89865	0.03077	0.68036
O(2)	0.48420	0.13494	0.71462	C(95)	0.88643	0.13256	0.69111
O(3)	0.62169	0.05113	0.67252	C(96)	0.80790	0.16563	0.67370
N(1)	0.71719	0.04202	0.82967	B(1)	0.06957	0.98808	0.87940
N(2)	0.54578	-0.05752	0.75348	F(1)	0.13761	1.01015	0.89725
N(3)	0.63234	0.23372	0.73164	F(2)	0.03399	1.08591	0.85916
C(11)	0.73313	0.05797	0.89412	F(3)	0.03588	0.94328	0.82528
C(12)	0.80656	0.06107	0.94181	F(4)	0.04626	0.96554	0.93004
C(13)	0.86393	0.04069	0.91668	B(2)	0.82479	0.18803	0.35241
C(14)	0.84927	0.01695	0.85105	F(5)	0.74336	0.24486	0.35675
C(15)	0.77432	0.01855	0.80837	F(6)	0.78023	0.15740	0.29033
C(21)	0.61348	-0.03446	0.92721	F(7)	0.83649	0.28813	0.33847
C(22)	0.54206	-0.04349	0.93042	F(8)	0.74786	0.28750	0.26708
C(23)	0.51234	-0.12953	0.93782				
C(24)	0.55533	-0.21509	0.94657				
C(25)	0.62688	-0.20466	0.94563				
C(26)	0.65632	-0.11815	0.93662				
C(31)	0.66364	0.15430	0.98301				
C(32)	0.70139	0.12164	1.04339				
C(33)	0.70953	0.17683	1.09795				
C(34)	0.67341	0.26617	1.08874				
C(35)	0.63303	0.30061	1.02772				
C(36)	0.62629	0.24328	0.97308				
C(41)	0.46865	-0.05965	0.73930				
C(42)	0.43137	-0.13914	0.74515				
C(43)	0.47022	-0.22618	0.75884				
C(44)	0.54675	-0.22574	0.77164				
C(45)	0.58139	-0.13931	0.76760				
C(51)	0.38686	0.09800	0.78266				
C(52)	0.32789	0.04475	0.79324				
C(53)	0.30183	0.08251	0.84253				
C(54)	0.33435	0.15841	0.87951				
C(55)	0.38919	0.20656	0.86825				
C(56)	0.41480	0.17884	0.81910				
C(61)	0.35051	0.05796	0.63690				
C(62)	0.28862	-0.01159	0.62007				
C(63)	0.23292	-0.00177	0.55988				
C(64)	0.23995	0.06155	0.51708				
C(65)	0.29463	0.12730	0.52921				
C(66)	0.35274	0.12660	0.58885				
C(71)	0.64701	0.24171	0.67452				
C(72)	0.65100	0.32870	0.64652				
C(73)	0.63840	0.41602	0.67714				
C(74)	0.62292	0.40429	0.73599				
C(75)	0.61898	0.31034	0.75983				
C(81)	0.60447	0.13381	0.55311				
C(82)	0.52642	0.12339	0.52952				
C(83)	0.48555	0.13733	0.46486				
C(84)	0.51918	0.15652	0.42257				
C(85)	0.59645	0.17329	0.44283				

Table III

Crystal data and Refinement for $Co(NO)_2(PPh_2(2\text{-}Py))I$

Parameter	Value
Crystal System	Monoclinic
Space Group	$P2_1/n$
a, Å	8.0450(6)
b, Å	14.7750(5)
c, Å	16.1600(6)
β, deg	91.540(5)
V, $Å^3$	1920.2
Z	4
D_{cal}, gm cm^{-3}	1.765
Radiation	MoKα
λ(Kα), Å	0.70932
$2\theta_{max}$, deg	45
Measured Reflection	4248
Unique Reflections	2497
Observed Reflection	1980
R_f	0.052
R_w	0.045
GOF	1.87

$Co(NO)_2(PPh_2(2\text{-}Py))_2I$

Table IV Atomic Parameters x,y,z and Biso. E.S.Ds. refer to the last digit printed.

	x	y	z	Biso
CO	.14086(9)	.17669(6)	.74918(5)	4.03 (4)
N1	.1541 (6)	.2404 (4)	.8322 (4)	4.8 (3)
N2	.2459 (7)	.1879 (5)	.6653 (4)	6.1 (3)
N3	-.1513 (6)	.0760 (3)	.5882 (3)	4.58 (25)
O1	.1420 (7)	.2926 (4)	.8850 (3)	6.8 (3)
O2	.3101 (8)	.2076 (6)	.6066 (4)	11.7 (5)
I	.13762(6)	.00869(3)	.79224(3)	5.905(25)
P	-.12751(17)	.19611(10)	.71009(9)	3.18 (6)
C11	-.2570 (7)	.2233 (4)	.7973 (3)	3.43 (25)
C12	-.3643 (8)	.2948 (5)	.7965 (4)	4.0 (3)
C13	-.4558 (9)	.3140 (6)	.8644 (5)	4.8 (4)
C14	-.4420 (9)	.2630 (5)	.9339 (5)	5.1 (4)
C15	-.3337 (9)	.1905 (5)	.9363 (4)	5.1 (4)
C16	-.2429 (11)	.1729 (6)	.8688 (5)	4.8 (4)
C21	-.1616 (6)	.2894 (3)	.6394 (3)	3.04 (24)
C22	-.0603 (9)	.3643 (4)	.6435 (4)	4.1 (3)
C23	-.0904 (9)	.4389 (5)	.5951 (4)	5.1 (3)
C24	-.2215 (10)	.4391 (5)	.5397 (4)	5.3 (4)
C25	-.3251 (10)	.3649 (5)	.5345 (4)	5.1 (3)
C26	-.2943 (9)	.2910 (5)	.5835 (4)	4.4 (3)
C31	-.2266 (7)	.1007 (4)	.6574 (3)	3.23 (24)
C32	-.2206 (10)	.0065 (5)	.5451 (5)	5.3 (4)
C33	-.3588 (9)	-.0394 (5)	.5710 (5)	5.1 (4)
C34	-.4319 (10)	-.0141 (5)	.6396 (5)	5.0 (3)
C35	-.3659 (8)	.0588 (4)	.6852 (4)	4.1 (3)
H12	-.381 (7)	.323 (4)	.758 (3)	3.6 (16)
H13	-.512 (8)	.357 (4)	.863 (4)	4.4 (17)
H14	-.506 (7)	.279 (4)	.981 (4)	4.6 (14)
H15	-.309 (9)	.162 (5)	.987 (4)	7.7 (21)
H16	-.192 (8)	.141 (4)	.869 (4)	2.3 (18)
H22	.016 (6)	.362 (3)	.675 (3)	1.1 (10)
H23	.001 (9)	.500 (4)	.604 (4)	6.2 (16)
H24	-.240 (8)	.491 (4)	.500 (4)	4.9 (14)
H25	-.417 (9)	.356 (4)	.497 (4)	5.7 (16)
H26	-.346 (8)	.248 (4)	.572 (4)	5.3 (18)
H32	-.170 (7)	-.005 (3)	.502 (4)	3.4 (14)
H33	-.397 (8)	-.090 (4)	.536 (4)	5.6 (15)
H34	-.538 (8)	-.040 (4)	.658 (3)	4.5 (13)
H35	-.422 (7)	.082 (3)	.732 (3)	3.5 (12)

Biso is the Mean of the Principal Axes of the Thermal Ellipsoid

Table V Table of u(i,j) or U values *100. E.S.Ds. refer to the last digit printed

	u11(U)	u22	u33	u12	u13	u23
CO	3.26(5)	6.17(6)	5.87(5)	-.23 (4)	-.30(4)	.05 (4)
N1	5.0 (3)	5.8 (3)	7.4 (4)	-.2 (3)	-1.7 (3)	.3 (3)
N2	4.3 (3)	10.9 (5)	8.1 (4)	.6 (3)	.8 (3)	2.1 (4)
N3	5.2 (3)	6.1 (3)	6.2 (3)	-.2 (3)	.4 (3)	-.8 (3)
O1	8.9 (4)	7.7 (4)	9.3 (4)	1.0 (3)	-1.8 (3)	-1.7(3)
O2	8.4 (5)	24.6 (9)	11.5 (5)	.3 (5)	2.6 (4)	5.9(6)
I	7.11(4)	6.18(3)	9.07(4)	1.195(24)	-1.25(3)	-.16(2)
P	3.35(8)	4.54(9)	4.21(8)	-.42 (7)	.24(6)	-.03(7)
C11	3.7 (3)	4.5 (3)	4.8 (3)	-.8 (3)	-.3 (3)	.1 (3)
C12	4.8 (4)	5.6 (4)	4.7 (4)	.1 (3)	.7 (3)	.3 (4)
C13	5.0 (4)	6.1 (5)	7.4 (5)	.5 (4)	1.1 (4)	-.6(4)
C14	6.0 (5)	6.8 (5)	6.7 (5)	-.9 (4)	2.4 (4)	-.6(4)
C15	7.6 (5)	6.7 (5)	5.1 (4)	-.4 (4)	2.1 (4)	.1(4)
C16	6.5 (5)	5.2 (5)	6.7 (5)	.8 (4)	.9 (4)	-.1(4)
C21	3.4 (3)	4.3 (3)	3.9 (3)	-.4 (3)	.2 (3)	-.32(25)
C22	4.4 (4)	6.3 (4)	4.7 (4)	-.6 (3)	-.2 (3)	-.3(3)
C23	7.7 (5)	5.4 (4)	6.3 (4)	-.9 (4)	.6 (4)	-.0(4)
C24	9.4 (6)	4.9 (4)	5.8 (4)	.7 (4)	.0 (4)	.6(4)
C25	6.9 (5)	6.5 (5)	6.0 (4)	.7 (4)	-1.3 (4)	-.1(4)
C26	5.7 (5)	5.1 (4)	5.8 (4)	-.7 (4)	-.5 (4)	-.2(3)
C31	3.7 (3)	4.7 (3)	3.9 (3)	.3 (3)	.6 (3)	.3(3)
C32	6.8 (5)	7.6 (5)	5.6 (5)	1.1 (4)	.2 (4)	-2.1(4)
C33	5.8 (5)	5.6 (4)	7.9 (5)	-.9 (4)	-1.3 (4)	-.6(4)
C34	5.4 (4)	6.0 (4)	7.5 (5)	-1.5 (4)	.2 (4)	-.5(4)
C35	4.3 (4)	5.4 (4)	6.1 (4)	-.5 (3)	.8 (3)	-.0(4)
H12	4.6(20)					
H13	5.6(22)					
H14	5.8(18)					
H15	9.7(26)					
H16	2.9(23)					
H22	1.4(13)					
H23	7.8(21)					
H24	6.2(18)					
H25	7.2(20)					
H26	6.7(23)					
H32	4.4(18)					
H33	7.1(20)					
H34	5.8(17)					
H35	4.4(16)					

Anisotropic Temperature Factors are of the form
Temp=-2*Pi*Pi*(h*h*u11*astar*astar+---+2*h*k*u12*astar*bstar+---)

Table VI

Crystal data and Refinement for $Co(NO)_2(PPh_2(2\text{-}Py))_2^+.BF_4^-$

Parameter	Value
Crystal System	Monoclinic
Space Group	P2/c
a, Å	14.3650(5)
b, Å	13.558(4)
c, Å	17.494(8)
β, deg	103.99(3)
V, $Å^3$	3306.08
Z	2
D_{cal}, gm cm^{-3}	1.471
Radiation	MoKα
λ(Kα), Å	0.70932
μ, mm^{-1}	2.76
$2\theta_{max}$, deg	25
Measured Reflection	5909
Unique Reflections	4325
Observed Reflection	2754
R_f	0.038
R_w	0.039
GOF	1.37

Table VII

$Co(NO)_2(PPh_2(2\text{-}Py))_2^{+}BF_4^{-}$

Atomic Parameters x,y,z and B_{iso}.

E.S.Ds. refer to the last digit printed.

	x	y	z	B_{iso}
CO A	0	0.76506(6)	1/4	2.67(4)
CO B	1/2	0.74926(6)	1/4	3.01(5)
P A	0.01844(9)	0.86253(8)	0.35848(7)	2.69(6)
P B	0.51751(9)	0.65003(9)	0.35663(7)	2.67(6)
F 1A	0.0125 (4)	0.5003 (3)	0.18960(25)	12.1 (3)
F 2A	0.0734 (4)	0.3863 (4)	0.2744 (3)	14.0 (4)
F 1B	0.4207 (3)	0.13870(23)	0.22602(24)	8.48(22)
F 2B	0.4925 (3)	0.0221 (3)	0.31015(24)	9.9 (3)
O A	0.1767 (3)	0.6710 (4)	0.2725 (3)	9.6 (3)
O B	0.3275 (4)	0.8287 (4)	0.2684 (3)	8.8 (3)
N A	0.1042 (3)	0.7104 (3)	0.26235(23)	4.05(23)
N B	0.3972 (4)	0.7990 (3)	0.25647(25)	4.9 (3)
N32A	-0.1458 (3)	0.9719 (3)	0.32225(24)	4.45(23)
N32B	0.3726 (3)	0.5343 (3)	0.29193(22)	3.61(20)
C11A	0.0675 (3)	0.7907 (3)	0.44690(25)	2.70(21)
C12A	0.0594 (4)	0.6907 (4)	0.4452 (3)	3.20(25)
C13A	0.0805 (4)	0.6360 (4)	0.5142 (3)	4.0 (3)
C14A	0.1127 (4)	0.6817 (4)	0.5848 (3)	4.5 (3)
C15A	0.1241 (4)	0.7813 (4)	0.5878 (3)	4.5 (3)
C16A	0.1007 (4)	0.8365 (4)	0.5194 (3)	3.8 (3)
C21A	0.0978 (4)	0.9681 (3)	0.36403(24)	2.84(24)
C22A	0.1947 (4)	0.9498 (4)	0.3761 (3)	3.7 (3)
C23A	0.2569 (5)	1.0265 (5)	0.3733 (3)	5.0 (4)
C24A	0.2226 (6)	1.1197 (5)	0.3585 (4)	5.4 (4)
C25A	0.1276 (6)	1.1366 (5)	0.3466 (3)	5.4 (4)
C26A	0.0644 (5)	1.0608 (4)	0.3498 (3)	3.9 (3)
C31A	-0.0956 (3)	0.9046 (3)	0.37476(24)	2.74(22)
C33A	-0.2348 (4)	0.9986 (4)	0.3300 (3)	4.2 (3)
C34A	-0.2741 (5)	0.9584 (5)	0.3863 (3)	4.3 (3)
C35A	-0.2245 (4)	0.8910 (4)	0.4381 (3)	4.3 (3)
C36A	-0.1340 (4)	0.8640 (4)	0.4325 (3)	3.7 (3)
C11B	0.6376 (3)	0.6303 (3)	0.4170 (3)	2.84(22)
C12B	0.7154 (4)	0.6274 (4)	0.3829 (3)	3.8 (3)
C13B	0.8065 (4)	0.6136 (5)	0.4294 (4)	4.5 (3)
C14B	0.8218 (5)	0.6047 (4)	0.5079 (4)	4.5 (3)
C15B	0.7470 (4)	0.6063 (5)	0.5432 (4)	4.9 (3)
C16B	0.6549 (5)	0.6184 (4)	0.4982 (3)	4.2 (3)
C21B	0.4547 (3)	0.7061 (3)	0.42421(24)	2.70(23)
C22B	0.4887 (5)	0.7963 (5)	0.4568 (4)	4.7 (3)
C23B	0.4451 (5)	0.8439 (5)	0.5089 (4)	5.5 (4)
C24B	0.3682 (5)	0.8023 (5)	0.5281 (4)	5.1 (3)
C25B	0.3337 (5)	0.7145 (5)	0.4961 (3)	4.8 (3)
C26B	0.3775 (4)	0.6658 (4)	0.4448 (3)	3.6 (3)
C31B	0.4631 (3)	0.5282 (3)	0.33512(24)	2.74(21)
C33B	0.3261 (4)	0.4493 (4)	0.2704 (3)	4.5 (3)
C34B	0.3683 (5)	0.3586 (4)	0.2882 (3)	4.7 (3)
C35B	0.4605 (5)	0.3543 (4)	0.3316 (3)	4.4 (3)
C36B	0.5095 (4)	0.4406 (3)	0.3565 (3)	3.32(24)
B A	0	0.4470 (7)	1/4	6.1 (7)
B B	1/2	0.0846 (7)	1/4	5.2 (6)

B_{iso} is the Mean of the Principal Axes of the Thermal Ellipsoid

Table VII

Crystal data and Refinement for $Co(NO)_2(Py)_2^+BF_4^-$

Parameter	Value
Crystal System	Monoclinic
Space Group	$P2_1/a$
a, Å	14.7633(6)
b, Å	13.9739(5)
c, Å	15.1667(6)
β, deg	109.334(4)
V, $Å^3$	2952.5
Z	8
D_{cal}, gm cm^{-3}	1.638
Radiation	Mokα
λ(Kα), Å	0.70926
μ, mm^{-1}	1.21
$2\theta_{max}$, deg	45
Measured Reflection	6038
Unique Reflections	3820
Observed Reflection	2225
R_f	0.054
R_w	0.023
GOF	2.462

Table IX Atomic parameters x, y, z and Biso of $Co(NO)_2(Py)_2^+BF_4^-$ (10).

E.S.Ds. refer to the last digit printed

	x	y	z	Biso
CO A	0.06232(8)	0.29287(7)	0.84672(7)	4.93(6)
N 1 A	0.0348 (6)	0.1544 (4)	0.8640 (4)	5.3 (4)
N 2 A	-0.0165 (4)	0.3404 (5)	0.9235 (5)	4.5 (4)
N 3 A	0.1768 (4)	0.3196 (5)	0.8985 (4)	6.5 (5)
N 4 A	0.0163 (4)	0.3260 (4)	0.7368 (4)	5.8 (4)
O 1 A	0.2538 (4)	0.3452 (5)	0.9227 (4)	10.6 (5)
O 2 A	-0.0037 (4)	0.3565 (4)	0.6620 (3)	8.3 (4)
C 1 A	0.1056 (6)	0.0889 (9)	0.8827 (6)	6.8 (6)
C 2 A	0.0899 (8)	-0.0072 (8)	0.8867 (7)	8.8 (8)
C 3 A	-0.0020 (11)	-0.0387 (7)	0.9749 (7)	8.0 (8)
C 4 A	-0.0736 (6)	0.0256 (9)	0.8555 (6)	6.4 (6)
C 5 A	-0.0531 (7)	0.1221 (7)	0.8503 (5)	5.5 (6)
C 6 A	-0.0125 (6)	0.3011 (6)	1.0057 (7)	5.4 (6)
C 7 A	-0.0644 (8)	0.3349 (8)	1.0590 (6)	6.6 (6)
C 8 A	-0.1250 (7)	0.4127 (8)	1.0270 (7)	6.5 (6)
C 9 A	-0.1288 (6)	0.4550 (6)	0.9468 (7)	5.9 (6)
C10 A	-0.0759 (7)	0.4171 (7)	0.8962 (5)	6.2 (6)
H 1 A	0.168 (4)	0.119 (4)	0.880 (4)	7.9
H 2 A	0.152 (4)	-0.057 (4)	0.894 (4)	7.9
H 3 A	0.001 (5)	-0.102 (4)	0.889 (5)	7.9
H 4 A	-0.142 (4)	0.009 (5)	0.852 (4)	7.9
H 5 A	-0.113 (4)	0.175 (4)	0.829 (4)	7.9
H 6 A	0.036 (4)	0.245 (4)	1.024 (4)	7.9
H 7 A	-0.060 (4)	0.298 (4)	1.120 (4)	7.9
H 8 A	-0.163 (4)	0.425 (5)	1.069 (4)	7.9
H 9 A	-0.174 (4)	0.529 (4)	0.910 (4)	7.9
H10 A	-0.081 (5)	0.435 (5)	0.838 (4)	7.9
CO B	0.28679(7)	0.06856(7)	0.40512(7)	4.72(6)
N 1 B	0.3391 (5)	-0.0166 (4)	0.5176 (4)	4.6 (4)
N 2 B	0.1494 (4)	0.0363 (5)	0.3903 (4)	4.8 (4)
N 3 B	0.3165 (4)	0.0303 (5)	0.3154 (4)	5.5 (4)
N 4 B	0.3122 (5)	0.1814 (4)	0.4348 (4)	6.1 (4)
O 1 B	0.3433 (4)	0.0154 (4)	0.2538 (3)	8.1 (4)
O 2 B	0.3335 (5)	0.2603 (3)	0.4427 (4)	9.9 (5)
C 1 B	0.4092 (7)	-0.0805 (7)	0.5247 (6)	6.0 (6)
C 2 B	0.4459 (7)	-0.1356 (7)	0.6038 (10)	8.0 (8)
C 3 B	0.4136 (10)	-0.1245 (10)	0.6756 (8)	8.8 (9)
C 4 B	0.3409 (8)	-0.0618 (9)	0.6691 (7)	7.5 (7)
C 5 B	0.3058 (6)	-0.0077 (6)	0.5897 (8)	5.7 (6)
C 6 B	0.1196 (6)	-0.0531 (6)	0.3947 (5)	5.3 (5)
C 7 B	0.0259 (8)	-0.0764 (6)	0.3813 (6)	6.6 (6)
C 8 B	-0.0414 (7)	-0.0048 (9)	0.3619 (7)	7.6 (7)
C 9 B	-0.0136 (7)	0.0864 (8)	0.3579 (7)	8.5 (7)
C10 B	0.0810 (8)	0.1052 (5)	0.3721 (6)	6.9 (6)
H 1 B	0.422 (4)	-0.098 (4)	0.449 (4)	7.9
H 2 B	0.496 (4)	-0.182 (4)	0.604 (4)	7.9
H 3 B	0.419 (5)	-0.158 (5)	0.725 (4)	7.9
H 4 B	0.303 (4)	-0.053 (5)	0.717 (4)	7.9
H 5 B	0.264 (4)	0.051 (4)	0.589 (4)	7.9
H 6 B	0.172 (4)	-0.109 (4)	0.402 (4)	7.9
H 7 B	0.004 (5)	-0.144 (4)	0.395 (4)	7.9
H 8 B	-0.099 (4)	-0.037 (5)	0.360 (4)	7.9
H 9 B	-0.069 (4)	0.142 (4)	0.334 (4)	7.9
H10 B	0.122 (4)	0.177 (4)	0.373 (4)	7.9
B A	0.2272 (10)	0.2303 (9)	0.6698 (10)	7.1 (9)
F 1 A	0.3060 (5)	0.2281 (4)	0.6491 (6)	16.8 (7)
F 2 A	0.2323 (5)	0.1674 (4)	0.7307 (4)	16.4 (6)
F 3 A	0.1582 (4)	0.2093 (4)	0.5964 (4)	17.0 (5)
F 4 A	0.2193 (4)	0.3197 (3)	0.6947 (4)	11.1 (4)
B B	0.2409 (9)	0.2539 (10)	0.1687 (8)	6.4 (8)
F 1 B	0.3309 (3)	0.2330 (3)	0.2234 (3)	9.6 (3)
F 2 B	0.2173 (4)	0.1931 (4)	0.0947 (4)	13.1 (4)
F 3 B	0.1795 (4)	0.2284 (4)	0.2130 (4)	11.3 (4)
F 4 B	0.2279 (4)	0.3394 (4)	0.1410 (4)	14.7 (5)

Biso is the Mean of the Principal Axes of the Thermal Ellipsoid

Table X

Crystal data and Refinement for $Co_2(NO)_3(PPPh_2(2\text{-}Py))_2{}^+BPh_4{}^-$

Parameter	Value
Crystal System	Triclinic
Space Group	$P\bar{1}$
a, Å	14.253(3)
b, Å	15.489(2)
c, Å	12.984(3)
α, deg	95.62(1)
β, deg	91.35(1)
γ, deg	106.8291)
V, A^3	2728.54
Z	2
D_{cal}, gm cm^{-3}	1.386
D_m, gm cm^{-3}	1.385
Radiation	CuKα
$\lambda(K\alpha)$, Å	1.5418
μ, mm^{-1}	6.877
$2\theta_{max}$, deg	130
Measured Reflection	9275
Unique Reflections	9275
Observed Reflection	6579
R_f	0.052
R_w	0.074
GOF	1.41

Table XI Atomic parameters x, y, z and B_{iso} of $Co_2(NO)_3(PPh_2(2\text{-}Py))_2^+$ BPh_4^- (12). E.S.Ds. refer to the last digit printed.

	x	y	z	B(E)
CO(1)	-793(5)	21036(5)	11685(5)	3.8
CO(2)	-9606(6)	9388(5)	23223(6)	4.4
P(1)	-4893(8)	29524(7)	24556(9)	2.7
P(2)	-14068(8)	15386(7)	650(9)	2.8
N(1)	842(3)	2796(3)	640(3)	4.2
N(2)	-584(3)	589(3)	3378(3)	4.7
N(3)	111(3)	1076(3)	1571(3)	3.8
O(1)	1405(4)	3358(4)	279(4)	8.6
O(2)	-157(4)	372(4)	4018(4)	8.8
O(3)	729(3)	704(3)	1505(4)	6.9
C(101)	-1734(3)	2483(3)	2879(3)	3.4
N(102)	-1989(3)	1571(3)	2802(3)	3.6
C(103)	-2872(4)	1137(4)	3150(4)	5.2
C(104)	-3487(4)	1581(5)	3563(4)	6.0
C(105)	-3230(4)	2510(5)	3641(5)	5.7
C(106)	-2333(4)	2971(4)	3303(4)	4.5
C(107)	-390(3)	4091(3)	2149(3)	3.3
C(108)	-1154(4)	4330(4)	1693(4)	4.7
C(109)	-1006(5)	5180(4)	1368(5)	6.2
C(110)	-118(6)	5794(4)	1492(5)	6.4
C(111)	648(5)	5580(4)	1935(5)	6.2
C(112)	523(4)	4730(3)	2252(4)	4.5
C(113)	232(3)	3157(3)	3680(3)	3.1
C(114)	-14(4)	3639(4)	4538(4)	4.0
C(115)	524(4)	3790(4)	5472(4)	4.9
C(116)	1320(5)	3467(4)	5550(4)	5.3
C(117)	1585(4)	3000(4)	4713(5)	5.3
C(118)	1039(4)	2834(3)	3785(4)	4.2
C(201)	-1992(3)	330(3)	206(3)	3.2
N(202)	-1860(3)	76(2)	1148(3)	3.5
C(203)	-2272(4)	-799(3)	1289(4)	4.3
C(204)	-2807(4)	-1443(3)	531(4)	4.6
C(205)	-2939(4)	-1172(4)	-433(4)	4.7
C(206)	-2522(4)	-282(3)	-590(4)	4.0
C(207)	-2438(3)	2000(3)	154(3)	3.5
C(208)	-3278(4)	1589(4)	642(4)	4.5
C(209)	-4043(4)	1990(5)	728(5)	6.3
C(210)	-3959(5)	2777(5)	316(5)	6.8
C(211)	-3145(5)	3190(5)	-173(5)	6.3
C(212)	-2371(4)	2815(4)	-246(5)	5.1
C(213)	-1140(3)	1544(3)	-1307(3)	3.3
C(214)	-1836(4)	1536(4)	-2077(4)	4.3
C(215)	-1584(4)	1552(4)	-3103(4)	5.1
C(216)	-661(5)	1583(4)	-3366(4)	5.2
C(217)	34(4)	1586(4)	-2606(5)	5.3
C(218)	-187(4)	1565(3)	-1577(4)	4.2
B(1)	4646(4)	2335(4)	6395(4)	3.3
C(301)	5639(4)	3076(3)	6067(4)	3.8
C(302)	6598(4)	3040(4)	6277(4)	4.9
C(303)	7420(4)	3695(5)	6013(5)	6.4

Table XII Tables of U (i,j) or U values for $Co_2(NO)_3(PPh_2(2\text{-}Py))_2^+ BPh_4^-$ (12)

	U11	U22	U33	U23	U13	U12
CO(1)	4854(38)	4956(33)	5003(34)	623(29)	455(31)	1717(31)
CO(2)	6901(47)	4958(44)	4898(42)	915(34)	43(36)	1528(36)
P(1)	3181(56)	3349(55)	3763(59)	343(43)	198(45)	1042(46)
P(2)	3739(56)	3593(55)	3416(59)	573(43)	351(45)	1158(46)
N(1)	441(23)	651(26)	497(24)	109(20)	79(19)	152(20)
N(2)	749(31)	600(26)	444(24)	160(20)	-4(21)	178(23)
N(3)	507(24)	472(22)	516(24)	31(18)	1(19)	228(19)
O(1)	844(34)	1167(41)	1120(40)	550(33)	279(29)	-73(29)
O(2)	1205(43)	1555(51)	813(33)	523(34)	-86(30)	632(39)
O(3)	945(33)	861(30)	1087(35)	308(26)	194(27)	636(27)
C(101)	362(24)	484(25)	386(24)	10(20)	36(19)	61(20)
N(102)	453(22)	489(22)	357(20)	45(17)	32(16)	19(18)
C(103)	670(36)	601(33)	488(30)	-29(25)	102(26)	-142(27)
C(104)	505(32)	1030(48)	538(33)	-39(32)	160(26)	-72(32)
C(105)	416(29)	1000(46)	629(35)	-195(32)	137(25)	112(29)
C(106)	394(26)	659(33)	621(33)	-112(26)	66(23)	127(24)
C(107)	485(26)	387(23)	410(24)	40(19)	34(20)	148(20)
C(108)	584(33)	533(30)	692(35)	70(26)	-39(27)	206(25)
C(109)	906(46)	653(37)	942(47)	190(34)	-80(37)	422(35)
C(110)	1142(55)	495(32)	869(46)	170(31)	-69(40)	316(34)
C(111)	1006(50)	507(32)	718(40)	198(29)	-51(35)	-7(32)
C(112)	613(33)	501(29)	555(31)	141(24)	-38(25)	89(24)
C(113)	408(24)	348(22)	408(24)	74(18)	19(19)	73(18)
C(114)	459(27)	597(30)	484(28)	60(23)	43(22)	203(23)
C(115)	711(37)	709(35)	419(28)	48(25)	52(25)	201(29)
C(116)	810(40)	631(34)	536(32)	62(26)	-190(28)	197(30)
C(117)	658(36)	754(37)	689(37)	37(30)	-144(29)	369(31)
C(118)	557(30)	576(30)	491(28)	-24(23)	-58(23)	269(25)
C(201)	447(25)	393(23)	400(24)	31(19)	39(20)	141(20)
N(202)	516(23)	380(20)	417(21)	54(16)	33(17)	109(17)
C(203)	669(34)	425(26)	489(29)	94(22)	49(24)	85(24)
C(204)	649(34)	401(26)	668(35)	75(24)	87(27)	99(24)
C(205)	643(34)	512(30)	534(31)	-24(24)	32(26)	13(25)
C(206)	543(30)	456(26)	469(28)	35(21)	43(23)	94(22)
C(207)	497(27)	501(26)	367(24)	11(20)	-11(20)	201(22)
C(208)	564(31)	765(36)	456(28)	44(26)	37(23)	296(27)
C(209)	608(37)	1276(58)	614(37)	-7(37)	34(29)	492(39)
C(210)	975(50)	1206(57)	654(39)	-103(37)	-103(34)	776(47)
C(211)	1051(52)	788(42)	727(41)	32(33)	-129(37)	544(40)
C(212)	748(39)	596(33)	658(35)	118(27)	-11(29)	292(29)
C(213)	487(26)	362(23)	401(24)	59(19)	75(20)	108(20)
C(214)	634(33)	576(30)	440(28)	48(23)	37(24)	192(25)
C(215)	781(39)	686(35)	418(29)	102(26)	-18(26)	124(29)
C(216)	822(40)	604(33)	458(30)	15(25)	166(28)	77(29)
C(217)	631(35)	627(34)	674(36)	-30(28)	252(28)	94(27)
C(218)	620(32)	504(28)	473(28)	34(22)	118(24)	152(24)
B(1)	393(27)	449(28)	401(28)	-37(22)	-29(22)	129(22)
C(301)	538(29)	461(26)	429(26)	-52(21)	87(22)	121(22)
C(302)	451(29)	679(35)	624(34)	-49(27)	-36(25)	59(25)
C(303)	541(35)	890(45)	797(43)	-195(35)	30(31)	1(32)

Table XII (Contd.)

Tables of U (i,j) or U values for $Co_2(NO)_3(PPh_2(2\text{-}Py))_2^+ BPh_4^-$ (12)

	U11	U22	U33	U23	U13	U12
C(304)	868(47)	632(39)	860(46)	-87(33)	187(37)	-164(33)
C(305)	1126(55)	429(31)	885(46)	86(30)	233(41)	40(33)
C(306)	721(37)	427(28)	680(35)	24(25)	110(28)	122(25)
C(307)	482(26)	450(24)	365(24)	25(19)	-16(20)	178(21)
C(308)	469(28)	635(32)	543(30)	-127(25)	-16(23)	193(24)
C(309)	673(35)	597(32)	533(31)	-150(25)	-47(26)	216(27)
C(310)	858(40)	607(33)	546(32)	-22(26)	149(28)	382(31)
C(311)	616(34)	887(42)	559(32)	38(29)	76(26)	406(32)
C(312)	563(30)	665(32)	382(25)	-8(23)	-11(22)	251(25)
C(313)	414(24)	421(24)	403(24)	-11(19)	-1(19)	180(20)
C(314)	534(29)	512(28)	416(26)	-4(21)	17(21)	185(23)
C(315)	749(37)	668(33)	397(27)	5(24)	-38(25)	274(29)
C(316)	736(39)	783(40)	539(33)	-180(28)	-204(28)	358(32)
C(317)	512(31)	569(32)	731(37)	-48(27)	-90(27)	67(25)
C(318)	554(30)	510(28)	471(28)	22(22)	-16(23)	121(23)
C(319)	367(24)	398(23)	439(25)	-19(19)	-30(19)	102(19)
C(320)	571(31)	562(30)	493(29)	28(23)	41(24)	224(24)
C(321)	521(31)	530(30)	718(36)	-84(26)	-22(26)	207(25)
C(322)	600(33)	478(29)	738(37)	21(26)	-198(28)	191(25)
C(323)	616(34)	583(31)	548(31)	104(25)	-77(25)	89(26)
C(324)	547(29)	456(26)	436(27)	12(21)	14(22)	124(22)
CL(1)	2454(54)	1444(34)	1445(34)	519(27)	942(36)	1016(36)
CL(2)	2054(50)	1825(45)	1430(37)	277(33)	-522(34)	308(38)
C(40)	1552(119)	924(80)	949(83)	-208(65)	292(81)	366(79)

Table XI (Contd.) Atomic parameters x, y, z and B_{iso} of $Co_2(NO)_3(PPh_2(2\text{-}Py))_2^+$ BPh_4^- (12). E.S.Ds. refer to the last digit printed.

	x	y	z	B(E)
C(304)	7343(5)	4421(4)	5550(5)	6.9
C(305)	6432(6)	4494(4)	5346(6)	6.7
C(306)	5577(4)	3840(3)	5601(4)	4.9
C(307)	4156(3)	2881(3)	7275(3)	3.4
C(308)	4748(4)	3405(4)	8124(4)	4.4
C(309)	4400(4)	3879(4)	8899(4)	4.8
C(310)	3434(5)	3879(4)	8856(4)	5.0
C(311)	2829(4)	3382(4)	8044(4)	5.1
C(312)	3186(4)	2895(4)	7280(4)	4.2
C(313)	3856(3)	1876(3)	5397(3)	3.2
C(314)	3972(4)	2117(3)	4389(4)	3.8
C(315)	3274(4)	1705(4)	3586(4)	4.7
C(316)	2465(4)	1029(4)	3740(4)	5.4
C(317)	2321(4)	751(4)	4723(5)	5.0
C(318)	3021(4)	1173(3)	5515(4)	4.1
C(319)	4942(3)	1493(3)	6872(3)	3.2
C(320)	5340(4)	927(4)	6219(4)	4.2
C(321)	5654(4)	236(4)	6549(4)	4.7
C(322)	5543(4)	47(4)	7565(5)	4.8
C(323)	5148(4)	573(4)	8228(4)	4.7
C(324)	4866(4)	1292(3)	7883(4)	3.8
CL(1)	5157(4)	3737(3)	2372(3)	13.0
CL(2)	3291(4)	3822(4)	1842(4)	14.4
C(40)	4297(11)	4255(8)	2678(9)	9.1

Table XIII

Crystal data and Refinement indicators for (PPh_2(2-Py)

Parameter	Value
Crystal System	Monoclinic
Space Group	$P2_1/n$
a, Å	9.9023(2)
b, Å	9.8780(3)
c, Å	14.8926(4)
β, deg	92.948(2)
V, $Å^3$	1454.8
Z	4
D_{cal}, gm cm^{-3}	1.202
Radiation	MoKα
λ(Kα), Å	0.709261
μ, mm^{-1}	0.17
$2\theta_{max}$, deg	45
Measured Reflection	3376
Unique Reflections	3346
Observed Reflection	1680
R_f	0.043
R_w	0.023
GOF	2.15

$PPh_2(2\text{-}Py))_2$

Table XIV Atomic Parameters x,y,z and B_{iso}

E.S.Ds. refer to the last digit printed.

	x	y	z	B_{iso}
P	0.96935(7)	0.15507(7)	0.29975(5)	4.13(3)
N18	1.14047(22)	0.3508 (3)	0.26210(15)	5.88(12)
C 1	0.88855(22)	0.1617 (3)	0.18700(15)	3.74(11)
C 2	0.8969 (3)	0.0488 (3)	0.13287(22)	4.87(15)
C 3	0.8419 (3)	0.0493 (5)	0.04591(25)	6.23(19)
C 4	0.7799 (3)	0.1627 (5)	0.01216(24)	6.64(20)
C 5	0.7704 (3)	0.2755 (4)	0.06388(24)	6.16(18)
C 6	0.8242 (3)	0.2750 (3)	0.15106(21)	4.87(15)
C 7	0.8292 (3)	0.1559 (3)	0.37458(16)	4.05(11)
C 8	0.6937 (3)	0.1622 (3)	0.34783(21)	4.98(14)
C 9	0.5956 (4)	0.1565 (4)	0.4115 (3)	6.78(20)
C10	0.6321 (5)	0.1470 (4)	0.5007 (3)	7.32(21)
C11	0.7649 (5)	0.1405 (4)	0.52758(24)	7.27(21)
C12	0.8625 (4)	0.1436 (3)	0.46535(20)	5.61(16)
C13	1.03095(22)	0.3302 (3)	0.30983(15)	3.86(11)
C14	0.9775 (3)	0.4308 (3)	0.36097(18)	4.35(13)
C15	1.0372 (3)	0.5563 (4)	0.36375(23)	5.77(17)
C16	1.1475 (4)	0.5793 (4)	0.31469(23)	6.55(18)
C17	1.1944 (4)	0.4745 (5)	0.26558(22)	7.33(20)
H 2	0.939 (3)	-0.024 (3)	0.1586 (17)	5.8 (8)
H 3	0.8487 (25)	-0.030 (3)	0.0117 (18)	6.0 (8)
H 4	0.751 (3)	0.161 (3)	-0.0468 (20)	7.4 (8)
H 5	0.726 (3)	0.358 (3)	0.0421 (20)	7.7 (9)
H 6	0.8137 (24)	0.3495 (24)	0.1837 (15)	4.3 (6)
H 8	0.6651 (23)	0.1679 (25)	0.2883 (15)	4.4 (6)
H 9	0.514 (3)	0.160 (3)	0.3908 (20)	7.2 (9)
H10	0.561 (3)	0.143 (3)	0.5420 (22)	8.8 (9)
H11	0.787 (3)	0.133 (3)	0.5882 (22)	8.4 (10)
H12	0.952 (3)	0.138 (3)	0.4815 (18)	6.3 (8)
H14	0.9034 (23)	0.4097 (24)	0.3936 (15)	4.6 (6)
H15	1.000 (3)	0.623 (3)	0.3962 (19)	6.6 (8)
H16	1.184 (3)	0.671 (3)	0.3086 (20)	8.5 (9)
H17	1.273 (3)	0.487 (3)	0.2330 (20)	8.8 (9)

B_{iso} is the Mean of the Principal Axes of the Thermal Ellipsoid